



UNIVERSIDAD DE OVIEDO

Departamento de Biología de Organismos y Sistemas

Programa de doctorado: “Biología aplicada a la sostenibilidad de recursos naturales”
(Mención de Calidad)

**ESTRUCTURA Y FISIOLÓGÍA DE LA COMUNIDAD PLANCTÓNICA A
PARTIR DE MÉTODOS DE DIGITALIZACIÓN Y ANÁLISIS DE IMAGEN.**

**PLANKTON COMMUNITY STRUCTURE AND PHYSIOLOGY FROM
AUTOMATED IMAGE-BASED METHODS.**

TESIS DOCTORAL

Eva Álvarez Suárez

Oviedo 2014



RESUMEN (en Inglés)

Phytoplankton organisms account for 50% of global primary production and hence are central to the comprehension of global biogeochemical cycles. The structural attributes of the planktonic community, such as abundance, size-structure or taxonomic diversity, are emergent properties of processes taking place at the cellular, individual level. The purpose of this PhD thesis is the development of techniques of characterization of the planktonic community, both structural and physiological, from the analysis of individual cells that could be applied in a routine basis to the study of the ecosystems. The Flow Cytometer and Microscope (FlowCAM) is an automatic sampling device that acquires images of the cells and uses pattern recognition techniques to identify them. It allows the acquisition of information on a single cell basis, which not only permits the size structure description but also the exploration of underlying processes, as aspect that has not been deeply explored.

The size-structure of planktonic communities must be considered when designing sampling methods whose objective is the enumeration of planktonic cells. Although the FlowCAM has been used during the past decade to estimate several structural attributes of plankton community, there is no a standard methodology that ensures the reliability of the obtained data. In Chapter I of the present PhD thesis, we tackle the task of determining the trade-offs between number of counted cells, size-range effectively sampled and time required for analysis. Those considerations are used to define proper sampling protocols. We demonstrate how, following those guidelines, the FlowCAM is capable to count reliably a mono-specific cell suspension but also to estimate the size-structure of natural samples.

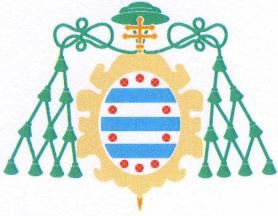
Automated sampling devices allow the increment of the sampling resolution and hence the number of images that can be acquired. Automatic classification of images appears, then, as a fundamental tool to deal with the identification of these extensive data bases. A common characteristic of image-based sampling devices is, however, the disregard of the tridimensional shape of the imaged particles, which can result in the bias of cellular biovolume estimates. In Chapter II, we introduce a method to improve the estimates of cellular biovolume obtained from image-based sampling devices coupled to a state of the art method for automated classification of images. The method of classification can be adapted to provide not only taxonomic information, but also a morphologic classification of the cells, allowing a trustworthy estimate of the cellular biovolume according to the cell shape predicted.



Once abundance, size and taxonomy have been obtained by FlowCAM analysis, one can wonder how this data compare with the traditional methods for plankton enumeration. In Chapter III, we compared FlowCAM and light microscopy as methods for the routine determination of the composition and size-structure of the planktonic community. The effects of the preservation of the sample and the inaccuracies in the automatic classification are the mainsprings discrepancies in the determination of size-structure between both methods. Nevertheless, the synoptic vision of the seasonal variation in abundance, biomass and diversity obtained was similar, which suggests that the fully automatic method is adequate for exploring these variations in natural samples.

The structural characterization of the phytoplankton community with FlowCAM can be applied for a variety of scales, from long to short-term. In Chapter IV, we analyze the dynamics of the phytoplankton community for a whole year and during two contrasted scenarios in summer and autumn in the Central Cantabrian Sea. The description of the hydrographic scenario showed temperature, light and nutrients as the main drivers of community size structure and physiology. The size structure and carbon biomass derived from FlowCAM were coupled with bulk measurements of chlorophyll, allowing a combined approximation to the phytoplankton community dynamics. The biomass and chlorophyll size spectra followed different trends which translated in changes in the chlorophyll to carbon ratio, for the whole community but also between size-fractions. The size dependence to the chlorophyll content was found to vary with field irradiance.

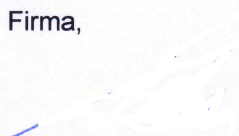
The structure of the community is the result of physiological processes taking place at the individual level. Hence, the description of the physiology of the phytoplankton community based on bulk measurements would go further if an estimate of pigment content per single cell was available. In Chapter V, we explored the relationship between the emission of fluorescence of phytoplankton single cells measured by the FlowCAM and their chlorophyll content. The size-dependence of chlorophyll content was found to vary with the irradiance experienced by the cells both at the inter- and intra-specific level. Hence, from a routine sampling of natural samples it is possible to estimate quantitatively the allometric exponent of chlorophyll content, which relates with the photosynthetic rates and hence, permits a more detailed description of the dynamics of the phytoplankton community.



**ACEPTACIÓN COAUTORES PRESENTACIÓN TRABAJOS FORMANDO
PARTE DE TESIS DOCTORAL COMO COMPENDIO DE PUBLICACIONES**

1.- Datos personales del coautor		
Apellidos: GUTIERREZ MORÁN	Nombre: XOSE ANXELU	
DNI/Pasaporte/NIE:	Teléfono:	Correo electrónico:

2.- Publicaciones que formarán parte de la tesis y de las que es coautor
Eva Álvarez, Enrique Nogueira, Ángel López-Urrutia and <u>Xose Ánxelu G. Morán</u> (2014) Autotrophic community size-structure and photoacclimation in a temperate shelf (Southern Bay of Biscay). (Manuscript).

ACEPTACIÓN:
Acepto que las publicaciones anteriores formen parte de la tesis doctoral titulada ESTRUCTURA Y FISIOLÓGÍA DE LA COMUNIDAD PLANCTÓNICA A PARTIR DE MÉTODOS DE DIGITALIZACIÓN Y ANÁLISIS DE IMAGEN. Y elaborada por Dña. Eva Álvarez Suárez. Firma,  En Gijón, a 10 de abril de 2014.

FOR-MAT-VOA-035

La investigación presentada en esta Tesis Doctoral se ha desarrollado en el Centro Oceanográfico de Gijón perteneciente al Instituto Español de Oceanografía - Ministerio de Economía y Competitividad.



Eva Álvarez fue beneficiaria de una ayuda para la formación de personal investigador “Severo Ochoa” (BP07-081) financiada por el Plan de Ciencia, Tecnología e Innovación del Gobierno del Principado de Asturias.



Los trabajos presentados se han desarrollado bajo la cobertura de los siguientes proyectos y convenios:

- PERPLAN - Efecto de las perturbaciones meteorológico-hidrográficas en la estructura de comunidad planctónica (CTM2006-04854/MAR)- Ministerio de Educación y Ciencia.
- IMAGINA - Integración de métodos de análisis de imagen de grupos planctónicos con técnicas de inteligencia artificial - Plan de Ciencia, Tecnología e Innovación del Gobierno del Principado de Asturias.
- ECOPEL - Estudio integrado del ecosistema pelágico, la distribución de las especies y su medio ambiente - UE-Plan Nacional de Datos Básicos + Instituto Español de Oceanografía.
- RADIALES - Programa de series temporales oceanográficas - Instituto Español de Oceanografía.
- METOCA - Predicción del Balance Metabólico de los Océanos (CTM2009-13882-MAR) - Spanish National Investigation + Development + Innovation (I+D+I) Plan.

Agradecimientos

Esta tesis hubiese sido imposible sin la participación de personas e instituciones que han facilitado las cosas para que este trabajo llegue a feliz término. Debo expresar mi agradecimiento a todas aquellas personas que con su ayuda no sólo han colaborado en la realización del presente trabajo si no también me han dado fuerza para finalizarlo.

Debo agradecer de manera especial y sincera a Enrique y Ángel por aceptarme para realizar esta tesis doctoral bajo su dirección. Su apoyo y confianza en mi trabajo y su capacidad para guiar mis ideas ha sido inestimable, no solamente en el desarrollo de esta tesis, sino también, creo, en mi formación como investigadora. Les agradezco también el haberme facilitado siempre los medios suficientes para llevar a cabo todas las actividades propuestas. Y especialmente quiero agradecerles todo el tiempo que han dedicado a esta tarea, su dedicación y su optimismo.

Han pasado varios años desde que esta andadura comenzó y durante este tiempo muchas personas han pasado por el Centro Oceanográfico de Gijón. A todos ellos, debo agradecerles su compañerismo y dedicación. También debo agradecer su ayuda a otros compañeros del IEO y de la Universidad de Oviedo, Jorge Lorenzo, Laura Escalera, Jorge Sostres... que aportaron sus conocimientos, recursos y sobre todo, su tiempo, para ayudarme a mejorar esta tesis. Gracias también a todas aquellas personas con quienes he compartido campañas oceanográficas y que no sólo me ayudaron con el trabajo sino que contribuyeron a hacer de ellas experiencias enriquecedoras.

En un ámbito más personal debo mencionar a mis familiares y amigos, que me han apoyado siempre y confiado en mí. Gracias a todos mis amigos por estar a mi lado y quererme como soy, Quique, Ángela, Marcos, Lu, Irene, Begoña, María... A Javi, sin su cariño todo hubiese sido mucho más difícil.

Gracias a mis padres, Marcelino y Mari, y a mi hermano, Hugo, nunca podré agradecerles suficiente su sacrificio y apoyo. A mis abuelos, Herminia y Suso, Arturo y Covadonga, por ser el espejo en el que mirarme. Si he heredado una pizca de la fuerza y capacidad de trabajo de todos ellos, estas han sido determinantes en la realización de esta tesis.

List of abbreviations and variables

ABD	area based diameter
ASS/BSS	abundance/biomass size spectrum
CBPM	carbon-based production models
CC	Coulter Counter
CTD	conductivity temperature depth
cv	coefficient of variation
DCM	deep chlorophyll maximum
EPM	epifluorescence microscopy
ESD	equivalent spherical diameter
FC	flow chamber / flow cell
FlowCAM	flow cytometer and microscope
IPC	Iberian poleward current
LIBSVM	library for support vector machines
LISST	laser in situ scattering and transmissometry
LM	light microscopy
mamsl	meters above mean sea level
MLD	mixed layer depth
NA	normalized abundance
NASS/NBSS	normalized abundance/biomass size spectrum
NPP	net primary production
PAR	photosynthetically active radiation
PMT	photomultiplier tube
PP	primary production
psu	practical salinity units
SBE	sea-bird electronics
SPB	spring phytoplankton bloom
SSD	side-scatter dispersion
SVM	support vector machine
TS	training set

A	autoimage
a	power law intercept
b	power law exponent
B	biomass
Chl-a	chlorophyll a
Chl-a:C	chlorophyll to carbon ratio
d	day
F	fluorescence
f/2	culture medium
FL2/FL3	flow cytometric fluorescences
H	Shannon's index
h	hour
I	irradiance
k	apparent growth rate
k_d	attenuation coefficient
L1	culture medium
N	abundance
P	relative abundance of taxonomic group
P_i	percentage analysed of the sample
q	number of taxonomic groups
S	side-scatter
S	taxonomic richness
s	size
s	second
t	time
V_i	sample volume per photograph
V_n	net volume analyzed
z	depth
z_{CM}	depth of the chlorophyll maximum
z_{eu}	depth of the euphotic zone
z_N	depth of the nitracline
Δs	size-interval

Contents

1. General introduction	1
2. Objectives	5
3. Results	7
Chapter I. How to effectively sample the plankton size spectrum? A case study using FlowCAM.....	7
Chapter II. Improvement of plankton biovolume estimates derived from image-based automatic sampling devices: application to FlowCAM.....	27
Chapter III. Routine determination of plankton community composition and size structure: a comparison between FlowCAM and light microscopy.....	49
Chapter IV. Autotrophic community size-structure and photoacclimation in a temperate shelf (Southern Bay of Biscay).....	69
Chapter V. In-vivo single-cell fluorescence and the size-scaling of phytoplankton chlorophyll content.....	93
Chapter VI. Other works related to the Thesis.....	113
4. General discussion	115
5. General conclusions	119
6. Conclusiones generales	121
7. Bibliography	123

General introduction

The autotrophic plankton has a fundamental role in functioning and dynamics of aquatic ecosystem, acting as a link among the chemical, geological and biological cycles in the ocean. The photosynthetic activity of the phytoplankton confined in the narrow illuminated layer of the oceans allows the transformation of the inorganic carbon in organic carbon that is then included in the trophic network. It is, therefore, an essential component in ecological models. Significant differences exist, nevertheless, in the location and extension of the maximum photosynthetic activity imposed by the physical and chemical conditions. The study of the factors and mechanisms that modulate the variability of populations of phytoplankton is a fundamental topic in marine ecology. It is recognized that the planktonic community is particularly sensitive to external factors, generally associated with changes in the oceanographic conditions promoted by the atmospheric variability, which operates in an ample range of temporal and spatial scales (Smayda, 1998).

Imaging cytometry: increased resolution and single cell approach

In the last decades, automatic sampling devices for the enumeration of plankton have been gaining relevance in oceanographic research (Babin *et al.*, 2005; Benfield *et al.*, 2007). At the cost of sacrificing certain taxonomic detail, these instruments provide a rapid analysis of samples that increases substantially the potential number of samples that can be analyzed. Imaging cytometry is uniquely suited to fill the need of increasing sampling resolution. Imaging cytometers are instruments triggered by optical properties and take microscopic pictures of particles directed at a camera's focal plane (Sieracki *et al.*, 1998; Olson & Sosik, 2007). Image-based flow cytometers can make observations at the level of a single cell in near real time, and collect data over a broad geographic regions and time-series observations.

The Flow Cytometer and Microscope (FlowCAM) combines elements of flow cytometry, microscopy and image analysis (Sieracki *et al.*, 1998), to count and to

General introduction

photograph particles that are embedded in a moving fluid. The sample fluid moves across the instrument thanks to a peristaltic pump and passes through a prismatic cell of glass that is focused by a microscope lens connected to a digital camera. One benefit of imaged based devices is that pattern recognition techniques can be used to identify the obtained images (MacLeod *et al.*, 2010). The properties of the planktonic community in the water column are the result of a series of processes at the individual level (Rodriguez, 1994). FlowCAM allows the acquisition of information on a single cell basis, which can be considered its great potential. The cell-level perspective provided and the capacity to measure large numbers of cells permits the description of the size distributions of the community.

The methodology used with FlowCAM is as diverse as diverse are their users, not existing an analysis of the reliability and limitations of the instrument. There is also a lack of tools for the analysis of data sets obtained from image-based sampling devices, which, given their own nature, require specific considerations that differ from those applied to data sets obtained by means of traditional methods. Also, although FlowCAM pretends to be an alternative to microscopy based methods, results produced for both methods have not been compared systematically. The fluorescence signals measured by FlowCAM have not been yet interpreted, opposite to cytometers employed for pico-phytoplankton analysis, where the detection of molecular probes by fluorescence signals allow single-cell physiological information to be garnered for a variety of algae, both in culture and in nature (Toepel *et al.*, 2005).

Phytoplankton community description

Classical models of primary productivity use chlorophyll as their index of phytoplankton biomass. Hence, net primary production (NPP) is commonly modeled as a function of chlorophyll concentration, even though it has been long recognized that variability in intracellular chlorophyll content from light acclimation and nutrient stress confounds the relationship between chlorophyll and phytoplankton biomass (Westberry *et al.*, 2008). As other variables become more readily available, both from remote sensing and *in situ* sampling, other indices of biomass take up the slack (Huot *et al.*, 2007). Phytoplankton carbon biomass is considered the more appropriately variable to describe algal standing stocks, especially as it relates to NPP which is a rate of carbon turnover (and not chlorophyll).

A recent advance is to consider both aspects of the community description when defining primary production models. On one side, aspects related with the standing stock of carbon, taxonomic composition and size structure are determinant for the fate of the production (Nielsen & Hansen, 1999). On the other side, organism size and

elemental composition constrain the rate of energy acquisition by the phytoplankton community and influences processes at the level of ecosystems. Hence, cell size and elemental composition appear as fundamental traits in phytoplankton growth models. The analysis of the structural and physiological aspects allows us to make inferences of energetic nature, relative to such questions as the maximum photosynthetic rate, the efficiency in the energy transfer across the food-web or the fate of the primary production.

Structural description of the community

The size-structure of the biomass in terrestrial and aquatic ecosystems has been an important point of attention in ecology in the last decades. The approximation "particle - size" began to develop in the decade of the twenties of the last century as a unifying theory that was establishing a relation between the biomass of the organisms in a certain size-classes and the individual size of these organisms (Rodriguez & Mullin, 1986). The concentration of particles depends on the type and on the status of the ecosystem and, for a given status, on the size of the organisms. The smallest organisms are much more abundant than the larger ones. This inverse relationship between size and abundance is described by means of spectrum of abundance in which the abundance of cells gathers in size-classes in a geometric scale and is represented against the individual size in double logarithmic scale (Sheldon *et al.*, 1972; Blanco *et al.*, 1994).

The normalized biomass-size spectrum (NBSS) is a structural representation of the plankton community (Rodriguez & Mullin, 1986) whose slope indicates the relative contribution of each size-class to the total phytoplankton community. When the NBSS covers several trophic levels, the slope of the NBSS is, thus, an integration of the efficiency of biomass transfer to larger organisms and indicates the number of large individuals that are maintained by small ones (Jennings & Mackinson, 2003).

The structure of the biological community, characterized on the basis of the species composition, the size-spectrum or the trophic relationships between its components, is one of the principal determinants of the functioning and the dynamics of the ecosystems (Tilman, 1999), with important implications in aspects related to the dynamics of populations, the energetics of the community or the stability of the ecosystem (Odum, 1969; Reynolds, 1997; Brown *et al.*, 2004). The analysis of the structural aspects (i. e. dominant species, species associations, diversity or size structure) allows to go deeper into the processes related to the dynamics of populations of the different planktonic components, from picoplankton (Calvo-Díaz & Morán, 2006) to mesozooplankton (Nogueira *et al.*, 2004).

Physiological description of the community

New generation ecosystem models are using physiological submodels to describe phytoplankton “behavior,” therefore future research needs to include, where practical, cell quotas for elements of interest that allow growth rates to be calculated from uptake rates. This approach opens the door to understand the range, variability, and controls on elemental stoichiometry at the population level. Advances in the use of proxies for intracellular biochemical pools in phytoplankton, if routinely applied, would help to resolve some of the outstanding questions based on cell counts and/or bulk measurements.

Cellular biovolume estimates coupled to bulk measurements of chlorophyll concentration can give a vision of the physiological status of the cells which can be translated to the community level. Changes in the amount of chlorophyll per biomass unit indicate an adjustment of cellular pigment levels to match the demands for photosynthesis, which is driven by changes in light, nutrients and temperature (Geider, 1987). Laboratory studies already showed that the phytoplankton responds to changes in light, nutrients and temperature fitting the cellular levels of pigment to cover the new requirements of the photosynthesis, and this response is easily quantifiable in the changes in the chlorophyll content per biomass unit (Geider, 1987; MacIntyre *et al.*, 2002). A trustworthy esteem of this ratio for routine methods would allow a characterization of the physiology of the community (Behrenfeld *et al.*, 2005).

Cell size and pigment content obtained on a single cell basis allows the exploration of the size-scaling of pigment content. The efficiency in the absorption of energy does not increase linearly with the increase of the concentration of pigment provided that the geometry of the cell imposes a packing of the molecules in the chloroplasts (Kirk, 1975a; Kirk, 1975b). This packaging effect must be taken into account to transform values of fluorescence measured with flow cytometry into chlorophyll. The size dependence of chlorophyll content changes with growth irradiance (Fujiki & Taguchi, 2002; Finkel, 2004), and relates directly with the size scaling of photosynthetic rates (Finkel, 2004; Marañón *et al.*, 2007). This can be determinant in primary productivity models since phytoplankton production can be modeled more realistically by improving current estimates derived from global primary production models.

Objectives

The global objective of the Thesis is to develop a semi-automated methodology for plankton enumeration based on FlowCAM that, applied routinely, allows the structural and physiological characterization of the phytoplankton community. Here are resumed the particular objectives of each chapter:

Chapter 1

1. To assess the reliability of FlowCAM to estimate the size-structure of natural samples.

Chapter II

2. To develop a technique to classify automatically images from an automatic sampling device.
3. To improve the estimation of the biovolume of the cells from two- dimensional images.

Chapter III

4. To compare the description of microplankton community provided by a traditional microscopy method and by FlowCAM.

Chapter IV

5. To characterize the hydrographical variability, at seasonal scales and at short-term scales in contrasted meteo-hydrographic situations (summer and autumn) in the Cantabrian Sea shelf.
6. To analyze changes in the size-structure of the phytoplankton community in relation to meteo-hydrographical drivers.
7. To explore the size dependence of photoacclimation processes trough the changes in the chlorophyll to carbon ratio on natural samples.

Chapter V

8. To interpret the fluorescence signals from FlowCAM to obtain a taxon- independent conversion from fluorescence to chlorophyll.
9. To describe the size dependence of chlorophyll content at the inter- and intra-specific level and the changes related to growth irradiance.

Chapter I. How to effectively sample the plankton size spectrum? A case study using FlowCAM

The size-structure of planktonic community must be considered when designing sampling methods whose objective is the enumeration of planktonic cells. Although the FlowCAM has been used during the past decade to estimate several structural attributes of plankton community, there is no a standard methodology that ensures the reliability of the obtained data. In this chapter we tackle the task of determining the trade-offs between number of counted cells, size-range effectively sampled and time of analysis. Those considerations are used to define proper sampling protocols. We demonstrate how, following those guidelines, the FlowCAM is capable to count reliably a mono-specific cell suspension but also it is useful to estimate the size-structure of natural samples.

Reference

Eva Álvarez, Ángel López-Urrutia, Enrique Nogueira and Santiago Fraga (2011) How to effectively sample the plankton size spectrum? A case study using FlowCAM. *Journal of Plankton Research*, 33(7): 1119-1133.

Candidate's contribution

My contribution to the work includes the co-design of the study and the establishment of methodology in collaboration with the rest of coauthors. I conducted the experiments with the help of SF, obtained and analyzed data and prepared tables and figures. I carried out the composition and co-writing of the article with substantial contributions and discussion of results of EN and AL-U. All authors commented on the manuscript.

How to effectively sample the plankton size spectrum? A case study using FlowCAM

EVA ÁLVAREZ^{1*}, ÁNGEL LÓPEZ-URRUTIA¹, ENRIQUE NOGUEIRA¹ AND SANTIAGO FRAGA²

¹INSTITUTO ESPAÑOL DE OCEANOGRAFÍA. CENTRO OCEANOGRÁFICO DE GIJÓN, 33212 GIJÓN, SPAIN AND ²INSTITUTO ESPAÑOL DE OCEANOGRAFÍA. CENTRO OCEANOGRÁFICO DE VIGO, 36200 VIGO, SPAIN

*CORRESPONDING AUTHOR: eva.alvarez@gi.ieo.es

Received October 27, 2010; accepted in principle January 20, 2011; accepted for publication January 23, 2011

Corresponding editor: John Dolan

Any technique developed to enumerate plankton must take into account the size structure of the plankton community. Automatic sampling devices must be capable of analysing a minimum number of cells of the largest size to cover the whole size range intended to be sampled effectively. The Flow Cytometer And Microscope (FlowCAM[®]) has been used in the last decade to estimate the size structure of the plankton community. Few attempts, however, have been made to compare FlowCAM measurements with the results provided by traditional microscopy methods for size-structure estimations. FlowCAM can operate in three working modes: autoimage, fluorescence triggered and side-scatter triggered. Autoimage and fluorescence triggered cannot only count accurately a mono-specific suspension of cells, but they are also useful to estimate the size structure of natural samples. The side-scatter-triggered mode is not effective to estimate the size structure of natural samples, although it can count a sparse mono-specific solution accurately. The analysis of natural samples with FlowCAM requires a planned pre-processing of the samples to adjust the density of triggering particles (concentrating or diluting the sample) and to pre-filtrate the sample to avoid cell clumping or obstruction of the flow chamber. The size structure obtained with FlowCAM and with microscopy counts on preserved samples are comparable. Sample preservation, however, alters the size structure of the sample, which suggests that results based on preserved samples must be taken with caution. Automatic sampling devices like FlowCAM could provide a more precise analysis of plankton communities, increasing the resolution of surveys and avoiding the effects of preservation and sample storage.

KEYWORDS: FlowCAM; light microscopy; community structure; size spectra; natural populations; sample preservation

INTRODUCTION

The variability of planktonic organisms occurs over a wide range of scales, from centimetres to basin-scales and from hours to decades (Haury *et al.*, 1978).

Characterizing these patterns of variability and understanding their causes and consequences require long-term high-resolution monitoring. Traditional methods for plankton enumeration, identification and sizing are,

however, time-consuming. In the last decades, interest in instruments capable of counting, sizing and identifying plankton automatically has increased (Babin *et al.*, 2005; Benfield *et al.*, 2007). At the cost of sacrificing taxonomic detail, the relatively fast analysis of samples obtained by these instruments substantially increases the potential number of samples that can be processed.

These new methods share with traditional methods for plankton enumeration the need to overcome an intrinsic feature of planktonic ecosystems: particle concentration depends both on the type and status of the ecosystem and, for a given status, on the size of the organisms. Smaller organisms are much more abundant than larger organisms, which results in the fact that when randomly picking a certain number of cells, a large proportion is small-sized whereas only a few are large-sized. This inverse relationship between size and abundance can be described through the normalized abundance size spectra (NASS) where the total abundance of cells is binned in size classes on an octave scale, divided by the width of the classes and plotted against size on a log–log scale (Sheldon *et al.*, 1972; Blanco *et al.*, 1994). The question that arises is, what is the minimum number of cells that must be counted to get a reasonable characterization of the larger particles? Techniques developed to enumerate plankton must be capable of analysing this minimum number of cells in a practical time interval.

The Flow Cytometer And Microscope (FlowCAM[®]) is one of such automatic sampling devices. It combines the capabilities of flow cytometry, microscopy and image analysis (Sieracki *et al.*, 1998). The FlowCAM counts and photographs particles moving in a fluid flow. To create this flow, the water sample is drawn into the instrument by means of a peristaltic pump. A digital camera photographs the particles as they pass through a prismatic glass chamber mounted on a cell holder in front of a microscope lens. Three working modes can be used with the FlowCAM: autoimage, fluorescence-triggered and side-scatter-triggered modes. The difference between them is in the way the camera is triggered. In the autoimage mode, photographs are taken at a constant rate regardless of the concentration of particles in the sample. The fluorescence-triggered and side-scatter-triggered modes take photographs only when a particle matching a triggering criterion passes through the chamber. This triggering criterion is the presence of fluorescent particles or the scatter of light due to any kind of particles. In the three working modes, after taking the photograph, the software extracts each particle present in it, a process named image segmentation. It also records the size and shape information for each particle. The user can then select

those particles that match a given criteria, for example a size range or fluorescence level.

The analysis of samples by FlowCAM has been used with several aims, such as the measurement of culture concentration in experimental studies or the estimation of biomass and size–frequency distribution of autotrophic or heterotrophic plankton in natural samples (Table I). Several studies have tested the sizing accuracy of FlowCAM (Sieracki *et al.*, 1998; Sterling *et al.*, 2004; Tauxe *et al.*, 2006) and all have shown that the FlowCAM can properly measure the size of the particles. Some authors have also verified the accuracy of FlowCAM estimates of abundance by comparison against traditional microscopy counts for monocultures, mixed cultures and natural samples (Table I). These comparisons, however, have been done over a limited size range and we lack a formal validation of the capability of the FlowCAM to estimate the size structure of natural plankton communities.

The characteristic flow and particle detection system of the FlowCAM makes it very sensitive to the concentration of particles in the sample being processed. This is supposed to impose important constraints on the size range that is effectively sampled in a given amount of time. The minimum number of cells counted to cover a given size range can saturate the instrument if they are contained in a very small processing volume, whereas it can increase substantially the time of analysis per sample if they are contained in a large processing volume.

The effects of the size structure of planktonic ecosystems on FlowCAM effectiveness for each of the three working modes has not been specifically addressed in the literature. The sensitivity of the FlowCAM to the concentration of particles being analysed is different for each working mode. While the autoimage mode is very sensitive to low concentrations, triggered modes are affected by high concentrations (Sieracki *et al.*, 1998). Consequently, FlowCAM's ability to count natural samples needs to be checked over realistic concentrations and compared with abundance size spectra determined through traditional microscopy. Microscopy counts are usually carried out on Lugol or formaldehyde preserved samples, while with the FlowCAM it is possible to process fresh samples. The effects of preservation and storage, such as cell losses and shrinkage (Menden-Deuer *et al.*, 2001), must be taken into account to make this comparison (Zarauz and Irigoien, 2008).

The general objective of this work is to assess the reliability of FlowCAM to estimate the size structure of natural samples. To this aim: (i) we have estimated the minimum number of cells to be counted to sample effectively a given size range. (ii) According to factory-defined FlowCAM specifications and depending on the total concentration of particles in the processing sample,

Table I: Literature review of FlowCAM applications

Reference	FlowCAM application	Methodological comparison
Sieracki <i>et al.</i> (1998)	Original paper	Comparable results of A and F against LM in mono-cultures
Vaillancourt <i>et al.</i> (2004)	Size frequencies of cultures	
Sterling <i>et al.</i> (2004)	Sizing of aggregates in aquatic sediments	
Lavrentyev <i>et al.</i> (2004)	Abundance of photosynthetic nano-eukaryotes	Comparable results of F against EPM in natural samples (size range: 3–20 μm) but not shown
See <i>et al.</i> (2005)	Abundance of micro-plankton	Comparable results of A against EPM in natural samples (>15 μm); not comparable results against LM
Clough and Strom (2005)	Abundance of <i>Heterosigma akashivo</i> in cultures	
Liu <i>et al.</i> (2005)	Size frequency of micro-plankton	
Tauxe <i>et al.</i> (2006)	Size frequency of flocs	
San Martin <i>et al.</i> (2006a, 2006b)	Size spectra of nano- and micro-plankton	
Koski <i>et al.</i> (2006)	Differentiation of species by fluorescence	
Buskey and Hyatt (2006)	Detection of <i>Karenia brevis</i> in cultures mixtures	Comparable results of A against LM in mono-cultures
Breier and Buskey (2007)	Abundance of phytoplankton	
Zarauz <i>et al.</i> (2007)	Size spectra of nano- and micro-plankton	
Ide <i>et al.</i> (2008)	Abundance of nano- and micro-plankton	Comparable results of F against LM and EPM in natural samples (3–40 μm)
Cotano <i>et al.</i> (2008)	Abundance and size structure of micro-plankton	
Zarauz and Irigoien (2008)	Preservation effect on FlowCAM performance	
Littman <i>et al.</i> (2008)	Abundance of <i>Sybiodium</i> sp. in coral reefs	Not comparable results of F or S against LM in natural samples (size around 10 μm)
Kudela <i>et al.</i> (2008)	Abundance of harmful algae	
Buskey (2008)	Abundance of micro-plankton	
Gribben <i>et al.</i> (2009)	Abundance of micro-plankton	
Zarauz <i>et al.</i> (2009)	Size spectra of nano- and micro-plankton	
Barofsky <i>et al.</i> (2010)	Abundance of protozoa	Comparable results of A against LM in mesocosms (11 m ³ , ~30–100 μm) but not shown
Pedersen <i>et al.</i> (2010)	Size structure and morphology of plankton community	
Tanoi <i>et al.</i> (2010)	Size and image colonies of <i>Botryococcus braunii</i>	
Töpper <i>et al.</i> (2010)	Visual identification of nano-eukaryotes	
Nielsen <i>et al.</i> (2010)	Total and size-fractionated biovolume of phytoplankton	
Reynolds <i>et al.</i> (2010)	Particle size distributions	Not comparable results of S against LISST and CC in monocultures and natural samples (15–30 μm)
Brzezinski <i>et al.</i> (2010)	Nano- and micro-plankton abundance	Not comparable results (mode not specified) against EPM in microcosms (20 L)
Bauman <i>et al.</i> (2010)	Phytoplankton abundance and diversity	

Those works which present results from FlowCAM comparison against other methods are shown: A, F and S stand for autoimage, fluorescence-triggered and side-scatter-triggered FlowCAM working modes. LM, light microscopy; EPM, epifluorescence microscopy; LISST, Laser In Situ Scattering and Transmissometry; CC, coulter counter.

we have converted this minimum number of cells in time of analysis, simulating a FlowCAM-specific relationship between the required time of analysis and the size range effectively sampled. (iii) We have also tested the different counting accuracy of the three FlowCAM working modes, the counting accuracy for samples with a realistic size structure, and whether the FlowCAM is capable of reproducing accurately the size spectrum of a natural sample taking into account the effects of preservation and storage.

METHOD

Effective sampling of the plankton size spectrum

To represent the abundance size spectra of plankton communities, we used the empirical relationship given

by Blanco *et al.* (Blanco *et al.*, 1994). They fitted a linear regression to a collection of NASS from different sources (the so-called superspectrum). We used this average “superspectrum” slope to calculate how many particles must be counted to sample effectively the size spectrum from pico- to meso-plankton. We arbitrarily defined that at least 10 particles should be counted to consider a size class to be representatively sampled. A size range from pico- to meso-plankton is too wide to be covered by a single methodology, so we estimated the number of cells to be counted for any possible size range between a lower and an upper size limit, both between 0.2 and 2000 μm . And finally, considering the mean abundance of cells in the ocean given by Blanco *et al.* (Blanco *et al.*, 1994), i.e. the “superspectrum” intercept, we estimated what sea-water volume needs to be collected to count such a representative number of cells.

Case study using FlowCAM: tradeoffs between time of analysis and size range effectively sampled

For the FlowCAM, the limitations in the volume analysed and the maximum concentration of particles impose important constraints on the number of cells, and thus the size range, that is effectively sampled in a given amount of time. In order to better understand these limitations, we conducted a series of simulations to understand the tradeoffs between time of analysis and size range that can be effectively sampled.

We calculated the amount of time necessary to obtain a representative count for a given size range and a given total concentration of particles in the sample within this size range. This representativeness will vary with the size of the particles considered. For the smallest particles, which are relatively more abundant, it will be possible to obtain a representative count in a lower amount of time than for large particles, which are scarcer. We used the average “superspectrum” (Blanco *et al.*, 1994) to simulate the size range that can be effectively sampled by taking into account the total concentration of particles, the size-spectrum slope and time of analysis. This would vary for the size range chosen and for each operating mode.

FlowCAM specifications

The FlowCAM used in this work belongs to the series VS4 and was purchased in 2008. FlowCAMs are provided with several microscope lenses. Each lens has its respective flow chamber and the focal depth of each lens is sufficient to cover the depth of the flow chamber (Sieracki *et al.*, 1998). The depth of the flow chamber sets the upper limit for the size of the particles that can be analysed, while the lower limit is determined by the smaller size resolved by the magnification. In this study, we have examined the performance at $\times 200$, $\times 100$ and $\times 40$ magnifications which have an optimum, factory defined, particle size range of 3–50, 15–100 and 30–300 μm , respectively (Table II).

The digital camera has a resolution of 1024×768 pixels. For each magnification, a size calibration constant gives the actual dimensions of the camera field-of-view. This field-of-view is not enough to cover the whole width of the flow chamber (at least for the FlowCAM model we have used). The relation between the total width of the flow chamber and the width of the field-of-view gives the percentage of the sample that is analysed (Pi). The volume sampled in one photograph (Vi) is a prism of dimensions: field-of-view width \times field-of-view height \times flow-chamber depth.

Table II: General characteristics of FlowCAM, setup for each working mode (autoimage, fluorescence- and side-scatter-triggered modes) and pre-treatment of the samples for the three magnifications ($200\times$, $100\times$ and $40\times$).

	Magnification		
	$\times 200$	$\times 100$	$\times 40$
General characteristics			
Flow chamber depth (μm)	50	100	300
Lower limit (μm)	3	15	30
Flow chamber width (μm)	1000	2000	3000
Calibration constant ($\mu\text{m pixel}^{-1}$)	0.2953	0.6151	1.6386
Field-of-view width (μm)	302.39	629.86	1677.93
Field-of-view height (μm)	226.79	472.4	1258.44
Pi: % sample view	30.24	31.49	55.93
Vi: volume per photo (mL)	3.43×10^{-6}	2.98×10^{-5}	6.33×10^{-4}
Max flow rate (mL min^{-1})	0.053	0.53	1.20
Min flow rate (mL min^{-1})	0.012	0.12	0.25
Max frame rate (photos s^{-1})	11	11	11
Autoimage			
Number of photos	20 000	20 000	10 000
Time of analysis (min)	30	30	33
Frame rate (photos s^{-1})	11	11	5
Flow rate (mL min^{-1})	0.05	0.4	0.5
Triggered modes			
Flow rate (mL min^{-1})	0.04	0.12–0.4	0.4
Time (min)	25	25	25
Pre-treatment			
Filtration (μm)	40	100	200
Concentration (μm)	–	15	15

The final net volume analysed (V_n) depends on the working mode. In the case of autoimage, photographs are taken at a constant frame rate. The frame rate must be low enough to avoid overlapping photos, consequently only a portion of the whole volume passing in front of the camera is photographed. The final V_n in autoimage is therefore calculated as the volume sampled in one photograph (V_i) times the number of photographs taken (frame rate \times time of analysis). Both triggered modes take a photograph of every particle matching the triggering criterion, so V_n is the whole volume passing in front of the camera and is equal to the volume pumped through the instrument (flow rate \times time of analysis) times the percentage of the sample analysed (Pi). In summary, for a given flow rate, the autoimage mode will analyse a smaller volume than the trigger modes.

The maximum concentration of particles in the sample that the instrument can handle also differs in autoimage and triggered modes. The limitation in autoimage is defined by the capability of the software to discriminate individual particles in the photographs (Sieracki *et al.*, 1998) and of the fluidics system to

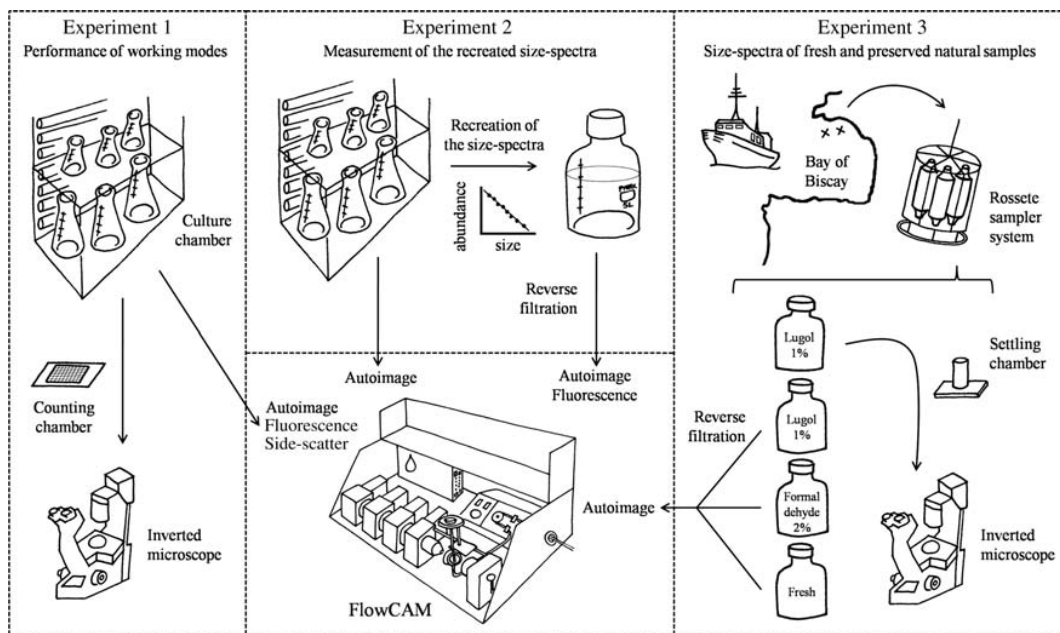


Fig. 1. Schematic representation of the set of experiments carried out to assess the FlowCAM reliability.

maintain all the particles homogeneously embedded in the fluid, avoiding obstructions of the flow chamber or aggregations of particles. For both triggered modes, the limitation is set by the fact that every particle within the size range covered by each lens/flow-chamber combination is capable of triggering the camera but only the particle that caused the trigger should be present in each photograph. In summary, the maximum concentration in triggered modes must be smaller than in the autoimage mode.

Experiments

A set of experiments have been carried out to tackle our objectives and validate the results arising from the simulations. In Experiment 1, we tested the performance of the three FlowCAM working modes using monocultures and latex-bead suspensions at different concentrations. Experiment 2 aimed to check if the FlowCAM is capable of counting accurately a community with a realistic size structure, so we have recreated size spectra with cultures of known concentration and then counted them with the FlowCAM in autoimage and in fluorescence-triggered modes. Finally, in Experiment 3, we compared, for several natural samples, the size spectra determined with FlowCAM, both on fresh and preserved samples, with those obtained using traditional microscopy on the preserved samples (Fig. 1).

General experimental procedures

All samples processed with FlowCAM were pre-filtered through a mesh smaller than the depth of the flow chamber in order to avoid obstructions. Dense samples were diluted with culture media (L1, 32 psu) in Experiment 1 or with filtered sea-water ($0.2 \mu\text{m}$, 32 psu) in Experiment 2. The samples analysed at $100\times$ and $40\times$ magnifications were concentrated by reverse filtration (Dodson and Thomas, 1978) with a $15 \mu\text{m}$ mesh (Table II). Although this concentration procedure resulted in some samples being analysed beyond the FlowCAM specification limits, this was done in order to validate the results arising from the simulations. The total number of cells counted was divided by the V_n and multiplied by the dilution factor to determine the cell concentration in the initial sample.

Experiment 1: performance of FlowCAM working modes

Seven phytoplankton cultures were used to test the performance of each of the three working modes. The cultures were obtained from the Toxic Phytoplankton Culture Collection from the Centro Oceanográfico de Vigo (Instituto Español de Oceanografía) and are summarized in Fig. 2 where their images, size and combination magnification/flow chamber used to count them are shown.

To determine the cell concentration in the cultures, an aliquot of 4 mL was fixed with $20 \mu\text{L}$ of Lugol solution, homogenized and then 1 mL was placed in a Sedgwick-Rafter counting chamber and counted under

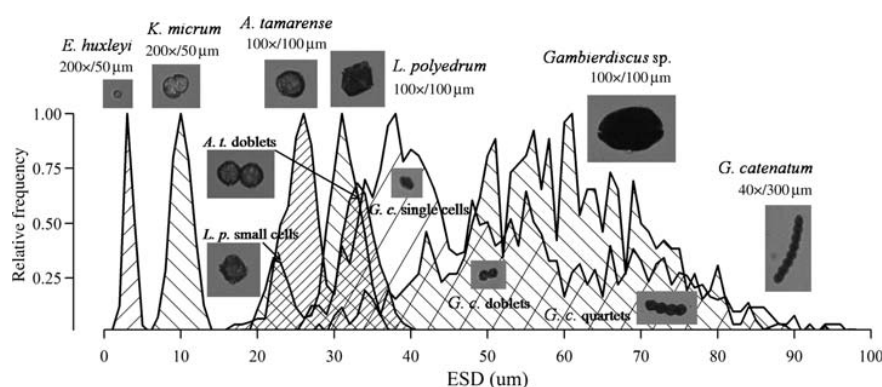


Fig. 2. Relative size frequencies of the seven cultures used in Experiment 1. Only six of them were used to reproduce the min, average- and max-NASS in Experiment 2 (see Table III).

Table III: Abundance (cells L⁻¹) predicted from the empirical NASS given by Blanco et al. (Blanco et al., 1994) for each biovolume class

Bio-volume class (μm ³)	ESD (μm)	Abundance (Blanco et al., 1994)	Species	Abundance min-NASS	Abundance average-NASS	Abundance max-NASS
16	3	2.33 × 10 ⁵				
32	4	1.19 × 10 ⁵	<i>E. huxleyi</i>	4.13 × 10 ⁴	4.13 × 10 ⁵	4.13 × 10 ⁶
64	5	6.06 × 10 ⁴				
128	6	3.09 × 10 ⁴				
256	8	1.57 × 10 ⁴	<i>K. micrum</i>	5.47 × 10 ³	5.47 × 10 ⁴	5.47 × 10 ⁵
512	10	8.03 × 10 ³				
1024	13	4.09 × 10 ³				
2048	16	2.09 × 10 ³	<i>A. tamarensis</i>	724	7.24 × 10 ³	7.24 × 10 ⁴
4096	20	1.06 × 10 ³				
8192	25	542				
16384	32	276	<i>L. polyedrum</i>	96	960	9.60 × 10 ³
32768	40	141				
65536	50	71.8				
131072	63	36.6	<i>Gambierdiscus</i> sp.	13	127	1.27 × 10 ³
262144	79	18.7				
524288	100	9.52				
1048576	126	4.85	<i>G. catenatum</i>	2	17	168
2097152	159	2.47				

The biovolume class is defined by its lower limit, from which the corresponding ESD is also shown. The cultured species used to recreate the size spectra are shown together with their abundances (cells L⁻¹) in each of the three reference size spectra: min-, average- and max-NASS.

a NIKON inverted microscope. Each culture was then diluted and counted again under the inverted microscope following the procedure previously described. The difference between the desired concentration and the actual one was calculated as a manipulation error and was on average 6%.

Each sample was processed with the FlowCAM in triplicate with the specifications shown in Table II. Samples counted with the 100× and the 40× magnifications were analysed in the three working modes. Samples counted with the 200× magnification were analysed only in autoimage and in the fluorescence-triggered mode because the side-scatter detection was unreliable at this magnification in the FlowCAM instrument used. An additional series of experiments with

latex beads were conducted to establish the limitations of the side-scatter-triggered mode (see Supplementary Data, Appendix A).

The results were compared to the microscopy counts with a *t*-test (Zar, 1999). Size information from this experiment was used to determine the size–frequency of each culture (Fig. 2) in order to decide which cultures to use in the recreation of the size spectra (Experiment 2).

Experiment 2: measurement of the recreated size spectra

With the regression line given by Blanco et al. (Blanco et al., 1994) (normalized abundance = 6.538 – 1.972 × biovolume), we predicted the abundances in each biovolume class for particles between 3 and 200 μm (Table III). The intercept of this regression was

increased and decreased one unit to obtain an upper and a lower limit of abundance, respectively, which means a variation of two orders of magnitude in abundance and encompasses most variability in the data compiled by Blanco *et al.* (Blanco *et al.*, 1994). These three reference size spectra are referred to as min-NASS, average-NASS and max-NASS.

To recreate these reference NASS, we combined six cultures from Experiment 1. *Prorocentrum balticum* was excluded because it was difficult to distinguish from *Karlodinium micrum* by size or morphology (Fig. 2). Each culture represented three biovolume-classes from Blanco *et al.* (Blanco *et al.*, 1994) and the desired concentration was calculated as the sum of these three classes (Table III). The six cultures were kept close to the optimal concentration tested in Experiment 1 in their respective culture flasks growing in L1 culture media with controlled photo-period (14:10 light–dark), irradiance ($\sim 90 \mu\text{mol quanta m}^{-2} \text{s}^{-1}$) and temperature ($24 \pm 1^\circ\text{C}$ for *Gambierdiscus* sp. and $18 \pm 1^\circ\text{C}$ for the rest). Each day, the cultures were counted with the FlowCAM in the autoimage mode taking 10 000 photos with $200\times$ and $100\times$ magnifications and 5000 photos with $40\times$ magnification since our results from Experiment 1 showed that this procedure resulted in reliable counts. Once the six concentrations were known, the culture volumes needed to recreate 5 L of each of the three reference size spectra were calculated. Each day of the experiment, one of the reference size spectra was recreated in filtered sea-water.

Three replicates of each sample were analysed (Table II). Each replicate was processed in autoimage and in the fluorescence-triggered mode with the $200\times$ and $100\times$ magnifications but only in autoimage with the $40\times$ magnification due to malfunction of the fluorescence-triggered mode at this magnification in the FlowCAM used. Cells from each species were separated by visual inspection of the images taken. Only bins with at least 10 counted particles in two of the replicates were included. The parameters of the regression line fitted to the measured NASS were compared with the slope and intercepts of the three reference NASS using a *t*-test (Zar, 1999).

Experiment 3: size spectra of fresh and preserved natural samples

Natural samples were taken with a rosette sampler system at a coastal (46.4219°N , 1.8477°W , 25 m) and a mid-shelf station (45.7943°N , 3.3714°W , 142 m) in the Bay of Biscay. At each site, three replicates, each using a separate Niskin bottle, were taken at the depth of the chlorophyll maximum, 12 and 30 m, respectively.

For each replicate, four 1-L samples were taken. One was kept fresh, stored in the dark and analysed with the FlowCAM in the autoimage mode within the next 12 h. Another was preserved with Lugol solution 1% final concentration and used to count and size microplankton under the inverted microscope. Two litres were preserved with Lugol 1% and formaldehyde 2%, respectively, and analysed with the FlowCAM in the autoimage mode within the next month.

For analysis under the microscope, 25 mL for the coastal and 100 mL for the mid-shelf station were dispensed into Utermöhl settling chambers and the phytoplankton cells were allowed to settle for 24 and 72 h, respectively (Utermöhl, 1958). Chambers were imaged at $100\times$ (two stripes) and $200\times$ (one stripe) using a LEICA inverted microscope equipped with a digital photo-camera. Length and width for each individual organism in the images were measured. The projected area of each particle was calculated based on its shape (rectangle or ellipse) and converted to an equivalent spherical diameter (ESD) comparable with that provided by FlowCAM. The images provided by the FlowCAM were manually classified in order to eliminate non-valid images (detritus, bubbles . . .) in both fresh and preserved samples. The V_n and total number of cells sized with each methodology are summarized in Table IV.

A *t*-test on the NASS calculated for Lugol-preserved samples was applied to compare the size spectra obtained with FlowCAM and traditional microscopy. To compare the effects of preservation, a one-way ANOVA and a Tukey test (Zar, 1999) were applied to the NASS calculated for fresh, and Lugol and formaldehyde-preserved samples analysed with FlowCAM.

Table IV: Net sampled volume (mL) and number of cells counted and sized (between 5 and 20 μm for $200\times$ magnification and 20–100 for $100\times$ magnification) with FlowCAM and microscopy for the two natural samples

Sample	Magnification	Volume FlowCAM	Volume microscope	Sized cells FlowCAM	Sized cells microscope
Mid-shelf	$\times 100$	23.8	10.28	33	16
	$\times 200$	0.14	2.17	11	104
Coastal	$\times 100$	9.84	2.57	750	384
	$\times 200$	0.08	0.54	39	243

RESULTS

What is the minimum number of counted cells needed to have a good representation of a given size range?

Figure 3 illustrates the total number of cells that must be counted to cover a given size range and how this number translates in sea-water collected volume. The total number of cells counted is independent of the total concentration of cells in the sample, and only depends on the relative abundance of each size class, i.e. the spectrum slope. Figure 3A shows the total number of cells that must be counted to cover the whole size spectrum from pico-plankton up to an upper limit. For instance, to sample effectively micro-plankton, we must count 6.24×10^9 cells between 0.2 and 200 μm .

However, to consider the total number of cells from pico-plankton to the size object of study seems not very practical. It is more useful to calculate a minimum number of cells within a downward-limited size range. Figure 3B shows the number of counted cells needed to cover a specific size range defined by a lower and an upper limit. Following the example with the micro-plankton, the total number of counted cells between 20 and 200 μm must be 8760 cells within this size range. Note that this number is not the simple difference between the required number of cells for sampling up to 20 μm and the cells for sampling up to 200 μm , but the cells needed for sampling up to 200 μm minus all cells smaller than 20 μm included in this minimum number and correspond to the dashed area in Fig. 3A.

Figure 3C translates the variable counted cells into collected volume considering the mean abundance of cells given by Blanco, i.e. the spectrum intercept. In our example of sampling micro-plankton, the required volume is 4.04 L.

Case study using FlowCAM: tradeoffs between time of analysis and size range effectively sampled

Figure 4 illustrates the results of the simulation obtained for the $\times 100$ magnification and the factory defined size range of 15–100 μm (similar simulations for $200\times/3-50\ \mu\text{m}$ and $40\times/30-300\ \mu\text{m}$ are shown in Supplementary Data, Figs S1 and S2 and Appendix B). The upper panels (Fig. 4A–C) show how as the concentration of particles increases, the time required to sample effectively decreases. Figure 4D–F shows examples of how these graphs should be interpreted. Taking into account that in natural samples the total concentration of particles in the size range of 15–100 μm is 8 cells per mL according to the “superspectrum” of Blanco *et al.* (Blanco *et al.*, 1994), the time required to sample effectively the whole factory defined size range would be 454 h in the autoimage mode (Fig. 4D) and 54 h in the triggered modes (Fig. 4E). This is achieved at the maximum frame rate of 11 frames per second in the autoimage mode and the maximum flow rate of $0.53\ \text{mL}\ \text{min}^{-1}$ in the triggered modes. These graphs are achieved by drawing vertical lines in Fig. 4A and B or C at this concentration of 8 cells per mL and plotting the intersection of this line with the isoclines of upper size range sampled effectively versus time.

In the triggered modes, there is a limitation in the number of events per second that the instrument can handle: 2 and 0.5 events per second in the fluorescence (Sieracki *et al.*, 1998) and side scatter triggered modes (Brown, 2010), respectively (see Supplementary Data, Appendix A). Thus, when the concentration in a sample is so high that this limit is surpassed at the maximum flow rate (above 226 and 57 cells mL^{-1} for fluorescence and side-scatter-triggered modes, respectively), the flow

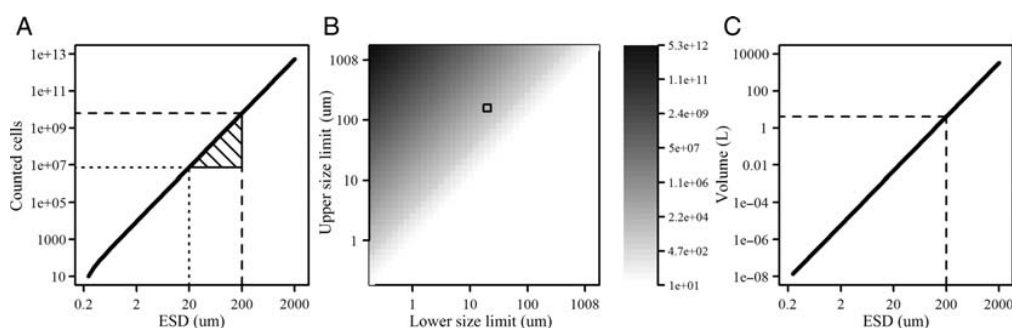


Fig. 3. Minimum number of counted cells needed to have a good representation of a given size range. **(A)** Total number of cells to be counted to sample effectively the size range from pico-plankton up to an upper limit (μm); **(B)** minimum number of cells to be counted to sample effectively a size range defined by a lower and a upper limit (μm); and **(C)** minimum sea-water volume needed to be collected to sample up to an upper limit (μm). Dotted line (A) indicates an example for the sampling up to nano-plankton (0.2–20 μm). Dashed lines (A and C) indicate an example for the sampling up to micro-plankton (0.2–200 μm) and the dashed area (A) and the little square (B) indicates an example for the sampling of micro-plankton (20–200 μm).

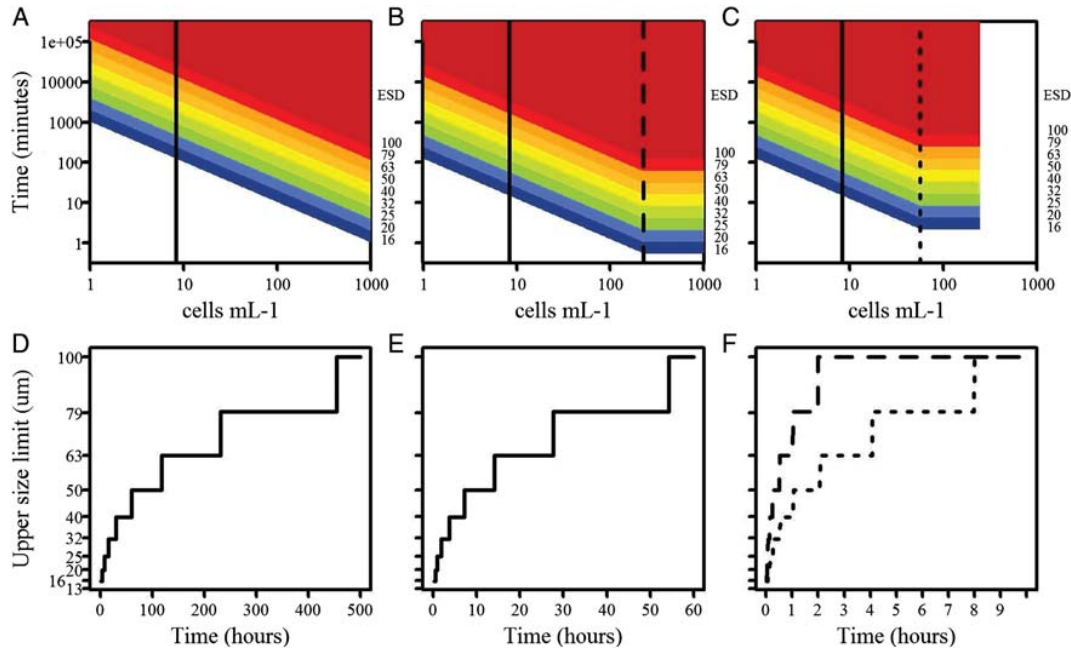


Fig. 4. Simulation for the combination magnification/flow chamber 100 × 100 μm. The upper panels show the upper size limit sampled effectively given the total concentration of particles in the size range of 15–100 μm and the time of analysis for the (A) autoimage mode, (B) fluorescence-triggered mode and (C) side-scatter-triggered mode. The correspondence of each shaded area with the ESD (μm) is indicated in the right axis of each panel. Lower panels show examples of upper size limit sampled versus time for (D and E) a mean natural sample concentration of 8 cells mL⁻¹, calculated according to Blanco *et al.* (Blanco *et al.*, 1994) and indicated as vertical lines in (A)–(C), for (D) autoimage and (E) triggered modes. (F) shows the same relationship for the concentrations at which the saturation of the triggered modes is reached, indicated as vertical dashed and dotted lines in (B) and (C), respectively.

rate should be reduced. So at concentrations higher than these thresholds, there are no means to reduce the amount of time necessary to sample effectively because the possible events per second is set. This results in the fact that above these threshold concentrations the isolines in Fig. 4B and C are horizontal and the time required to sample effectively is constant as represented in Fig. 4F: 2 h in fluorescence-triggered and 8 h in side-scatter-triggered modes. However, the flow rate cannot be decreased infinitely so the cell density at which the events per second limit is reached at minimum flow rate sets an overall upper limit for the densities each trigger mode can count accurately (1000 and 250 cells mL⁻¹ for fluorescence- and side-scatter-triggered modes, respectively).

Obviously 454 and 54 h is unacceptably long for a sample analysis, which explains the need for concentrating natural samples to obtain reliable estimates of the size spectra. Considering 30 min to be a reasonable amount of time for processing each sample, in the side-scatter mode, the maximum total number of particles that can be analysed in 30 min is 279 (i.e. 30 events per minute times $\Pi = 0.31$). This implies that in 30 min only the size range between 15 and 32 μm can be sampled, even if the

sample is concentrated. In the fluorescence mode, this maximum total number of particles that can be analysed in 30 min is 1116 (i.e. 120 events per minute times $\Pi = 0.31$). So in 30 min, it is possible to cover effectively the range between 15 and 50 μm.

Experiment 1: performance of each working mode

The performance in the autoimage mode was good (Fig. 5). The slope of the relationship between autoimage and microscopy counts was 1.038 ± 0.045 ($R^2 = 0.9648$, P -value < 0.0001, $n = 21$), not significantly different to the 1:1 line (P -value = 0.4163). The average percentage error, calculated as the absolute difference between FlowCAM and microscopy counts relative to the microscopy counts, was 14.8%. As an index of the reproducibility of the counts, we calculated the coefficient of variation within the three replicates for each culture. The average coefficient of variation in the autoimage mode was 12.4%.

In the fluorescence-triggered mode, the relationship had a slope of 0.905 ± 0.030 ($R^2 = 0.9824$, P -value < 0.0001, $n = 18$) not statistically different from the 1:1

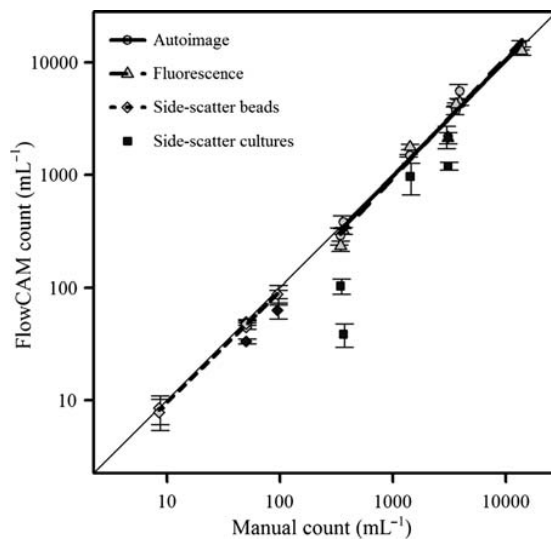


Fig. 5. FlowCAM counting accuracy. Comparison between microscopy and FlowCAM counts for seven different phytoplankton cultures in the three FlowCAM working modes and three latex beads solutions in the side-scatter-triggered mode. Solid thin line shows the 1:1 relationship. The dark triangle and dark rectangles represent points not included in the comparison because they did not meet the factory defined settings.

relationship (P -value = 0.0528). The average percentage error in the fluorescence-triggered mode was 18.1% and the average coefficient of variation was 6.6%. One of the samples had a concentration that was too high for this mode and was analysed at an events per second rate above FlowCAM specifications. As expected, this point fell below the 1:1 line and if included in the calculations caused the slope to be statistically different from 1 (P -value = 0.0231, $n = 21$).

In the side-scatter-triggered mode, the relationship considering only those samples processed under 0.5 events per second (experiment using bead solutions, see Supplementary Data), within the factory specifications for this triggered mode, had a slope of 0.9243 ± 0.044 ($R^2 = 0.9579$, P -value < 0.0001, $n = 21$) marginally statistically different to the 1:1 relationship (P -value = 0.010). The percentage error was on average of 5.6% and an average coefficient of variation of 14.8%. The performance with the other samples exceeding the events per second limitation was poor, with a percentage of error on average of 53.0%.

Experiment 2: measurement of the recreated size spectra

FlowCAM sizing capability is a useful tool to analyse the size–frequency of the samples and we have used it

to decide which cultures to include in our simulated size spectra (Fig. 2). The size–frequency distributions of *Emiliana huxleyi*, *K. micrum* and *Gambierdiscus* sp. were unimodal, *Alexandrium tamarense* and *Lygulodinium polyedrum* distributions were bimodal, caused by the presence of doublets and two separate sizes, respectively, and *Gymnodinium catenatum* shows three modal peaks given its appearance in single cells, doublets, quartets and even octets, a consequence of its division mechanism. The size distributions were overlapped which forced the experimental design to use each culture to represent one bin of the recreated size spectra and not to use the biovolume of the particles to build the NASS (Table III).

To cover the size range of 3–200 μm , each of the three recreated NASS was analysed with the three magnifications. Those bins with less than 10 counted particles because of the relative low volume analysed result in curvature of the spectrum and were not included as they could cause potential error in the calculation of the parameters. For instance, bin 6 represented by *G. catenatum* was not properly sampled in any of the three size spectra due to the low volume analysed.

According to this representativeness criterion, the bins properly sampled in the autoimage mode were: 1 (*E. huxleyi*), 3 (*A. tamarense*) and 4 (*L. polyedrum*) for the min-NASS; 1, 3, 4 and 5 (*Gambierdiscus* sp.) for the average-NASS; and from 1 to 5 for the max-NASS

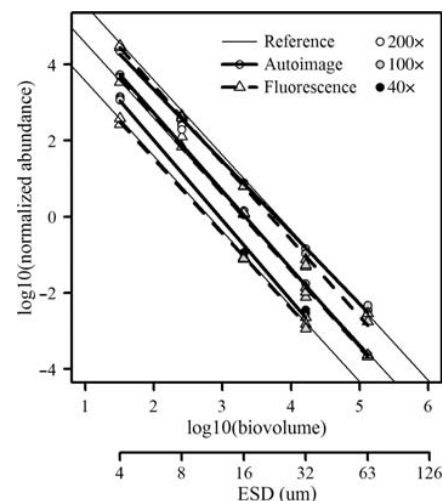


Fig. 6. Measurement of the recreated size spectra. NASS obtained with FlowCAM in the autoimage (solid line) and fluorescence-triggered modes (dashed line) sampling the three recreated spectra, min-, average- and max-NASS (solid thin lines). Each sample was analysed as the combination of three subsamples: 200 \times (white), 100 \times (gray) and 40 \times (black). In the x-axis, in addition to \log_{10} (biovolume), the geometric mean of the ESD covered by each sampled bin is shown.

(Fig. 6). Bins number 2 (*K. micrum*) (the larger size class analysed at 200× magnification) and 5 (the larger size class analysed at 100× magnification) were not adequately sampled because the time of analysis (net volume analysed) was too short (low) to obtain representative counts, in accordance with the simulation experiments. Taking into account only those bins that were representatively sampled, the autoimage mode can reproduce accurately the three reference NASS (Fig. 6; min-NASS: P -value = 0.0606, n = 9; average-NASS: P -value = 0.7055, n = 12; max-NASS: P -value = 0.2113, n = 15).

In the fluorescence-triggered mode, the bins that were properly sampled were 1, 3 and 4 for the min-NASS and from 1 to 5 for the average-NASS (Fig. 6). Taking into account these bins, the fluorescence-triggered mode can reproduce accurately the reference min- and average-NASS (P -value = 0.1946, n = 8; P -value = 0.3529, n = 14). However, for the max-NASS, which was analysed at a trigger rate higher than 2 events per second, the measured size spectrum was significantly different from the reference NASS (P -value < 0.0001, n = 14).

Experiment 3: size spectra of fresh and preserved natural samples

When analysing fresh and preserved samples (Lugol or formaldehyde) with FlowCAM in the autoimage mode, the spectra were significantly different (mid-shelf station:

P -value < 0.001, n = 44, Fig. 7B–D; coastal station: P -value < 0.001, n = 101, Fig. 7F–H). The size-spectrum slope was higher in the fresh samples compared to the preserved samples due to an underestimation of the abundance of small cells and an overestimation of the abundance of the medium-sized particles in the preserved samples. The variance of the NASS bins was larger in the preserved samples than in the fresh samples.

When comparing FlowCAM and microscopy on preserved samples, using only those size bins sampled by both methods, there were no significant differences in the size-spectrum slopes in the mid-shelf sample (P -value = 0.111, n = 31, Fig. 7A and C), but significant differences in the coastal one (P -value < 0.001, n = 81, Fig. 7E and G). It must be taken into account, however, that the size ranges covered by each method do not overlap completely. The lower limit of detection was 3 μm for FlowCAM and 5 μm for the microscope technique. The upper limit was determined by the net volume sampled (Table IV), 32 μm in the mid-shelf sample and 100 μm in the coastal station. In the coastal samples, although the sampled volume was representative (Table IV), the FlowCAM did not sample the last size class (Fig. 7F–H).

Another difference between microscopy and FlowCAM methods is that the former can sample the size spectra continuously from the lower to the upper limit, while the later does not sample several bins in the middle of the size range, one in the coastal sample and

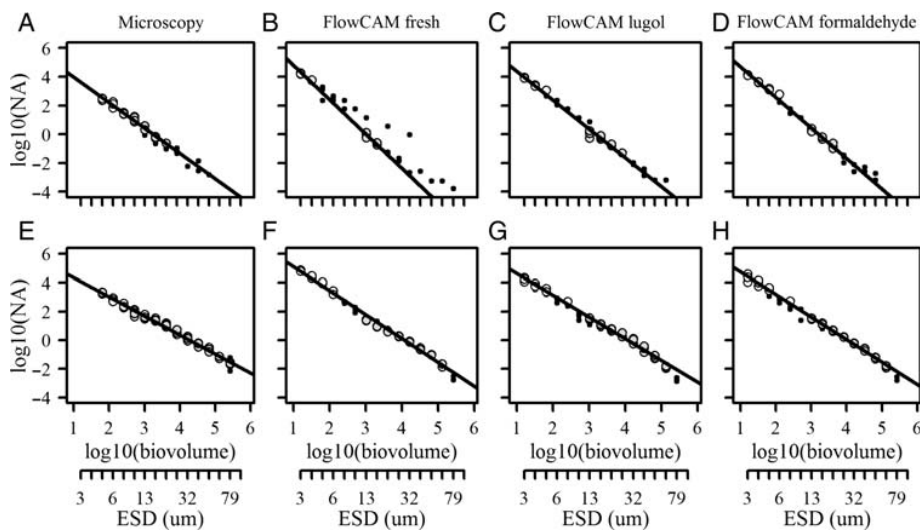


Fig. 7. NASS obtained with microscopy and FlowCAM with different preservation techniques. The upper panels (A–D) correspond to the mid-shelf sample and the lower panels (E–H) to the coastal sample. The sample analysed with microscopy was preserved only with lugol solution, whereas the fresh sample and two preservation treatments (lugol and formaldehyde) were examined with FlowCAM. Each sample was analysed as the combination of two subsamples: 200× (white) and 100× (grey). In the x-axis, in addition to log₁₀(biovolume), the min ESD of each sampled bin is shown. Size bins with less than 10 cells imaged are included in the representation (●) but not in the regression analysis.

three in the mid-shelf sample. The un-sampled bins are due to the low volume analysed with the 200 \times (Table IV). As a consequence, there were few bins in common to compare the size spectra obtained with microscopy and FlowCAM in the mid-shelf sample reducing the power of the statistical test. From the simulations, it is possible to calculate that the additional time necessary to fill the gap with the 200 \times would be 911 min in the mid-shelf sample and 45 min in the coastal one. The time of analysis in the side-scatter-triggered mode would have been 139 and 22 min, respectively.

DISCUSSION

We have described the scenario in which any plankton sampling methodology must operate, in terms of counted cells and sampled volume. We have then tested the capacity of FlowCAM to work within these limits describing its specific tradeoff between time of analysis and size range effectively sampled.

The main concern when using automatic sampling devices is whether they provide reliable results. For this reason, we have tested the accuracy of FlowCAM in estimating the size structure of natural samples against the results obtained with light microscopy, the traditional method for plankton enumeration and sizing. As long as the factory-defined limitations are considered, our results show that the three working modes can provide accurate abundance estimates. Phytoplankton cultures or latex bead suspensions with concentrations within the factory-defined limits were measured accurately, whereas the suspensions with concentrations beyond the limits were not (Fig. 5). Some studies have reported poor performance of FlowCAM compared with other methodologies (Table I), but it appears that they operate the FlowCAM outside the factory-defined limits (Reynolds *et al.*, 2010).

When the purpose is to reproduce the size spectra (Fig. 6), it is necessary to count enough cells in each size class. We have defined an arbitrary value of 10 sampled cells as the minimum to consider a size class to be effectively sampled. We consider it important to establish this representativeness criterion because a size bin sampled only with a couple of cells can potentially bias the size-spectrum estimation. Our simulations to calculate the size range of particles effectively sampled by each magnification/flow-chamber combination are based on factory-defined parameters (Table II), so they can be reproduced before experimental work to identify the required processing time and sample concentration protocol.

The first point that arises from the simulation is the need to analyse the same sample using several

magnification/flow-chamber combinations to cover the complete size spectra. The second point is the necessity to concentrate natural samples in some of the magnification/flow-chamber combinations, because the time of analysis required to estimate the complete size spectra is too high for routine work. The need to concentrate the sample also depends on the status of the ecosystem. For example in Fig. 7, at the coastal site, the 3–15 μm size range is effectively sampled by the $\times 200$ magnification without the need for concentration, but in the mid-shelf sample concentration was required. For micro-plankton, the sample will always require concentration due to their relative low concentration in natural systems.

The degree of sample concentration required will depend on the chosen working mode. In autoimage, the sample can be concentrated up to the limitations imposed by the software and the fluidics (i.e. segmentation of the images and homogeneous distribution of particles in the fluid). These limits are sufficiently high to permit the concentration of natural samples and their accurate analysis in less than 30 min.

For triggered modes, in contrast, the number of events per second sets an upper limit to the concentration of the samples. This maximum trigger rate in the fluorescence-triggered mode is sufficiently high to measure the size structure of most natural samples in a reasonable amount of time. In the side-scatter-triggered mode, in contrast, the trigger rate is so low that, even concentrating the sample to the limit, the processing time is too high; consequently, it is not the appropriate working mode to estimate the size structure of natural samples. The problem with the need to concentrate the sample, in addition to possible artefacts and damage to the cells, is that it is necessary to know beforehand the natural cell densities to determine the degree of sample concentration required (maybe using proxies such as fluorescence or transmittance from automatic sensors).

The discrete sampling rate in autoimage requires that the cell distribution must be homogeneous to obtain reliable results, so it is very important to stir carefully the sample before and during the analysis especially if it contains large cells. Also, many particles are cut in the images as they can be placed in any of the four borders of the photograph and a too high concentration can increase the probability of coincident counts (Buskey and Hyatt, 2006). In the fluorescence-triggered mode, the counting is not as dependent on the homogeneity of the sample as in autoimage. Coincidence counting is unusual if the factory-defined limits regarding cell density are followed. Also, particles are captured preferably in the middle of the field-of-view so they can only be cut in the left and right borders of the image.

Depending on the study aim, it might be also necessary to analyse several subsamples each with a different working mode. For instance, if the aim is to distinguish autotrophic from heterotrophic organisms, and since autoimage and fluorescence-triggered modes cannot work together given their different designs, the only option would be to activate side-scatter and fluorescence together to count every particle differentiating the fluorescent ones. However, then the sample has to be processed within the strict analysing time limitations imposed by the side-scatter mode (Fig. 4F). Besides, some heterotrophic organism can have a fluorescence signal due to gut contents. In summary, to estimate the size spectrum of a natural sample, differentiating autotrophic and heterotrophic individuals could take a prohibitive amount of time, if the experimental protocol is not planned very carefully and taking the limitations of the instrument into account. Another option is to use only autoimage mode and try to classify the FlowCAM images in taxonomic or functional groups. This classification can be done *a posteriori* through visual inspection of the images, but it is time-consuming. Alternatively, the images can be classified automatically using classification algorithms (Blaschko *et al.*, 2005).

If FlowCAM can reproduce accurately the size structure of natural samples, at least working in autoimage and fluorescence-trigger modes, the next question is whether it can work with preserved samples. Our results show that there are not major differences between the size spectra obtained with FlowCAM and with light microscopy for preserved samples. It must be noted, however, that the size range each method can sample effectively is different. To cover the size range between 3 and 100 μm , both methods need to combine at least two magnifications. The lower size limit of the $\times 100$ magnification in FlowCAM is 15 μm which requires that the $\times 200$ magnification samples from 3 to 15 μm . In the microscope, the lower limit of the $\times 100$ magnification is around 10 μm and the volume sampled with the $\times 200$ is larger than in the FlowCAM (Table IV), so it is easier to sample the complete size spectrum with the traditional microscopy method.

The FlowCAM tends to underestimate the cell abundance in the size classes close to the upper size limit of the magnification/flow chamber. This underestimation of large cells can be caused by obstruction of the flow chamber. Cell clumping was not a problem with the cultures in Experiments 1 and 2 because cells are all elliptical without spines or chaetae, but it can be a problem in natural samples, where clumped cells can cause underestimation of cell abundance or even obstruction of the flow chamber. This effect is greater in preserved samples where cells tend to form aggregates

larger than the flow-chamber depth (Zarauz and Irigoien, 2008).

Therefore, and considering all their limitations, the size-spectrum estimates obtained with FlowCAM can be as valid as the estimates obtained with microscope, but the time spent with each methodology is very different. FlowCAM can be slow, as we have shown previously, and can take a couple of hours to estimate the size spectrum of a sample over a wide size range, but to do exactly the same task, that is, count and size every particle, with a microscope can take more than a day. If the aim of the study is not size structure but simple enumeration, the microscope can be competitive in terms of time with FlowCAM (Littman *et al.*, 2008).

The size structure of preserved samples can be different to the size spectra of fresh samples (Zarauz and Irigoien, 2008). There are two effects causing this change, the different preservation response of organisms to fixation and the different effect of shrinkage (Leakey *et al.*, 1994; Menden-Deuer *et al.*, 2001). The decrease in the intercept and slope suggests a degradation of small cells due to a lack of rigid structures or a strong shrinkage what might cause the size of these particles to fall below the detection limit (James, 1991). The decrease in the slope can also be due to a disintegration of larger cells (Zarauz and Irigoien, 2008). This implies that the results from size-structure studies based on preserved samples, although correctly estimated, must be considered with caution, because they might not be showing the actual size structure of the community. If the actual size structure of the community can only be described with fresh samples, automatic sampling methods like FlowCAM are not only a faster alternative to traditional methods but the only choice. To be used in routine work, it is necessary that the device is highly robust or, at least, that there is a low incidence of mechanical failure, which, from our experience, may not always be the case with the present design of FlowCAM. For instance, during our experiments, we have experienced malfunction in the fluorescence and side-scatter detectors that have required shipment of the instrument back to the manufacturer for fixing. This has been the case with three FlowCAM devices our lab has worked with.

SUMMARY AND CONCLUSIONS

The inverse relationship between size and abundance in nature determines the sampling techniques used to estimate the size structure of the planktonic community. Automatic sampling devices must be capable of analysing a sufficient number of cells within a size range to ensure the representation of the largest/scarcest particles

of the range. We provide an analysis which allows the estimation of the volume or total number of particles that have to be counted to obtain a representative sample of the size spectrum. Some automatic devices, like the FlowCAM, have characteristic flow and particle detection systems which impose limits to the concentration of the samples to be processed leading to important constraints on the size range that can be effectively sampled in a given amount of time. Thus, the analysis of the size structure of natural samples with FlowCAM requires a planned pre-processing of the samples.

The side-scatter-triggered mode can count accurately a sparse solution of particles, but it has an analysis rate that is too low to estimate the size structure of natural samples. In contrast, autoimage and fluorescence-triggered modes cannot only count a mono-specific solution of cells accurately but can also estimate the size structure of natural samples. However, the requirements of each working mode in terms of sample concentration are different so the concentration procedure should be carefully chosen and some *a priori* knowledge about the cell density in the sample is needed.

The size structure obtained with FlowCAM and with light microscopy on preserved samples coincides but they differs from the size structure obtained on fresh samples. This suggests that automatic sampling devices could provide a more precise vision of plankton community avoiding the effects of sampling preservation and storage and increasing the resolution of the surveys.

SUPPLEMENTARY DATA

Supplementary data can be found online at <http://plankt.oxfordjournals.org>

ACKNOWLEDGEMENTS

This is a contribution to SCOR Working Group 130 on Automatic Visual Plankton Identification. We are indebted to all components of the Red Tides and Harmful Algae team of the Centro Oceanográfico de Vigo (IEO) for their help at the laboratory and the access to the Toxic Phytoplankton Culture Collection. We thank the captain and crew in the R/V Thalassa for their assistance during the Pelacus1009 cruise.

FUNDING

This work was supported by the Plan de Ciencia, Tecnología e Innovación del Gobierno del Principado

de Asturias (project IMAGINA and research grant BP07-081 to E.A.) and the Ministerio de Ciencia e Innovación (project PERPLAN, CTM2006-04854).

REFERENCES

- Babin, M., Cullen, J. J., Roesler, C. *et al.* (2005) New approaches and technologies for observing harmful algal blooms. *Oceanography*, **18**, 210–227.
- Barofsky, A., Simonelli, P., Vidoudez, C. *et al.* (2010) Growth phase of the diatom *Skeletonema marinoi* influences the metabolic profile of the cells and the selective feeding of the copepod *Calanus* spp. *J. Plankton Res.*, **32**, 263–272.
- Bauman, A. G., Burt, J. A., Feary, D. A. *et al.* (2010) Tropical harmful algal blooms: an emerging threat to coral reef communities? *Mar. Pollut. Bull.*, doi: 10.1016/j.marpolbul.2010.08.015.
- Benfield, M. C., Grosjean, P., Culverhouse, P. *et al.* (2007) RAPID: research on automated plankton identification. *Oceanography*, **20**, 12–26.
- Blanco, J. M., Echevarría, F. and García, C. M. (1994) Dealing with size-spectra: some conceptual and mathematical problems. *Sci. Mar.*, **58**, 17–29.
- Blaschko, M. B., Holness, G., Mattar, M. A., Lisin, D., Utgoff, P. E., Hanson, A. R., Schultz, H., Riseman, E. M., Sieracki, M. E., Balch, W. M. and Tupper, B. (2005) Automatic in situ identification of plankton. *Proceedings of the Seventh IEEE Workshops on Application of Computer Vision (WACV/MOTION'05)*, **1**, 79–86.
- Breier, C. F. and Buskey, E. J. (2007) Effects of the red tide dinoflagellate, *Karenia brevis*, on grazing and fecundity in the copepod *Acartia tonsa*. *J. Plankton Res.*, **29**, 115–126.
- Brown, L. (2010) *Using Laser-scatter Triggering in an Imaging Particle Analysis System to Increase Particle Counting Accuracy in Sparse Samples*. Fluid Imaging Technologies, Yarmouth, ME, 8 pp.
- Brzezinski, M. A., Baines, S. B., Balch, W. M. *et al.* (2010) Co-limitation of diatoms by iron and silicic acid in the equatorial Pacific. *Deep-Sea Res. II*, doi: 10.1016/j.dsr2.2010.08.005.
- Buskey, E. J. (2008) How does eutrophication affect the role of grazers in harmful algal bloom dynamics? *Harmful Algae*, **8**, 152–157.
- Buskey, E. J. and Hyatt, C. J. (2006) Use of the FlowCAM for semi-automated recognition and enumeration of red tide cells (*Karenia brevis*) in natural plankton samples. *Harmful Algae*, **5**, 685–692.
- Clough, J. and Strom, S. (2005) Effects of *Heterosigma akashiwo* (Raphidophyceae) on protist grazers: laboratory experiments with ciliates and heterotrophic dinoflagellates. *Aquat. Microb. Ecol.*, **39**, 121–134.
- Cotano, U., Irigoien, X., Etxebeste, E. *et al.* (2008) Distribution, growth and survival of anchovy larvae (*Engraulis encrasicolus* L.) in relation to hydrodynamic and trophic environment in the Bay of Biscay. *J. Plankton Res.*, **30**, 467–481.
- Dodson, A. N. and Thomas, W. H. (1978) Reverse filtration. In Sournia, A. (ed.), *Phytoplankton Manual*. UNESCO, Paris, pp. 104–107.
- Gribben, P. E., Wright, J. T., O'connor, W. A. *et al.* (2009) Reduced performance of native infauna following recruitment to a habitat-forming invasive marine alga. *Oecologia*, **158**, 733–745.

- Haurv, L. R., Mcgowan, J. A. and Wiebe, P. H. (1978) Patterns and processes in the time-space scales of plankton distributions. In: Steele, J. H. (ed.), *Spatial Pattern in Plankton Communities*. Plenum Press, New York, pp. 277–327.
- Ide, K., Takahashi, K., Kuwata, A. *et al.* (2008) A rapid analysis of copepod feeding using FlowCAM. *J. Plankton Res.*, **30**, 275–281.
- James, M. R. (1991) Sampling and preservation methods for the quantitative enumeration of microzooplankton. *N. Z. J. Mar. Freshw.*, **25**, 305–310.
- Koski, M., Breteler, W. K., Schogt, N. *et al.* (2006) Life-stage-specific differences in exploitation of food mixtures: diet mixing enhances copepod egg production but not juvenile development. *J. Plankton Res.*, **28**, 919–936.
- Kudela, R. M., Lane, J. Q. and Cochlan, W. P. (2008) The potential role of anthropogenically derived nitrogen in the growth of harmful algae in California, USA. *Harmful Algae*, **8**, 103–110.
- Lavrentyev, P. J., McCarthy, M. J., Klarer, D. M. *et al.* (2004) Estuarine microbial food web patterns in a Lake Erie coastal wetland. *Microbial. Ecol.*, **48**, 567–577.
- Leakey, R. J. G., Burkill, P. H. and Sleight, M. A. (1994) A comparison of fixatives for the estimation of abundance and biovolume of marine planktonic ciliate populations. *J. Plankton Res.*, **10**, 375–389.
- Littman, R. A., Van Oppen, M. J. H. and Willis, B. L. (2008) Methods for sampling free-living *Symbiodinium* (zooxanthellae) and their distribution and abundance at Lizard Island (Great Barrier Reef). *J. Exp. Mar. Biol. Ecol.*, **364**, 48–53.
- Liu, H., Dagg, M. J. and Strom, S. (2005) Grazing by the calanoid copepod *Neocalanus cristatus* on the microbial food web in the coastal Gulf of Alaska. *J. Plankton Res.*, **27**, 647–662.
- Menden-Deuer, S., Lessard, E. J. and Satterberg, J. (2001) Effect of preservation on dinoflagellate and diatom cell volume and consequences for carbon biomass predictions. *Mar. Ecol. Prog. Ser.*, **222**, 41–50.
- Nielsen, L. T., Jakobsen, H. H. and Hansen, P. J. (2010) High resilience of two coastal plankton communities to twenty-first century seawater acidification: evidence from microcosm studies. *Mar. Biol. Res.*, **1**, 1–14.
- Pedersen, T. M., Almeda, R., Fotel, F. L. *et al.* (2010) Larval growth in the dominant polychaete *Polydora ciliata* is food-limited in a eutrophic Danish estuary (Isefjord). *Mar. Ecol. Prog. Ser.*, **407**, 99–110.
- Reynolds, R. A., Stramski, D., Wright, V. M. *et al.* (2010) Measurements and characterization of particle size distributions in coastal waters. *J. Geophys. Res.*, **115**, doi: 10.1029/2009JC005930.
- San Martín, E., Harris, R. P. and Irigoien, X. (2006a) Latitudinal variation in plankton size spectra in the Atlantic Ocean. *Deep-Sea Res. II*, **53**, 1560–1572.
- San Martín, E., Irigoien, X., Harris, R. P. *et al.* (2006b) Variation in the transfer of energy in marine plankton along a productivity gradient in the Atlantic Ocean. *Limnol. Oceanogr.*, **51**, 2084–2091.
- See, J. H., Campbell, L., Richardson, T. L. *et al.* (2005) Combining new technologies for determination of phytoplankton community structure in the northern Gulf of Mexico. *J. Phycol.*, **41**, 305–310.
- Sheldon, R. W., Prakash, A. and Sutcliffe, W. H. Jr. (1972) The size distribution of particles in the ocean. *Limnol. Oceanogr.*, **17**, 327–340.
- Sieracki, C. K., Sieracki, M. E. and Yentsch, C. S. (1998) An imaging-in-flow system for automated analysis of marine microplankton. *Mar. Ecol. Prog. Ser.*, **168**, 285–296.
- Sterling, M. C. Jr., Bonner, J. S., Ernest, A. N. S. *et al.* (2004) Characterizing aquatic sediment-oil aggregates using in situ instruments. *Mar. Pollut. Bull.*, **48**, 533–542.
- Tanoi, T., Kawachi, M. and Watanabe, M. M. (2010) Effects of carbon source on growth and morphology of *Botryococcus braunii*. *J. Appl. Phycol.*, doi: 10.1007/s10811-010-9528-4.
- Tauxe, L., Steindorf, J. L. and Harris, A. (2006) Depositional remanent magnetization: toward an improved theoretical and experimental foundation. *Earth Planet. Sci. Lett.*, **244**, 515–529.
- Töpper, B., Larsen, A., Thingstad, T. F. *et al.* (2010) Bacterial community composition in an Arctic phytoplankton mesocosm bloom: the impact of silicate and glucose. *Polar Biol.*, doi: 10.1007/s00300-010-0846-4.
- Utermöhl, H. (1958) Zur Vervollkommnung der quantitativen Phytoplankton-Methodik. *Mitt. Int. Ver. Theor. Angew. Limnol.*, **9**, 1–38.
- Vaillancourt, R. D., Brown, C. W., Guillard, R. R. L. *et al.* (2004) Light backscattering properties of marine phytoplankton: relationships to cell size, chemical composition and taxonomy. *J. Plankton Res.*, **26**, 191–212.
- Zar, J. H. (1999) *Biostatistical Analysis*. Prentice-Hall, Englewood Cliffs, New Jersey.
- Zarauz, L. and Irigoien, X. (2008) Effects of Lugol's fixation on the size structure of natural nano-microplankton samples, analyzed by means of an automatic counting method. *J. Plankton Res.*, **30**, 1297–1303.
- Zarauz, L., Irigoien, X. and Fernandes, J. A. (2009) Changes in plankton size structure and composition, during the generation of a phytoplankton bloom, in the central Cantabrian sea. *J. Plankton Res.*, **31**, 193–207.
- Zarauz, L., Irigoien, X., Urtizberea, A. *et al.* (2007) Mapping plankton distribution in the Bay of Biscay during three consecutive spring surveys. *Mar. Ecol. Prog. Ser.*, **345**, 27–39.

Supplementary material

Appendix A: Maximum events per second in triggered modes.

In the triggered modes, there is a limitation in the number of events per second that the instrument can handle. For fluorescence-triggered mode we considered the limit of 2 events per second given by (Sieracki *et al.*, 1998). For the side-scatter-triggered mode the available information states that cell densities up to 100 cells mL⁻¹ can be counted accurately in this mode (Brown, 2010). No information about the maximum number of events per second is given, so we carried out a series of tests (Table SI) to establish the maximum events per second of this mode.

We prepared three bead solutions with the same concentrations tested in (Brown, 2010). They were counted by triplicate under the microscope and with the FlowCAM in side-scatter-triggered mode with different flow rates. Counting accuracy in the solution of 94 beads mL⁻¹ decreased when flow rate was above 0.35 mL min⁻¹, which means a maximum number of events per second to count accurately of 0.5.

Table SI. Counting accuracy in side-scatter-triggered mode for the combination magnification/flow-chamber 100x/100µm with 45 µm latex beads solutions at three concentrations and different flow rates.

Flow rate (mL min ⁻¹)	Concentration (beads mL ⁻¹)		
	8.5	50	94.7
0.24		99.5	92.8
0.35		88.9	92.8
0.43	99.6	95.3	66.5
0.53	92.1	67.0	

Appendix B: Sampling effectively, a function of particle concentration and time.

Fig. S1 and S2 illustrate the simulation for the 200× and 40× magnification and their respective factory defined size ranges in a similar manner as it is shown for the 100x magnification in Fig. 4.

Taking into account that in natural samples the total concentration of particles in the size range of 3-50 µm is 475 cells mL⁻¹ according to the “superspectrum” of Blanco *et al.* (Blanco *et al.*, 1994), the time required to sample effectively the whole factory defined size range would be 522 hours in autoimage mode (Fig. S1D), and 74.4 hours in the triggered modes (Fig. S1E). This is achieved at the maximum frame rate of 11 frames per second in autoimage mode and the maximum flow rate of 0.053 mL min⁻¹ in the triggered modes.

Results

E. ÁLVAREZ ET AL. | PLANKTON SIZE-STRUCTURE ESTIMATION

The points of inflection in the simulations, corresponding to the concentration of particles at which the events per second limit is reached at the maximum flow rate are 2264 and 566 cells mL⁻¹ for fluorescence and side-scatter-triggered modes respectively. When the concentration is higher than this value, the time required to sample effectively turns constant as represented in Fig. S1F: 15.6 hours in fluorescence-triggered and 62.5 hours in side-scatter-triggered modes. The concentration at which the events per second is reached at the minimum flow rate sets the overall maximum concentration that can be processed (10000 and 2500 cells mL⁻¹ for fluorescence and side-scatter-triggered modes respectively). Considering 30 minutes to be a reasonable amount of time for processing each sample, in the side-scatter mode, only the size range between 3 and 8 μm can be sampled, even if the sample is concentrated. In the fluorescence mode, in 30 minutes it is possible to cover effectively the range between 3 and 13 μm.

Fig. S2 illustrates the simulation obtained for the 40x magnification and the factory defined size range of 30-300μm. In natural samples the total concentration of particles in the size range of 3-

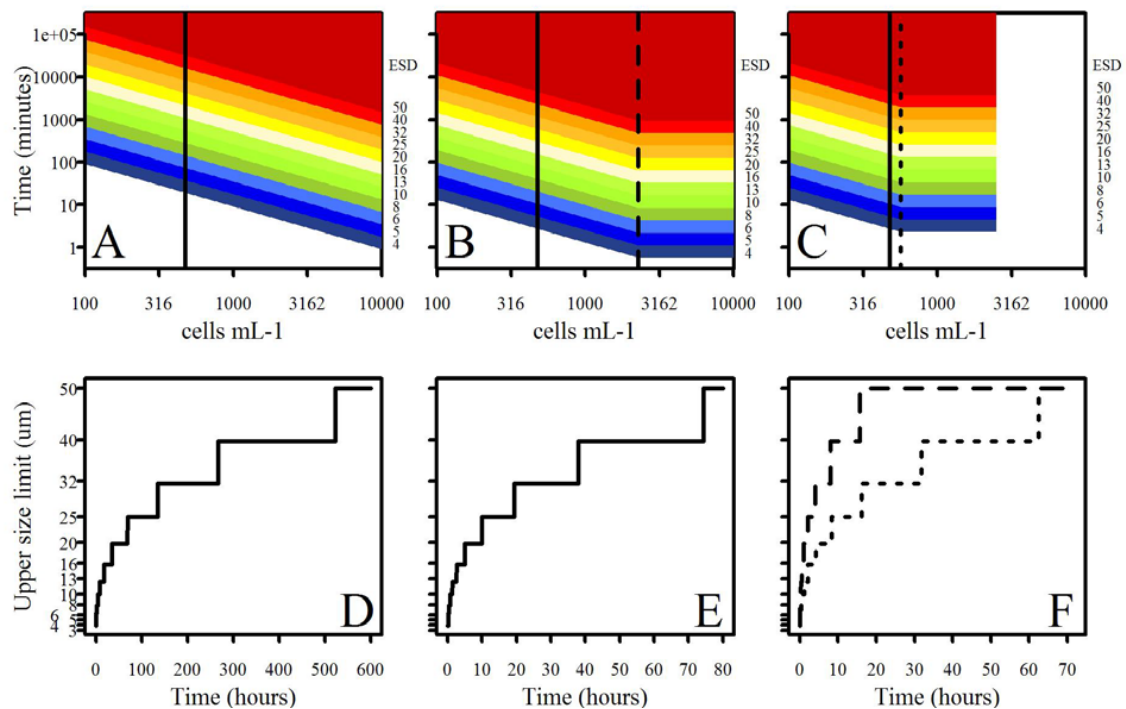


Fig. S1. Simulation for the combination magnification/flow-chamber 200x/50μm. The upper panels show the upper size limit sampled effectively given the total concentration of particles in the size range 3-50 μm and the time of analysis for (A) autoimage, (B) fluorescence-triggered mode and (C) side-scatter-triggered mode. The correspondence of each coloured area with the equivalent spherical diameter (μm) is indicated in the right axis of each panel. Lower panels show examples of upper size limit sampled versus time for (D and E) a mean natural sample concentration of 475 cells mL⁻¹, calculated according to Blanco *et al.* (Blanco *et al.*, 1994) and indicated as vertical lines in A-C, for (D) autoimage and (E) triggered modes. (F) shows the same relationship for the concentrations at which the saturation of the triggered modes is reached, indicated as vertical dashed and dotted lines in B and C respectively.

300 μm is 0.56 cells mL⁻¹ according to the “superspectrum” of Blanco *et al.* (Blanco *et al.*, 1994), so the time required to sample effectively the whole factory defined size range would be 620 hours in autoimage mode (Fig. S2D), and 386 hours in the triggered modes (Fig. S2E). This is achieved at the maximum frame rate of 11 frames per second in autoimage mode and the maximum flow rate of 1.2 mL min⁻¹ in the triggered modes.

Above the points of inflection (100 and 25 cells mL⁻¹ for fluorescence and side-scatter-triggered mode respectively) the time required to sample effectively is constant: 2.2 hours in fluorescence-triggered and 8.7 hours in side-scatter-triggered mode (Fig. S2F). The overall maximum concentration that can be processed is 480 and 120 cells mL⁻¹ for fluorescence and side-scatter-triggered mode respectively. In 30 minutes, in the side-scatter mode, only the size range between 30 and 100 μm can be sampled, even if the sample is concentrated. In the fluorescence mode, in 30 minutes it is possible to cover effectively the range between 30 and 160 μm .

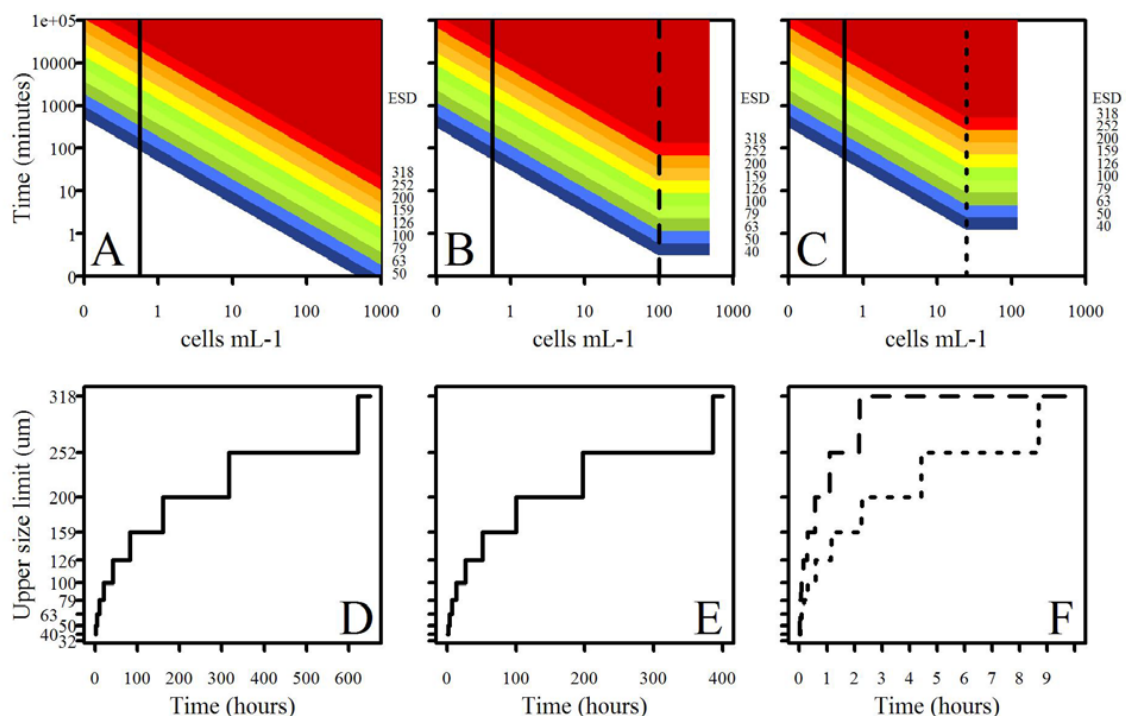


Fig. S2. Simulation for the combination magnification/flow-chamber 40 \times /300 μm . The upper panels show the upper size limit sampled effectively given the total concentration of particles in the size range 30-300 μm and the time of analysis for (A) autoimage, (B) fluorescence-triggered mode and (C) side-scatter-triggered mode. The correspondence of each coloured area with the equivalent spherical diameter (μm) is indicated in the right axis of each panel. Lower panels show examples of upper size limit sampled versus time for (D and E) a mean natural sample concentration of 0.56 cells mL⁻¹, calculated according to Blanco *et al.* (Blanco *et al.*, 1994) and indicated as vertical lines in A-C, for (D) autoimage and (E) triggered modes. (F) shows the same relationship for the concentrations at which the saturation of the triggered modes is reached, indicated as vertical dashed and dotted lines in B and C respectively.

Impact factor report

Abbreviated Journal Title	J Plankton Res
ISSN	0142-7873

JCR Data	Total Cites	5753
	Impact Factor	2.435
	5-Year Impact Factor	2.423
	Immediacy Index	0.725
	Articles	91
	Cited Half-life	>10.0
<i>Eigenfactor</i>[®] Metrics	<i>Eigenfactor</i>[®] Score	0.00975
	<i>Article Influence</i>[®] Score	0.894

Source: Journal Citation Reports, Science Edition 2012 (Thomson Reuters).

Chapter II. Improvement of plankton biovolume estimates derived from image-based automatic sampling devices: application to FlowCAM

Automated sampling devices allow the increment of the sampling resolution and hence the number of images that must be managed. Automatic classification of images appears, then, as a fundamental tool to deal with the identification of these growing data bases. A common characteristic of image-based sampling devices is, however, the ignoring of the tridimensional shape of the imaged particles which can misestimate the cellular biovolume. In this chapter we introduce a method to improve the estimates of cellular biovolume obtained from image based sampling devices coupled to a state of the art method for automated classification of images. The method of classification can be adapted to provide not only taxonomic information, but also a morphologic classification of the cells that allows obtaining a trustworthy estimate of the cellular biovolume according to the cell shape predicted.

Reference

Eva Álvarez, Ángel López-Urrutia and Enrique Nogueira (2012) Improvement of plankton biovolume estimates derived from image-based automatic sampling devices: application to FlowCAM. *Journal of Plankton Research*, 34(6): 454-469.

Candidate's contribution

My contribution to the work includes the co-design of the study and the establishment of methodology in collaboration with the rest of coauthors. I conducted the experiments, obtained and analyzed data and prepared tables and figures. All authors discussed the results and co-write the article.

Improvement of plankton biovolume estimates derived from image-based automatic sampling devices: application to FlowCAM

EVA ÁLVAREZ*, ÁNGEL LÓPEZ-URRUTIA AND ENRIQUE NOGUEIRA

CENTRO OCEANOGRÁFICO DE GIJÓN, INSTITUTO ESPAÑOL DE OCEANOGRAFÍA, 33212 GIJÓN, SPAIN

*CORRESPONDING AUTHOR: eva.alvarez@gi.ico.es

Received November 16, 2011; accepted in principle January 23, 2012; accepted for publication February 17, 2012

Corresponding editor: Roger Harris

The most commonly used biomass estimate for microalgae is obtained from cell biovolume, usually calculated from microscopically measured linear dimensions. Although reliable, this is a highly time-consuming and specialized technique. Automated sampling devices that acquire images of cells and use pattern recognition techniques to identify the images have been developed as an alternative to microscopy-based methods. There are some aspects of automatic sampling and classification methods, however, which can be improved for the analysis of field samples including living and non-living particles. In this work, we demonstrate how the accuracy of a state-of-the-art technique for plankton classification (Support Vector Machine) can be improved up to 86% if a previous automated step designed to remove non-living images is included. There is a tendency with the currently applied automatic methods to misestimate cell biovolume due to the two-dimensionality of the images. Here, we present a data set of more than 500 samples to show that the greatest effect is caused by the incorrect estimation of biovolume of the chain-forming diatoms. This results in an overestimate of biomass of between 20 and 100% where chain-forming diatoms represent more than the 20% of the biomass of the sample. We show how the classification method can be adapted to provide not only taxonomic but also the morphological classification of cells in order to obtain a more reliable estimate of biovolume according to the predicted cell shape, in a way comparable with microscopy-based estimates.

KEYWORDS: biovolume; biomass; size spectra; machine learning; Support Vector Machine (SVM); FlowCAM

INTRODUCTION

The biomass size distribution in aquatic and terrestrial ecosystems has been an important focus of research in ecology during the last decades. The “particle-size” approach began to develop in the last century as a

unifying theory that established a relationship between the biomass of organisms in any size category and the individual body weight of these organisms (Rodríguez and Mullin, 1986). The planktonic community soon appeared to be a very appropriate object of study to test

the hypotheses of the “particle-size” approach due to its wide size range (Quiñones *et al.*, 2003). An extensive oceanic survey carried out by Sheldon *et al.* (Sheldon *et al.*, 1972) provided the first empirical evidence of a general feature of marine ecosystems: the same amount of biomass is allocated in logarithmically equal biovolume ranges (Sheldon *et al.*, 1972). The study of this relationship was carried out with a Coulter counter (Sheldon and Parsons, 1967), a device capable of counting and sizing particles in a fluid, which enabled the authors to analyse more than a hundred of un-preserved samples distributed all over the world ocean.

The introduction of automated sampling devices designed to characterize the abundance and size of planktonic organisms in a reasonable amount of time has furthered the application of this “particle-size” approach. One disadvantage, however, of these faster methods such as the Coulter counter is the lack of identification of the particles analysed. In an attempt to solve the problem of knowing what kind of particles are sampled, several automated devices that acquire images of the particles have been developed. These new technologies brought together the need to examine, identify and automatically measure large numbers of images (Benfield *et al.*, 2007). The automated classification of plankton images has specific challenges because of the highly variable proportion of taxonomic groups depending upon location, time and nature of the survey, morphological heterogeneity, variable proportion of non-living targets, different orientations, partial occlusion and single images containing more than one particle. In order to overcome these challenges, several authors have developed automatic classification techniques based on pattern recognition that have yielded very promising results. These classification techniques are general mathematical techniques that can be applied to the images obtained from different instruments, e.g. the Video Plankton Recorder (Tang *et al.*, 1998; Davis *et al.*, 2004), the Shadow Imaging Particle Profiling Evaluation Recorder (Luo *et al.*, 2004), the ZooScan (Grosjean *et al.*, 2004; Gorsky *et al.*, 2010), the FlowCytobot (Sosik and Olson, 2007) or the Flow Cytometer And Microscope (FlowCAM; Blaschko *et al.*, 2005; Zarauz *et al.*, 2009).

With the exception of holographic methods, all image-based automatic sampling devices have in common that they do not capture the three-dimensional shape of the particles. To calculate the volume of planktonic cells, the methods based on two-dimensional images usually consider all cells as spheres and use the equivalent spherical diameter (ESD) of the area projected by the cell on a flat surface. This is a good approximation in the case of spherical or elliptical cells but a poor one in the case of

cylindrical cells. A cylinder with an aspect ratio of 0.5 has a volume 26% lower than the volume of a sphere with the same projected area; the underestimate reaches 54% if the aspect ratio is of 0.2. On the other hand, a discus with an aspect ratio of 0.5 has a volume 47% higher than the volume of the equivalent sphere; the overestimate reaches 136% if the aspect ratio is of 0.2. This can bias the estimation of biovolume when the particles are placed preferably in some orientations, a typical effect that occurs when particles lay on a flat surface (e.g. microscopy, scanner) or are embedded in a moving fluid (e.g. FlowCAM). The effect is dependent on the proportion of cylindrical cells in the sample. Under these conditions, the simplification of assuming that all particles are spheres can render poor biovolume or biomass estimates per group, genera or species, even with a perfect classification at these prescribed taxonomic levels.

Microscopy-based methods are considered the most accurate for plankton enumeration and biovolume estimate and have been the most extensively used methodology for the study of microplankton community size structure (Cermeño and Figueiras, 2008). The most widely used protocol is the one proposed by Utermöhl (Utermöhl, 1958), in which the preserved water sample is settled on a microscope slide. An expert taxonomist examines the slide under the microscope, identifies the taxonomic groups and estimates the abundance of each group. To estimate the biovolume of the cells, the expert needs to assign a geometrical shape to each taxonomic group, measure a certain number of linear dimensions and estimate the hidden dimensions following aspect ratios previously calculated. Hillebrand *et al.* (Hillebrand *et al.*, 1999) proposed a set of 20 geometric models to be used for the determination of microalgal biovolume. Although this set of shapes was thought to minimize the effort of microscopic measurement, it also aims to be as close to the actual shape of the organism as possible, so the shape that describes a cell can be as simple as a sphere, or complex, formed by various geometrical bodies that require the measurement of several dimensions. However, the description of a cell with a complex shape usually requires accommodating structures that do not constitute a large proportion of the total volume of the cell, such as spines or setae (Menden-Deuer *et al.*, 2000). For this reason, considering the intrinsic error of microscopic volume measurements and the sometimes inaccurate designation of composite shapes, the description of complex shapes can be approximated by three simple shapes: sphere, ellipsoid and cylinder (Menden-Deuer *et al.*, 2000). The effort needed to process samples according to this technique turns it into a highly time-consuming and specialized task, although this technique is considered the most reliable and is used as a

benchmark for the assessment of new techniques for plankton enumeration and biovolume estimation.

In order to provide biovolume estimates comparable to those obtained with microscopy-based techniques using automated classification devices, it is necessary to consider the three-dimensional shape of the cells. Our strategy in the present work has been to imitate the working procedures followed by microscopy-based techniques, that is, to predict the shape of the cells and make some assumptions about the hidden dimension. To do this, we adapted the currently used techniques to automatically classify the images not only taxonomically but also morphologically. The aim of this work is to develop a technique to classify automatically images from an automatic sampling device (FlowCAM) that permits at the same time a more accurate estimate of the biovolume of the cells. With this aim we have: (i) adapted the state-of-the-art classification techniques to classify images from FlowCAM in order to obtain morphological information of the cells; (ii) used the morphological information to improve the estimate of the biovolume of the cells digitized in two-dimensional images and (iii) used the taxonomic information to identify situations where poor size-structure characterization or biomass estimation may result.

METHOD

A total of 526 natural samples were taken with a rosette sampler system in the Bay of Biscay between August 2008 and April 2010 at 313 different sampling stations. Figure 1 shows the geographic location of all sampling stations and the season of the year when they were sampled. At all the stations, samples were collected at the surface, and additional 213 samples were obtained between 10 and 75 m. All samples were pre-filtered at sea through a 200- μm mesh-size net, kept fresh, stored in the dark and analysed with FlowCAM on board or in the laboratory within a few hours. All samples constituted our data set, subdivided into: a training set used to train the automated classifier, a test set to evaluate it and a field evaluation set to illustrate the application of the automatic classification method. The training set was built using images from 86 randomly selected samples and indicated in Fig. 1 as grey dots. The test set consisted of 17 samples, obtained over 2 years in a monthly sampling of a coastal station located in the Cantabrian Sea, so these samples cover the whole seasonal cycle. Another two samples, taken on the French shelf, were collected in triplicate and used to explore the different calculations of biovolume. Finally, the rest of the samples constituted the field evaluation set.

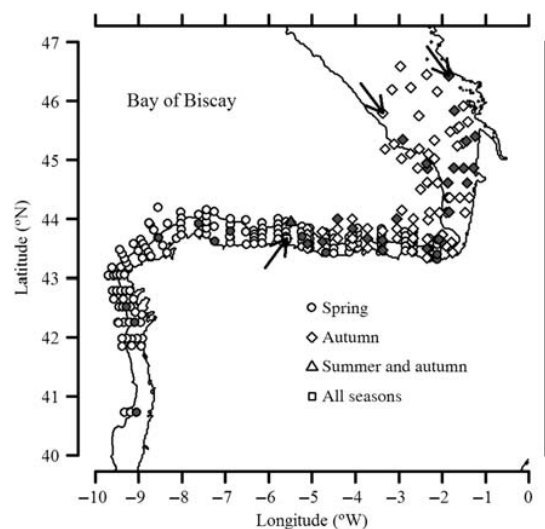


Fig. 1. Geographical location of the sampling stations. The shape of the point indicates the season when the samples were taken. Grey dots indicate samples used to build the training set. The upward arrow indicates the location of the series of samples used as the test set. Downward arrows indicate the location of samples used to explore the effect of different ways of calculating the cell biovolume.

Automatic processing of FlowCAM samples

The automatic processing of FlowCAM samples consists of several steps:

Digitalization of samples

Each sample was split in an un-concentrated subsample for analysis with the 200 \times magnification to digitize particles between 3 and 50 μm , and in a concentrated subsample (1 L concentrated by reverse filtration (Dodson and Thomas, 1978) down to around 20 mL) for the 100 \times magnification to digitize particles between 6 and 100 μm . The lower limit for both magnifications corresponds to particles covering an area smaller than 10×10 pixels that do not have enough resolution to be identified, even by a human expert, and thus they are not considered. Photographs can be captured following three working modes: in autoimage mode photographs are taken at a constant rate (in our case, 11 frames s^{-1}), while in fluorescence-triggered and side-scatter-triggered modes photographs are taken only when a particle that emits fluorescence or scatters light, respectively, passes in front of the camera. Samples were analysed in autoimage and fluorescence-triggered modes; side-scattered mode was not used as it has been shown to give unreliable results (Álvarez *et al.*, 2011). Thirty minutes were considered a maximum running time for each subsample. In the subsamples processed with autoimage, 20 000 photos were taken, which corresponds to

a net volume of 0.072 mL in 20× and 14.91 mL in 10×. In the subsamples processed with fluorescence triggered mode, 1 mL was processed at 0.0333 mL min⁻¹ in the 20× and 10 mL at 0.3333 mL min⁻¹ in the 10×. The FlowCAM software, Visual SpreadSheet, extracts each particle present in a photograph (a process called image segmentation), and stores the rectangular section on disk. The result is a plankton sample turned into a collection of images, each containing an individual particle. All rectangular sections are combined in collages that constitute the raw output of the VisualSpreadSheet.

Description of the images

We followed the philosophy of the SCOR 130 working group (Benfield *et al.*, 2007) promoting the intercomparison of plankton pictures from various origins. Zoo/PhytoImage is an open source software based on R for plankton image analysis that can be modified to meet the requirements of the user and accommodate many different imaging systems (Grosjean, 2005). We followed the instructions proposed by the Zoo/PhytoImage platform in terms of the conventional names of the samples, the inclusion of metadata and the format of the images and the data.

In order to import the raw data into the Zoo/PhytoImage convention, we used the EBIImage R package from Bioconductor (Sklyar and Huber, 2006; Pau *et al.*, 2010), which provides general purpose functionality for the reading, writing, processing and analysis of images as well as tools to transform the images, segment cells and extract quantitative cellular descriptors. The collage files provided by the FlowCAM software were separated in individual images and a series of morphological features were calculated for each image. To localize the particle within each rectangular section we used the intensity-based method proposed by Tang (Tang *et al.*, 1998). Once the particle was located, new features were extracted. These included simple shape and texture descriptors (Blaschko *et al.*, 2005), invariant moments (Hu, 1962), granulometric features (Luo *et al.*, 2004; Blaschko *et al.*, 2005), edge features (Sklyar and Huber, 2006), texture features from the co-occurrence matrix (Haralick *et al.*, 1979) and Zernike features (Zernike, 1934). In total, 136 features or image attributes described each particle (see Supplementary Data).

Generation of a training and a test set

A training set is a group of example images classified by a human expert that is used to train the classification algorithm. In our case, these images come from 86 randomly selected samples of the data set. To manage the images we used the tools provided by the Zoo/PhytoImage software. The training set was established

by means of the *ad hoc* method, that is, with a variable number of items within each group as chosen by the user (Davis *et al.*, 2004), so that the largest diversity of organisms could be considered. We have created three different training sets (TS): (1) for the images obtained with the 200× magnification (TS200×, composed by 3600 images); (2) for the images smaller than 20 μm in ESD obtained with the 100× magnification (TS100×_{<20}, 9500 images); and (3) for the images larger than 20 μm ESD obtained with the 100× magnification (TS100×_{>20}, 9500 images). We divided each of the training sets in a group of artefacts, a group of detritus and a variable number of living-particle groups indicated in Table I and Fig. 2. These living groups were made based on three criteria: size, taxonomy and morphology (Bakker *et al.*, 1985). Each group was homogeneous for each of the criteria, containing cells of the same size range, same taxon and same shape. The training sets TS200× and TS100×_{<20} separate organisms based only on their shape and size, without taxonomic differentiation (Groups 1 to 4 in Table I). In the TS100×_{>20}, each living group includes individuals which are taxonomic and morphologically homogeneous (Groups 5 to 34 in Table I).

The test set is a group of images classified by a human expert and not included in the training set that is used to evaluate the efficiency of the classifier. The test set consisted of 19 samples of the data set with 70 900 images between 3 and 100 μm. The living particles were separated from detritus and artefacts by visual inspection and compared with predictions of the classifier to estimate the efficiency of the automated method.

Pretreatment of the images for the elimination of artefacts and detritus

The relative importance of non-living particles, which include artefacts (bubbles, background images and repeated images) and detritus, and the living particles differs depending on the FlowCAM working mode used to digitize the sample. The fluorescence-triggered mode does not record many non-living particles because they are not photographed due to their absence of red fluorescence, whereas autoimage mode captures a variable and usually large amount of images of non-living particles that interferes with the classification of living particles.

Instead of eliminating artefacts and detritus manually, as it is commonly done (Zarauz *et al.*, 2007), we implemented a series of cleaning filters. For the artefacts, we designed the filters using the information of the time of recording and the position in the field of view of the particles. We considered as bubbles, those images segmented with a frequency higher than 10 per second; as

Table I: Classification of FlowCAM images in groups according to size, shape and taxonomic affiliation

Taxon class	Groups	Shape class	
1. Others (all <20 μm)	Spherical cells (1)	Sphere	
	Elliptical cells (2)	Ellipsoid	
	Discoid cells (3)	Disc	
	Cylindrical cells (4)	Cylinder	
	Cells unidentified (5)	Ellipsoid	
2. Others >20 μm	Flagellates (6)	Ellipsoid	
	Silicoflagellates (7)	Ellipsoid	
3. Silicoflagellates	Small dinoflagellates (8)	Ellipsoid	
4. Dinoflagellates	<i>Prorocentrum micans</i> (9)	Ellipsoid	
	Genera <i>Prorocentrum</i> (10)	Ellipsoid	
	Genera <i>Dinophysis</i> (11)	Ellipsoid	
	Globose un-horned cells (e.g. <i>Protoperidinium</i>) (12)	Ellipsoid	
	Globose horned cells (e.g. <i>Ceratium</i>) (13)	Ellipsoid	
	<i>Mesodinium rubrum</i> (14)	Ellipsoid	
	Few cilia in apical position (e.g. <i>Laboea</i> , <i>Strombidium</i>) (15)	Ellipsoid	
	Few cilia in lateral position (e.g. <i>Euplotes</i> , <i>Diophrys</i>) (16)	Ellipsoid	
	Tintinnids with extended lorica (e.g. <i>Salpingella</i>) (17)	Ellipsoid	
	Tintinnids with globular lorica (e.g. <i>Codonella</i> , <i>Dictyocysta</i>) (18)	Ellipsoid	
6. Diatoms	Pennate cells (19)	Ellipsoid	
	Centric cells with height < diameter (20)	Disc	
	Centric cells with height > diameter (21)	Cylinder	
	Cylindrical cells with round ends (e.g. <i>Ditylum</i> , <i>Stephanopyxis</i> , <i>Corethron</i>) (22)	Cylinder	
	Cylindrical cells with spine-like ends (e.g. <i>Rhizosolenia</i>) (23)	Cylinder	
	Wide chains with closed connected cells (e.g. <i>Detonula</i> , <i>Guinardia</i>) (24)	Cylinder	
	Narrow chains with closed connected cells (e.g. <i>Leptocylindrus</i>) (25)	Cylinder	
	Chains with slightly connected cells (e.g. <i>Eucampia</i>) (26)	Cylinder	
	Chains with long setae (e.g. <i>Chaetoceros</i>) (27)	Cylinder	
	Chains with intercellular spaces (e.g. <i>Skeletonema</i>) (28)	Cylinder	
	Chains with cells connected by gelatinous threads (e.g. <i>Thalassiosira rotula</i>) (29)	Cylinder	
	Chains of needle-like cells (e.g. <i>Nitzschia</i>) (30)	Cylinder	
	Colonial star-shaped (e.g. <i>Asterionellopsis</i>) (31)	Sphere	
	Colonial zig-zag (e.g. <i>Thalassionema</i>) (32)	Sphere	
	Gelatinous spheres (e.g. <i>Phaeocystis</i> , <i>Thalassiosira subtilis</i>) (33)	Sphere	
	7. Crustaceans	Crustaceans (34)	Ellipsoid
	8. Detritus	Faecal pellets, exuvia, dead fragments	—
9. Artefacts	Bubbles, empty images, background noise	—	

The name of the groups that contains a description of the species included are based on the classification of Bakker *et al.* (Bakker *et al.*, 1985). These groups are merged, after automatic classification, in the taxon and shape classes indicated.

background images, those recorded more than 10 times in the same position of the camera field of view; and as repeated images, those recorded in consecutive photographs and with an Euclidean distance between their image attributes lower than 50. For the detritus, we have explored the 136 image attributes searching for a selected subset of them able to discriminate between detritus and living particles. In Fig. 3, two of these selected attributes are shown to illustrate the procedure we have followed: the mean value of grey intensity for each particle (Fig. 3A), that represented a lower limit for living particles, and the skewness of grey intensity (Fig. 3B), that represented an upper limit for living particles. Thus, setting a lower and an upper limit value, respectively, for these two attributes permits the identification of many non-living particles. Obviously, there is not a single image attribute that can distinguish between detritus and living particles unequivocally, but a combination of attributes can be used to establish a statistical

filter to identify most of detritus particles. In total, a subset of 50 attributes were selected as they discriminate living particles in their upper limit and a subset of 10 attributes were selected as they discriminate living particles in their lower limit. The range of these attributes for the living particles in the training set were extended a 5% for the 200 \times images and a 2% for the 100 \times images in their discrimination limit, to establish a confidence interval within the living particles are expected to be included. We labelled as detritus those images in the test and field evaluation sets that show values of any of the attributes selected outside its confidence interval.

Training the algorithm

Support Vector Machine (SVM) was used to classify the rest of the particles after the pretreatment of the images. We used the library LIBSVM (Chang and Lin, 2009) with its R interface: *e1071* package (Karatzoglou *et al.*, 2006) and *ipred* package (Peters and Hothorn, 2009).

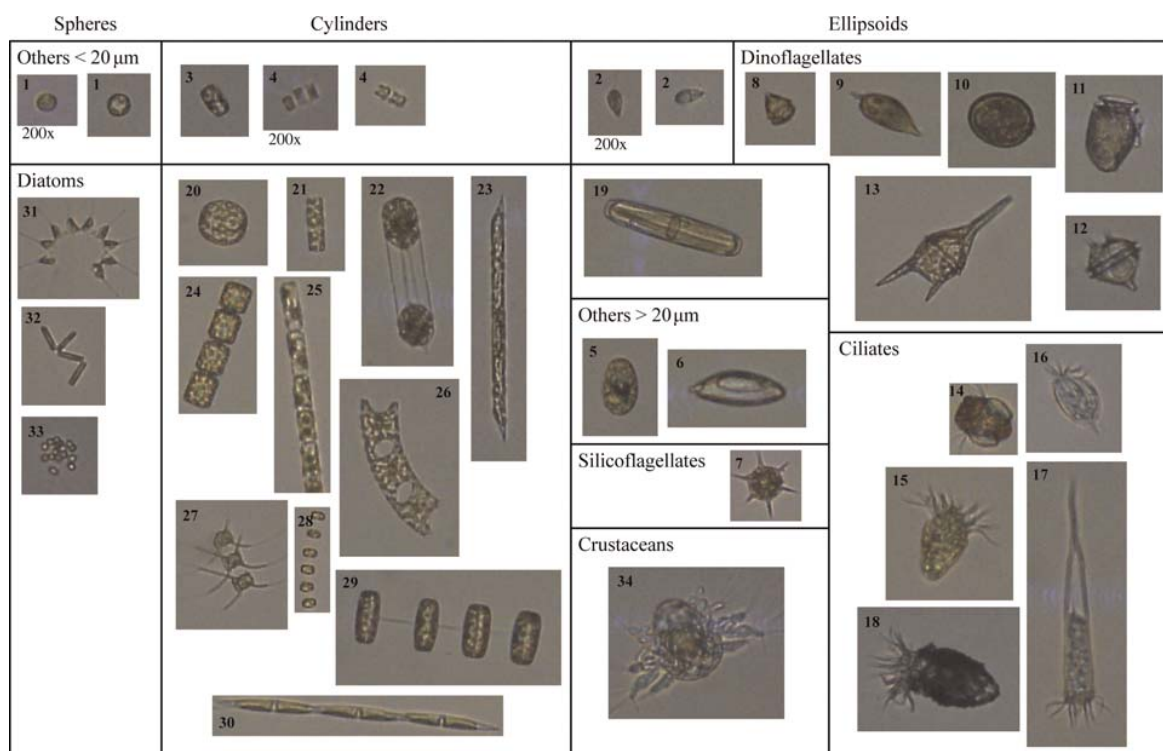


Fig. 2. Groups in the automatic classification and their correspondence in taxonomic and morphological classes. Dashed lines separate morphological classes, dotted lines taxonomic classes and solid lines both. The number in the left upper corner of the images corresponds to the description of the group given in Table I. All image magnifications are $\times 100$ except when indicated.

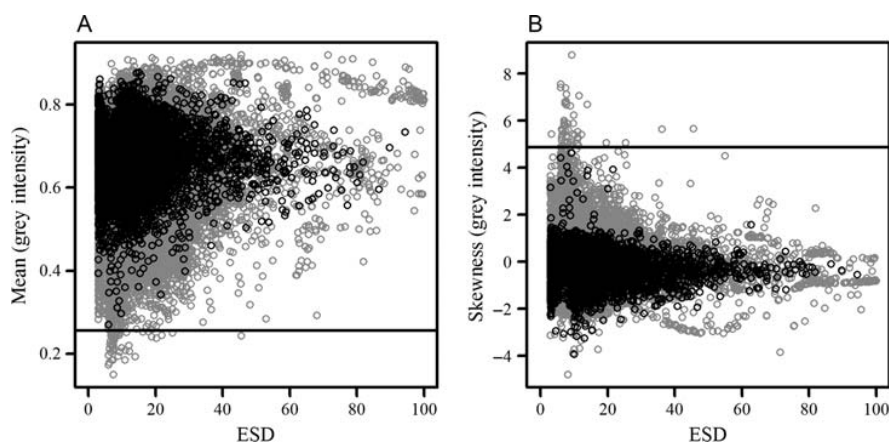


Fig. 3. Example of two attributes selected to design a statistical filter to eliminate non-living particles prior to the automatic classification. Both are texture attributes related to grey intensity that range from 0 to 1: (A) mean and (B) skewness versus the ESD of the particles. Living particles are plotted in black and detritus and artefacts in grey. Horizontal lines show the value used to discriminate living from non-living particles in the lower and the upper limit of the variable, respectively.

Each training set of images with its 136 attributes per image, scaled previously, constitutes the input for the LIBSVM. The Gaussian Radial Basis Function was used as the kernel and parameters were tuned using a

grid search over parameter ranges, testing the maximization of accuracy by 5-fold cross-validation. Cross validation randomly separates the training set in several sets of images (five sets in our case); the images of each

of these sets are classified with a tool built with the remainder (four) sets. The predicted assignments are compared with the actual assignments, and the number of elements correctly classified with respect to the total number of elements gives the global accuracy of the classifier.

Predicting new samples

The three classifiers obtained (i.e. for 200x, 100x_{<20} and 100x_{>20}) make up a classifier tool that can predict any FlowCAM sample described in the same way as the example images. Each image was classified in one of the 34 groups and assigned to the corresponding taxon class and shape class (Table I). The result was each particle being classified in one of the 6 taxonomic categories (diatoms, dinoflagellates, silicoflagellates, ciliates, crustaceans and other living particles) and of the 4 morphological categories (spheres, ellipsoids, cylinders and discuses) (Table I). For instance, a species of the genus *Lauderia* is included in the taxon-class diatoms but also in the shape-class cylinders, while a species of the genus *Proocentrum* is included in the taxon-class dinoflagellates and in the shape-class ellipsoids.

Evaluation of the classifier

The most widely used technique to estimate the efficiency of the automatic classification is the cross validation, described above. The cross validation, however, has been shown to give higher efficiencies than the estimate over a test set of independent samples (Davis *et al.*, 2004; Sosik and Olson, 2007). The testing over natural samples consists in automatically classifying a set of images (i.e. the test set) that has been previously classified by an expert and are not included in the training set.

The efficiency is tested with the construction of a confusion matrix, a table where the manual classes are placed in rows and automatic classes in columns and each image counted in the cell determined by its manual and automatic assignment. The efficiency of the automatic classification was assessed by: (i) global accuracy, that is the percentage of elements correctly classified, estimated as the ratio between total elements in the diagonal of the confusion matrix (true positives) and the total number of elements, and (ii) accuracy per class, that is the ratio between the number of particles classified as belonging to a class and the actual number of particles in that class. The global accuracy can not be higher than one, whereas the accuracy per class is lower than one when the automatic classification counts fewer particles than actual ones and is higher than one when automatic classification overestimates the number of particles. It should be noted that the accuracy per

class only takes into account the total number classified and does not consider whether particles are correctly classified or not. For instance, in a sample with 100 diatoms where we classify 10 diatoms correctly and 80 detrital particles as diatoms, the accuracy per class is 90% (90 of 100 particles were classified as diatoms). Two measures are used to evaluate this type of error: (i) specificity, that is the percentage of the elements that really belong to the class where they have been classified (true positives/total classified), and (ii) probability of detection, that is the percentage of elements in a class which are correctly classified (true positives/total manual). In the previous example, the specificity would have been 11.1% (10 of the 90 particles were correctly classified as diatoms), and the probability of detection 10% (10 of the 100 diatoms were classified correctly).

To estimate these parameters for the taxonomic classification, 17 samples of the test set, obtained during 2 years in a monthly sampling of a coastal station located in the Cantabrian Sea (at 46.42°N, 1.85°W, $z = 100$ m), were analysed. Only the living particles were selected and separated into six taxonomic classes (dinoflagellates, silicoflagellates, diatoms, ciliates, crustaceans and other living particles) by visual inspection, constituting a test set of 61 700 images between 3 and 100 μm . The other two natural samples of the test set, corresponding to a coastal (at 46.42°N, 1.85°W, $z = 25$ m) and a mid-shelf location (at 45.79°N, 3.37°W, $z = 142$ m) in the Bay of Biscay (October 2009), were used to estimate the parameters for the morphological classification, constituting a test set of 9200 images between 20 and 100 μm separated into four morphological classes (spheres, ellipses, cylinders and discuses).

To account for the possible variation in the accuracy of each sample (i.e. changes in taxonomic composition and variations in image quality related to lightning and focus), we have computed for each sample the abundance of living particles in the size range 3–100 μm manually and automatically classified and compared with an expected one-to-one relationship with a *t*-test.

Estimation of biovolume

Two natural samples were used to explore the effect of the different ways of calculating the biovolume of the particles. These two samples were taken in triplicate, each replicate taken using a separate Niskin bottle and analysed as described above. Only the living particles were selected, obtaining 1378, 1475 and 1470 particles in the coastal sample and 243, 170 and 205 particles in the shelf sample. Particles were separated in four shape classes (spheres, ellipses, cylinders and discuses) by visual inspection.

The biovolume of each living particle recorded by the FlowCAM was calculated in three ways: (i) the projected area of each particle was used to calculate their biovolume considering a spherical shape (i.e. area-based); (ii) the length and width were measured manually and the biovolume calculated as a revolution volume according to the shape manually assigned (i.e. shape-based); and (iii) the biovolume was calculated according to the shape predicted by the classification algorithm and the automatic measurements made by the image analysis (i.e. automatic-shape-based). Depth and width dimensions were considered equivalent since the orientation of the particles results in one or the other being measured randomly. The normalized abundance size spectra (NASS) obtained with area-based, shape-based and automatic-shape-based biovolumes were compared with a one-way ANOVA and a Tukey test. Only those bins of the spectra for which a minimum of five particles were measured were considered for the comparison.

Field evaluation

For the field evaluation set of samples ($n = 509$), the same calculations were done but only for those corresponding to automatic assignments. The total abundance of living cells was estimated and the biovolume for each living particle was calculated based on the area-based and the automatic-shape-based method. The NASS for both data sets were built and compared with a t -test.

The area-based and the automatic-shape-based biovolume obtained for the living particles were converted to carbon. Different conversion factors were applied for cells: smaller than $3000 \mu\text{m}^3$, larger than $3000 \mu\text{m}^3$ except diatoms, and diatoms larger than $3000 \mu\text{m}^3$ (Menden-Deuer *et al.*, 2000). The abundance and biomass per taxon class were calculated and the percentage that each taxon represents in the sample was

estimated. The misestimation of autotrophic biomass was calculated comparing the area-based and the shape-based biomass only for autotrophic and mixotrophic taxa.

RESULTS

Automatic classification of FlowCAM images

We used the test set to estimate the efficiency of the automated method to classify living particles. The global accuracy of the automatic processing of FlowCAM sorting living from non-living particles was 86% (Table II). The accuracy per class for both types of images is close to 1 which means that the number of particles given for each class fits the actual value. The specificity is lower because it does not consider the false positives, but it is still above 80% and the probability of detection is above the 84%.

There are no significant differences in the global accuracy of autoimage and fluorescence (87 and 85% respectively). The accuracy per class is, however, different depending on the working mode. Whereas the accuracy per class in fluorescence is close to 1 for detritus and living particles, in autoimage the misclassification of living particles is high (124%). This is caused by the large amount of detritus present in autoimage samples; even with a good classification of detritus (95%), their proportion is so high (32 000 non-living from 38 000 particles) that it causes the inclusion of many false positives in the counts of living particles.

The efficiency estimated over the confusion matrix depends on the size and composition of the test set (Solow *et al.*, 2001). Since our test set is constituted by complete samples, a very abundant sample well classified can determine the efficiency of the classification. The abundance of living particles in the size range 3–100 μm manually and automatically classified for each sample is

Table II: Confusion matrix for the automatic classification of living and non-living particles, digitized with the two FlowCAM working modes

Mode	Manual	Automatic		Global accuracy	Accuracy per class	Specificity	Probability of detection
		Non-living	Living				
Total	Non-living	38 324	5628	0.86	0.97	0.90	0.87
	Living	4408	22 525				
Autoimage mode	Non-living	31 699	3701	0.87	0.95	0.94	0.90
	Living	1972	5298				
Fluorescence-triggered mode	Non-living	6625	1927	0.85	1.06	0.73	0.77
	Living	2436	17 227				

The parameters that account for the efficiency of the classifier are: global accuracy (true positives/total particles), accuracy per class (total classifier/total manual), specificity (true positives/total classifier) and probability of detection (true positives/total manual).

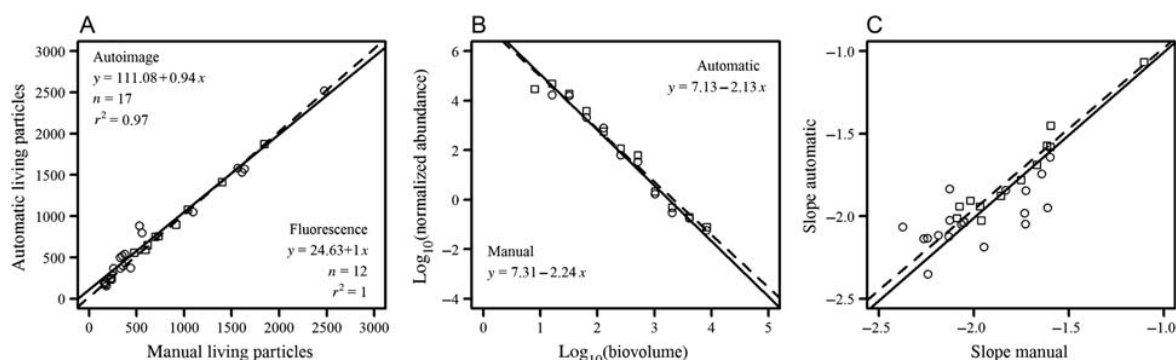


Fig. 4. Accuracy classifying living particles. **(A)** Counts of living particles manually and automatically classified in the size range 3–100 μm for each sample of the test set. Autoimage samples in dots and solid line and fluorescence-triggered samples in squares and dashed line. **(B)** NASS built with living cells manually (dots and solid line) and automatically (squares and dashed line) classified for an example sample. **(C)** Comparison of the slope of the NASS obtained with the living particles manually and automatically classified between 3 and 100 μm . Autoimage samples in dots and solid line and fluorescence samples in squares and dashed line.

shown in Fig. 4A. The relationship between the abundances is not different from 1 in autoimage ($P = 0.1868$, $n = 17$) and in fluorescence-triggered mode ($P = 0.4760$, $n = 12$). In autoimage, the r^2 is lower than in fluorescence (0.97 versus 1) given the higher error on classification explained above. A sample with 5009 living particles in manual assignment and 4668 in automatic assignment was considered an outlier and eliminated.

The NASS were built only with living particles, so the efficiency classifying living particles also determines the accuracy of the parameters of the spectra. Figure 4B shows the NASS and the parameters of the regression line fitted to the NASS, for an example sample that has been manually and automatically classified. The slope of the regression line fitted to the NASS based on manual and automatic estimates of abundance of all samples in the test set (Fig. 4C), did not differ significantly. The relationship for the whole test set of samples is not different from the expected one-to-one relationship, both for autoimage (slope automatic = $1.0056 \times$ slope manual, $P = 0.8127$, $n = 17$) and fluorescence working modes (slope automatic = $0.9793 \times$ slope manual, $P = 0.0564$, $n = 13$). Since the NASS include all living organisms it means that the error in the classification is smaller than the variations in abundance needed to observe a change in the parameters of the NASS.

The confusion matrix of abundance for taxon-class assignment and the parameters of efficiency are shown in Table III. The global accuracy of taxon assignment, once the detritus is eliminated, is 87%. The accuracy per class is low in classes with fewer individuals (ciliates and crustaceans) and in diatoms. The specificity is above 74% in all classes except in ciliates, a very heterogeneous class. The probability of detection is above 60% in all classes. Figure 5 shows a comparison between the counts

obtained by the manual and automatic classification in each sample for the different taxonomic classes of microplankton (20–100 μm). In autoimage, the relationship was different from the expected one-to-one for ciliates, crustaceans and the “others” class, which are the taxonomic classes with fewer individuals (ciliates: $P = 0.0031$, $n = 13$; crustaceans: $P = 0.0105$, $n = 6$; others: $P < 0.0001$, $n = 15$). The relationship for diatoms, dinoflagellates and silicoflagellates was not different from the expected one-to-one (diatoms: $P = 0.2209$, $n = 14$; dinoflagellates: $P = 0.3422$, $n = 15$; silicoflagellates: $P = 0.5910$, $n = 6$). In fluorescence-triggered mode, the only relationship different from the expected one-to-one was the class “others” ($P < 0.0001$, $n = 12$).

The confusion matrix of abundance for shape-class assignment and the parameters of efficiency are shown in Table IV. The global accuracy of shape assignment, once the detritus was eliminated, is 78%, although the accuracy per class is variable. The class that is better classified is that of cylinders (104%), which is in fact the class that may cause the highest overestimate of biovolume (see below). There is high misclassification between spheres and ellipses but, since the geometrical body of a sphere is a particular case of an ellipse, the error does not greatly influence the estimate of biovolume. However, if the shape classification is used for other purposes, this must be improved. The specificity is high for cylinders and low for ellipses and spheres. The probability of detection followed the same pattern but always above the 60%.

Cell biovolume estimation

Figure 6 shows the NASS built with biovolume data calculated from area-based, shape-based and automatic-

Table III: Confusion matrix for the taxonomic classification with the parameters to account for the efficiency of the classifier

Manual	Automatic										Probability of detection
	Diatoms	Silicoflagellates	Dinoflagellates	Ciliates	Crustaceans	Others	Detritus	Artefacts	Accuracy per class	Specificity	
Diatoms	3590	10	35	28	1	1915	393	240	1.50	0.97	0.64
Silicoflagellates	3	244	—	2	—	74	51	4	1.18	0.89	0.76
Dinoflagellates	9	2	201	12	—	34	28	2	0.95	0.74	0.78
Ciliates	9	—	7	42	—	11	21	—	0.70	0.42	0.61
Crustaceans	1	—	—	—	3	1	7	1	1.25	0.75	0.60
Others	96	17	28	15	—	11 078	1921	419	0.86	0.84	0.99
Detritus	285	33	59	93	4	4242	27 713	889	—	—	—
Artefacts	101	—	1	4	5	28	729	6944	—	—	—

Efficiency parameters are calculated only for the living organisms groups.

shape-based methods. The NASS of the coastal station has an ordinate higher than the NASS of the shelf station given the higher concentration of particles in the coastal one. The slopes of the regression lines fitted to the NASS were different at the coastal station ($P = 0.0024$, $n = 23$), whereas they were not significantly different at the oceanic station ($P = 0.7283$, $n = 15$). The coastal station is dominated by chain-forming diatoms, and thus the proportion of cylinders relative to the other basic shapes is 75%, with an average aspect ratio (height/diameter) of 0.35. In the oceanic sample, there were a significantly lower proportion of cylinders, around 14%, with an average aspect ratio of 0.40. Given the overestimation of biovolume caused by the utilization of the area-based method, more conspicuous when the cylinders are abundant and with a large height, the regression lines were different. On the other hand, the spectra calculated with the shape-based method, with manual or automatic measures, were not different (coastal: $P = 0.6393$, $n = 21$; oceanic: $P = 0.6016$, $n = 14$), which suggests that the efficiency in shape assignment is sufficiently high to improve the biovolume estimate.

Field evaluation

The parameters of the regression line fitted to the NASS calculated with area-based and automatic-shape-based methods were different only in 13 samples (2.5%). Even when the parameters of the NASS were not different in many cases, the misestimation of biomass is higher than the 20% in 132 samples (14%). In Fig. 7A, where the concentration of carbon ($\mu\text{g C L}^{-1}$) in the sample is plotted against the concentration of carbon that corresponds to chain-forming centric or pennate diatoms, these samples are indicated with grey solid dots. It must be noted that the samples with overestimation higher than 20% are the points closer to the 1:1 relationship, that is, the samples where the biomass of chain-forming diatoms is dominant.

In Fig. 7B the percentage that the biomass of chain-forming centric or pennate diatoms represents of the total biomass in the sample against the percentage of misestimation of the autotrophic biomass is shown. The overestimate of autotrophic biomass is directly proportional to the percentage of biomass that corresponds to chain-forming diatoms. The slope of the regression line between both variables is significantly different from zero ($P < 0.0001$, $n = 882$). The percentage of chain-forming diatoms reaches 71% and their average aspect ratio (height/diameter) per sample range from 0.04 to 0.72 with an average of 0.35.

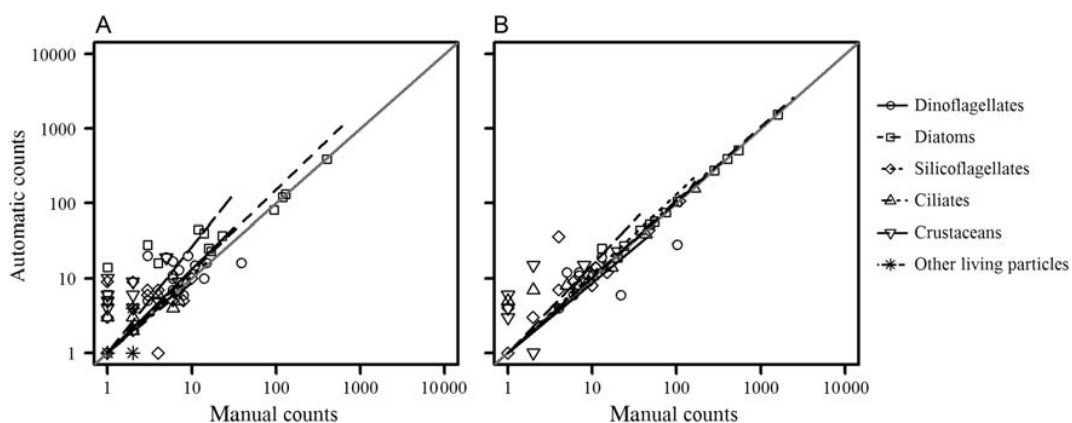


Fig. 5. Comparison of manual and automatic counts per taxonomic class (size range 20–100 μm) for the test samples analysed in (A) autoimage and (B) fluorescence-triggered modes.

Table IV: Confusion matrix for the morphological classification with the parameters to account for the efficiency of the classifier

Manual	Automatic						Accuracy per class	Specificity	Probability of detection
	Cylinder	Discus	Ellipsoid	Sphere	Detritus	Artefacts			
Cylinder	2332	12	161	25	282	593	1.04	0.96	0.92
Discus	28	208	64	1	4	64	1.27	0.88	0.69
Ellipsoid	54	8	974	571	196	89	1.20	0.72	0.61
Sphere	18	9	145	447	40	53	0.59	0.43	0.72
Detritus	241	4	256	72	1047	820	—	—	—
Artefacts	174	—	19	7	59	123	—	—	—

Efficiency parameters are calculated only for the living organisms groups.

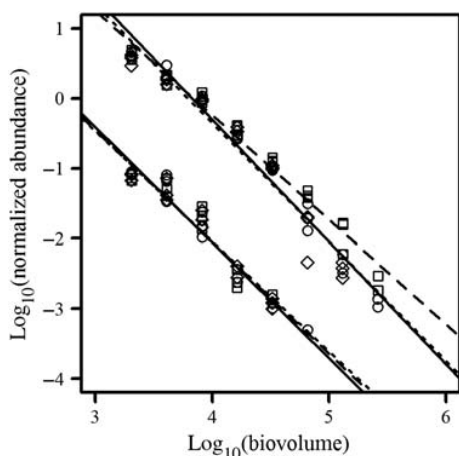


Fig. 6. NASS for FlowCAM counts of two samples, a coastal station in the upper part (i.e. higher normalized abundance) and a shelf station in the lower part of the figure. Biovolume data are calculated with area-based (squares and dashed line), shape-based (dots and solid line) and automatic shape-based methods (diamonds and dotted line).

However, the situation is not the same with the single cell centric diatoms, whose geometrical shape is expected to cause the opposite effect to chain-forming

diatoms (Fig. 7C). The slope of the regression line between the underestimate of autotrophic biomass and the percentage of biomass that corresponds to single cell centric diatoms is not significantly different from zero ($P = 0.1359$, $n = 882$). The percentage of single cell centric diatoms does not exceed 35% in any sample and their aspect ratios (diameter/height) ranged from 0.29 to 0.99 with an average of 0.84.

This means that a relatively high error in biomass estimation could not be detected in the parameters of the size spectrum. However, when more than 20% of the biomass of the sample corresponds to chain-forming centric or pennate diatoms, using the area-based method to estimate the biovolume causes an overestimate of autotrophic biomass higher than the 20%. A 20% or larger biomass corresponding to chain-forming diatoms is not unusual, very common in fact during the spring bloom at temperate and boreal locations.

DISCUSSION

The main objective of automated classification techniques is, most frequently, to estimate the abundance of

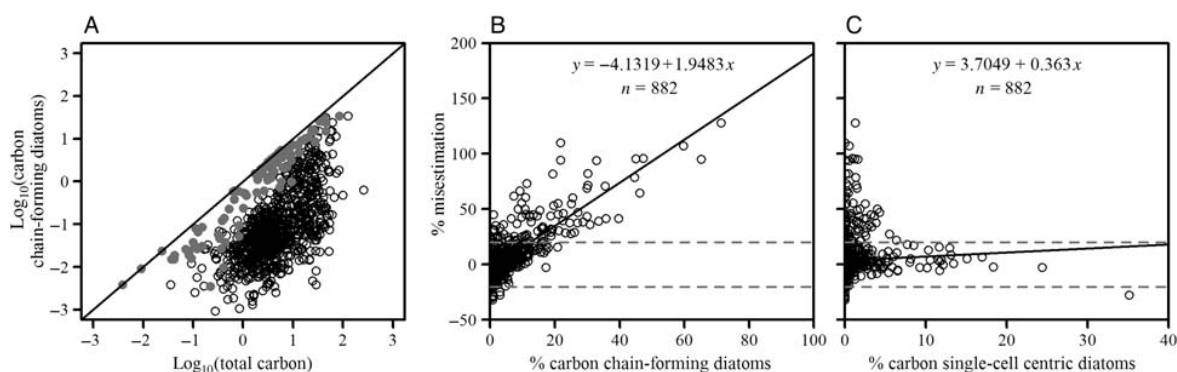


Fig. 7. (A) Relationship between the concentration of total carbon in the samples of the field evaluation set ($\mu\text{g C L}^{-1}$, size range 4–100 μm) and the carbon corresponding to chain-forming diatoms in the size range 20–100 μm . Samples with a misestimate of autotrophic biomass higher than 20% are marked with grey dots. Misestimation of autotrophic biomass versus the relative biomass of (B) chain-forming diatoms (y versus x in A) and (C) single-cell centric diatoms in the sample, with the lineal regression adjustment. Horizontal dotted lines show the error of 20% in the biomass estimate.

each predicted class. Sometimes, however, the research focuses on other ecosystem properties, such as biovolume, biomass or cell attributes (i.e. pigment or carbon content), for which the estimation of cell biovolume is required. The goal of the present study was to improve the estimation of cell biovolume using automated classification of FlowCAM images. With this aim we solved two challenges of the automated classification of plankton images with no additional effort using state-of-the-art automatic classification methods: (1) the need to classifying automatically and with a high specificity (i.e. correct assignation to a given class) a heterogeneous set of images, which include living and non-living particles (artefacts and detritus); and (2) the tendency to misestimate cell biovolume due to the two-dimensionality of the images. These two characteristics of the FlowCAM are common to other image-based devices for plankton identification and enumeration.

The automated classification of plankton images has improved over the last years. For instance, the methods and algorithms explored have been diverse, although in the last years SVM has been the most widely used algorithm. Other authors who have used linear discriminant analysis or random forest algorithms obtained comparable results (Irigoien *et al.*, 2009). In the first attempts at automatic classification of plankton samples the number of classified groups was below 10 while in the last years it has increased to more than 20 (Sosik and Olson, 2007). The description of images began being merely based on shape features but, later, texture features were included, increasing the accuracy of classification considerably (Tang *et al.*, 1998). The accuracy of classification has increased from below 75% to near the 90% (Gorsky *et al.*, 2010), although it depends on the digitization device.

Several aspects can be improved in automated classification of plankton samples. We have carried out a series of tests in order to improve the prediction of particle biomass by the algorithm. However, even when the results have been promising (González *et al.*, 2010), further room for improvement, may arise, according to our experience, from the refinement of the image acquisition stage. One challenge is in the digitization of high-quality images, which permits the extraction of new attributes. Some of them more class-specific, as it has been done with mesoplankton organisms, considering specific structures of each taxonomic class (Tang *et al.*, 2006). Another challenge relies on the improvement of the digitization protocols, in order to be more selective with the particles that are going to be included in the classification. When the training set used to train the classifier is large enough the accuracy of the classification is a property of the classifier and does not depend on the composition of the predicted samples (Solow *et al.*, 2001). However, even if the training set was representative and the accuracy of classification was constant, a large number of non-target images reduce the specificity and probability of detection of the classification, and hence the biovolume or biomass estimates per class are incorrect. Related to this we have shown that the fluorescence-triggered mode obtains better classification efficiencies because it is a much more selective digitization method, recording fewer detritus images. On the other hand, autoimage, a non-selective digitization method, has lower efficiencies.

Non-living particles (i.e. device-specific artefacts and detritus) form a group of recurrent images in the digitization devices that can affect the prediction of new samples, providing poor estimates of biomass of living particles. Artefacts are images recorded by the

digitization devices that do not correspond to any particle in the sample. The characteristics of these artefacts are very specific to the process of acquisition of images of each type of automatic sampling device, and thus it is not possible to develop a general tool to remove them. The ideal situation is to minimize their appearance, but, in case this cannot be achieved, we have shown how a series of filters can be designed taking into account the characteristics of the digitization mechanism. These filters allowed us to remove the artefacts with high confidence, avoiding the need to eliminate them manually, which can be a highly time-consuming process.

The presence of detritus in the samples is, however, a common feature of plankton imaging devices. The problem has been addressed with different strategies by other authors. Some have included detritus in their calculations since they consider it part of the energetics of the ecosystem (San Martín *et al.*, 2006), while others have eliminated it by visual recognition (Barofsky *et al.*, 2010), avoided the digitization of detritus using cell staining (Alcaraz, 2003) or, as we have done, tried to classify them automatically (Irigoin *et al.*, 2009; Zarauz *et al.*, 2009). The automatic method we have developed, based on statistical differences between certain image attributes of detritus and living particles, has improved the classification. We have shown that it is possible to automate the elimination of non-target images before the classification in order to obtain acceptable classification efficiencies in a non-selective digitization method, although the uncertainty in the autoimage samples is still higher than in fluorescence mode. This demonstrated that a previous step designed to eliminate artefacts and detritus is highly recommended. It can be done recording with the images a discriminative variable such as the presence of fluorescence or staining, or using a statistical filter that applied to the description of the images permits discrimination of most of the non-target images.

The second challenge addressed, the problem with the two-dimensionality of the images, is common to several sampling methods including sedimentation techniques for microscopy (Ütermöhl, 1958) or continuous sampling with sample-in-flow techniques such as FlowCAM (Sieracki *et al.*, 1998). In this work the classification scheme we adopted permits not only a taxonomic but also a morphological characterization of the particles. We used the morphological information of the particles provided by the automatic classification to calculate their biovolume, a method similar to the one used by microscopists. The unique requirement is to form groups in the training set having in mind that they must contain individuals of the same taxonomic class and the same morphological class. For instance, if the desired taxonomic resolution includes a taxon class of

diatoms, we can create a group with various diatom species as long as all they can be assigned univocally to a shape class. This way, the prediction of an image to belong to a group provides taxonomic and morphological information that permits the calculation of the biovolume of each particle as a revolution volume specific for its geometric shape. With this information we can implement an automatic-based method that renders comparable results to the microscopy-based method. For nanoplankton cells, smaller than 20 μm in ESD, taxonomic information is not available, since the resolution of the images does not permit the separation of taxonomic groups. Without taxonomy, information about the third dimension cannot be inferred but it has been demonstrated that in nanoplankton cells the measurement of the third dimension can be omitted since most cells can be assumed to be spheres or ellipsoids with equal depth and width (Verity *et al.*, 1992).

SVM classification algorithms have been shown to classify plankton images obtained with FlowCAM with relatively high accuracy (Blaschko *et al.*, 2005). We have applied SVM trained with our morphologically oriented training set together with the filters described above successfully to a data set of FlowCAM plankton images obtained on a seasonal basis in the Bay of Biscay area. The extent of our training set and testing and field evaluation data ensures that the approach is robust and reliable across a range of conditions. The global accuracy we have obtained in classifying morphological and taxonomic classes is comparable to that obtained in similar studies, specifically, in those focused on the classification of microplankton that tested the accuracy over independent natural samples and with a similar number of taxonomic categories considered (Sosik and Olson, 2007). The accuracy per class differs from one class to another; it is lower for the less abundant and more heterogeneous taxonomic classes, such as crustaceans and ciliates. This is a common feature in the automatic classification of plankton due to its heterogeneity and poses, in fact, a specific challenge for the automatic classification of plankton images. The accuracy per class compensates for false negatives excluded from a class with false positives included within it, provided the error is homogeneously distributed. This parameter is a good estimator of the effectiveness in the estimate of abundance per class. On the other hand the specificity evaluates the percentage of cells that really correspond to a certain class in relation to the total cells classified in that class. The specificity must be taken into account as an evaluation parameter when the aim is not only the estimate of abundance but the estimate of another variable related with size. A high specificity is desirable because the error in biovolume estimates can not be

compensated between false assignments. At class level, in the prediction of a taxon class, a high specificity is an indicator of high accuracy in the estimate of biovolume or biomass per class. At individual level, a high specificity in the prediction of shape indicates that the probability of the correct geometrical calculation of biovolume is also high, which implies that the estimate of biovolume per class can be improved.

The shape assignment has been demonstrated to be sufficiently accurate to correct the biovolume estimates based on two-dimensional images. Thus, the discrepancies between the NASS of natural samples constructed using area-based and automatic-shape-based biovolume estimates are expected to be caused by the misestimation of biovolume associated with the area-based method. Cylinders and discuses are the geometric shapes that have more different biovolumes considering area-based or shape-based biovolume. The biovolume of discuses is underestimated and the biovolume of cylinders is overestimated when area-based biovolume is considered: the higher the aspect ratio, the higher the misestimation of biovolume. Single cell centric diatoms, which usually present high aspect ratios, do not cause large underestimation of biovolume if it is calculated with the area-based method. Chain-forming centric or pennate diatoms present lower aspect ratios and can cause large overestimation of biovolume when the area-based method is applied. Thus, in samples with a large proportion of chain-forming centric or pennate diatoms the effect can be conspicuous, although determined by the aspect ratio of the chains. For instance, in a hypothetical sample composed of a 100% of chain-forming diatoms with an aspect ratio of 0.2 or 0.1, the biomass would be, respectively, duplicated or triplicated. A similar effect occurs with the Coulter counter, which tends to underestimate the biomass of cells with a shape differing strongly from spheres (Bakker *et al.*, 1985). That is important when analysing samples, because depending on where and when they are collected and their taxonomic composition, they can be susceptible to poor estimation of biomass or even poor size-structure characterization. The misestimation of autotrophic biomass is presented as an example of the error that can be made assigning biomass to a certain trophic status. This can be important in the analysis of trophic webs or when applying a modelling approach. For instance, in samples collected during the spring bloom, when the abundance of diatoms is high and they represent the main part of the microplankton community, an accurate estimate of biomass is important to estimate, for instance, the transfer of energy and/or the sedimentation of biological carbon.

However, it does not matter how good this new approximation is if it cannot be applied easily to the

analysis of plankton samples. Our approach is easy to use since it adapts the state of the art techniques of automatic classification of plankton. Only two aspects must be considered, the morphological division of the training set and the calculation of biovolume depending on the shape predicted. Both tasks do not imply necessary additional work. For instance, the classification scheme applied by Sosik and Olson (Sosik and Olson, 2007) is susceptible to use this approximation, since their 22 categories are morphologically independent. Besides, the linear dimensions of the cells needed to calculate biovolume as a revolution volume are attributes extracted routinely from plankton images. In fact they have been used recently to estimate biovolume as a revolution volume (Jakobsen and Carstensen, 2011), although without shape differentiation. Gathering both aspects permits substantial improvement of biovolume estimates in a routine work, making our approach a candidate to join the available set of tools developed for automated classification of plankton images.

In summary, an improved method to estimate the biovolume of the cells coupled with an automated image acquisition system, such as FlowCAM, presents obvious advantages. The system can deal with many images providing information at scales of variability that have been inaccessible with traditional methods, but, at the same time providing more accurate biovolume estimation resulting in this information being more reliable.

SUPPLEMENTARY DATA

Supplementary data can be found online at <http://plankt.oxfordjournals.org>.

FUNDING

This work was supported by the Plan de Ciencia, Tecnología e Innovación del Gobierno del Principado de Asturias [project IMAGINA (“Integración de métodos de análisis de imagen de grupos planctónicos con técnicas de inteligencia artificial”) and research grant BP07-081 to E.A.], the Ministerio de Ciencia e Innovación (project PERPLAN, CTM2006-04854/MAR) and the Instituto Español de Oceanografía (projects ECOPEL and RADIALES).

ACKNOWLEDGEMENTS

This is a contribution to SCOR Working Group 130 on Automatic Visual Plankton Identification. We thank the

captain and crew in the R/V Thalassa, the R/V Francisco de Paula Navarro and the R/V José Rioja for their assistance during the cruises of the projects ECOPEL (“Ecología de pequeños pelágicos”), PERPLAN (“Efecto de las perturbaciones meteorológico-hidrográficas en la estructura de comunidad planctónica”, CTM2006-04854/MAR) and RADIALES (“Programa de series temporales oceanográficas”) that provided the data set for the present work. We are indebted to all participants in the cruises for their work at sea and in the laboratory.

REFERENCES

- Alcaraz, M. (2003) Estimating zooplankton biomass through image analysis. *Mar. Biol.*, **143**, 307–315.
- Álvarez, E., López-Urrutia, A., Nogueira, E. *et al.* (2011) How to effectively sample the plankton size spectrum? A case study using FlowCAM. *J. Plankton Res.*, **33**, 1119–1133.
- Bakker, C., Prins, T. C. and Tackx, M. L. M. (1985) Interpretation of particle spectra of electronic counters by microscopical methods. *Hydrobiol. Bull.*, **19**, 49–59.
- Barofsky, A., Simonelli, P., Vidoudez, C. *et al.* (2010) Growth phase of the diatom *Skeletonema marinoi* influences the metabolic profile of the cells and the selective feeding of the copepod *Calanus* spp. *J. Plankton Res.*, **32**, 263–272.
- Benfield, M. C., Grosjean, P., Culverhouse, P. *et al.* (2007) RAPID: research on automated plankton identification. *Oceanography*, **20**, 12–26.
- Blaschko, M. B., Holness, G., Mattar, M. A. *et al.* (2005) Automatic *in situ* identification of plankton. *Proceedings of the Seventh IEEE Workshops on Application of Computer Vision (WACV/MOTION'05)*, **1**, 79–86.
- Cermeno, P. and Figueiras, F. G. (2008) Species richness and cell-size distribution: size structure of phytoplankton communities. *Mar. Ecol. Prog. Ser.*, **357**, 79–85.
- Chang, C.-C. and Lin, C.-J. (2009) LIBSVM: a Library for Support Vector Machines. <http://www.csie.ntu.edu.tw/~cjlin/libsvm/>.
- Davis, C. S., Hu, Q., Gallager, S. M. *et al.* (2004) Real-time observation of taxa-specific plankton distributions: an optical sampling method. *Mar. Ecol. Prog. Ser.*, **284**, 77–96.
- Dodson, A. N. and Thomas, W. H. (1978) Reverse filtration. In Sournia, A. (ed.), *Phytoplankton Manual*. UNESCO, Paris, pp. 104–107.
- González, P., Díez, J., Del Coz, J. J. *et al.* (2010) Predicción taxonómica de muestras de microplankton usando técnicas de Aprendizaje Automático. In Troncoso, A. and Riquelme, J. C. (eds), *Actas del V Simposio de Teoría y Aplicaciones de Minería de Datos (TAMIDA 2010)*. Ibergaceta Publicaciones, Madrid, pp. 319–328.
- Gorsky, G., Ohman, M. D., Picheral, M. *et al.* (2010) Digital zooplankton image analysis using the ZooScan integrated system. *J. Plankton Res.*, **32**, 285–303.
- Grosjean, P. (2005) Analyze your plankton through digitized images. <http://www.sciviews.org/zooimage/index.html>.
- Grosjean, P., Picheral, M., Warembourg, C. *et al.* (2004) Enumeration, measurement and identification of net zooplankton samples using the ZOOSCAN digital imaging system. *ICES J. Mar. Sci.*, **61**, 518–525.
- Haralick, R. M., Shanmugam, K. and Deinstein, I. (1979) Textural features for image classification. *IEEE Trans. Syst. Man Cyber.*, **6**, 610–621.
- Hillebrand, H., Dürselen, C.-D., Kirschtel, D. *et al.* (1999) Biovolume calculation for pelagic and benthic microalgae. *J. Phycol.*, **35**, 403–4424.
- Hu, M. K. (1962) Visual pattern recognition by moment invariants. *IRE Trans. Info. Theory*, **8**, 179–187.
- Irigoien, X., Fernandes, J. A., Grosjean, P. *et al.* (2009) Spring zooplankton distribution in the Bay of Biscay from 1998 to 2006 in relation with anchovy recruitment. *J. Plankton Res.*, **31**, 1–17.
- Jakobsen, H. H. and Carstensen, J. (2011) FlowCAM: sizing cells and understanding the impact of size distributions on biovolume of planktonic community structure. *Aquat. Microb. Ecol.*, **65**, 75–87.
- Karatzoglou, A., Meyer, D. and Hornik, K. (2006) Support Vector Machines in R. *J. Stat. Softw.*, **15**, 1–28.
- Luo, T., Kramer, K., Goldgof, D. B. *et al.* (2004) Recognizing plankton images from the shadow image particle profiling evaluation recorder. *IEEE Trans. Syst. Man Cyber. B*, **34**, 1753–1762.
- Menden-Deuer, S., Lessard, E. J. and Satterberg, J. (2000) Carbon to volume relationships for dinoflagellates, diatoms and other protist plankton. *Limnol. Oceanogr.*, **45**, 569–579.
- Pau, G., Fuchs, F., Sklyar, O. *et al.* (2010) EBImage—an R package for image processing with applications to cellular phenotypes. *Bioinformatics*, **26**, 979–981.
- Peters, A. and Hothorn, T. (2009) ipred: Improved Predictors. R Package Version 0.8-8. <http://CRAN.R-project.org/package=ipred>.
- Quiñones, R. A., Platt, T. and Rodríguez, J. (2003) Patterns of biomass-size spectra from oligotrophic waters of the Northwest Atlantic. *Prog. Oceanogr.*, **57**, 405–427.
- Rodríguez, J. and Mullin, M. M. (1986) Relation between biomass and body weight of plankton in a steady state oceanic ecosystem. *Limnol. Oceanogr.*, **31**, 361–370.
- San Martín, E., Irigoien, X., Harris, R. P. *et al.* (2006) Variation in the transfer of energy in marine plankton along a productivity gradient in the Atlantic Ocean. *Limnol. Oceanogr.*, **51**, 2084–2091.
- Sheldon, R. W. and Parsons, T. R. (1967) *A Practical Manual on the Use of the Coulter Counter in Marine Science*. Coulter Electronics, Toronto, pp. 66.
- Sheldon, R. W., Prakash, A. and Sutcliffe, W. H. Jr (1972) The size distribution of particles in the ocean. *Limnol. Oceanogr.*, **17**, 327–340.
- Sieracki, C. K., Sieracki, M. E. and Yentsch, C. S. (1998) An imaging-in-flow system for automated analysis of marine microplankton. *Mar. Ecol. Prog. Ser.*, **168**, 285–296.
- Sklyar, O. and Huber, W. (2006) Image analysis for microscopy screens—image analysis and processing with EBImage. *The Newsletter of the R Project*, **6**, 12–16.
- Solow, A., Davis, C. and Hu, Q. (2001) Estimating the taxonomic composition of a sample when individuals are classified with error. *Mar. Ecol. Prog. Ser.*, **216**, 309–311.
- Sosik, H. M. and Olson, R. J. (2007) Automated taxonomic classification of phytoplankton sampled with imaging-in-flow cytometry. *Limnol. Oceanogr. Meth.*, **5**, 204–216.
- Tang, X., Lin, F., Samson, S. *et al.* (2006) Binary plankton image classification. *IEEE J. Oceanic Eng.*, **31**, 728–735.
- Tang, X., Stewart, W. K., Vincent, L. *et al.* (1998) Automatic plankton image recognition. *Artif. Intell. Rev.*, **12**, 177–199.

- Utermöhl, H. (1958) Zur Vervollkommnung der quantitativen Phytoplankton-Methodik. *Mitt. Int. Ver. Theor. Angew. Limnol.*, **9**, 1–38.
- Zarauz, L., Irigoien, X. and Fernandes, J. A. (2009) Changes in plankton size structure and composition, during the generation of a phytoplankton bloom, in the central Cantabrian Sea. *J. Plankton Res.*, **31**, 193–207.
- Zarauz, L., Irigoien, X., Urtizberea, A. *et al.* (2007) Mapping plankton distribution in the Bay of Biscay during three consecutive spring surveys. *Mar. Ecol. Prog. Ser.*, **345**, 27–39.
- Zernike, F. (1934) Beugungstheorie des Schneidenverfahrens und seiner verbesserten Form, der Phasenkontrastmethode (Diffraction theory of the cut procedure and its improved form, the phase contrast method). *Physica*, **1**, 689–704.

Supplementary material

R implementation of the importation and image analysis of FlowCAM files to the Zoo/PhytoImage convention

Introduction

Various functions were written in R (R_Development_Core_Team, 2010) to transform the raw files generated by the FlowCAM software (VisualSpreadsheet) into a file that matches the Zoo/PhytoImage (Grosjean, 2005) requirements. The result follows the Zoo/PhytoImage convention in terms of name of the samples, inclusion of metadata, name and format of the images and description of the images. Thanks to this adaptation FlowCAM images can be compared with images coming from other sources, analyzed in the Zoo/PhytoImage or other platforms.

Requirements

The R package EBIImage (Sklyar *et al.*, 2011) was used for this implementation. The function `make.RData()` provided in Zoo/PhytoImage (Grosjean, 2005) and the package `svMisc` (Grosjean, 2011) were also needed. The functions are checked for R running on Windows and for FlowCAM samples obtained with software versions of VisualSpreadsheet between 1.5.14 and 2.2.7.

Previous work

The disposition of the archives to be processed is shown in Figure S1. Our functions are prepared to process a folder (Cruise) containing one or various samples. Each sample processed has an independent folder (Sample_1); inside this folder the raw files generated by the FlowCAM, that can be a variable number, must be placed. The raw files generated by the FlowCAM must maintain the format of the name given by the FlowCAM (000-000001). For each raw file the data of all particles must be exported to a CSV file with the option File>Export Data in VisualSpreadsheet. It is necessary to generate a metadata file named ZIM.csv and placed in the basis folder (Fig. S1). The metadata file must contain the fields shown in Table SI, which must be populated for each sample.

R implementation

The functions contained in *Alvarez_et_al_Rfunctions.txt* implement the importation method as it is described by Álvarez *et al.* The function `process()` is the one to work with, it will call the other functions, all must be read previously with a `source()` function. At the end of the processing a warning is displayed but it must be omitted.

The function `process()` has two inputs:

folder: path to the folder where the samples together with the ZIM.csv file are placed. All the result files will be placed on this location (Fig. S1).

COLOR: if FALSE is specified the particle images are stored in grey scale, if TRUE the colour images are stored when available.

The function returns three new folders:

1_Ordered: that contains the original files with the conventional name and their metadata in a notes file to make self-referenced. It can be used to store in disk.

2_Processed: that contains the processed files, one folder per sample containing the separated images with the conventional name, their metadata and data in a .zim file and data in a Rdata file. It can be used to collect images for the training set or to store in disk.

3_ProRdata: that contains a .Rdata file for each sample, if the sample was formed by various FlowCAM analysis, they are all merged in one file to facilitate the calculations. It can be used to be predicted and analyzed.

Table SI Fields to be populated in the metadata file (ZIM.csv), their description and examples. Fields from *Series* to *Code* are used to form the name of the sample under the Zoo/PhytoImage convention (in the example it will be *WEE006.2010-03-28.000.F1+C*). To find details about the formation of sample names under the Zoo/PhytoImage convention see (Grosjean, 2005). The three fields concerning sample volume are crucial; in the example exposed volumes correspond to a sample processed in triggered mode: 1000 mL were concentrated down to 20 mL and only 10 mL were processed with the FlowCAM. In samples processed in autoimage, the three volumes must be populated with the same value.

Field	Content	Example
File	Raw name of the sample	14
Series	Code for the series (maximum one digit)	W
Cruise	Code for the cruise (maximum two digits)	EE
Station	Code for the sampling station (maximum three digits)	6
Year	Year	2010
Month	Month	3
Day	Day	28
Mode	Code to distinguish working modes (maximum one digit)	F
Replicate	Code to distinguish replicates(maximum one digit)	1
Code	Code to distinguish size-fractions or subsamples. (maximum one digit)	C
Min	Minimum size in μm (if there are not lower limit: -1)	15
Max	Maximum size in μm (if there are not higher limit: -1)	100
LocationName	Name of the sampling location	BayofBiscay
LocationLatitude	Decimal latitude ($^{\circ}$)	42.2548
LocationLongitude	Decimal longitude ($^{\circ}$)	-8.9497
LocationDepth	Depth of sampling (m)	0
TotalVolume	Initial volume (mL)	1000
ConcentratedVolume	Concentrated volume (mL)	20
NetVolume	Volume processed with the FlowCAM (mL)	10

The files obtained match the requirements of Zoo/PhytoImage. So, from here, all calculations can be done with the Zoo/PhytoImage platform. In *Alvarez et al.* we use Zoo/PhytoImage functions for the generation of the training and testing tests but we choose to work with the LIBSVM (Chang & Lin, 2009) for image classification, since the Support Vector Machine (SVM) algorithm is not implemented in Zoo/PhytoImage yet.

Example:

```
source("C:/.../Alvarez_et_al_Rfunctions.txt")
folder<-"C:/.../Cruise"
process(folder, COLOR=TRUE)
```

Reproducing Álvarez et al. results

All this code, as well as some pre- and post-processed examples, can be found at: <http://planktonimages.wordpress.com>

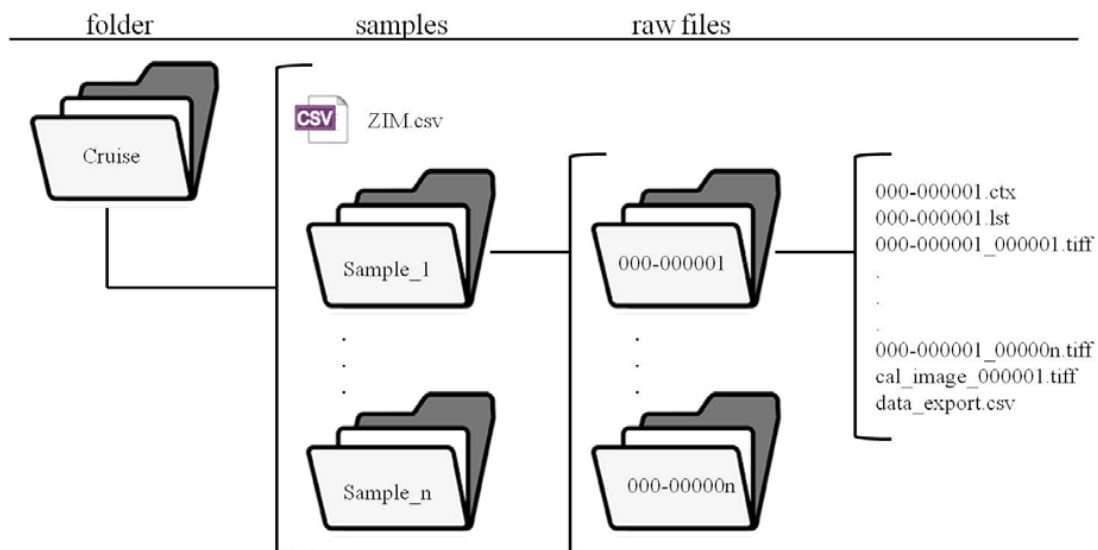


Figure S1 Input for the function process(). The argument folder corresponds to the path where the samples are contained. Additionally a ZIM.csv file containing all the metadata of the samples must be included. Each sample folder must contain the original folders stored by FlowCAM with its raw name (ddd-hhmmss), it can go from one to n, later they will be combined into one file. Along the files generated by VisualSpreadsheet must be the data_export.csv file, exported after each FlowCAM analysis.

References

- Chang, C.-C. and Lin, C.-J. (2009) LIBSVM: a Library for Support Vector Machines. <http://www.csie.ntu.edu.tw/~cjlin/libsvm/>.
- Grosjean, P. (2005) Analyze your plankton through digitized images. <http://www.sciviews.org/zooimage/index.html>.
- Grosjean, P. (2011) SciViews: A GUI API for R. <http://www.sciviews.org/SciViews-R/>.
- R_Development_Core_Team (2010) R: A language and environment for statistical computing. <http://www.R-project.org>.
- Sklyar, O., Pau, G., Smith, M. and Huber, W. (2011) EBImage: Image processing toolbox for R. <http://bioconductor.org/packages/2.9/bioc/html/EBImage.html>.

Impact factor report

Abbreviated Journal Title	J Plankton Res
ISSN	0142-7873

JCR Data	Total Cites	5753
	Impact Factor	2.435
	5-Year Impact Factor	2.423
	Immediacy Index	0.725
	Articles	91
	Cited Half-life	>10.0
<i>Eigenfactor</i>[®] Metrics	<i>Eigenfactor</i>[®] Score	0.00975
	<i>Article Influence</i>[®] Score	0.894

Source: Journal Citation Reports, Science Edition 2012 (Thomson Reuters).

Chapter III. Routine determination of plankton community composition and size structure: a comparison between FlowCAM and light microscopy

Once abundance, size and taxonomy have been obtained from FlowCAM one can wonder how this data compare with the traditional methods for plankton enumeration. In this chapter we compared FlowCAM and light microscopy as methods for the routine determination of the composition and size-structure of the planktonic community. The effects of the preservation of the sample and the inaccuracies in the automatic classification are the mainsprings discrepancies in the determination of size-structure between both methods. Nevertheless, the synoptic vision of the seasonal variation in abundance, biomass and diversity obtained was similar, which suggests that the fully automatic method is adequate for exploring these variations.

Reference

Eva Álvarez, Marta Moyano, Ángel López-Urrutia, Enrique Nogueira and Renate Scharek (2014) Routine determination of plankton community composition and size structure: a comparison between FlowCAM and light microscopy. *Journal of Plankton Research*, 36(1): 170-184.

Candidate's contribution

My contribution to the work includes the co-design of the study and the establishment of methodology. I conducted the experiments and obtained data from FlowCAM whereas RS and MM obtained data from light microscopy. I analyzed data, prepared tables and figures and composed and co-write the article with substantial contributions of EN and AL-U. All authors discussed the results and commented on the manuscript.



J. Plankton Res. (2014) 36(1): 170–184. First published online July 28, 2013 doi:10.1093/plankt/fbt069

Routine determination of plankton community composition and size structure: a comparison between FlowCAM and light microscopy

EVA ÁLVAREZ*, MARTA MOYANO†, ÁNGEL LÓPEZ-URRUTIA, ENRIQUE NOGUEIRA AND RENATE SCHAREK
INSTITUTO ESPAÑOL DE OCEANOGRAFÍA, CENTRO OCEANOGRÁFICO DE GIJÓN, 33212 GIJÓN, SPAIN

†PRESENT ADDRESS: INSTITUTE FOR HYDROBIOLOGY AND FISHERIES SCIENCE, UNIVERSITY OF HAMBURG, OLBERSWEG, 24, 22767, HAMBURG, GERMANY

*CORRESPONDING AUTHOR: eva.alvarez@gi.ieo.es

Received November 2, 2012; accepted July 4, 2013

Corresponding editor: John Dolan

Samples from a monthly monitoring programme in the Cantabrian Sea were analysed with a FlowCAM-based automated technique. The estimates of abundance, biomass size spectra and taxonomic diversity of nano- and microplankton communities were compared with those obtained by traditional microscopical analysis of the same samples. The structure and abundance of a preserved plankton sample determined using FlowCAM showed minimal differences compared with traditional microscopical estimates. The effects of sample preservation and inaccuracies in the automatic classification are the main causes of discrepancies in the size structure determination between the two approaches. However, the synoptic understanding of the seasonal variation in the abundance, biomass and diversity obtained from the two methods is similar. Our results suggest that the natural variations in the community attributes explored are of greater magnitude than the error introduced by the methods and that the fully automatic method is adequate to explore these variations.

KEYWORDS: abundance; biovolume; biomass; size spectra; diversity; seasonal cycle; light microscopy; FlowCAM

INTRODUCTION

The demanding task of gathering information on plankton composition and abundance has traditionally relied on taxonomists who identify and enumerate specimens under the microscope. The Utermöhl method is the most widely used protocol to enumerate nano- and microplankton (Utermöhl, 1958). To estimate cell biovolume, experts describe each taxonomic group by a geometrical shape (Hillebrand *et al.*, 1999), and estimate a suitable number of linear dimensions, either by direct measurement or by using known aspect ratios (Olenina *et al.*, 2006). This traditional method is highly time-consuming and thus imposes limitations on the number of samples that can be processed. In addition, the use of fixatives to preserve samples introduces biases in the biovolume estimates due to cell shrinkage (Montagnes *et al.*, 1994). This traditional technique is considered to be the most accurate for the identification and enumeration of nano- and microplankton and is the benchmark methodology. Nevertheless, several human factors such as fatigue and inexperience of the operator can affect the quality of the analysis (Culverhouse *et al.*, 2003).

Over the past two decades, combinations of automated sampling devices, image analysis technologies and machine learning algorithms have been developed to count and size plankton organisms more rapidly (Benfield *et al.*, 2007). However, all methods for plankton enumeration have uncertainties when estimating the actual composition and abundance of the community, and the proper interpretation of the results requires assessment of the confidence limits of each method. The reliability of the data provided by new automated methods based on image analysis is still under assessment. There is a need to demonstrate their benefits and disadvantages through comparison against the standard, traditional methods (Jakobsen and Carstensen, 2011).

The Flow Cytometer And Microscope (FlowCAM) is an automated technique for particle enumeration that combines flow cytometry and microscopy (Sieracki *et al.*, 1998). It adds to the growing collection of methods for plankton enumeration based on image analysis. The characteristic step of all these systems is representation of the organisms present in a water sample by a set of images, a process called digitalization. In the FlowCAM, digitalization is based on the capture of images from a water sample flowing through a rectangular glass chamber, the flow cell. A microscope lens coupled to the digital camera magnifies the particles up to 200 times and a calibration factor (microns per pixel) provides their actual size. Depending on the instrument setup and microscope objective used, the FlowCAM can detect

cells or particles that range from 3 to 3000 μm in size. One advantage of FlowCAM is that samples can be digitized *in vivo* eliminating the need for preservation (Zarauz and Irigoien, 2008). Image analysis of FlowCAM digitized images provides precise estimates of the abundance and size of particles (Sieracki *et al.*, 1998; See *et al.*, 2005; Buskey and Hyatt, 2006; Ide *et al.*, 2008; Álvarez *et al.*, 2011). Automatic classification techniques based on pattern recognition provide accuracies reliable enough for most ecological studies (Blaschko *et al.*, 2005; Zarauz *et al.*, 2009; Álvarez *et al.*, 2012). However, traditional microscopy can easily identify cells to the species level, whereas automated methods that utilize automatic classification of images (obtained from FlowCAM or other automatic sampling devices) usually attain a taxonomic level of genus or above. The tendency to misestimate cell biovolume due to the two-dimensionality of the images can be overcome with the currently applied analysis algorithms that take into account the three-dimensional shape of the particles in estimating their biovolume (Álvarez *et al.*, 2012; Moberg and Sosik, 2012). Hence, FlowCAM sampling coupled with an automatic classification of the images generated aims to obtain information comparable with that provided by microscopy but with minimum human intervention, considerably reducing the sample processing time and the dependence on the operator.

FlowCAM can be considered complimentary to microscopy. It provides an analysis with low taxonomic resolution at a high rate, while traditional microscopy can achieve higher taxonomic resolution for a lesser number of samples. Nevertheless, the estimates of abundance, size structure and taxonomic composition obtained by both methods should be comparable. The aim of this work is to assess the similarity in the characterization of nano- and microplankton communities obtained with FlowCAM and with traditional microscopy. Sample acquisition for the comparison was simultaneous, but sample treatment and counting strategy followed the specific protocol for each method. The intention was to compare not only the counting and sizing ability of the methods, but their full capability to characterize the attributes of the plankton community.

METHOD

Monthly sampling was carried out in the central Cantabrian Sea in the framework of the time series monitoring program RADIALES (Oceanographic Time Series Program; <http://www.seriestemporales-ieo.com>).

Seawater samples were taken with a rosette sampler system at 2, 30 and 75 m from November 2008 to March 2010 at a coastal station (43.67°N, 5.58°W, bottom-depth = 100 m). Subsamples (1 L) to be analysed fresh with FlowCAM were pre-filtered at sea with a 200 µm mesh, kept fresh, stored in the dark and analysed in the laboratory within 3 h after collection. Subsamples (100 mL) for analysis of preserved samples with both microscopy and FlowCAM were poured into brown glass bottles with acid Lugol's solution and kept in the dark until analysis.

FlowCAM counts

Fresh samples were analysed with FlowCAM using two working modes. In autoimage mode, FlowCAM takes photographs at a fixed rate and the net sample volume imaged depends on the number of photographs taken. In fluorescence-triggered mode, digital images are taken of only those particles that emit red fluorescence, and the net sample volume imaged is roughly a third of the volume poured into the instrument. In both working modes, FlowCAM images only a subset of the particles in the sample and calculates their concentration taking into account the net sampled volume. An un-concentrated subsample was filtered with a 53 µm mesh and used for analysis at ×200 magnification (×20 objective and 50 µm flow cell), both in autoimage (20 000 photos, 30 min sample processing time) and in fluorescence-triggered mode (1 mL, 30 min sample processing time). A concentrated subsample (1 L down to around 20 mL) was filtered with a 100 µm mesh and used for analysis at ×100 magnification (×10 objective and 100 µm flow cell), both in autoimage (20 000 photos, 30 min sample processing time) and in fluorescence-triggered mode (10 mL, 30 min sample processing time). To minimize the damage to living cells, samples were concentrated by reverse filtration (Dodson and Thomas, 1978) through a 15 µm mesh. The preserved samples were not concentrated because of the small volume of the sample. They were analysed in two working modes: autoimage and side-scatter-triggered. In the latter, FlowCAM digitizes all particles scattering light and the net sample volume imaged is roughly a third of the volume poured into the instrument. Preserved samples were filtered with a 53 µm mesh and analysed at ×200 magnification in autoimage mode (40 000 photos, 1 h sample processing time) and filtered with a 100 µm mesh and analyzed with ×100 magnification in side-scatter-triggered mode (15 mL, 3 h sample processing time). Hence, three subsamples described each sample: one analysed in fluorescence-triggered mode to account for the autotrophic nano- and microplankton community, one

analysed in autoimage mode to account for the whole nano- and microplankton community in fresh samples and one analysed in both autoimage and side-scatter-triggered mode to account for the whole nano- and microplankton community in preserved samples.

Classification of FlowCAM images

For preserved samples, the images were sorted as living versus non-living particles by visual inspection. Biovolume was calculated from the equivalent spherical diameter of the particle (called ABD diameter in the FlowCAM software), corrected for shrinkage (Montagnes *et al.*, 1994) and converted to carbon content (Menden-Deuer *et al.*, 2000). For fresh samples, in order to obtain taxonomic information from the FlowCAM images, we applied the automatic classification technique described by Álvarez *et al.* (Álvarez *et al.*, 2012). Briefly, the technique applies an image analysis algorithm to describe numerically each image recorded by the FlowCAM. The Support Vector Machine (SVM) algorithm then separates the particles into 34 groups. These 34 groups are merged from a taxonomic point of view into seven “functional classes” (diatoms, silicoflagellates, dinoflagellates, ciliates, crustaceans, other living particles and detritus) and from a morphological perspective as four “shape classes” (spheres, ellipsoids, cylinders and discs). Simplification of taxonomic categories permits comparison with other methods whose taxonomic resolution is not the same as that attained by the automatic classification. Morphological description of particles, although only as simple geometrical shapes, gives a better estimation of cell biovolume and allows comparison with methods not based on two-dimensional images. Hence, the automated classification of the samples produced both a functional class and a simple shape assignment for each image. Particle biovolume was calculated as a revolution volume appropriate to the assigned simple shape and the dimensions (length and width) measured by the image analysis. Biovolume was converted to carbon according to the functional class predicted. Different conversion factors were applied for cells smaller than 3000 µm³, cells larger than 3000 µm³ except diatoms and diatoms larger than 3000 µm³ (Menden-Deuer *et al.*, 2000).

Microscopy counts

For microscopical analyses, the samples preserved in Lugol's solution were enumerated following the Utermöhl technique (Utermöhl, 1958; Edler and Elbrächter, 2010). Between 25 and 50 mL of the sample were dispensed into settling chambers and cells were allowed to settle for at least 15 and up to 30 h. Cells were

counted with $\times 100$, $\times 200$ and $\times 400$ magnifications using a NIKON inverted microscope in evenly spaced stripes. Whenever possible, organisms were classified at the species or genus level. A total of 144 taxonomic groups were identified in the 17 samples analysed. Some of these taxa were separated into several size classes (e.g., *Chaetoceros* subgenus *Phaeoceros* 10–20 μm and 20–40 μm) given their wide size ranges (Olenina *et al.*, 2006).

Biovolume estimation on microscopy counts


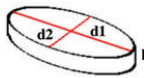
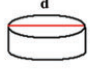
The initial database for microscopical counts consists of a series of taxonomic groups and their estimated abundances in each sample. Starting from the taxonomic information, we made several inferences to obtain information about the biovolume and the trophic status of each taxonomic group. Table I shows an example of this treatment for a given taxon (*Chaetoceros compressus*). Each taxon was assigned to a functional class (diatoms, silicoflagellates, dinoflagellates, ciliates or other living particles) to match the taxonomic resolution of the FlowCAM (Supplementary data, Correspondances). In addition, each taxon was assigned to a trophic status (heterotrophic or autotrophic/mixotrophic) in order to make possible comparison with the results provided by the different FlowCAM working modes. The shape of each taxonomic group was defined according to composite geometric bodies extracted from the literature (Hillebrand *et al.*, 1999; Sun and Liu, 2003; Olenina *et al.*, 2006), obtaining a total of 24 composite shapes for the taxonomic groups present in the samples analysed. Those 24 composite shapes were simplified to three: sphere, ellipsoid and cylinder (Supplementary data, Correspondances). The linear measurements needed to describe a composite shape ranged from only one (e.g. sphere) to seven (e.g. flattened ellipsoid + cylinder + two

cones). For each taxonomic group, the range of these composite cell dimensions was taken from the literature (Cupp, 1977; Dodge, 1982; Tomas, 1997; Bérard-Therriault *et al.*, 1999; Olenina *et al.*, 2006). Since simple shapes are only defined by two linear measurements (length and width), composite cell dimensions were reduced to simple cell dimensions considering only the main body of the cell and its most likely orientation on a flat surface. Minimum and maximum cell biovolume for each taxonomic group was calculated as a revolution volume considering the simple shape and the range of cell dimensions. Cell biovolumes were converted to carbon as previously described (Menden-Deuer *et al.*, 2000).

Cell biovolume inferred from a subset of cells

An important difference between traditional and automated methods for plankton enumeration is the fact that with the latter it is possible to count and measure all cells imaged during the analysis of a sample. Traditional microscopic methods only allow measurement of a limited number of cells or use previously published cell dimensions. In order to analyse the effect of measuring only a subset of cells during microscopical analyses, we used two approximations to assign biovolume to each of the cells counted in the taxonomic group. First, the biovolume of every cell counted was assumed to be equal to the average biovolume of the taxon (“average biovolume”), which is the most widely used method for analysis of the size structure of nano- and microplankton using microscopy (e.g. Cermeño and Figueiras, 2008; Huete-Ortega *et al.*, 2010). However, cells within a population do not have equal sizes, rather their biovolumes distribute within the range defined by the maximum and

Table I: Example of the treatment given to each taxonomic group found in the microscopy counts to obtain information about the biovolume of each cell

Taxonomical group	Functional class	Trophic status	Composite shape			Simple shape				
<i>Chaetoceros compressus</i>	Diatoms	Autotrophic	Oval cylinder			Cylinder				
			Composite cell dimensions (μm)		min	max	Simple cell dimensions (μm)		min	max
			Height (h)	5	14		Height (h)	5	14	
			Diameter (d1)	5	10		Diameter (d)	5	10	
			Diameter (d2)	4.25	8.5					
Biovolumerange of the group:			Min and max simple biovolumes							

Two biovolume data sets were considered: average and distributed biovolume. Composite shape and cell dimensions from Olenina *et al.* (2006). See online supplementary data for a colour version of this table.

the minimum of the species. Consequently, the second approximation assigns a biovolume to each cell within the biovolume range of the group (“distributed biovolume”). In the case of species counted only in one size category, we considered the cell biovolumes to be normally distributed and assigned a random-Normal value from a distribution with the appropriate mean size and a standard deviation equal to 0.21 times the range (maximum–minimum). In the case of groups combining several species (i.e. Ciliates) or species divided in several size classes (i.e. the taxonomist counted cells of taxon in two size categories; for example, *Chaetoceros* subgenus *Phaeoceros* 10–20 μm and *C. sg Phaeoceros* 20–40 μm), we considered uniform distributions of biovolumes.

Size spectra

In order to establish a basis for further comparisons, the characteristics of the community were estimated separately for distinct biovolume classes. In order to obtain the abundance size spectrum (ASS) and the biomass size spectrum (BSS), cell abundance (cells L^{-1}) and biomass ($\mu\text{g C L}^{-1}$) were distributed in biovolume classes established on an octave scale, from 2^4 to 2^{18} μm^3 in biovolume, which corresponds to a size range from 3 to 100 μm of equivalent spherical diameter. The ASS and the BSS conform to a power law:

$$N_s = a \times S^b \quad (1)$$

where s is the lower limit of the biovolume class, s is also the width of the class interval, N is the abundance in the biovolume class and a and b are the parameters of the power law. The ASS and the BSS were normalized by dividing each class by its width in biovolume units (Δs), obtaining the normalized abundance size spectrum (NASS) and the normalized biomass size spectrum (NBSS), both of which follow a linear relationship when plotted in a log–log scale:

$$\log\left(\frac{N_s}{\Delta s}\right) = \log(a) + b \times \log(S) \quad (2)$$

The slope (b) and the intercept ($\log(a)$) of the NASS for each sample were estimated by fitting a linear regression model to the points of each normalized spectrum. To avoid biases in the calculation of the spectra due to curvature at the extremes of the size range, we rejected those biovolume classes with less than 5 cell counts or located to the left of the modal class (García *et al.*, 1994).

Diversity

Species diversity may be defined as a measure of species composition, in terms of both the number of species and

their relative abundances (Legendre and Legendre, 1998). The taxonomic richness (S) simply takes into account the number of taxonomic groups present in the community, whereas higher order indices, such as Shannon’s index (H), consider also the relative abundance of each group:

$$H = - \sum_{i=1}^q p_i \times \log(p_i) \quad (3)$$

where q is the number of taxonomic groups and P the abundance of each group relative to the total abundance. Indices S and H were estimated from both FlowCAM and microscopical counts. For microscopy data, we considered the 144 taxonomic groups identified and their abundances, whereas for FlowCAM data, we used the 34 groups and their abundances provided by the automatic classification. The calculation of diversity indices only considered individuals in reliably sampled biovolume classes. A biovolume class was considered reliably sampled when the abundance obtained with FlowCAM did not exceed double or fall below half of the abundance obtained with light microscopy.

RESULTS

Size spectra estimation from microscopy counts

As previous studies have shown, there are no significant differences between composite shapes and simple shapes for estimating the biovolume of cells in order to characterize size spectra (Menden-Deuer *et al.*, 2000), with the advantage that the latter method requires measurement of only two cell dimensions. The most widely used biovolume method for microscopy is to estimate an average for a subset of cells and assign that average biovolume to all cells of a given taxon. That is not realistic. When we measured every cell counted during analysis of a sample using the FlowCAM analysis, distributions of cell biovolumes emerged (Fig. 1). The biovolume distributions estimated from FlowCAM images for four exemplary species of microplankton span at least two biovolume classes of the size spectra (delimited by the vertical lines in Fig. 1). These biovolume distributions were approximately Normal. Hence, to infer the Normal distribution for the species analysed by microscopy for which only the biovolume range was available, we calculated the ratio between the standard deviation of the biovolume distribution and the biovolume range based on these four exemplary species. This ratio was very similar for the four species (0.2125 ± 0.0374). Hence, the Normal distribution for each species was calculated using the average of the

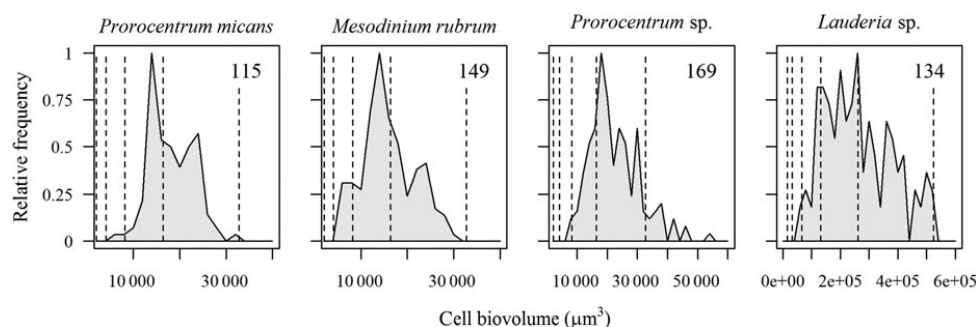


Fig. 1. Biovolume frequency for cells of four selected species present in natural samples analysed with FlowCAM: *Prorocentrum micans*, *Prorocentrum* sp. (dinoflagellates), *Mesodinium rubrum* (ciliate) and *Lauderia* sp. (chain-forming diatom). Vertical lines show the limits of the biovolume classes of the size spectra to indicate how a single species can spread through several biovolume classes. The number in the upper right corner of each panel indicates the total number of cells.

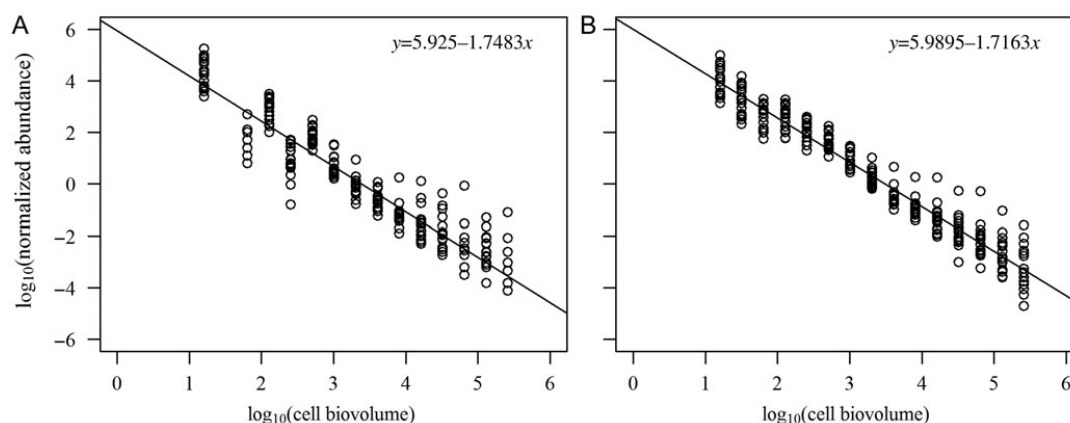


Fig. 2. Normalized abundance size spectra of analysed samples (NASS) from microscopy counts for (A) the “average biovolume” data set and (B) the “distributed biovolume” data set.

biovolume range limits and 0.2125 times that range as the standard deviation. The NASS constructed using this new abundance distribution for each taxon in its biovolume range (Fig. 2B) do not show the peak-valley pattern of the average biovolume spectra (Fig. 2A), in which several classes had abundance/biomass lower than expected, whereas other bins had higher abundances/biomass.

To determine which parameters of the size spectra (slope and/or intercept) were affected, we compared both methods of biovolume assignment (average and distributed) in the microscopy data sets (Fig. 3). The slopes of the average and distributed NASS were not statistically different ($P = 0.0830$, $n = 17$), whereas the intercepts were significantly different ($P < 0.0001$, $n = 17$). To determine which parts of the size spectra were most affected, we compared the means of the abundance and

biomass in each biovolume class for the average and distributed microscopy data sets using a Student’s t -test (Fig. 4). Artefacts in the average biovolume data set were more conspicuous in the smallest biovolume classes. When applying the distribution of biovolume to the counts of each taxonomic group, the variability between contiguous biovolume class decreases. When comparing the mean abundance and biomass for each biovolume class, as determined by the average and distributed data sets, significant differences appeared in the biovolume classes below $10 \mu\text{m}$ ESD ($P < 0.05$, $n = 17$). The differences between the two data sets for the remaining biovolume classes were not significant. Differences in the larger size classes, however, cannot be ruled out, as the power of the statistical test is reduced due to the smaller numbers of cells in the larger biovolume classes.

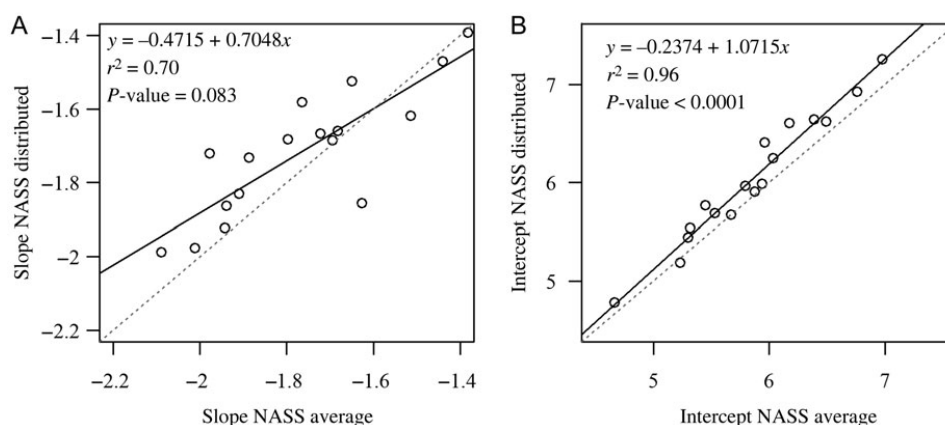


Fig. 3. Comparison of the parameters of the NASS, (A) slope and (B) intercept, constructed using the “average biovolume” data set (x-axis) versus the “distributed biovolume” data set (y-axis) from microscopy counts. For each parameter, the slope, the r -squared of the relationship and the P -value of the t -test that examines whether the relationship is 1:1 are displayed. The grey dotted line shows the 1:1 relationship.

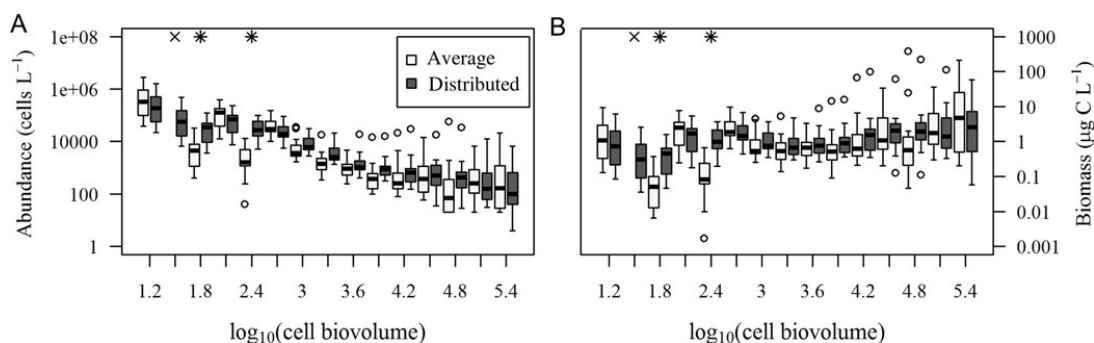


Fig. 4. Box and whisker plot for comparison of the mean (dark bar), standard deviation (box) and range (whisker) of (A) the abundance (cells L^{-1}) and (B) biomass ($\mu\text{g C L}^{-1}$) in each biovolume class calculated with the “average biovolume” and the “distributed biovolume” data sets from microscopy counts. Biovolume classes are indicated for which the means were different by Student’s t -test (* above) and where the comparison was not possible because the bin was absent from one of the data sets (x above).

Comparison between FlowCAM and light microscopy

Analysis of the intra-method variability has been reported previously for FlowCAM, as well as for light microscopy. Previous studies evaluated the variability of FlowCAM measurements by triplicate counting of single-species cultures, obtaining coefficients of variation (cv) within replicates ranging only from 2 to 11% for the fluorescence-triggered mode (Sieracki *et al.*, 1998) and from 6.6 to 53.0% when considering the three FlowCAM working modes (12.4% in autoimage, 6.6% in fluorescence triggered and 53.0% in side-scatter triggered mode) (Álvarez *et al.*, 2011). Microscopical counts of subsamples analysed by the same taxonomist yield cv’s ranging from 4 to 19%, increasing to 13–42% when the samples are counted by different experts (Willén, 1976; Vuorio *et al.*, 2007). To include the effect of this

intra-method variability in the comparison between FlowCAM and microscopy, we established a margin of error of 100% as an acceptable threshold, meaning that the difference in estimated cell concentrations between the methods is lower than a factor of two. The comparisons between FlowCAM and microscopy counts for each sample included estimates of abundance, biomass and community attributes such as size structure and diversity. The results obtained with FlowCAM for preserved and fresh samples in autoimage mode were compared with the distributed biovolume data set obtained with microscopy. The results obtained with FlowCAM in fluorescence-triggered mode were compared with the distributed biovolume data set obtained with microscopy only for autotrophic cells.

Figure 5 shows the abundance (cells L^{-1}) and biomass ($\mu\text{g C L}^{-1}$) per biovolume class estimated with microscopy

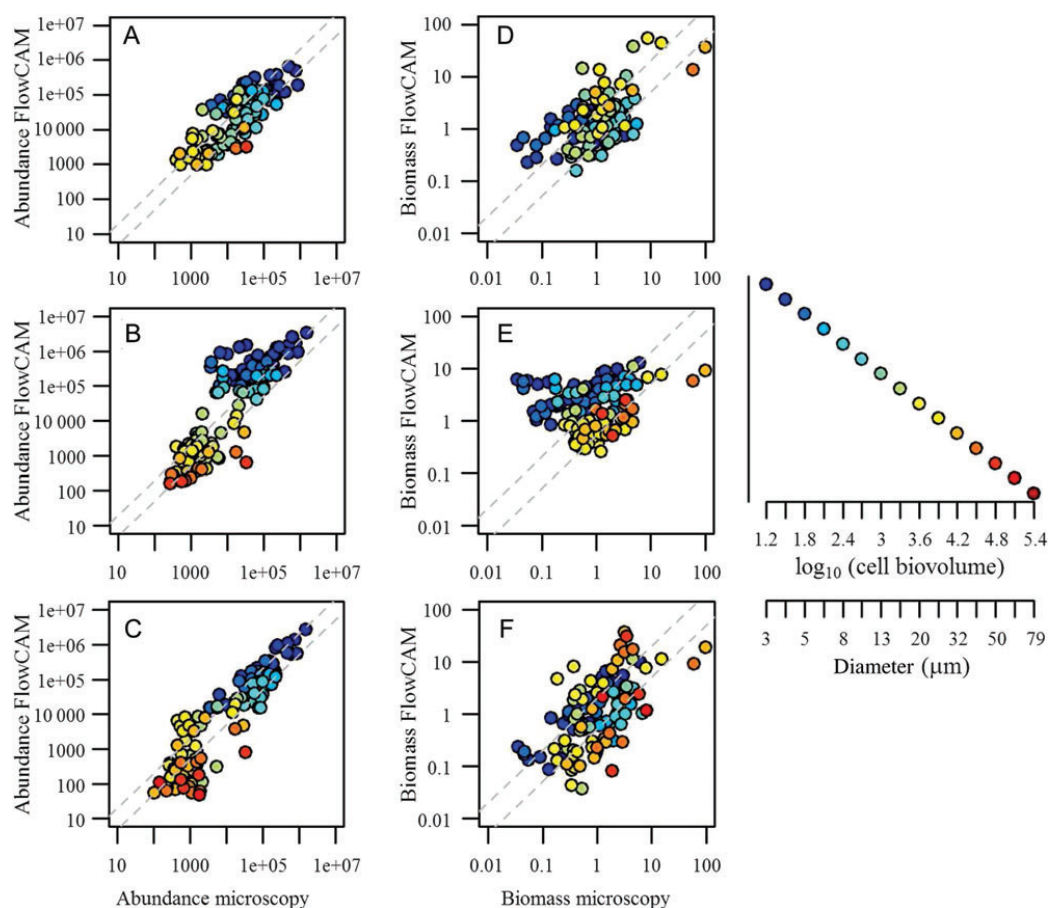


Fig. 5. Comparison of abundance (cells L^{-1}) (left panels) and biomass ($\mu\text{g C L}^{-1}$) (right panels) obtained with light microscopy (x -axis) versus the abundance or biomass obtained with FlowCAM (y -axis) in each biovolume class of the size spectra for (A and D) preserved samples and fresh samples analysed in (B and E) autoimage and (C and F) fluorescence-triggered mode. The colour of the point indicates to which biovolume class the abundance/biomass belongs, and the schematic size spectrum to the right shows the distribution of colours. The dashed lines represent the 100% scatter lines. See online supplementary data for a colour version of this figure.

against those estimated with FlowCAM. Differences arose in preserved samples as well as in fresh samples analysed in autoimage and fluorescence-triggered modes. Regarding abundance, the percentages of biovolume classes falling within a scatter area of 100% around the 1:1 relationship, were: 66.67% for preserved samples (Fig. 5A), 52.31% for fresh samples considering the total community (Fig. 5B) and 73.28% for fresh samples considering only autotrophic cells (Fig. 5C). In terms of biomass, the percentages of biovolume classes that meet the counting precision criteria of 100% were: 61.17% for preserved samples (Fig. 5D), 48.80% for the total community (Fig. 5E) and 68.14% when considering only autotrophic cells (Fig. 5F). For each FlowCAM working mode, the points deviating from the 1:1 relationship can be grouped by biovolume class. Whereas in the preserved samples, the error is homogeneously distributed, in the autoimage

samples the FlowCAM overestimated the smaller biovolume classes. On the other hand, FlowCAM generally underestimated larger biovolume classes in fresh samples.

Within functional classes (Fig. 6), there were differences in the abundance (cells L^{-1}) and biomass ($\mu\text{g C L}^{-1}$) per biovolume class estimated with microscopy and FlowCAM on fresh samples analysed with autoimage (Fig. 6A for ASS and Fig. 6C for BSS) and with fluorescence-triggered modes (Fig. 6B for ASS and Fig. 6D for BSS). Table II shows the percentages of biovolume classes that fall in the 100% scatter area around the 1:1 relationship. The percentage is relatively high for diatoms (from 64.29 to 84.31%) and dinoflagellates (from 86.67 to 100.00%), and lower for ciliates (from 33.33 to 62.50%), silicoflagellates (50.00 to 60.00%) and other living particles smaller than $20 \mu\text{m}$ (from 15.49 to 66.13%). Particularly low is the percentage of other living particles larger that

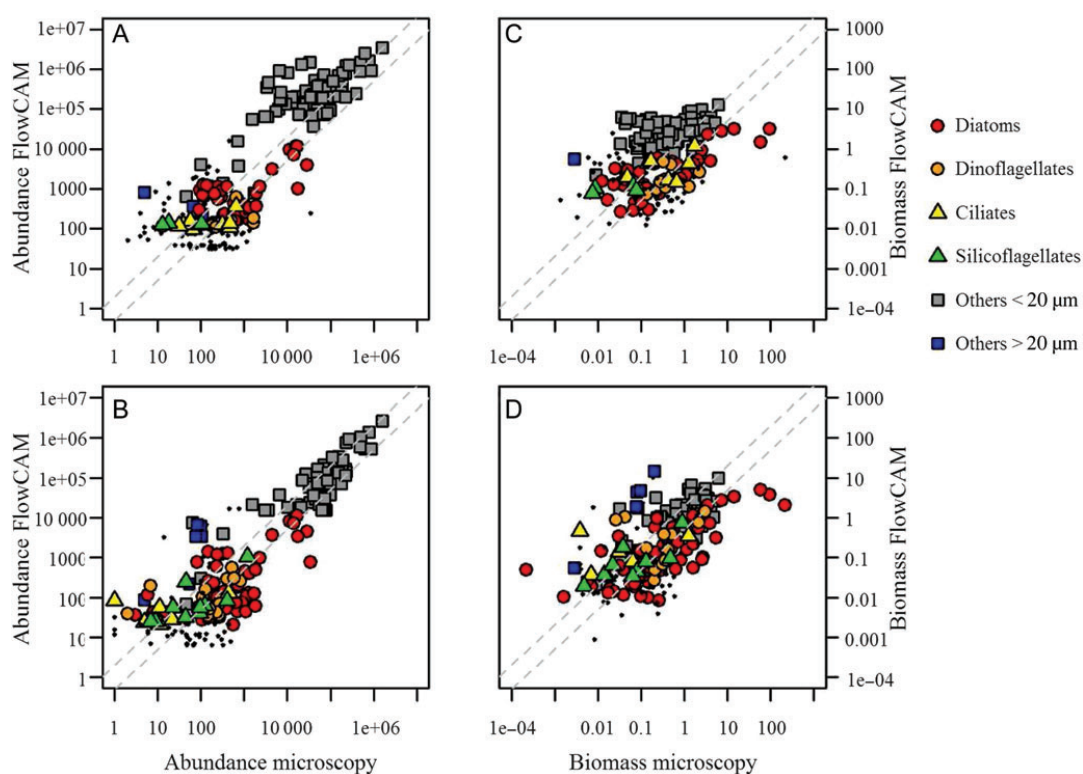


Fig. 6. Comparison of abundance (cells L⁻¹) (left panels) and biomass (µg C L⁻¹) (right panels) obtained with light microscopy (*x*-axis) versus the abundance/biomass obtained with FlowCAM (*y*-axis) in each functional class for fresh samples analysed in (A and C) autoimage and (B and D) fluorescence-triggered modes. The colour and shape of the point indicates to which functional class the abundance/biomass belongs. The dashed lines represent the 100% scatter lines. See online supplementary data for a colour version of this figure.

Table II: Percentage of biovolume classes of the size spectra for each functional class whose difference in estimated cell concentrations between FlowCAM and microscopy was less than a factor of two, which means a margin of error of 100%

Variable	Community	Others <20 µm	Others >20 µm	Diatoms	Dinoflagellates	Ciliates	Silicoflagellates
Abundance	Total	21.33	16.67	64.29	100.00	62.50	50.00
	Autotrophic	66.13	14.29	80.77	86.67	50.00	60.00
Biomass	Total	15.49	0.00	71.05	100.00	62.50	50.00
	Autotrophic	61.67	14.29	84.31	86.67	33.33	60.00

“Total nano- and microplankton community” compares the results obtained with FlowCAM in autoimage mode with all cells counted in microscopy, whereas the “autotrophic community” compares the results obtained with FlowCAM in fluorescence-triggered mode to only the autotrophic cells counted with microscopy.

20 µm (from 0.00 to 16.67%). The catch-all nature of the group “others > 20 µm” in the FlowCAM methodology explains its poor comparison. This group is designated as living particles that are not classified within a functional class due to the poor FlowCAM image quality. It is a group that is usually absent in traditional microscopy analyses, since cells greater than 20 µm are usually always classified. In the “others < 20 µm” group, there are large differences in the accuracy of fluorescence-triggered

(63.90% on average) and autoimage modes (18.41%), due, as seen previously, to the overestimation of small cells by the FlowCAM in autoimage mode.

Regarding community attributes, we explored the size structure and the diversity of the samples obtained with both methodologies. Figure 7 compares the parameters of the NASS from microscopy counts with the parameters of the NASS from FlowCAM. The adjustments to the 1:1 relationship of the slopes of the NASS from

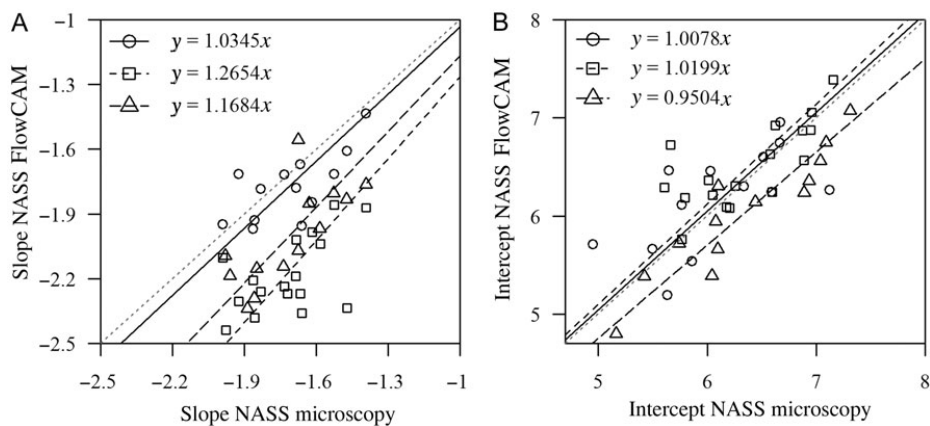


Fig. 7. Comparison of the parameters of the NASS, (A) slope and (B) intercept, obtained with light microscopy versus the parameters obtained with FlowCAM on preserved samples (circles and solid line) and FlowCAM on fresh samples analysed in autoimage (squares and short-dashed line) and in fluorescence-trigger mode (triangles and long-dashed line). The grey dotted line shows the 1:1 relationship.

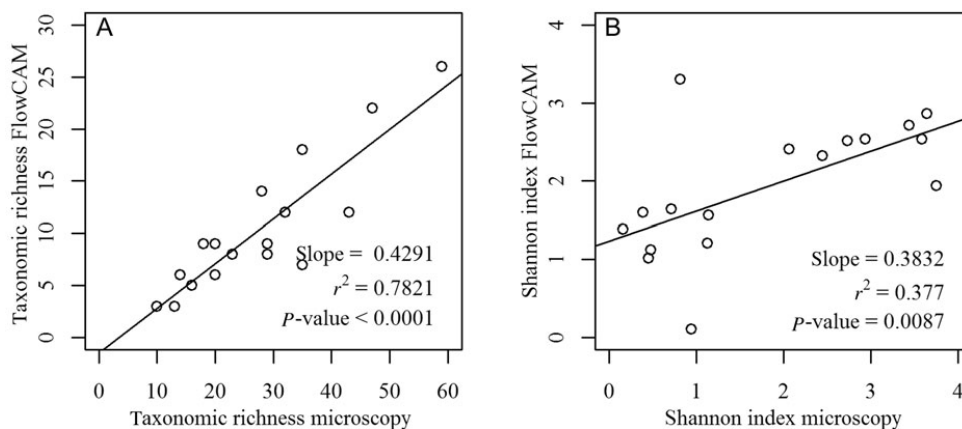


Fig. 8. Comparison of the diversity, (A) taxonomic richness and (B) Shannon index, for each sample obtained with light microscopy against the diversity obtained with the automatic classification of FlowCAM images. For each index, the slope, the r -squared of the relationship and the P -value of the t -test that examines whether the correlation is significant are displayed.

microscopy against FlowCAM were tested with a Student's t -test. When the slopes were not significantly different, the intercepts were calculated assuming a constant slope, and the 1:1 relationship between the intercepts of FlowCAM and microscopy were tested with a t -test. The slope relationship for preserved samples was not different from the 1:1 line (slope: $P = 0.1434$, intercept $P = 0.7265$, $n = 13$). The relationships were different from the 1:1 relationship for fresh samples analysed with FlowCAM in autoimage and preserved samples with microscopy (slope: $P < 0.0001$, $n = 17$), and for the fluorescence-triggered mode (slope: $P < 0.0001$, $n = 13$).

Figure 8 shows the comparison of diversity indices obtained for each sample with both methodologies. Obviously, the categories the classification tool was

trained to discriminate limit the maximum number of groups that can appear in FlowCAM samples. An image of an organism whose taxon was not included in the training set of images is assigned to one or another of the pre-defined categories. On the other hand, the taxonomic resolution of traditional microscopy is limited by the expertise of the taxonomist who can identify a new taxon even when it has not been observed in previous samples. Therefore, the relationship between diversity indices is not expected to fit a 1:1 relationship, and consequently the correlation between the estimates provided by FlowCAM and microscopy was evaluated with a Student's t -test and by reporting the value of r -squared for each diversity index. For taxonomic richness, the correlation was significant ($P < 0.0001$, $n = 17$) and the r^2 was 0.78. For the Shannon index, although the

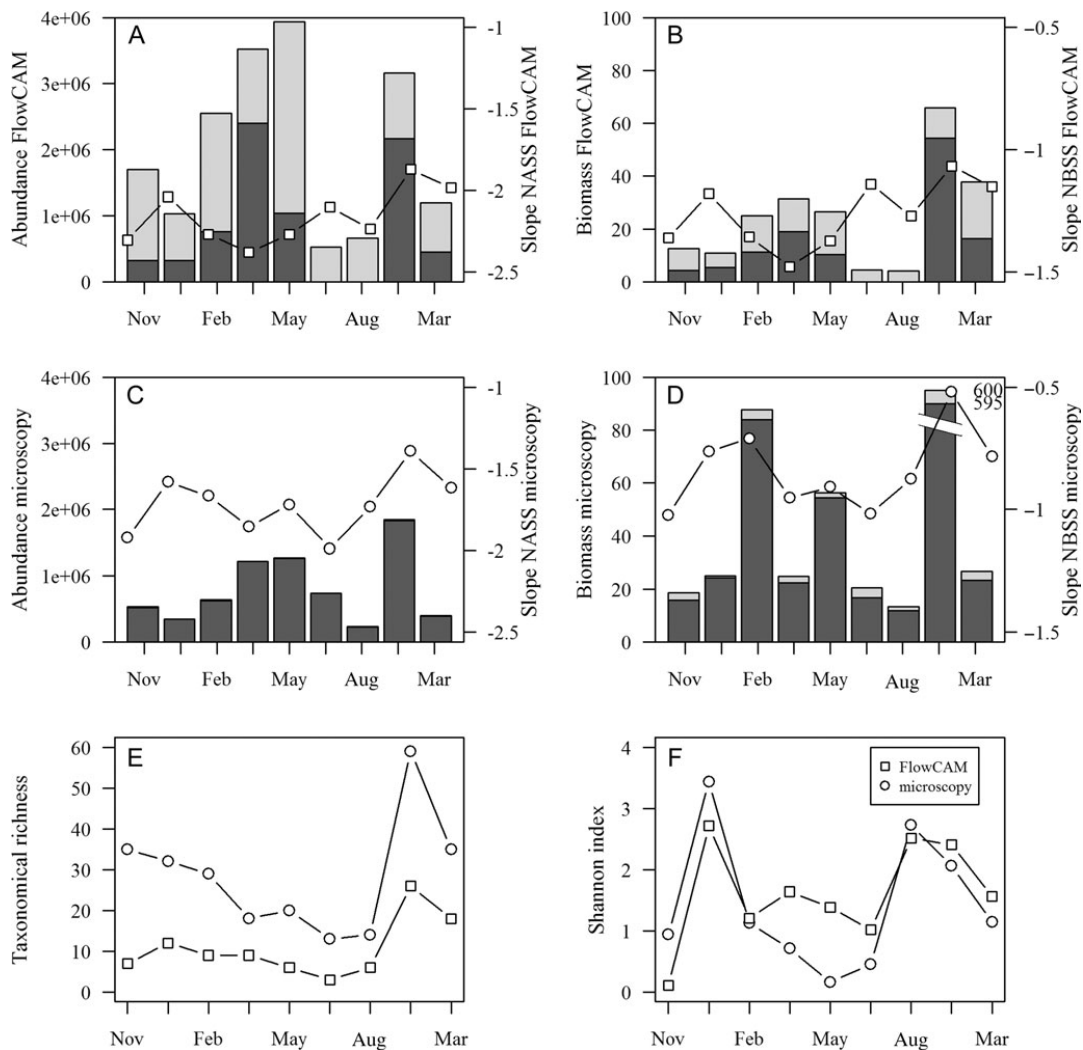


Fig. 9. Variation in the community attributes explored in the work during the sampling period at the surface of a coastal station (46.42°N, 1.85°W, bottom-depth = 100 m). Abundance of cells (autotrophic in dark grey bars and heterotrophic in light grey bars, cells L⁻¹) and slope of the NASS (points) with **(A)** FlowCAM and **(C)** light microscopy. Biomass (µg C L⁻¹) and slope of the NBSS with **(B)** FlowCAM and **(D)** light microscopy. Diversity indices: **(E)** taxonomic richness and **(F)** Shannon index.

correlation was also significant ($P = 0.0087$, $n = 17$), the r^2 was only 0.38.

Finally, the temporal variation of community attributes during the study period illustrates the output obtained by both methodologies (Fig. 9). The abundance (cells L⁻¹, Fig. 9A) and biomass (µg C L⁻¹, Fig. 9B) of nano- and microplankton estimated with FlowCAM followed the same pattern as the abundance (Fig. 9C) and biomass (Fig. 9D) estimated with microscopy. Thanks to the use of two different working modes, fluorescence triggered and autoimage modes, respectively, FlowCAM was capable of discriminating the autotrophic (dark grey bars) from the heterotrophic community (light grey bars) without

additional sample treatment. For the whole nano- and microplankton community and for the autotrophic community, the timing of maxima and minima of abundance and biomass matched. The same happened with the parameters of the size spectra as well as with the diversity indices explored (Fig. 9E and F). Although the trends were similar with both methodologies, the absolute values differed.

DISCUSSION

The scientific community has focused much effort on comparisons between automated and traditional techniques for plankton enumeration, given the growing interest

in the automated techniques. We have compared traditional light microscopy and the automatic, FlowCAM-based technique for routine analyses of nano- and microplankton samples. The wide sample variability covered, in both cell abundance and taxonomic composition, ensures the reliability of the comparison. This was attained by considering samples collected during a time series monitoring programme, which covered the whole seasonal cycle at different depths within the photic layer of the coastal Cantabrian Sea. Our results broaden knowledge about the reliability of automated methods, clarify which tasks the FlowCAM can tackle and which it currently cannot.

Performance of FlowCAM on routine sample analyses

Microscopy-based biovolume estimations have been the main source of information for size structure studies of nano- and microplankton. In most routine sample analyses, taxonomists measure only a subset of cells and assign a unique average biovolume to each taxonomic group. But any taxonomic group, even at the species level, can span several biovolume classes. Consequently, the use of a unique average biovolume misestimates the abundance and biomass of certain biovolume classes. The presence of these artefacts in size spectra based on average biovolumes is common in the literature (e.g. Marañón *et al.*, 2007; Huete-Ortega *et al.*, 2010). We suggest that these artefacts can be avoided by considering the distribution of cell biovolume within each taxon. We have shown that even if we lack the actual biovolume distribution, making gross approximations of the distribution of biovolumes removes these artefacts from the size spectra. Taxonomists usually have some knowledge about biovolume distributions, since they have measured a representative number of cells, sometimes even for several size classes within each taxonomic group (Olenina *et al.*, 2006). Our advice is not to lose this information by summarizing it in an average value, but to use it to obtain more realistic size spectra. The use of average cell biovolumes to assign a biovolume value to each of the cells counted does not significantly affect the estimated slope of the size spectrum, but it can affect the biological and/or ecological parameters derived from the intercept of the size spectrum, such as the standing stock of phytoplankton. It also introduces significant differences in the estimates of abundance and biomass of specific biovolume classes and can generate deviations from the linearity of the phytoplankton size structure.

Another problem with microscopy-based methods for characterizing size structure is the need for sample preservation. Changes in cell size and shape in response to

the use of fixatives have been reported extensively (Leakey *et al.*, 1994; Montagnes *et al.*, 1994; Stoecker *et al.*, 1994; Menden-Deuer *et al.*, 2001) and also in samples analysed with FlowCAM (Zarauz and Irigoien, 2008). The absence of differences in the size spectra obtained from preserved samples with FlowCAM and microscopy suggests that both methodologies are closely comparable when applied to samples with the same preservation and classified by an expert. Hence, the effect of fixatives can explain the differences between fresh samples analysed with FlowCAM and preserved samples analysed with microscopy. The inaccuracy in the automatic classification of FlowCAM images is another source of error, which is likely to be reduced as image classification algorithms improve. Additionally, the representativeness of the sampled volume needs further study to develop protocols that are more robust in order to avoid undersampling. Although with the data presented in this work these sources of error are indistinguishable, the degree to which they affect the results provided by each of the FlowCAM working modes permits us to outline their relative importance.

Samples analysed with FlowCAM in autoimage mode are illustrative of the discrepancies between microscopy and FlowCAM. At the lower size limit of the nanoplankton fraction, the effect of fixatives on the inverted microscope samples causes an underestimation of cell numbers, resulting in flatter spectra than those obtained with FlowCAM. On the other hand, the images digitized in autoimage mode are classified with less accuracy than under the microscope, and many non-living particles are classified as living cells. This error is especially problematic in the smaller biovolume classes for which image quality is less and translates as steeper spectra. In addition, in the FlowCAM data, the sampled volume is insufficient to cover the whole spectrum, and the upper limits of the nanoplankton and the microplankton size ranges suffer from undersampling. In microscopy, the sedimentation method and the possibility of changing magnification during the sample analysis allow good estimation of particle abundances across the complete size range. Hence, since traditional microscopy underestimates the cell abundance and biomass (due to preservation) and the FlowCAM overestimates the cell abundance and biomass (due to classification of non-living particles), the actual slopes of size spectra lie between those from the two methods. The overall slope of the NASS reported by Blanco *et al.* (Blanco *et al.*, 1994) in a size spectrum including size distribution information from samples with multiple origins was -1.98 . That value is intermediate between our -1.77 for preserved samples analysed with microscopy and our -2.11 for fresh samples analysed in autoimage mode.

The fluorescence-triggered FlowCAM mode provides a better estimation of cell abundance in the smaller bio-volume classes than the autoimage mode. The presence of red fluorescence in planktonic cells is an unambiguous discriminatory variable to distinguish living autotrophic particles, avoiding the effects in autoimage mode of reduced optical resolution and the contamination by detritus. The larger sampled volume permits good coverage of the complete size range, with fewer missing bio-volume classes than in the autoimage mode. As expected, the overall slope of the NASS in our data from the fluorescence-triggered mode, -1.99 , is closer to the value of -1.98 reported by Blanco *et al.* (Blanco *et al.*, 1994). The effects of uncertainties in cell enumeration should be minimal when an ample size range of planktonic organisms (from pico- to macroplankton) is included in the analysis and several methodologies enumerate them. The global trend that arises compensates for the method-specific biases in nano- and microplankton estimation. However, in marine ecosystems, most size spectrum studies have been conducted at local scales and/or for only a small size range of planktonic organisms. In those cases, biases affecting the enumeration of the target size range can determine the estimated values of sample parameters.

The diversity indexes presented add a new facet to the capacities of automatic classification. The *a priori* selection of classification groups and the lower taxonomic resolution provided by automatic image classification derived from FlowCAM caution against its use in biodiversity studies. Despite these limitations, we have shown that estimates of taxonomic richness derived from FlowCAM are reasonably comparable with those obtained by microscopy. This opens the possibility to use a simple index obtained with FlowCAM to determine the variations of community diversity at large scales where sampling using traditional microscopy is not feasible. Some authors have used indices of taxonomic richness (e.g. mean number of species) as an indicator of community diversity and changes in ecosystem function (Beaugrand *et al.*, 2000), even though they do not reflect the actual number of taxa. For higher-order indices, such as the Shannon index, which include in their calculation both the number of taxa and their relative abundances, the difference between the two methods is larger, because the uncertainties in cell enumeration explained above affect the abundance values.

Scope of application of FlowCAM

Relevant information has been gathered in recent years about the comparability of FlowCAM and traditional methods. Nevertheless, when designing a sampling

strategy, deciding whether FlowCAM is a reliable option remains challenging. We have reviewed the aspects in which it differs from microscopy in order to provide a global vision of the abilities of the automated technique and to help establish in which situations FlowCAM can substitute and/or complement microscopy with reliability and in which not.

FlowCAM has been used with success in several research scenarios. Its counting accuracy has been proved for cultures (Buskey and Hyatt, 2006) and natural samples (See *et al.*, 2005; Ide *et al.*, 2008). And it has given comparable results in cell sizing when compared with light microscopy (Sieracki *et al.*, 1998; Spaulding *et al.*, 2012). Hence, FlowCAM has become a useful tool in size-related studies needing extensive numeric information from the samples (Chisholm, 1992), particularly size structure determination (Álvarez *et al.*, 2011). In the current work, we have shown how routine application of FlowCAM analysis can provide results comparable with those obtained with light microscopy, not only in size structure determination but also in the discrimination of broad categories within the nano- and microplankton community, such as functional classes or autotrophic cells. However, although the overall error in the automatic classification of FlowCAM images is around 10% (Blaschko *et al.*, 2005; Zarauz *et al.*, 2009; Álvarez *et al.*, 2012), the number of categories that FlowCAM discriminates is still very low when compared with light microscopy. This limits its application in research scenarios that demand extensive taxonomic detail.

When used in studies for which their limits are acceptable, the results obtained with the two methods are comparable with each other, supporting the confident application of FlowCAM methodology. Although the fully automatic method seems appropriate for the analysis of variations in the planktonic community at broad spatial and temporal scales, further work is needed to standardize the protocols to avoid undersampling and to improve the automated classification of particles. The currently applied protocols are a weak point when dealing with waters with very low concentrations of particles. Such oligotrophic environments need substantial sample concentration to be properly characterized by FlowCAM. The reliable use of the FlowCAM for very dilute samples needs further protocol development.

CONCLUSIONS

FlowCAM is a useful advance for size structure studies, providing a way to analyse many samples in a reasonable amount of time and to obtain extensive numeric information. It is also capable of differentiating broad

taxonomic categories. However, the automatic classification of FlowCAM images currently only attains a low taxonomic resolution, thus when the aim is high taxonomic resolution, microscopy is still the unique choice. When limited to scenarios for which the two methodologies are comparable, ancillary factors must be considered to choose the most suitable technique: the scale of variation of the target variables, the time available for analysis, the possibility of analyzing fresh samples, the dependence on the operator and the need to discriminate the autotrophic community. The scope of application of the FlowCAM cannot be elucidated completely with the available literature, since that depends on methodological considerations needing further study. However, FlowCAM complements traditional techniques by improving the sampling resolution available for study of highly dynamic communities and providing the detailed descriptions of particle-size spectra necessary for ecological studies.

SUPPLEMENTARY DATA

Supplementary data can be found online at <http://plankt.oxfordjournals.org>.

ACKNOWLEDGEMENTS

This is a contribution to SCOR Working Group 130 on Automatic Visual Plankton Identification. We thank the captain and crew in the R/V José Rioja for their assistance during the sampling of the project RADIALES (“Programa de series temporales oceanográficas”; <http://www.seriestemporales-ieo.com>) that provided the data set for the present work. We are indebted to all participants in the monthly sampling for their work at sea and in the laboratory and to three anonymous reviewers for their valuable comments and suggestions.

FUNDING

This work was supported by the Plan de Ciencia, Tecnología e Innovación del Gobierno del Principado de Asturias [project IMAGINA (“Integración de métodos de análisis de imagen de grupos planctónicos con técnicas de inteligencia artificial”) and research grant BP07-081 to E.A.] and the Instituto Español de Oceanografía [project RADIALES (“Programa de series temporales oceanográficas”)]. M.M. was supported by an Alexander von Humboldt Postdoctoral Fellowship.

REFERENCES

- Álvarez, E., López-Urrutia, A., Nogueira, E. *et al.* (2011) How to effectively sample the plankton size spectrum? A case study using FlowCAM. *J. Plankton Res.*, **33**, 1119–1133.
- Álvarez, E., López-Urrutia, A. and Nogueira, E. (2012) Improvement of plankton biovolume estimates derived from image-based automatic sampling devices: application to FlowCAM. *J. Plankton Res.*, **34**, 454–469.
- Beaugrand, G., Reid, P. C., Ibañez, F. *et al.* (2000) Biodiversity of North Atlantic and North Sea calanoid copepods. *Mar. Ecol. Prog. Ser.*, **204**, 299–303.
- Benfield, M. C., Grosjean, P., Culverhouse, P. *et al.* (2007) RAPID: research on automated plankton identification. *Oceanography*, **20**, 12–26.
- Bérard-Therriault, L., Poulin, M. and Bossé, L. (1999) *Guide d'identification du phytoplancton marin de l'estuaire et du Golfe du Saint-Laurent*. CNRC-NRC, Ottawa, Canada, pp. 387.
- Blanco, J. M., Echevarría, F. and García, C. M. (1994) Dealing with size-spectra: some conceptual and mathematical problems. *Sci. Mar.*, **58**, 17–29.
- Blaschko, M. B., Holness, G., Mattar, M. A. *et al.* (2005) Automatic in situ identification of plankton. *Proceedings of the Seventh IEEE Workshops on Application of Computer Vision (WACV/MOTION'05)*, **1**, 79–86.
- Buskey, E. J. and Hyatt, C. J. (2006) Use of the FlowCAM for semi-automated recognition and enumeration of red tide cells (*Karenia brevis*) in natural plankton samples. *Harmful Algae*, **5**, 685–692.
- Cermeño, P. and Figueiras, F. G. (2008) Species richness and cell-size distribution: size structure of phytoplankton communities. *Mar. Ecol. Prog. Ser.*, **357**, 79–85.
- Chisholm, S. W. (1992) Phytoplankton size. In Falkowski, P. G. and Woodhead, A. D. (eds), *Primary Productivity and Biogeochemical Cycles in the Sea*. Plenum Press, New York, pp. 213–237.
- Culverhouse, P. F. R. W., Reguera, B., Herry, V. *et al.* (2003) Do experts make mistakes? A comparison of human and machine identification of dinoflagellates. *Mar. Ecol. Prog. Ser.*, **247**, 17–25.
- Cupp, E. E. (ed) (1977) *Marine Plankton Diatoms of the West Coast of North America*. Otto Koeltz Science Publishers, Koenigstein, Germany, pp. 237.
- Dodge, J. D. (ed) (1982) *Marine Dinoflagellates of the British Isles*. Her Majesty's Stationary Office, London, United Kingdom, pp. 303.
- Dodson, A. N. and Thomas, W. H. (1978) Reverse filtration. In Sournia, A. (ed.), *Phytoplankton Manual*. UNESCO, Paris, pp. 104–107.
- Edler, L. and Elbrächter, M. (2010) The Utermöhl method for quantitative phytoplankton analysis. In Karlson, B., Cusack, C. and Bresnan, E. (eds), *Microscopic and Molecular Methods for Quantitative Phytoplankton Analysis*. UNESCO, Paris, pp. 13–20.
- García, C. M., Jimenez-Gómez, F. and Rodríguez, J. (1994) The size-structure and functional composition of ultraplankton and nanoplankton at a frontal station in the Alboran Sea. Working groups 2 and 3 report. *Sci. Mar.*, **58**, 43–52.
- Hillebrand, H., Dürselen, C.-D., Kirschtel, D. *et al.* (1999) Biovolume calculation for pelagic and benthic microalgae. *J. Phycol.*, **35**, 403–4424.
- Huete-Ortega, M., Marañón, E., Varela, M. *et al.* (2010) General patterns in the size scaling of phytoplankton abundance in coastal waters during a 10-year time series. *J. Plankton Res.*, **32**, 1–14.
- Ide, K., Takahashi, K., Kuwata, A. *et al.* (2008) A rapid analysis of copepod feeding using FlowCAM. *J. Plankton Res.*, **30**, 275–281.

- Jakobsen, H. H. and Carstensen, J. (2011) FlowCAM: sizing cells and understanding the impact of size distributions on biovolume of planktonic community structure. *Aquat. Microb. Ecol.*, **65**, 75–87.
- Leakey, R. J. G., Burkill, P. H. and Sleight, M. A. (1994) A comparison of fixatives for the estimation of abundance and biovolume of marine planktonic ciliate populations. *J. Plankton Res.*, **10**, 375–389.
- Legendre, P. and Legendre, L. (1998) *Numerical Ecology*. Elsevier Science B. V., Amsterdam.
- Marañón, E., Cermeño, P., Rodríguez, J. *et al.* (2007) Scaling of phytoplankton photosynthesis and cell size in the ocean. *Limnol. Oceanogr.*, **52**, 2190–2198.
- Menden-Deuer, S., Lessard, E. J. and Satterberg, J. (2000) Carbon to volume relationships for dinoflagellates, diatoms and other protist plankton. *Limnol. Oceanogr.*, **45**, 569–579.
- Menden-Deuer, S., Lessard, E. J. and Satterberg, J. (2001) Effect of preservation on dinoflagellate and diatom cell volume and consequences for carbon biomass predictions. *Mar. Ecol. Prog. Ser.*, **222**, 41–50.
- Moberg, E. A. and Sosik, H. M. (2012) Distance maps to estimate cell volume from two-dimensional plankton images. *Limnol. Oceanogr. Meth.*, **10**, 278–288.
- Montagnes, D. J. S., Berges, J. A., Harrison, P. J. *et al.* (1994) Estimating carbon, nitrogen, protein and chlorophyll a from volume in marine phytoplankton. *Limnol. Oceanogr.*, **39**, 1044–1060.
- Olenina, I., Hajdu, S., Edler, L. *et al.* (2006) Biovolumes and size-classes of phytoplankton in the Baltic Sea. *HELCOM Balt. Sea Environ. Proc.*, **106**, 144.
- See, J. H., Campbell, L., Richardson, T. L. *et al.* (2005) Combining new technologies for determination of phytoplankton community structure in the northern Gulf of Mexico. *J. Phycol.*, **41**, 305–310.
- Sieracki, C. K., Sieracki, M. E. and Yentsch, C. S. (1998) An imaging-in-flow system for automated analysis of marine microplankton. *Mar. Ecol. Prog. Ser.*, **168**, 285–296.
- Spaulding, S. A., Jewson, D. H., Bixby, R. J. *et al.* (2012) Automated measurement of diatom size. *Limnol. Oceanogr. Meth.*, **10**, 882–890.
- Stoecker, D. K., Gifford, D. J. and Putt, M. (1994) Preservation of marine planktonic ciliates: losses and cell shrinkage during fixation. *Mar. Ecol. Prog. Ser.*, **110**, 293–299.
- Sun, J. and Liu, D. (2003) Geometric models for calculating cell biovolume and surface area for phytoplankton. *J. Plankton Res.*, **25**, 1331–1346.
- Tomas, C. R. (ed) (1997) *Identifying Marine Phytoplankton*. Academic Press, San Diego, CA, pp. 858.
- Utermöhl, H. (1958) Zur Vervollkommnung der quantitativen Phytoplankton-Methodik. *Mitt. Int. Ver. Theor. Angew. Limnol.*, **9**, 1–38.
- Vuorio, K., Lepisto, L. and Holopainen, A.-L. (2007) Intercalibrations of freshwater phytoplankton analyses. *Boreal Environ. Res.*, **12**, 561–569.
- Willén, E. (1976) A simplified method of phytoplankton counting. *Br. Phycol. J.*, **11**, 265–278.
- Zarauz, L. and Irigoien, X. (2008) Effects of lugol's fixation on the size structure of natural nano-microplankton samples, analyzed by means of an automatic counting method. *J. Plankton Res.*, **30**, 1297–1303.
- Zarauz, L., Irigoien, X. and Fernandes, J. A. (2009) Changes in plankton size structure and composition, during the generation of a phytoplankton bloom, in the central Cantabrian sea. *J. Plankton Res.*, **31**, 193–207.

Supplementary material

Plankton enumeration data provided by the light microscopy technique attain high taxonomic resolution, classifying organisms at the species or genus level. However, methods for plankton enumeration based on image analysis and automatic classification, such as the FlowCAM-based technique, discriminate organisms in much broader groups. Similarly, when an expert taxonomist assigns a geometrical shape that describes a taxonomic group, he or she can choose a shape as simple as a sphere, or more complex, formed by various geometrical bodies. However, the description of a cell with a complex shape usually accommodates structures that do not constitute a high proportion of the total biovolume of the cell, such as spines or setae (Menden-Deuer *et al.*, 2000); those can generally be neglected. For that reason the description of shapes can be approximated by three simple shapes: sphere, ellipsoid and cylinder (Menden-Deuer *et al.*, 2000). Hence the microscopy data needed to be simplified regarding taxonomy and morphology to meet the taxonomical and morphological resolution of the FlowCAM-based technique.

Each taxon enumerated with microscopy was assigned to a functional class (diatoms, silicoflagellates, dinoflagellates, ciliates or other living particles) in order to match the taxonomic resolution of FlowCAM counts, as can be seen in the correspondences in Table SI. The shape of each taxonomical group was defined according to composite geometric bodies extracted from the literature (Hillebrand *et al.*, 1999; Sun & Liu, 2003; Olenina *et al.*, 2006) obtaining a total of 24 composite shapes for the taxonomical groups present in the analyzed samples. Those 24 composite shapes were simplified to three simple shapes: sphere, ellipsoid and cylinder, using the conversion indicated in Table SII.

References

- Bérard-Therriault, L., Poulin, M. and Bossé, L. (1999) *Guide d'identification du phytoplancton marin de l'estuaire et du Golfe du Saint-Laurent*. CNRC-NRC, Ottawa, Canada, pp. 387.
- Cupp, E. E. (ed) (1977) *Marine plankton diatoms of the west coast of North America*. Otto Koeltz Science Publishers, Koenigstein, Germany, pp. 237.
- Dodge, J. D. (ed) (1982) *Marine dinoflagellates of the British Isles*. Her Majesty's Stationary Office, London, United Kingdom, pp. 303.
- Hillebrand, H., Dürselen, C.-D., Kirschtel, D., Pollinger, U. and Zohary, T. (1999) Biovolume calculation for pelagic and benthic microalgae. *J. Phycol.*, **35**, 403-4424.
- Menden-Deuer, S., Lessard, E. J. and Satterberg, J. (2000) Carbon to volume relationships for dinoflagellates, diatoms and other protist plankton. *Limnol. Oceanogr.*, **45**, 569-579.
- Olenina, I., Hajdu, S., Edler, L., Andersson, A., Wasmund, N., Busch, S., Göbel, J., Gromisz, S., Huseby, S., Huttunen, M., Jaanus, A., Kokkonen, P., Ledaine, I. and Niemkiewicz, E. (2006) Biovolumes and size-classes of phytoplankton in the Baltic Sea. *HELCOM Balt. Sea Environ. Proc.*, **106**, pp. 144.
- Sun, J. and Liu, D. (2003) Geometric models for calculating cell biovolume and surface area for phytoplankton. *J. Plankton Res.*, **25**, 1331-1346.
- Tomas, C. R. (ed) (1997) *Identifying marine phytoplankton*. Academic Press, San Diego, California, pp. 858.

Table S1 Degree of taxonomic resolution attained for microscopy and FlowCAM methods and the gathering of the two classifications into common functional classes.

FlowCAM Taxonomy	Functional class	Microscopy Taxonomy
	Diatoms	
Centric cells with height<diame	<i>Asterionellopsis glacialis</i>	<i>Haslea</i> sp.
Centric cells with height>diame	<i>Asteromphalus sarcophagus</i>	<i>Haslea trompii</i>
Cylindrical cells with round ends (e.g. <i>Ditylum</i> , <i>Stephanopyxis</i> , <i>Corethron</i>)	<i>Bacteriastrium delicatulum</i>	<i>Lauderia annulata</i>
Cylindrical cells with spine-like ends (e.g. <i>Rhizosolenia</i>)	<i>Bacteriastrium</i> sp.	<i>Leptocylindrus danicus</i>
Wide chains with closed connected cells (e.g. <i>Detonula</i> , <i>Guinardia</i>)	<i>Cerataulina pelagica</i>	<i>Leptocylindrus mediterraneus</i>
Narrow chains with closed connected cells (e.g. <i>Leptocylindrus</i>)	<i>Chaetoceros</i> sp.*	<i>Lioloma pacificum</i>
Chains with slightly connected cells (e.g. <i>Eucampia</i>)	<i>Corethron</i> sp.	<i>Navicula</i> sp.
Chains with long setae (e.g. <i>Chaetoceros</i>)	<i>Cylindrotheca closterium</i>	<i>Navicula transitans</i>
Chains with intercellular spaces (e.g. <i>Skeletonema</i>)	<i>Dactyliosolen fragilissimus</i>	<i>Paralia sulcata</i>
Chains with cells connected by gelatinous threads (e.g. <i>Thalassiosira rotula</i>)	<i>Dactyliosolen phuketensis</i>	<i>Pleurosigma / Gyrosigma</i>
Chains of needle-like cells (e.g. <i>Pseudo-nitzschia</i>)	<i>Dactyliosolen</i> sp.	<i>Pleurosigma</i> sp.
Colonial star-shaped (e.g. <i>Asterionellopsis</i>)	<i>Detonula pumila</i>	<i>Proboscia alata</i>
Colonial zigzag (e.g. <i>Thalassionema</i>)	<i>Ditylum</i> sp.	<i>Proboscia truncata</i>
Gelatinous spheres (e.g. <i>Phaeocystis</i> , <i>Thalassiosira subtilis</i>)	<i>Eucampia zodiacus</i>	<i>Pseudo-nitzschia delicatissima</i> complex
Pennate cells	<i>Guinardia delicatula</i>	<i>Pseudo-nitzschia seriata</i> complex
	<i>Guinardia striata</i>	<i>Pseudo-nitzschia</i> sp.
	Dinoflagellates	
Small dinoflagellates	<i>Amphidinium</i> sp.	<i>Gyrodinium</i> sp.
<i>Prorocentrum micans</i>	<i>Amphidoma caudata</i>	<i>Micracanthodinium claytonii</i>
Genera <i>Prorocentrum</i>	<i>Amphisolenia globifera</i>	<i>Minuscula bipes</i>
Genera <i>Dinophysis</i>	<i>Ceratium</i> sp.**	<i>Oxytoxum</i> sp.
Globose un-horned cells (e.g. <i>Protoperidinium</i>)	<i>Cochlodinium / Warnowia</i>	<i>Phalacroma</i> sp.
Globose horned cells (e.g. <i>Ceratium</i>)	<i>Cochlodinium</i>	<i>Pronoctilica pelagica</i>
	<i>Dinophysis acuminata</i>	<i>Pronoctilica</i> sp.
	<i>Dinophysis acuta</i>	<i>Prorocentrum micans</i>
	<i>Dinophysis rotundata</i>	<i>Prorocentrum vaginula</i>
	<i>Dinophysis</i> sp.	<i>Prorocentrum</i> sp.
	<i>Gymnodinium</i> sp.	<i>Protoperidinium curtipes</i>
	Ciliates	
<i>Mesodinium rubrum</i>	<i>Mesodinium</i> sp.	
Few cilia in apical position (e.g. <i>Laboea</i> , <i>Strombidium</i>)	<i>Tintinnidae</i>	
Few cilia in lateral position (e.g. <i>Euplates</i> , <i>Diophrys</i>)	<i>Gilphora</i>	
Tintinnids with extended lorica (e.g. <i>Salpingella</i>)		
Tintinnids with globular lorica (e.g. <i>Codonella</i> , <i>Dictyocysta</i>)		
	Silicoflagellates	
Silicoflagellates	<i>Dictyocha fibula</i>	<i>Dictyocha speculum</i>
	Others>20um	
Cells unidentifed<20um	<i>Commatia cryoporinum</i>	Radiolaria
Flagellates	<i>Eutreptia</i> spp.	Flagellates > 20 µm
	Others (all<20um)	
Cells unidentifed<20um	Choanoflagellates	Flagellates < 20µm

Table SII Composite-to-simple shape conversions for microscopy counts. Composite shapes were integrated by the set proposed by Hillebrand *et al.* (1999) plus the shapes from Sun & Liu (2003) for the genus *Ceratium*. The source for the assignment of shape and cell dimensions to each taxonomic group is indicated in brackets: (A) the authors; (B) Bérard-Therriault *et al.* (1999); (C) Cupp (1977); (D) Dodge (1982); (H) Hillebrand *et al.* (1999); (O) Olenina *et al.* (2006); (S) Sun & Liu (2003); (T) Tomas (1997).

Simple shape	Composite shape	Taxonomical group (shape source : size source)
Cylinder	Cylinder	<i>Amphisolenia globifera</i> (A: D), <i>Bacteriasterium delicatulum</i> (A: T), <i>Bacteriasterium</i> sp. (A: T), <i>Cerataulina pelagica</i> (O: O), <i>Corethron</i> sp. (A: T/ C), <i>Dactyliosolen fragilissimus</i> (O: T), <i>Dactyliosolen phuketensis</i> (A: T), <i>Dactyliosolen</i> sp. (A: T), <i>Detonula pumila</i> (O: T), <i>Guinardia delicatula</i> (O: O), <i>Guinardia striata</i> (A: T), <i>Lauderia annulata</i> (O: T), <i>Leptocylindrus danicus</i> (O: C), <i>Leptocylindrus mediterraneus</i> (A: T), <i>Paralia sulcata</i> (A: T), <i>Proboscia alata</i> (O: C), <i>Proboscia truncata</i> (A: A), <i>Rhizosolenia imbricata</i> (A: T), <i>Rhizosolenia setigera</i> (O: T), <i>Rhizosolenia</i> sp. (A: A), <i>Skeletonema costatum</i> (O: O), <i>Thalassiosira</i> sp. (O: O/ A), <i>Thimnidae</i> sp. (A: A), Centric Diatoms (O: O/ A), Disc-like Diatoms (A: A).
Oval cylinder	Oval cylinder	<i>Asteromphalus sarcophagus</i> (A: T), <i>Chaetoceros affinis</i> (O: O), <i>Chaetoceros atlanticus</i> (A: T), <i>Chaetoceros compressus</i> (O: O), <i>Chaetoceros concavicornis</i> (O: T/ C), <i>Chaetoceros convolutus</i> (O: O), <i>Chaetoceros curvisetus</i> (O: T/ C), <i>Chaetoceros danicus</i> (O: T/ C), <i>Chaetoceros decipiens</i> (O: O), <i>Chaetoceros didymus</i> (O: C), <i>Chaetoceros subgenus Hyalochaete</i> (A: A), <i>Chaetoceros lorenzianus</i> (O: C), <i>Chaetoceros peruvianus</i> (O: T/ C), <i>Chaetoceros subgenus Phaeoceros</i> (A: A/ T/ C), <i>Chaetoceros similis</i> (A: C/ A), <i>Chaetoceros socialis</i> (O: T), <i>Chaetoceros tortissimus</i> (O: T), <i>Eucampia zodiacus</i> (O: C), <i>Haslea</i> sp. (A: T), <i>Haslea trompii</i> (A: T), <i>Gyrosigma</i> sp. (A: A), <i>Pleurosigma</i> sp. (A: T), <i>Pseudo-nitzschia delicatissima</i> complex (A: T), <i>Pseudo-nitzschia serriata</i> complex (A: T), <i>Pseudo-nitzschia</i> spp. (A: T), Diatoms (A: A), <i>Ditylum</i> sp. (O: O).
Sphere	Prism on triangle base	<i>Phalacroma</i> sp. (A: T), <i>Protoperidinium tuba</i> (A: A), <i>Mesodinium</i> sp. (O: O), Dinoflagellate cyst (A: A), Radiolaria (A: A).
Ellipsoid	Sphere	<i>Dictyocha fibula</i> (A: T), <i>Dictyocha speculum</i> (O: T), <i>Dictyocha</i> sp. (A: T).
	Half sphere	<i>Warnowia</i> sp. (A: A), <i>Gochlodinium</i> (A: A), <i>Cylindrotheca closterium</i> (O: O/ T), <i>Eutreptia</i> sp. (O: O), <i>Prorocentrum vaginula</i> (A: A), <i>Micrarcantodinium claytonii</i> (A: D), <i>Thalassionema frauenfeldii</i> (A: T), Thecate dinoflagellates (A: A), Dinoflagellates (in slime) (A: A), Flagellates (O: A).
	Rotational ellipsoid	Athecate dinoflagellates (A: A).
	Rotational ellipsoid -10%	
	Flattened ellipsoid	<i>Amphidinium</i> sp. (O: A), <i>Dinophysis acuminata</i> (O: O), <i>Dinophysis acuta</i> (O: O), <i>Dinophysis rotundata</i> (O: T), <i>Dinophysis</i> sp. (O: O), <i>Gymnodinium</i> sp. (O: O), <i>Gyrodinium</i> sp. (O: A), <i>Pronoctilica pelagica</i> (O: O), <i>Pronoctilica</i> sp. (A: A), <i>Prorocentrum micans</i> (O: T), <i>Prorocentrum</i> sp. (O: O), <i>Torodinium</i> sp. (O: A), <i>Torodinium teredo</i> (A: T).
	Parallelepiped	<i>Lioloma pacificum</i> (A: T/ C), <i>Meuniera membranacea</i> (A: T/ C), <i>Thalassionema nitzschoides</i> (O: O), <i>Thalassiothrix</i> sp. (A: T).
	Parallelepiped -40%	<i>Navicula</i> sp. (O: O), <i>Navicula transitans</i> (O: T), <i>Oxytoxum</i> sp. (A: D/ B).
	Half parallelepiped	Pennate Diatoms (O: O/ A).
	Cone	Ciliates (A: A), Choanoflagellates (A: A).
	Half cone	<i>Minuscula bipes</i> (O: O).
	Cone+half sphere	<i>Amphidoma caudata</i> (A: D).
	(Cone+half sphere) -20%	<i>Protoperidinium curtipes</i> (A: D), <i>Protoperidinium depressum</i> (O: O/ T/ D).
	(Cone+half sphere) -25%	<i>Protoperidinium steinii</i> (O: O/ D), <i>Protoperidinium</i> sp. (O: O).
	(Cone+half sphere) -40%	<i>Asterionellopsis glacialis</i> (O: O).
	Monoraphidoid	<i>Pyrocystis lunula</i> (A: T).
	Rotational ellipsoid / parallelepiped	<i>Lioloma</i> sp. (A: T/ O), <i>Thalassionema</i> sp. (A: T/ O).
	Rotational ellipsoid + cylinder	<i>Commation cryoporinum</i> (A: B).
	2 cones	<i>Ceratium fuscus</i> (H: T).
	Cone+2 cones+cylinder	<i>Ceratium arietinum</i> (H: D), <i>Ceratium tripos</i> (H: T).
	Flattened ellipsoid+3cylinders	<i>Ceratium macroceros</i> (H: D).
	Flattened ellipsoid+2 cones+cylinder	<i>Ceratium candelabrum</i> (H/ S: T), <i>Ceratium furca</i> (H/ S: T), <i>Ceratium horridum</i> (H: T), <i>Ceratium kojoidii</i> (H: T), <i>Ceratium lineatum</i> (H: T), <i>Ceratium</i> sp. (A: A).

Impact factor report

Abbreviated Journal Title	J Plankton Res
ISSN	0142-7873

JCR Data	Total Cites	5753
	Impact Factor	2.435
	5-Year Impact Factor	2.423
	Immediacy Index	0.725
	Articles	91
	Cited Half-life	>10.0
<i>Eigenfactor</i>[®] Metrics	<i>Eigenfactor</i>[®] Score	0.00975
	<i>Article Influence</i>[®] Score	0.894

Source: Journal Citation Reports, Science Edition 2012 (Thomson Reuters).

Chapter IV. Autotrophic community size-structure and photoacclimation in a temperate shelf (Southern Bay of Biscay)

The structural characterization of the phytoplankton community with FlowCAM can be applied for a variety of scales, from long to short-term. In this chapter we analyze the dynamics of the phytoplankton community for a whole year and during two contrasted scenarios in summer and autumn in the Central Cantabrian Sea. The description of the hydrographical scenario showed temperature, light and nutrients as the main drivers of community size structure and physiology. The size structure and carbon biomass derived from FlowCAM were coupled with chlorophyll bulk measurements allowing a combined approximation to the phytoplankton community dynamics. The biomass and chlorophyll size spectra followed different trends which translated in changes in the chlorophyll to carbon ratio, for the whole community but also between size-fractions. The size dependence to the chlorophyll content was found to vary with field irradiance.

Reference

Eva Álvarez, Enrique Nogueira, Ángel López-Urrutia and Xose Anxelu G. Morán (2014) Autotrophic community size-structure and photoacclimation in a temperate shelf (Southern Bay of Biscay). (Manuscript).

Candidate's contribution

My contribution to the work includes the co-design of the study and the establishment of methodology in collaboration with the rest of coauthors. I obtained data from FlowCAM whereas XM obtained data from flow cytometry. I analyzed data and prepared tables and figures. All authors discussed the results, composed and co-write the article.

Autotrophic community size-structure and photoacclimation in a temperate shelf (Southern Bay of Biscay)

Eva Álvarez*, Enrique Nogueira, Ángel-López Urrutia and Xosé Anxelu G. Morán.

Instituto Español de Oceanografía. Centro Oceanográfico de Gijón, 33212, Gijón, Spain.

*e-mail corresponding author: eva.alvarez@gi.ieo.es

Running Head: *Community size-structure and photoacclimation*

KEYWORDS: phytoplankton, community structure, light, nutrients, carbon to chlorophyll ratio, size-spectra, southern Bay of Biscay shelf.

Shelf waters of the Cantabrian Sea (Southern Bay of Biscay) are productive ecosystems with a marked seasonality. The size-structure of the autotrophic community (from pico- to micro-phytoplankton) is tightly coupled with the meteo-climatic and hydrographic conditions, and has important implications for primary productivity in this region. We present here the results from one year of monthly monitoring together with an intensive sampling carried out in two contrasting scenarios during summer and autumn in a mid-shelf area of the Central Cantabrian Sea. Stratification was apparent on the shelf in summer, while the water column was comparatively well-mixed in autumn. At short-term, variations in the size-structure and chlorophyll content of phytoplankton cells were related with changes in the physical-chemical environment, through changes in the availability of nutrients and light. Uncoupling between dynamics of carbon biomass and chlorophyll resulted in chlorophyll to carbon ratios dependent on body size. The size-scaling of chlorophyll content increased with increased irradiance, reflecting different photoacclimation plasticity from pico- to micro-phytoplankton. The results have important implications for productivity and the fate of biogenic carbon in this region.

Introduction

The observed attributes of the autotrophic plankton community, such as productivity, community structure or diversity, are the result of a combination of a variety of biological processes occurring at different organisation levels, from individuals to populations, and the variability of the physical environment acting at a wide range of spatial and temporal scales (Rodriguez, 1994). The structure of the community, characterised by its species composition, size-spectra or trophic relationships among its components are important for the fate of productivity and the transfer of energy and matter across the food web (Nielsen & Hansen, 1999). The study of the whole autotrophic community on the basis of size as a scaling factor and aggregation criterion permits inferences about ecosystem energetics and metabolism to be made, which are relevant to ascertain energy transfer efficiency across the food web and the amount of biomass that can be sustained at higher trophic levels.

The introduction of flow cytometry techniques in oceanography allowed the enumeration and sizing of single cells (Yentsch *et al.*, 1983; Sieracki *et al.*, 1998) and the estimation of cellular carbon biomass from cell biovolume. The normalized biomass-size spectrum (NBSS) is a structural representation of the plankton community (Rodriguez & Mullin, 1986) whose slope indicates the relative contribution of each size-class to the total phytoplankton community. Unproductive ecosystems are characterized by more negative slope values (steeper spectra), whereas productive waters show less negative slope values (flatter spectra) (Cavender-Bares *et al.*, 2001).

The size-spectra derived from flow cytometry methods allow the estimation of phytoplankton carbon biomass, a measure that is hard to measure directly. Instead, phytoplankton biomass is often inferred from chlorophyll *a* (named Chl-*a*, hereafter), a pigment that is common to all planktonic autotrophs and can be easily measured. It is well known that the phytoplankton Chl-*a* to carbon (Chl-*a*:C) ratio increases with increasing irradiance under nutrient replete conditions, a phenomenon called photoacclimation. Hence, the content in pigments is an indicator of the physiological status of the cells (Geider, 1987), and the intracellular concentration of chlorophyll can be used to estimate the productivity of the ecosystem (Behrenfeld *et al.*, 2002). It has been argued that focusing on eco-physiological traits may lead to improved mechanistic linkages between environmental drivers and community composition (McGill *et al.*, 2006; Litchman & Klausmeier, 2008) and may ultimately allow prediction of community structure from first principles on physiology and morphology (Edwards *et al.*, 2013). Hence, cell size and elemental stoichiometry appear as basic eco-physiological traits that can account for a physiological description of the community focusing on aspects such as

Results

pigment content or photosynthesis rate. The combined effects of light, nutrients and temperature on the phytoplankton Chl-a:C ratio in the real ocean are not well known. Moreover, little is known about the relative roles of light, temperature and nutrients regulating the large scale variability in the phytoplankton Chl-a:C ratio. Also, there is a lack in field sampling that accounts for the size-dependence of the Chl-a:C ratio.

The Bay of Biscay is a typical temperate ecosystem, and as such is characterized by strong seasonality of the water column mixing-stratification cycle. Besides, the spring to summer transition in the Cantabrian Sea is associated with a shift from coastal downwelling to upwelling conditions (Fernández & Bode, 1991). The general circulation is anticyclonic (Pingree & LeCann, 1990) but hydrodynamics along the northern and western Iberian shelf are also affected by the presence of subtropical and saline waters transported by the Iberian Poleward Current (IPC, Peliz *et al.*, 2005) from late autumn to early spring. Phytoplankton physiology and production are highly influenced by hydrographical conditions, and hence the abundance of phytoplankton cells follows strong seasonal cycles. The phytoplankton dynamics on the area are characterized by an annual maximum of phytoplankton biomass and production in late winter / early spring when enhanced solar radiation and surplus of inorganic nutrients allow the accumulation of phytoplankton biomass. During winter, when the solar radiation is greatly reduced, the production keeps in annual minimum levels. Phytoplankton production is not, however, a single spring feature, the spring bloom, but extend into the rest of the year with different intensity, contributing significantly to regional productivity. Autumn blooms take place thanks to replenishment of nutrients in surface layer under sufficient light levels. During summer, the strong thermal stratification and the consumption of nutrients that have been taken place previously associated to the spring bloom drive the depletion of nutrients in the surface layer, promoting the dominance of pico- and nanoplankton, the development of a sub-surface chlorophyll maximum and relatively low values of depth-integrated biomass and production (Granda & Anadón, 2008).

In the present work, we analysed the seasonal and short-term dynamics of the meteo-hydrographic scenario and phytoplankton community in the southern Bay of Biscay shelf. We present a complete year of monthly sampling in a mid-shelf station coupled to two intensive (daily) surveys at the same location carried out in summer and autumn, during which the hydrographic situation, and biomass stocks, size structure and chlorophyll to carbon ratios of the phytoplankton community were monitored. Our goal was to study two different meteo-hydrographic scenarios with high between-regime differences in phytoplankton carbon biomass and pigment content within the context of the seasonal cycle.

Material and Methods

Sampling at sea

Intensive sampling was carried out at a mid-shelf oceanographic station (43.67° N, 5.58° W, ca. 110 m depth in low water) in the central Cantabrian Sea (Southern Bay of Biscay) during summer (17th-29th August) and autumn (6th-23rd November) of 2008. The station was visited almost daily around noon (maximum sampling interval 3 days) during these contrasting seasonal scenarios. Supplementary oceanographic data acquired monthly at this location within the frame of the time-series monitoring programme RADIALES (<http://www.seriestemporales-ieo.net/>) were used to define the seasonal context (from April 2008 to April 2009).

The water column was sampled with a rosette sampler equipped with Niskin bottles and a conductivity-temperature-depth probe CTD (SBE 25), with auxiliary sensors for the measurement of fluorescence (SCUFA Turner) and photosynthetic active radiation (PAR) (Biospherical/Licor). Vertical profiles of temperature, salinity, *in vivo* fluorescence and PAR were obtained from the surface (3 m depth) down to 100 m. The mixed layer depth (MLD) was defined as the depth where the temperature decreases 0.8 °C from the surface value (Kara *et al.*, 2000). The euphotic zone depth (Z_{eu} , m) was estimated as the depth where light represents 1% PAR level at the surface (Kirk, 1994). Water samples were collected from Niskin bottles at eight fixed depths of 3, 10, 20, 30, 40, 50, 75 and 100 m for the analysis of nutrients and chlorophyll concentrations. For the analysis of the autotrophic community by means of flow cytometry and FlowCAM, water samples from the bottles were collected at 5 depths in summer (3, 20, 40, deep chlorophyll maximum (DCM) and 75 m) and 3 depths in autumn (3, 20 and 75 m). The DCM was established on the basis of the vertical profiles of *in vivo* fluorescence.

Analytical procedures

Biogeochemical variables

Water samples for the analysis of inorganic nutrients (around 5 mL) were frozen (-20 °C) and kept in the dark until analysis in the laboratory with a Skalar San Plus System auto-analyzer. Nutrient concentrations (μM of ammonium, nitrite, nitrate, silicate and phosphate) were estimated by replicated segmented flow analysis (Grasshoff *et al.*, 1983). The nitracline was defined as the depth where the concentration of nitrate was 1 μM .

Results

Total chlorophyll was estimated from 100 mL of water filtered onto Whatman GF-F filters. For the analysis of size-fractionated chlorophyll, another 100 mL were filtered sequentially through 20, 2 and 0.2 μm nominal pore-size polycarbonate filters (Millipore). In both cases, filtrations were carried out at low vacuum pressure (<100 mm Hg), and filters were frozen in the dark until analysis. Pigments were extracted in 3 mL of acetone 90% during 24 h at 4°C. Total and size-fractionated concentrations of chlorophyll a were determined spectrofluorimetrically (Perkin Elmer LB-50s).

Autotrophic community

Phototrophic pico-plankton within the size-range 0.2-3 μm equivalent spherical diameter (ESD) was analysed from water samples of 1.8 mL, fixed with 1% paraformaldehyde plus 0.05% glutaraldehyde solution, deep-frozen in liquid N_2 and stored at -70°C until analysis. The abundance and size of pico-planktonic cells was determined by flow cytometry (FACSalibur, Becton & Dickinson). After analysis, cells found in the cytograms were separated into five categories according to size estimations based on side-scattered light and emitted fluorescence properties (FL2, 585 nm and FL3, >650 nm) (Olson *et al.*, 1993): *Synechococcus* and *Prochlorococcus* cyanobacteria, two groups of eukaryotic cells, distinguished according to their SSC signal as 'small' and 'large' eukaryotes, and Cryptophyta cells. Mean cell diameters of the different groups were obtained after sequential filtration through polycarbonate filters ranging from 0.2 to 3.0 μm pore-size (Zubkov *et al.*, 1998). A spherical shape was assumed for all groups. Biomass was finally calculated applying volume-to-carbon conversion factors (Worden *et al.*, 2004). A detailed description of the flow cytometry methods that have been applied can be found elsewhere (Calvo-Díaz & Morán, 2006).

Samples for the analysis of nano and micro-phytoplankton (5-100 μm) by means of the Flow Cytometer And Microscope (FlowCAM) were collected from the oceanographic bottles by filtering gently through a 200 μm mesh-size 1.1L water, that was kept fresh in the dark until analysis in the lab within the next few hours after collection. Details of FlowCAM design and image acquisition procedures are available elsewhere (Sieracki *et al.*, 1998). Samples were processed in fluorescence-triggered mode, by means of which only those particles emitting red fluorescence (PMT1, >650 nm) when excited by a blue laser fan (488 nm) are photographed. Samples were split in two subsamples, one for nanoplankton and the other for microplankton size-fractions. The nanoplankton aliquot was pre-filtered by a 53 μm mesh and processed un-concentrated, pouring 1 mL of sample into the sample inlet and using a FC50-200x flow chamber-lens combination. For microplankton, 1L was pre-filtered by 100 μm mesh and concentrated to around 20 mL by reverse filtration (Dodson & Thomas, 1978) through a 15 μm net. 10 mL of this

subsample was processed using a FC100-100x flow chamber-lens combination. The instrument was cleaned with distilled water between sub-samples and with a 2% bleach solution at the end of the day (maximum 10 samples). The application of the described sample processing protocol provides reliable estimates of abundance in the ESD range 5 - 100 μm (Álvarez *et al.*, 2011). The images provided by the FlowCAM were automatically classified as described in (Álvarez *et al.*, 2012) to discriminate among different categories (nano-eukaryota, diatoms, silicoflagellates, dinoflagellates, ciliates and micro-eukaryota) and remove detritus from the analysis. Particle biovolume was calculated as a revolution volume according to the shape of the particles and the dimensions (length and width) measured by image analysis. Biovolume was converted to carbon according to the functional group predicted, applying different conversions factors for cells smaller than 3000 μm^3 , cells larger than 3000 μm^3 except diatoms, and diatoms larger than 3000 μm^3 (Menden-Deuer *et al.*, 2000).

Data analysis

The three phytoplankton subsamples corresponding to the pico- (analysed by flow cytometry), nano- and micro-plankton size fractions (both analysed by FlowCAM) were combined to produce normalised biomass size spectra (NBSS). To this aim, biomass (mg C m^{-3}) was distributed in biovolume-classes established on an octave scale (from 2^{-6} to 2^{18} μm^3 in biovolume, which is equivalent to a size range from 0.2 to 100 μm ESD). Only those size classes with statistically reliable counts (>5 counts per biovolume class) and to the left of the modal class (García *et al.*, 1994) were considered. The biomass size spectrum (BSS) obtained in this way were normalized by dividing each bin by the width of the biovolume-class. A linear regression was fitted to the log-log transformed data to estimate the parameters, slope and intercept, of the NBSS.

We used the parameters of the linear regressions fitted to the NBSS to estimate biomass in specific size ranges by integrating the area under the linear function within this size range. This procedure has the advantage of minimizing the effect of missing bins or bins deviating from linearity. Biomass was integrated in three size fractions, pico- (0.2-2 μm), nano- (>2-20 μm) and micro-phytoplankton (>20-200 μm), for which size-fractionated chlorophyll was also determined. Then, the ratio between chlorophyll and carbon biomass (Chl-a:C ratio), which represents an index of phytoplankton acclimation to different growth irradiances (Geider, 1987), was estimated for the total autotrophic community and for each size-fraction.

The three size-fractions of chlorophyll and Chl-a:C ratio were combined to estimate normalized chlorophyll size spectra (NCSS) and normalized Chl-a:C size spectra (NChl-a:CSS). The lower limit of the size interval was considered as nominal size of the

Results

size-class. The parameters of the linear relationship in a log-log scale (slope and provisional value of the intercept) were estimated by fitting a linear regression model to the points of each spectrum. The provisional value of the intercept was corrected by a factor that depends on the geometric progression of the size-classes and the nominal size chosen (Blanco *et al.*, 1994).

From the *in situ* PAR profiles, the attenuation coefficient (k_d) for each day was estimated with the light extinction equation ($I_z = I_0 \times e^{-k_d z}$), where I_z and I_0 represent irradiance at a given depth and in the surface, respectively, and z is the depth in the water column. Surface PAR on an hourly basis was recorded on a meteorological station sited on land near the sampling area (43.54°N, 5.62°W, at 30 mamsl). The daily profiles of irradiance were estimated from the average surface solar radiation during the hours of light and assuming a constant k_d . To estimate the history of irradiance for each sample, the irradiance at the depth of the sample was estimated in the 24 hours previous to the sampling hour (only light hours) from surface solar radiation and assuming a constant k_d . The irradiance values were weighted and averaged taking into account the elapsed time.

The dependency of Chl-a:C on light can be modelled as an exponential function of light (Cloern *et al.*, 1995; Behrenfeld *et al.*, 2002). Chl-a:C_{N,T-max} is the function that accounts for the maximum potential community Chl:C value for a given irradiance level (Chl-a:C_{N,T-max} = Chl-a:C_{min} + [Chl-a:C_{max} - Chl-a:C_{min}] × [exp^{-3I_z}]) where Chl-a:C is the chlorophyll to carbon ratio of the sample and I_z is the irradiance level at the sampled depth z . For each size fraction, the Chl-a:C_{min} and Chl-a:C_{max} were estimated by quantile regression as the equation that enveloped the 90% of the Chl-a:C vs. irradiance points ($\tau=0.90$) (Vázquez-Domínguez *et al.*, 2013).

To explore the variations of the main variables in the water column we used two dimensional contour graphs of time (x-axis) vs. depth (y-axis) with isoclines representing the variable (z). The data points were irregularly spaced so we performed a bivariate interpolation onto a regular grid (Akima, 1978).

Results

Seasonal context

Hydrographic conditions showed the characteristic seasonality of a northern temperate shelf, defined by the alternation of a thermal stratified period from May to October and a well-mixed period from December to March, with transitional phases in spring and autumn (Fig. 1A). The mixed layer depth (MLD) ascended sharply from the bottom (110 m) to 30 m during the spring transition, remained between 20 and 40 m during the summer stratified period and descended gradually down to the bottom between the autumn transition and early winter (Fig. 1A). The level of underwater PAR (daily averaged) exhibited also two contrasting phases, with higher irradiance levels during the thermally stratify period than during the well-mixed and transitional periods (Fig. 1B). The seasonal variation of nutrients (exemplified by nitrate in Fig. 1C) is modulated by the annual cycles of hydrographic conditions and phytoplankton production. The surface concentration of nutrients decreased to minimum levels during the spring bloom (both in April 2008 and 2009). In 2008, the nitracline depth (Z_N , proxy for the nutricline depth due to high co-variation among inorganic nutrients) deepened down to 60 m, and remained below 40 m during the stratified period. The vertical gradient of nutrients relaxed in early autumn, and subsequent winter mixing caused the replenishment of the surface nutrients pool (February 2009).

The annual evolution of the autotrophic was coupled with the seasonality of hydrographical scenario. The spring bloom was dominated by large- or medium-size autotrophic components, which translates in size-spectra with relatively steeper slopes (Fig 1D). At the end of the spring, concurrent with the exhaustion of nutrients, the spring bloom decayed (Fig 1E). The dominance of small cells in these nutrient poor conditions translates into steeper size spectra (i.e. lower slope values). The stratified period was characterize by relatively low Chl-a:C ratios with an increase in the Chl:C ratio with depth (Fig. 1F). The autumn bloom was characterized by flatter size-spectra (i.e. higher slope values) and autotrophic community was characterised by high Chl-a:C ratios with a narrow range of vertical variation.

Short-term dynamics during summer stratification and autumn transition

Hydrographic conditions during the summer survey were characterised by a strong thermal stratification (surface to bottom temperature ranged from 22-12 °C) and the ascent of the MLD from 40 m at the beginning of the cruise to 20 m towards its end (Fig. 2A). Underwater PAR levels within the MLD were high during the whole survey:

Results

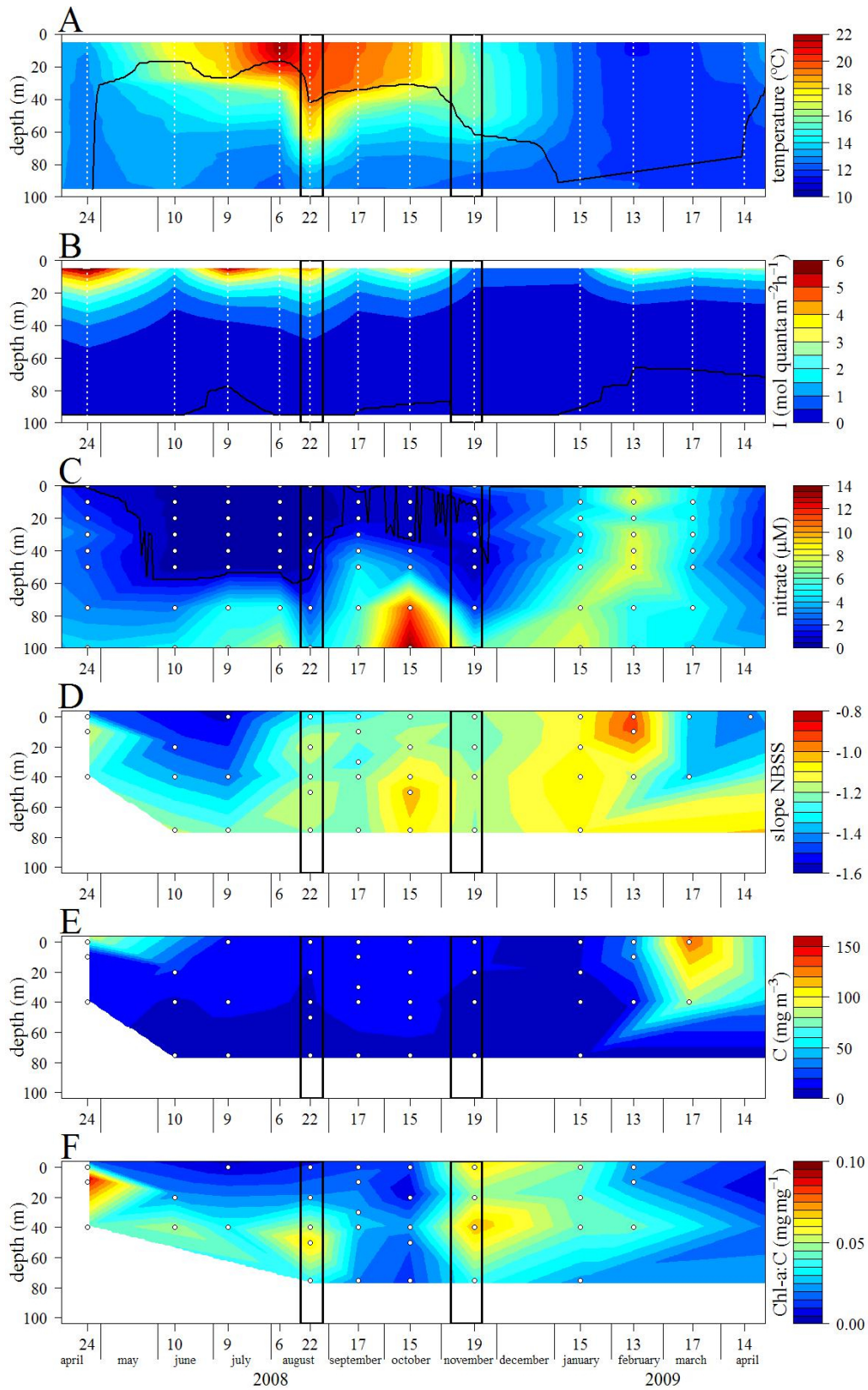


Figure 1 Seasonality of physical and biogeochemical variables. **(A)** Temperature and mixed layer depth (MLD); **(B)** Photosynthetically active radiation (PAR) and euphotic depth (z_{eu} , 1% PAR); **(C)** Nitrate and depth of the nitracline (z_{N3} , 1 μM isocline); **(D)** Slope of the NBSS; **(E)** Total carbon biomass; **(F)** Chlorophyll to carbon ratio.

surface values reached $5 \text{ mol quanta m}^{-2} \text{ h}^{-1}$ and Z_{eu} kept below 100 m (Fig. 2B). The opposite trends of MLD and Z_{eu} resulted in the increment of the $Z_{\text{eu}}:\text{MLD}$ ratio from 2 to 5. The concentration of nutrients showed a sharp vertical gradient. Nitrate was below detection limits at the surface, except for a short period during the first two sampling days, and reached maximum concentrations at the bottom (around $9 \mu\text{M}$). The nitracline deepened from 20 m at the beginning of the cruise to a maximum of 60 m on the 23rd, lifting up from this depth to the surface during the following days (Fig. 2C).

The concentration of autotrophic carbon biomass was low at all depths, with larger contribution of pico-, and to a lesser extent nano-, size-fractions, which translates into steeper and relatively constant size spectra slopes (-1.26 ± 0.08) during the whole period (Fig. 2D). Relatively high carbon biomass values (around $20\text{-}30 \text{ mg C m}^{-3}$) occurred not only at the subsurface but also at the surface (Fig. 2E). The pattern of chlorophyll differed from that of autotrophic carbon biomass, since total chlorophyll during the summer survey reached maximum values only at the sub-surface. The discrepancies between chlorophyll and carbon biomass fields translates in the variability of the C:Chl-a ratio (Fig. 2F), which decreased with depth, reflecting the acclimation of the pigment content of phytoplankton cells to progressively decreasing light levels.

During the autumn transition, the MLD fluctuated between 50 and 80 m. Temperature within the mixed layer was almost homogeneous and thermal inversion developed in association to buoyancy driven plumes that reached the mid-shelf (Fig. 2G). Daily averaged solar radiation was significantly lower than in August, with maxima of $3.5 \text{ mol quanta m}^{-2} \text{ h}^{-1}$ at the beginning of the sampling descending to less than 1.5 towards the end. Although underwater irradiance levels at noon decreased sharply in the first 10 m of the water column, the euphotic zone still ranged from 75 to 100 m, with $\text{MLD}:Z_{\text{eu}}$ ratios from 1.5 to 1 (Fig. 2H). The vertical gradient of nutrients persisted during the studied period, although it was less intense than in August and was eroded several times due to successive surface nutrient enrichment episodes associated to runoff pulses, causing Z_{N} to oscillate between 40 m and the surface (Fig. 2I).

Maximum carbon biomass values were higher than in the summer and took place at the surface. The distribution of total biomass was characterised by a marked vertical gradient, with surface peak values of 50 mg C m^{-3} and increased biomass within the MLD towards the end of the studied period (Fig. 2K). Despite the variability of total biomass, the partaking of carbon among size-fractions kept relatively constant during the whole period, which summarized in flatter spectra than in August and nearly constant (-1.18 ± 0.08) NBSS slopes (Fig. 2J). The average C:Chl-a ratios of the autotrophic community were significantly higher than in the summer (Fig. 2L). The ratios also decreased with

Results

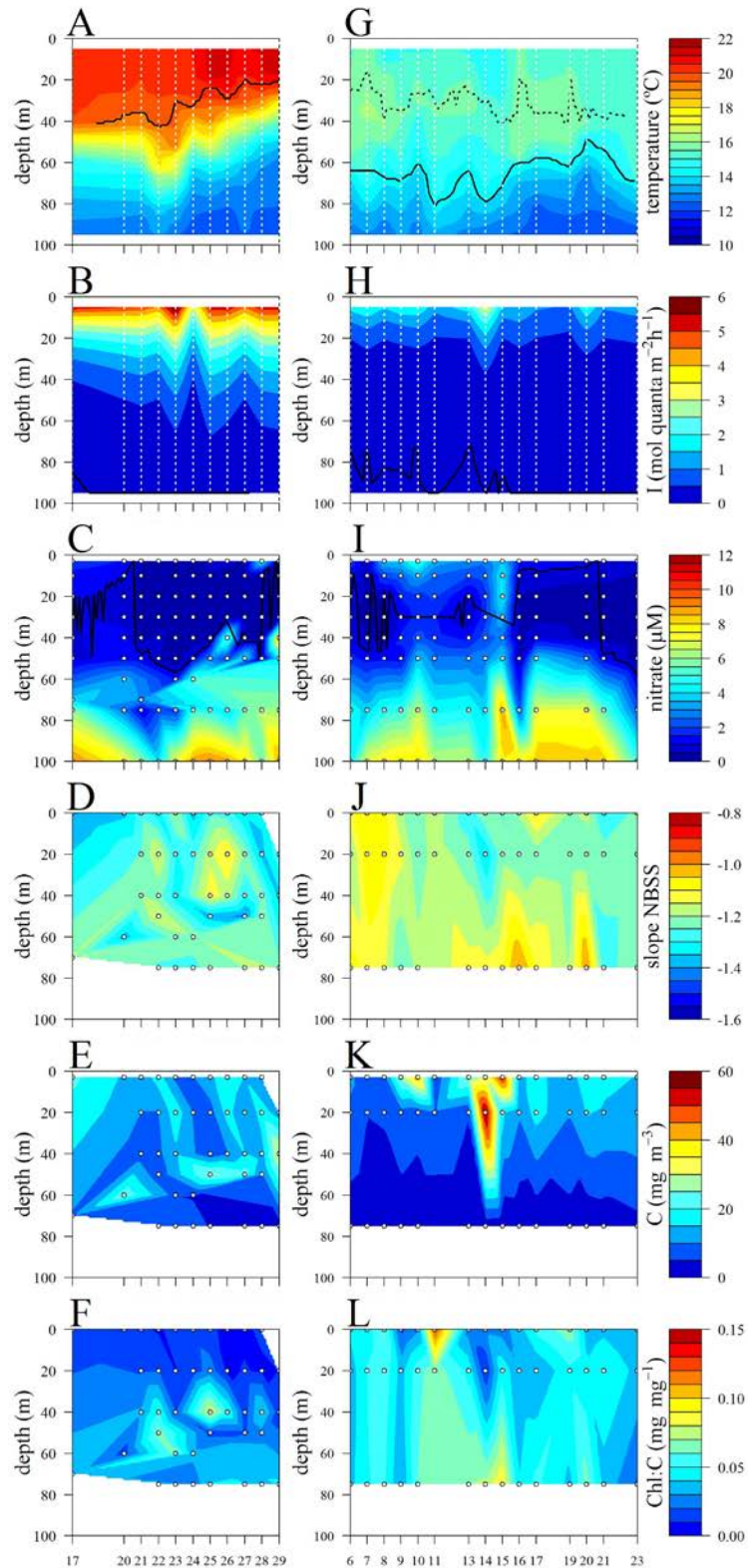


Figure 2 Physical and biogeochemical variables during the intensive cruises carried out in August (left column) and November (right column): **(A and D)** Temperature and MLD (dotted line indicates thermal inversion); **(B and E)** Photosynthetic Active Radiation (PAR) and Z_{eu} (1% PAR); **(C and F)** Concentration of nitrate (μM) and Z_N ($1 \mu\text{M}$ isoline); **(D and J)** Slope of the NBSS; **(E and K)** Total autotrophic carbon biomass; **(F and L)** Chlorophyll to carbon ratio.

depth, although the vertical gradient was not so sharp (from 0.1 at the surface to round 0.05 at 75 m depth). The high Chl-a:C ratios reflected the acclimation of the community to reduced solar radiation levels during autumn, and the diminished difference between surface and bottom ratios reflect the mixing regime that the phytoplankton cells experienced during this period.

Coupling of community size structure with meteo-hydrographical drivers

We observed a descriptive relationship between the variability of the slope of the NBSS and nitrate concentrations, especially at the seasonal scale (Fig. 1C and D). To evaluate the role of nutrients and temperature as potential drivers of the variability of the NBSS slope, we first eliminated the dependence on temperature with a linear regression model between the slope of the NBSS and temperature (Fig. 3A). It is not possible to correct efficiently the relationship between nutrients and temperature, due to co-linearity between both variables, since temperature is an indicator variable of other processes which are driving the observed variability in nutrients, i. e. coastal upwelling-downwelling events and mixing-stratification cycles (Fig. 3B). So, we cannot quantify the effect of temperature and nutrients on the slope of the NBSS, but the significant correlation between the residuals of slope vs. temperature and the residuals of the nutrients vs. temperature indicated that nutrients have indeed an effect on the slope, even filtering out the effect of temperature on both the independent and dependent variables and, hence, both nutrients and temperature control the slope of the NBSS (Fig. 3C).

We then explored the effect of light on the Chl-a:C ratio (Fig. 4). Given the oligotrophic conditions in summer, the functional groups that contributed larger to carbon biomass were eukaryotic pico- and nano- phytoplankton. Micro-phytoplankton was much less abundant. Then the parameters of the NBSS remained relatively constant during August and the global spectra for the period had a slope of -1.24 (Fig. 4A). In autumn, on the other hand, the whole community contribute to the increase in biomass, and microplankton was more abundant than in summer. Although the increment of biomass took place in form of pulses on days 9th, 14th and 20th, the NBSS remained relatively constant during November with slopes flatter than in August: the global spectra had a slope of -1.13 (Fig. 4B). The patterns were different for the chlorophyll size-spectra, since the slope of the Chl-a global spectra was -1.08 in summer (Fig. 4C) decreasing to -1.12 in autumn (Fig. 4D). This opposite patterns between carbon and chlorophyll size spectra in the two periods resulted in different scaling of the Chl-a:C ratio. The slope of the size spectra of the Chl-a:C ratio in November was close to 1 (-0.94, Fig. 4F) given the similarity between the NBSS and NCSS slopes. This means that the

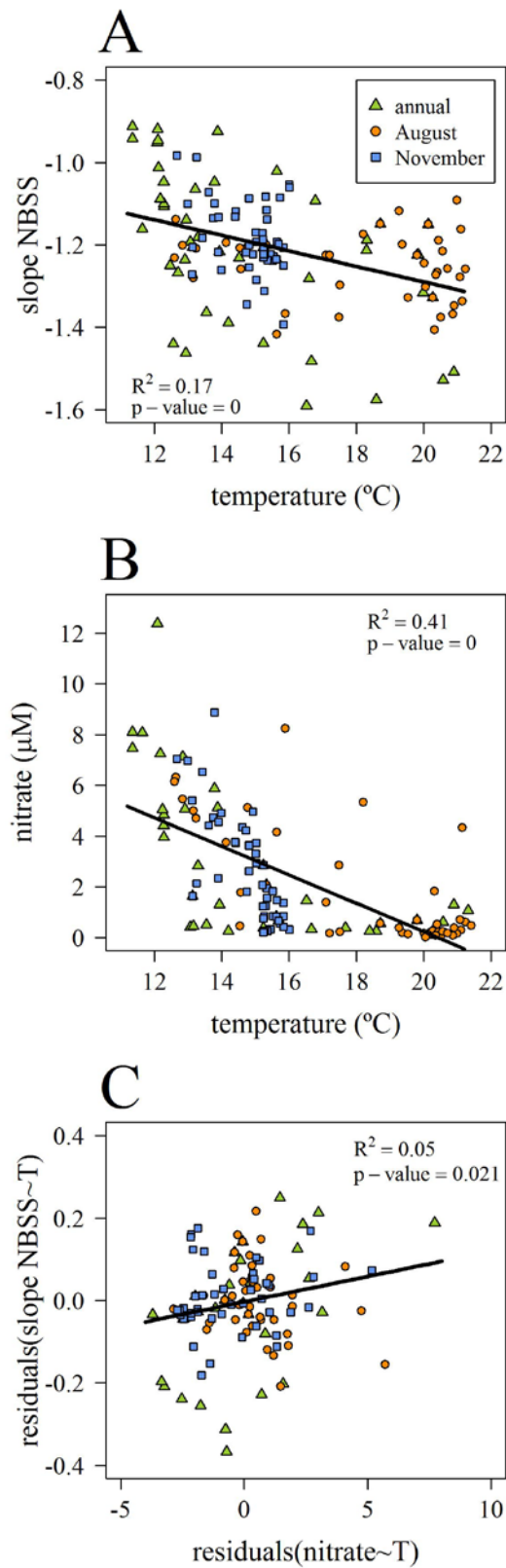


Figure 3 (A) Slope of the normalized biomass size spectra (NBSS) as a function of temperature and (B) nitrate concentration as a function of temperature. (C) Residuals of the correlation in A (slope of the NBSS eliminating the effect of temperature) as a function of the residuals in B (nitrate concentration eliminating the effect of temperature).

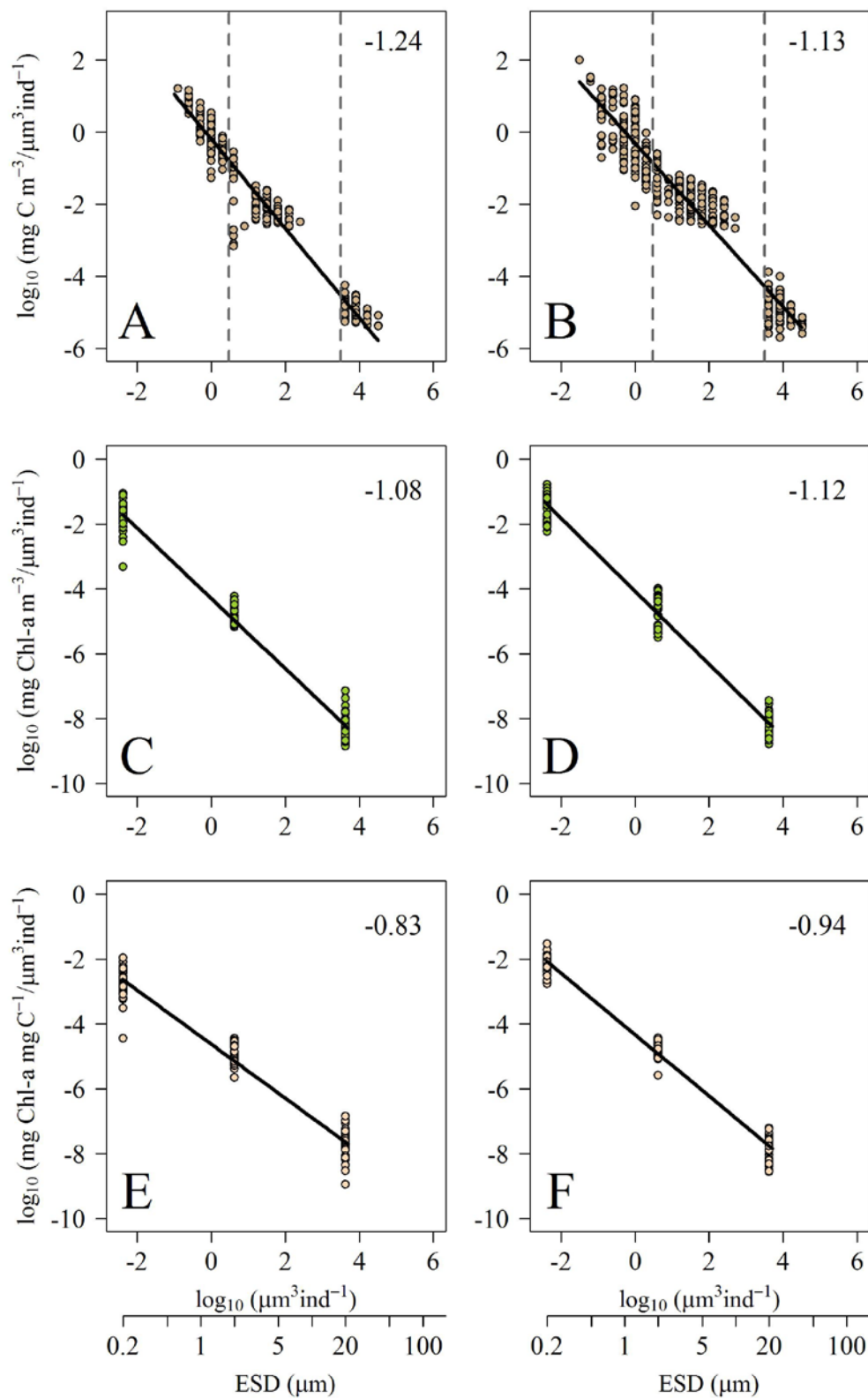


Figure 4 Global biomass size spectra of phytoplankton for all the samples taken during the intensive cruises carried out in August (left column) and November (right column): (A and B) normalized biomass size spectra; (C and D) normalized chlorophyll size spectra; (E and F) normalized chlorophyll to carbon ratio size spectra.

Results

concentration of chlorophyll was homogeneous between size-classes. The Chl-a:C ratio size spectra slope in August was steeper than one (-0.83, Fig. 4E) indicating that the concentration of chlorophyll was relatively lower in the small cells. This differences between August and Autumn in the Chl-a:C slopes can be explained by the different irradiance conditions.

Size scaling of the photoacclimation

The complex effect of light, nutrients and temperature lead to a variable chlorophyll to carbon ratio in phytoplankton cells. Picophytoplankton had in general lower Chl-a:C ratios at all depths than the nano- and micro- size-fractions and hence the $\text{Chl-a:C}_{N,T-\max}$ functions were scaled (Fig. 5). The values of Chl-a:C_{\min} and Chl-a:C_{\max} varied for the three size fractions (0.04-0.06 for pico, 0.09-0.12 for nano and 0.18-0.26 for micro-phytoplankton) which means that the photoacclimation through the variation of the Chl-a:C ratio was size dependent (Fig. 6A).

To clarify this fact and its implications of the size scaling of the photoacclimation we made a series of predictions with the parameters of the $\text{Chl-a:C}_{N,T-\max}$ functions obtained. The three $\text{Chl-a:C}_{N,T-\max}$ functions were used to predict the Chl-a:C for each size-fraction for a sequence of irradiances (Fig. 6B). The relationship between Chl-a:C and the lower biovolume limit of the size fraction in a log-log scale shows the size scaling of chlorophyll concentration and the exponent of the size scaling for each irradiance level was obtained with a reduced major axis model. The exponent of the size scaling increased with increasing irradiance (Fig. 6C).

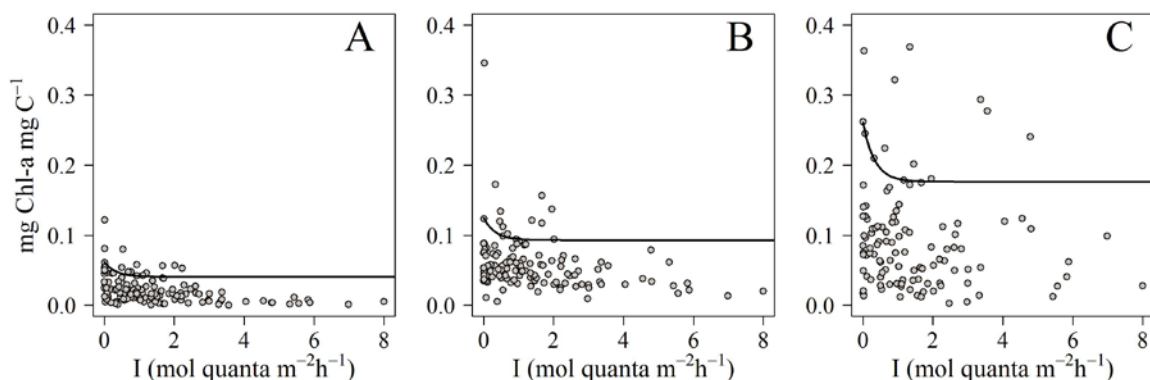


Figure 5 Chlorophyll to carbon ratio ($\text{mg Chl-a mg C}^{-1}$) as a function of irradiance at the sampling depth for the (A) pico-, (B) nano- and (C) micro-phytoplankton size fractions. Solid line denotes the $\text{Chl-a:C}_{N,T-\max}$ function fitted by quantile regression.

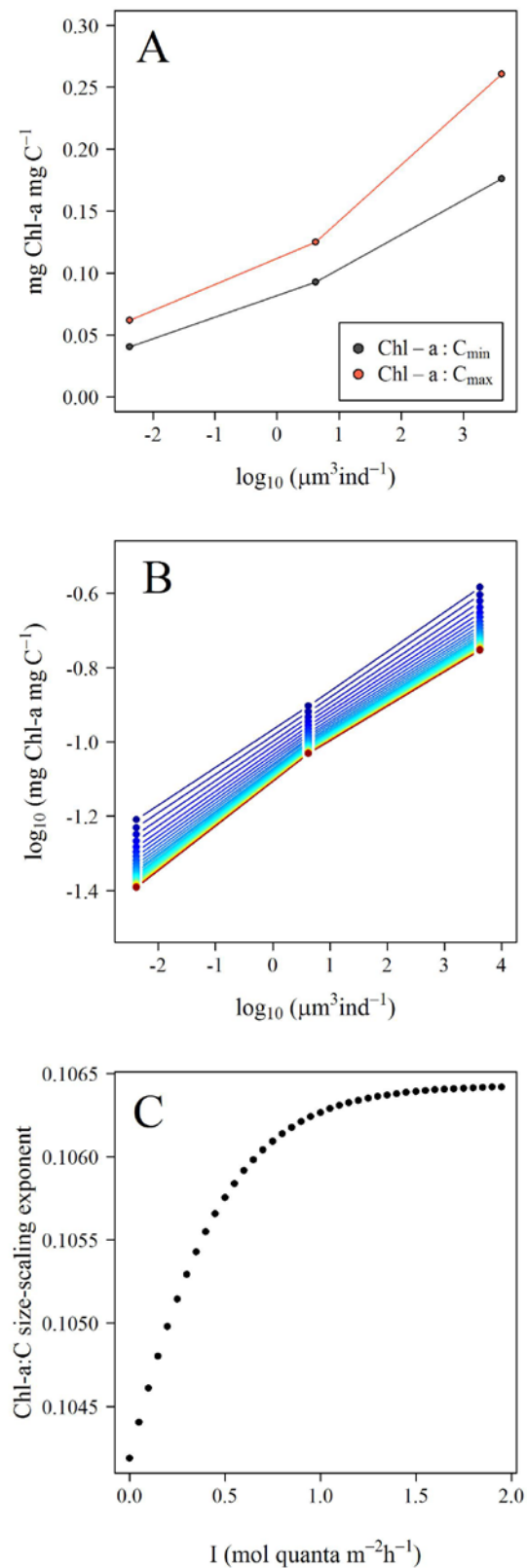


Figure 6 Size-dependence of photoacclimation: **(A)** parameters of the Chl:C_{N,T-max} function as a function of body size; **(B)** prediction of the size scaling of the Chl-a:C ratio for a sequence of irradiance values (cold to hot colours indicates low to high irradiance); **(C)** variation in the size-scaling exponent of Chl-a:C ratio as a function of irradiance.

Discussion

The seasonal scale addressed in this work allows to cover an ample range of oceanographic conditions. Also, the daily sampling scale of the intensive surveys permits a synoptic vision of the short-term dynamics of phytoplankton under contrasting scenarios. We have described the characteristic seasonality of the hydrographical conditions in a temperate shelf. The phytoplankton production appeared related to the MLD, the Z_{eu} and the Z_N , and the absolute levels of temperature, light and nutrients. The classical theories of spring bloom development invoke the relationship between the MLD and Z_{eu} . Accordingly, for the development of the spring phytoplankton bloom (SPB) the photosynthetic production must exceed losses due to respiration, provided that other loss terms such as grazing and exportation are negligible. This happens in spring in northern temperate ecosystems, when the cells keep limited within a shallow MLD when compared to the Z_{eu} , which allows the movement of the cells within the well illuminated part of the water column and the daily primary production remains positive (Sverdrup, 1953). However, water column stratification is not a requisite to keep cells above the critical depth. A relatively deep penetration of light coupled to weak turbulence can keep the growth rate of the cells above the exclusion rates, which causes the accumulation of biomass (Townsend *et al.*, 1992). Late-winter blooms has been described in the area following this mechanism (Álvarez *et al.*, 2009).

This study considers also short-term variability during two contrasting periods: summer, characterised by strong thermal stratification, depletion of nutrients within the surface mixed layer and deep light penetration; and autumn, characterised by mixing of the water column, replenishment of nutrients in surface layer and low light levels in the whole water column. The absence of nutrients in the surface layer during the summer period limited the phytoplankton biomass to the subsurface, where nutrients and light where sufficient to permit the growth of small cells, good competitors in the harvesting of light and nutrient resources. The low Chl-a:C ratios reflected the high levels of light regime experienced by phytoplankton cells. Light is primary responsible for the vertical increase of phytoplankton Chl-a:C ratio in the euphotic zone, a consequence of the water column stability in summer. On the other hand, the increase in nutrients into the upper layer during November allowed there to be enough nutrients and light available to trigger population increase. The phytoplankton pigment content during the autumn survey was highly dependent on mixing events, which caused that the Chl-a:C was homogeneous with depth. In this situation of low light availability, Chl-a:C ratios were relatively high, thus allowing phytoplankton cells to harvest light efficiently even when becoming drawn to low depths, and hence low light levels.

Since the size structure of phytoplankton community was driven by changes in temperature and nutrients, the NBSS slopes estimated during August are lower than in November, reflecting a dominance of small cells in the oligotrophic conditions characteristic of summer. During November, the NBSS were flatter (higher slope values), reflecting a relative increment of larger cells, explained by the replenishment of surface nutrients due to mixing and the inputs associated to buoyancy driven plumes due to to runoff episodes. On the other hand, the light levels drive the size-scaling of chlorophyll content. During November, the chlorophyll values were higher but the slope of the NCSS was more negative, while during August, chlorophyll content were lower, the NCSS flatter. Hence, the relationship between the phytoplankton carbon biomass and Chl-a concentration was non-linear because of the complex, and presumably interacting, influences of light, nutrients and temperature in the euphotic zone. During the autumn survey, phytoplankton carbon and chlorophyll were highly coupled, which means that chlorophyll is a good proxy for phytoplankton biomass, while during summer, phytoplankton carbon and chlorophyll were uncoupled, which indicates that chlorophyll concentration does not reflect the phytoplankton biomass. Results as those exposed in this work show that the description of community can change substantially when using chlorophyll or biovolume as a proxy for biomass.

An accurate estimation of the biovolume of the cells allows deriving their carbon content (Menden-Deuer *et al.*, 2000; Álvarez *et al.*, 2012). Chl:C ratios have been estimated for the whole autotrophic community or for specific compartments (Cermeño *et al.*, 2005; Vázquez-Domínguez *et al.*, 2013), *in situ* and even from space (Behrenfeld *et al.*, 2005). The C:Chl-a ratios showed a large degree of variability, but the Chl-a:C ratios obtained in this study fall in the range of those previously reported for another coastal and shelf realms (Gutiérrez-Rodríguez *et al.*, 2010). This fact, together with the expected observations of a increase in Chl-a:C ratios over depth during stratification, give us further confidence in the validity of our estimates.

The size-scaling exponent of Chl-a:C ratio increases with irradiance, reflecting a different photoacclimation per size class. This fact has been observed in laboratory experiments (Fujiki & Taguchi, 2002) and predicted by models (Finkel, 2004). Although the variations in Chl-a:C ratios in field studies has been described and follow similar trends as those exposed here (Cermeño *et al.*, 2005), the size scaling of chlorophyll content from *in situ* sampling is a less explored issue. Uncertainties arose, however, from this study, such as the need to deal with the low resolution of the size fractions of chlorophyll. Whereas flow cytometric techniques allow the enumeration and sizing of single cells, the data must be aggregated to compare with chlorophyll fractionation. However, flow cytometric techniques based on fluorescence, such as flow cytometry and

Results

FlowCAM, open the scope to the interpretation of fluorescence signals and the use of these signals as a proxy of the chlorophyll content on single cells (Sosik *et al.*, 1989).

Since the variability of the intracellular chlorophyll content from light acclimation and nutrient stress confounds the relationship between chlorophyll and phytoplankton biomass, there is a tendency to the development of carbon-based models (Behrenfeld *et al.*, 2005; Westberry *et al.*, 2008) that circumvents the problem of using chlorophyll as a proxy for biomass. Remote sensing approaches rely on realistic conversion between the phytoplankton carbon biomass and Chl-a concentration, hence the prediction of Chl-a:C ratios is fundamental.

Acknowledgements

The authors thank the captain and crew of the RV *Francisco de Paula Navarro* and the RV *José Rioja* for their work during the cruises of the project. We are indebted to all participants in the cruises for their work and dedication at sea and in the laboratory. We also thank F. Ronzón who kindly provided meteorological data from his meteorological station in Gijón.

Funding

This work was supported by the *Ministerio de Ciencia e Innovación* [project PERPLAN, '*Efecto de las perturbaciones meteorológico-hidrográficas en la estructura de la comunidad planctónica*', CTM2006-04854/MAR], the *Plan de Ciencia, Tecnología e Innovación del Gobierno del Principado de Asturias* [project IMAGINA and research grant BP07-081 to E.A.] and the *Instituto Español de Oceanografía* [project RADIALES].

References

- Akima, H. (1978) A method of bivariate interpolation and smooth surface fitting for irregularly distributed data points. *ACM Transactions on Mathematical Software*, **4**, 148-164.
- Álvarez, E., López-Urrutia, A. and Nogueira, E. (2012) Improvement of plankton biovolume estimates derived from image-based automatic sampling devices: application to FlowCAM. *J. Plankton Res.*, **34**, 454-469.
- Álvarez, E., López-Urrutia, A., Nogueira, E. and Fraga, S. (2011) How to effectively sample the plankton size spectrum? A case study using FlowCAM. *J. Plankton Res.*, **33**, 1119-1133.
- Álvarez, E., Nogueira, E., Acuña, J. L., López-Álvarez, M. and Sostres, J. A. (2009) Short-term dynamics of late-winter phytoplankton blooms in a temperate ecosystem (Central Cantabrian Sea, Southern Bay of Biscay). *J. Plankton Res.*, **31**, 601-617.
- Behrenfeld, M. J., Boss, E., Siegel, D. A. and Shea, D. M. (2005) Carbon-based ocean productivity and phytoplankton physiology from space. *Global Biogeochemical Cycles*, **19**.
- Behrenfeld, M. J., Marañón, E., Siegel, D. A. and Hooker, S. B. (2002) Photoacclimation and nutrient-based model of light-saturated photosynthesis for quantifying oceanic primary production. *Mar Ecol Prog Ser*, **228**, 103-117.
- Blanco, J. M., Echevarría, F. and García, C. M. (1994) Dealing with size-spectra: some conceptual and mathematical problems. *Sci. Mar.*, **58**, 17-29.
- Calvo-Díaz, A. and Morán, X. A. G. (2006) Seasonal dynamics of picoplankton in shelf waters of the southern Bay of Biscay. *Aquat. Microb. Ecol.*, **42**, 159-174.
- Cavender-Bares, K. K., Rinaldo, A. and Chisholm, S. W. (2001) Microbial size-spectra from natural and nutrient enriched ecosystems. *Limnol. Oceanogr.*, **46**, 778-789.
- Cermeño, P., Marañón, E., Rodríguez, J. and Fernández, E. (2005) Large-sized phytoplankton sustain higher carbonspecific photosynthesis than smaller cells in a coastal eutrophic ecosystem. *Mar. Ecol. Prog. Ser.*, **297**, 51-60.
- Cloern, J. E., Grenz, C. and Vidergar-Lucas, L. (1995) An empirical model of the phytoplankton chlorophyll/carbon ratio - The conversion factor between productivity and growth rate. *Limnol. Oceanogr.*, **40**, 1313-1321.
- Dodson, A. N. and Thomas, W. H. (1978) Reverse filtration. In: S. A. (ed) *Phytoplankton manual*. UNESCO, Paris, pp. 104-107.
- Edwards, K. F., Litchman, E. and Klausmeier, C. A. (2013) Functional traits explain phytoplankton community structure and seasonal dynamics in a marine ecosystem. *Ecology Letters*, **16**, 56-63.
- Fernández, E. and Bode, A. (1991) Seasonal patterns of primary production in the Central Cantabrian Sea (Bay of Biscay). *Scientia Marina*, **55**, 629-636.
- Finkel, Z. V. (2004) Resource limitation alters the 3/4 size scaling of metabolic rates in phytoplankton. *Mar Ecol Prog Ser*, **273**, 269-279.

Results

- Fujiki, T. and Taguchi, S. (2002) Variability in chlorophyll a specific absorption coefficient in marine phytoplankton as a function of cell size and irradiance. *J. Plankton Res.*, **24**, 859-874.
- García, C. M., Jimenez-Gómez, F. and Rodríguez, J. (1994) The size-structure and functional composition of ultraplankton and nanoplankton at a frontal station in the Alboran Sea. Working groups 2 and 3 report. *Sci. Mar.*, **58**, 43-52.
- Geider, R. J. (1987) Light and temperature dependence of the carbon to chlorophyll a ratio in microalgae and cyanobacteria: implications for physiology and growth of phytoplankton. *New Phytologist*, **106**, 1-34.
- Granda, A. P. and Anadón, R. (2008) The annual cycle of nanoflagellates in the Central Cantabrian Sea (Bay of Biscay). *Journal of Marine Systems*, **72**, 298-308.
- Grasshoff, K., Ehrhardt, M. and Kremling, K. (eds) (1983) *Methods of seawater analysis*. Verlag Chemie, Weinheim.
- Gutiérrez-Rodríguez, A., Latasa, M., Estrada, M., Vidal, M. and Marrasé, C. (2010) Carbon fluxes through major phytoplankton groups during the spring bloom and post-bloom in the Northwestern Mediterranean Sea. *Deep-Sea Research I*, **57**, 486-500.
- Kara, A. B., Rochford, P. A. and Hurlburt, H. E. (2000) An optimal definition for ocean mixed layer depth. *Journal of Geophysical Research*, **105**, 16803-16821.
- Kirk, J. T. O. (1994) *Light and photosynthesis in aquatic ecosystems*. Cambridge Univ. Press, New York., pp. 662.
- Litchman, E. and Klausmeier, C. A. (2008) Trait-based community ecology of phytoplankton. *Annu. Rev. Ecol. Evol. Syst.*, **39**, 615-639.
- Mcgill, B. J., Enquist, B. J., Weiher, E. and Westoby, M. (2006) Rebuilding community ecology from functional traits. *Trends Ecol. Evol.*, **21**, 178-185.
- Menden-Deuer, S., Lessard, E. J. and Satterberg, J. (2000) Carbon to volume relationships for dinoflagellates, diatoms and other protist plankton. *Limnol. Oceanogr.*, **45**, 569-579.
- Nielsen, T. G. and Hansen, B. W. (1999) Plankton community structure and carbon cycling on the western coast of Greenland during the stratified summer situation. I. Hydrography, phytoplankton and bacterioplankton. *Aquat Microb Ecol*, **16**, 205-216.
- Olson, R. J., Zettler, E. R. and Durand, M. D. (1993) Phytoplankton analysis using flow cytometry. In: P. F. Kemp, B. F. Sherr, E. B. Sherr and J. J. Cole (eds) *Handbook of methods in aquatic microbial ecology*. Lewis publishers, Boca Raton, Florida, pp. 175-186.
- Peliz, A., Dubert, J., Santos, A. M. P., Oliveira, P. B. and Le Cann, B. (2005) Winter upper ocean circulation in the Western Iberian Basin - fronts, eddies and poleward flows: an overview. *Deep-Sea Research I*, **52**, 621-646.
- Pingree, R. D. and Lecann, B. (1990) Structure, strength and seasonality of the slope currents in the Bay of Biscay region. *J. Mar. Biol. Assoc. UK*, **70**, 857-885.
- Rodríguez, J. (1994) Some comments of the size-based structural analysis of the pelagic ecosystems. *Sci. Mar.*, **58**, 1-10.

- Rodriguez, J. and Mullin, M. M. (1986) Relation between biomass and body weight of plankton in a steady state oceanic ecosystem. *Limnol. Oceanogr.*, **31**, 361-370.
- Sieracki, C. K., Sieracki, M. E. and Yentsch, C. S. (1998) An imaging-in-flow system for automated analysis of marine microplankton. *Mar. Ecol. Prog. Ser.*, **168**, 285-296.
- Sosik, H. M., Chisholm, S. W. and Olson, R. J. (1989) Chlorophyll fluorescence from single cells: interpretation of flow cytometric signals. *Limnol. Oceanogr.*, **34**, 1749-1761.
- Sverdrup, H. U. (1953) On conditions for the vernal blooming of phytoplankton. *Journal du Conseil pour la Exploration de la Mer*, **18**, 287-295.
- Townsend, D. W., Keller, M. D., Sieracki, M. E. and Ackleson, S. G. (1992) Spring phytoplankton blooms in the absence of vertical water column stratification. *Nature*, **360**, 59-62.
- Vázquez-Domínguez, E., Morán, X. A. G. and López-Urrutia, A. (2013) Photoacclimation of picophytoplankton in the central Cantabrian Sea. *Mar Ecol Prog Ser*, **493**, 43-56.
- Westberry, T., Behrenfeld, M. J., Siegel, D. A. and Boss, E. (2008) Carbon-based primary productivity modeling with vertically resolved photoacclimation. *Global Biogeochemical Cycles*, **22**, GB2024.
- Worden, A. Z., Nolan, J. K. and Palenik, B. (2004) Assessing the dynamics and ecology of marine picophytoplankton: the importance of the eukaryotic component. *Limnol. Oceanogr.*, **49**, 168-179.
- Yentsch, C. M., Horan, P. K., Muirhead, K., Dortch, Q., Hangen, F., Legendre, L., Murphy, L. S., Perry, M. J., Phinney, D. A., Pomponi, S. A., Spinrad, R. W., Wood, M., Yentsch, C. S. and Zahuranec, B. J. (1983) Flow cytometry and cell sorting: a technique for analysis and sorting of aquatic particles. *Limnol. Oceanogr.*, **28**, 1275-1280.
- Zubkov, M. V., Sleigh, M. A., Tarran, G. A., Burkill, P. H. and Leakey, R. J. G. (1998) Picoplankton community structure on an Atlantic transect from 50° N to 50° S. *Deep-Sea Res. I.*, **45**, 1339-1355.

Chapter V. In-vivo single-cell fluorescence and the size-scaling of phytoplankton chlorophyll content

The structure of the community is the result of physiological processes taking place at the individual level. Hence, the description of the physiology of the phytoplankton community based on bulk measurements would go further if an estimate of pigment content per single cell was available. In this chapter we explored the relationship between the emission of fluorescence of phytoplankton single cells measured by the FlowCAM and their chlorophyll content. The size-dependence of chlorophyll content was found to vary with the irradiance experienced by the cells both at the inter- and intra-specific level. Hence, from a routine sampling of natural samples it is possible to estimate quantitatively the allometric exponent of chlorophyll content, which relates with the photosynthetic rates and hence, permits a more detailed description of the dynamics of the phytoplankton community.

Reference

Eva Álvarez, Enrique Nogueira and Ángel López-Urrutia (2014) In-vivo single-cell fluorescence and the size-scaling of phytoplankton chlorophyll content. (Manuscript).

Candidate's contribution

My contribution to the work includes the co-design of the study and the establishment of methodology in collaboration with the rest of coauthors. I conducted the experiments, obtained and analyzed data, and prepared tables and figures. All authors discussed the results, composed and co-write the article.

In-vivo single-cell fluorescence and the size-scaling of phytoplankton chlorophyll content

Eva Álvarez*, Enrique Nogueira, and Ángel López-Urrutia.

Instituto Español de Oceanografía. Centro Oceanográfico de Gijón, 33212, Gijón, Spain.

*e-mail corresponding author: eva.alvarez@gi.ieo.es

Running Head: *In-vivo single-cell chlorophyll content*

KEYWORDS: fluorescence, chlorophyll, single-cell, irradiance, size-scaling, primary production, FlowCAM.

Red fluorescence measured by the Flow Cytometer and Microscope (FlowCAM) is correlated with the chlorophyll content of phytoplankton cells. This is revealed by a series of incubations with monocultures exposed to different light levels to induce a gradient in the chlorophyll content of the cells. All species increased their chlorophyll concentration in response to decreasing light conditions, and this pattern was also observed for the fluorescence measured by the FlowCAM. This correspondence between chlorophyll and fluorescence per cell was used to estimate chlorophyll contents on a single cell basis. The size dependence of chlorophyll content in unicellular phytoplankton changes when cells are exposed to light limitation. This was observed at the inter-specific scale but also at the intra-specific level, as a pattern of decrease of the allometric exponent of chlorophyll content at increased light limitation. Our results show that the single cell perspective provided by the FlowCAM can be applied to field samples to account for changes in the size dependence of chlorophyll content in response to environmental variables affecting primary production.

Introduction

Phytoplankton organisms account for 50% of global primary production and hence are central to the comprehension of global biogeochemical cycles (Falkowski & Raven, 2007). Organism size and elemental composition constrain the rate of energy acquisition by the phytoplankton community, which influences processes at the ecosystems level. Hence, cell size and composition are fundamental ecophysiological traits in growth/production models. Because all autotroph plankton contain chlorophyll a (named Chl-a, hereafter), it is arguably the best known and most widely used proxy for autotrophic biomass (Huot *et al.*, 2007). However, cell surface area to volume ratio constrains the absorptive efficiency of Chl-a molecules and, as a result, larger cells tend to have relatively lower intracellular concentrations of Chl-a than smaller cells (Finkel, 2001; Finkel, 2004). Thus, the concentration of Chl-a is a biased estimator of phytoplankton biomass expressed in organic carbon terms (Cullen, 1982). Instead, the intra-cellular Chl-a concentration can give a vision of the physiological status of the cells which can be translated to the community level. Changes in the ratio of Chl-a to carbon biomass (Chl-a:C ratio) indicate an adjustment of cellular pigment levels to match the demands for photosynthesis, which is driven by changes in light, nutrients and temperature (Geider, 1987).

When resources are limiting, the surface area to volume ratio imposes fundamental constraints on the rates of resource acquisition (Mei *et al.*, 2009). The growth rate of a majority of the phytoplankton cells in the oceans is limited by light (Cullen, 1982). In order to maximize the efficiency of resource acquisition in a variable environment, cellular physiology adjusts through a suite of acclimation processes. Photoacclimation refers to phenotypic adjustments of the cells in response to variation in irradiance and it is typically reflected in a graded reduction/increase in the photosynthetic pigment content with increasing/decreasing irradiance levels (MacIntyre *et al.*, 2002). This physiological acclimation to light conditions leads to altered cellular pigment composition, particularly regarding Chl-a content. This photoacclimation response changes with cell-size, resulting in different allometric exponents in the size-scaling of Chl-a content with changing irradiance (Fujiki & Taguchi, 2002; Finkel, 2004).

Chl-a emits fluorescence in the red portion of the spectrum. Hence, the fluorescence of Chl-a reflects the endogenous concentration of this pigment. This is the rationale for the estimation of Chl-a *in situ* by means of fluorometers (Lorenzen, 1966) or for the measurement on discrete samples by means of fluorometric (Yentsch &

Results

Menzel, 1963) or spectrophotometric methods (Jeffrey & Humphrey, 1975). The introduction of flow cytometry techniques in oceanography allowed the quantification of these optical properties, such as Chl-a fluorescence, on individual cells in a fluid stream as they cross one or more light beams (Yentsch *et al.*, 1983). The cell-level perspective provided by flow cytometry and the capacity to measure large numbers of cells has been used extensively by biological oceanographers to define the distributions and dynamics of marine pico-phytoplankton. Chl-a fluorescence intensity quantified by flow cytometry has been shown to scale with cellular Chl-a levels in nano-phytoplankton (Sosik *et al.*, 1989), but the relationships reported are not constant for all phytoplankton taxa due to differences in intracellular pigment structure or, even for the same phytoplankton taxa, due to differences in growth conditions. Hence, none of these studies provide a taxon-independent conversion from fluorescence to Chl-a that can be applied to natural samples.

In addition, traditional flow cytometers have a limited capacity to analyze large-sized phytoplankton (>5 μm). There are no measurements of fluorescence on a single cell basis for microplankton, a compartment where a significant proportion of the autotrophic activity takes place. The Flow Cytometer And Microscope (FlowCAM) is an automated technique for plankton enumeration that combines flow cytometry and microscopy (Sieracki *et al.*, 1998). Although the FlowCAM is not a flow cytometer *per se*, it contains the needed elements to aboard the task of measure the fluorescent response of single cells: a source of light, a fluidics system in which the cells are embedded and a detection sensor. When a solution of autotrophic cells runs through the fluidics system, the detected fluorescence signals trigger the digital camera to obtain images that allows counting and sizing the cells in the sample. However, the fluorescence signals measured by FlowCAM have not been yet interpreted. The detection of molecular probes by fluorescence signals and a taxon-independent conversion from fluorescence to that probe, may allow single-cell physiological information to be garnered for a variety of algae, both in culture and in natural samples.

Here, we present a reliable methodology for the estimation of the content of Chl-a on single cells that can be applied to field studies. The aim of the work is to test the relationship between the FlowCAM measured fluorescence per cell and the content of Chl-a per cell. With this purpose six species of marine phytoplankton where grown over a range of irradiances and their content in pigments and fluorescence monitored. With those cultured species we explored the changes in the inter-specific size scaling of chlorophyll content when cells are exposed to light limitation. We then explore these capabilities of the FlowCAM to investigate the patterns at the intra-specific scale. Finally, the size scaling of Chl-a content in field samples was explored and related to the

irradiance levels in the water column. Our results show that a taxon independent conversion from fluorescence to Chl-a content can be obtained for FlowCAM, which allows the analysis of single-cell physiological responses and the size-dependence of Chl-a content both in cultures and natural samples.

Materials and methods

Phytoplankton cultures and growth conditions

We performed a series of incubations to induce photoacclimation in cultured phytoplankton, exposing mono-specific solutions of cells to different light intensities in order to obtain a gradient of intracellular Chl-a concentrations. The species used were: *Isochrysis galbana*, *Emiliana huxleyi*, *Rhodomonas salina*, *Karlodinium veneficum* (*micrum*), *Alexandrium tamarense* and *Protoceratium reticulatum*. The inocula were maintained in exponential growth in F2 media at 15 °C in a culture chamber with photoperiod 12L/12D and low light conditions. With those initial solutions we conducted eight experiments, summarized in Table I.

Each experiment took place in a linear incubator illuminated at one end by a spot light. The incubator was divided into compartments along its axis by means of transverse partitions consisting on a double layer of nylon mesh. The initial solution of cells was divided in 50 mL cellstack culture chambers (Corning), and the chambers placed into the compartments of the incubator. Total irradiance (photosynthetically active radiation, PAR) in each compartment was measured with a LICOR radiometer (Biospherical). The irradiances varied slightly between experiments but in any one experiment light levels ranged between 10 and 400 W m⁻² of PAR (0.17-6.62 mol photons m⁻² h⁻¹). Running water through the incubator kept the temperature stable at 15.5 ± 0.5 °C. Incubations were kept with photoperiod for six days, except *E. huxleyi* that was maintained for five days, and were shook manually twice daily. Microscopy counts, pigment extraction and *in vivo* FlowCAM analysis were conducted on the first and last days of each incubation experiment; additionally in two experiments we took measurements also in the fourth day (Table I).

Results

Table I Description and growth conditions of the incubation experiments carried out to obtain a gradient of Chl-a content per cell.

Experiment	Species	Nº of light treatments	Photoperiod	Total days	Days of measurement	Lens / flow chamber	Points for calibration
1	<i>I. galbana</i>	5	12/12	6	1 and 6	200×/FC50	5
2	<i>E. huxleyi</i>	5	12/12	5	1 and 5	200×/FC50	5
3	<i>R. salina</i>	5	12/12	6	1 and 6	200×/FC50	5
4	<i>R. salina</i>	6	14/10	6	1, 4 and 6	200×/FC50	12
5	<i>K. veneticum</i>	5	12/12	6	1 and 6	200×/FC50	5
6	<i>A. tamarensis</i>	5	12/12	6	1 and 6	100×/FC100	5
7	<i>A. tamarensis</i>	6	14/10	6	1, 4 and 6	100×/FC100	12
8	<i>P. reticulatum</i>	5	12/12	6	1 and 6	100×/FC100	5

Microscopy counts of each treatment were carried out placing 1 mL of sample in a Sedgwick-Rafter counting cell slide under a NIKON inverted microscope. For the analysis of the Chl-a concentration, 10mL of each sample was filtered onto Whatman GF/F filters, frozen at -18°C during 24h and extracted in 3 mL of acetone during 24h. Single measurements for Chl-a were determined using a spectrofluorometer (Perkin Elmer LB-50s) with excitation set at 488 nm and emission at 663.5 nm. The signal of the spectrofluorometer was calibrated against Chl-a solutions of known concentration. The concentration of extracted Chl-a was divided by the number of cells to obtain the Chl-a per cell value, and by the total cellular volume to obtain the intracellular Chl-a concentration.

For each treatment, measurements of single cell fluorescence, cell size and cell concentration were acquired with FlowCAM. Excitation illumination consisted on a blue laser fan of 488 ± 0.04 nm, and fluorescence was measured as the emitted light passing a 650 long-pass filter reaching a photomultiplier tube (PMT 1). When the fluorescent light reaches the PMT generates a voltage pulse that is described numerically by three parameters: the maximum value reached by the pulse, known as height or peak, the number of consecutive measurements that exceeded the threshold value, called width, and the integrated area under the pulse. The width and the area of the pulse are strongly influenced by the flow speed of sample analysis, while the peak of the signal is expected to reflect the total fluorescence of the cell and therefore was the parameter used to ascertain the intra-cellular Chl-a content.

Field sampling

Field data consisted on a series of 21 samples taken from 12th to 14th April of 2013 in coastal, shelf and oceanic waters of the Cantabrian Sea (Southern Bay of Biscay) (43.51-43.80°N, 5.55-3.73°W, 25-1625 m depth). Sea-water samples were collected at selected depths (ranging from 3 to 100 meters) with Niskin bottles mounted on a rosette sampler system equipped with a CTD (conductivity-temperature-depth) probe (SBE), and auxiliary sensor for the measurement of underwater PAR (Biospherical/Licor radiometer). Surface PAR on an hourly basis was recorded on a meteorological station sited on land near the sampling area (43.54°N, 5.62°W, 30 mamsl).

From the *in situ* PAR profile, the attenuation coefficient (k_d) was estimated with the light extinction equation ($I_z = I_0 \times e^{-k_d z}$), where I_z and I_0 represent, respectively, irradiance at a given depth and in the surface, and z is the depth in the water column. To integrate the irradiance regime experienced by the cells of a given sample the field irradiance at the sample depth was estimated taking into account the 24h PAR regime previous to the time of acquisition of the sample, calculated from surface solar radiation and assuming a constant k_d , weighting the calculated underwater PAR by the elapsed time.

Phytoplankton samples were analyzed on board with FlowCAM. They were maintained fresh and dark until analysis, which started immediately after collection to minimise pigment degradation. Each sample was split in two: an un-concentrated subsample pre-filtered by 40 μm for analysis with 200 \times magnification (1 mL), and a concentrated subsample pre-filtered by 100 μm (1 litre down to around 20 mL) for analysis with 100 \times magnification (10 mL). The sample concentration was carried out by reverse filtration (Dodson & Thomas, 1978) through a 15 μm mesh to prevent the damage of living cells.

FlowCAM data analysis

For each analyzed sample, either cultured or natural, abundance of autotrophic cells was estimated from all cells imaged by the FlowCAM in the fluorescence-triggered mode. The size of the cells was estimated considering only properly focused and uncut single cells. The spherical equivalent diameter (ESD) and geometrical section of each cell were obtained directly from the digital image taken by the FlowCAM, and particle biovolume was calculated as a revolution volume from the ESD from the particles. Fluorescence signals were selected considering only uncut cells captured in the proximities of the laser beam. FlowCAM photographs with more than one particle were rejected.

Results

Phytoplankton incubations

During all incubations, the cells within each treatment differentiated their attributes, in terms of Chl-a content and fluorescence signal, from the beginning to the last day of measurements. Figure 1 shows the variation in the average fluorescence per unit volume and the average intracellular Chl-a concentration as a function of growth irradiance in the last day of incubation. The pigment concentration obtained through Chl-a extraction decreased as expected with increased irradiance in all experiments. The same pattern was captured by the FlowCAM-measured fluorescence: fluorescence intensity decreased with irradiance in parallel to intra-cellular pigment content, with the exception of experiment 7 that showed higher fluorescence at intermediate growth irradiances.

Fluorescence to Chl-a conversion

Our cultured species had different intracellular pigment concentration and different cell size. Hence, to explore the relationship between the measured fluorescence and the Chl-a content, we analysed the relationship between fluorescence per cell (arbitrary units cell⁻¹) and the intracellular pigment content (pg Chl-a cell⁻¹) (Figure 2). Since the fluorescence signals measured with different combinations of FlowCAM magnification lenses / flow chamber dimensions (FC) were not comparable due to optical differences, the relationship was explored for each of the applied combinations (200x/FC50, 100x/FC100).

We performed a linear regression over the log-log transformed data to adjust an exponential curve to the experimental data obtained with the 200x/FC50 ($F = 75.46 \times \text{Chl-a}^{0.4}$, $R^2 = 0.85$, $p\text{-value} < 0.001$, Fig 2A) and the 100x/FC100 ($F = 40.63 \times \text{Chl-a}^{0.28}$, $R^2 = 0.91$, $p\text{-value} < 0.001$, Fig 2B). The best fit between fluorescence and Chl-a per cell was given by a curvilinear model, since the fluorescence emitted does not only depend on the pigment content but also on the way those pigments are packaged within the cell. The package effect implies that larger cells can expose relatively less pigments for light harvesting than smaller cells due to constraints imposed by the relationship between cell surface area to volume.

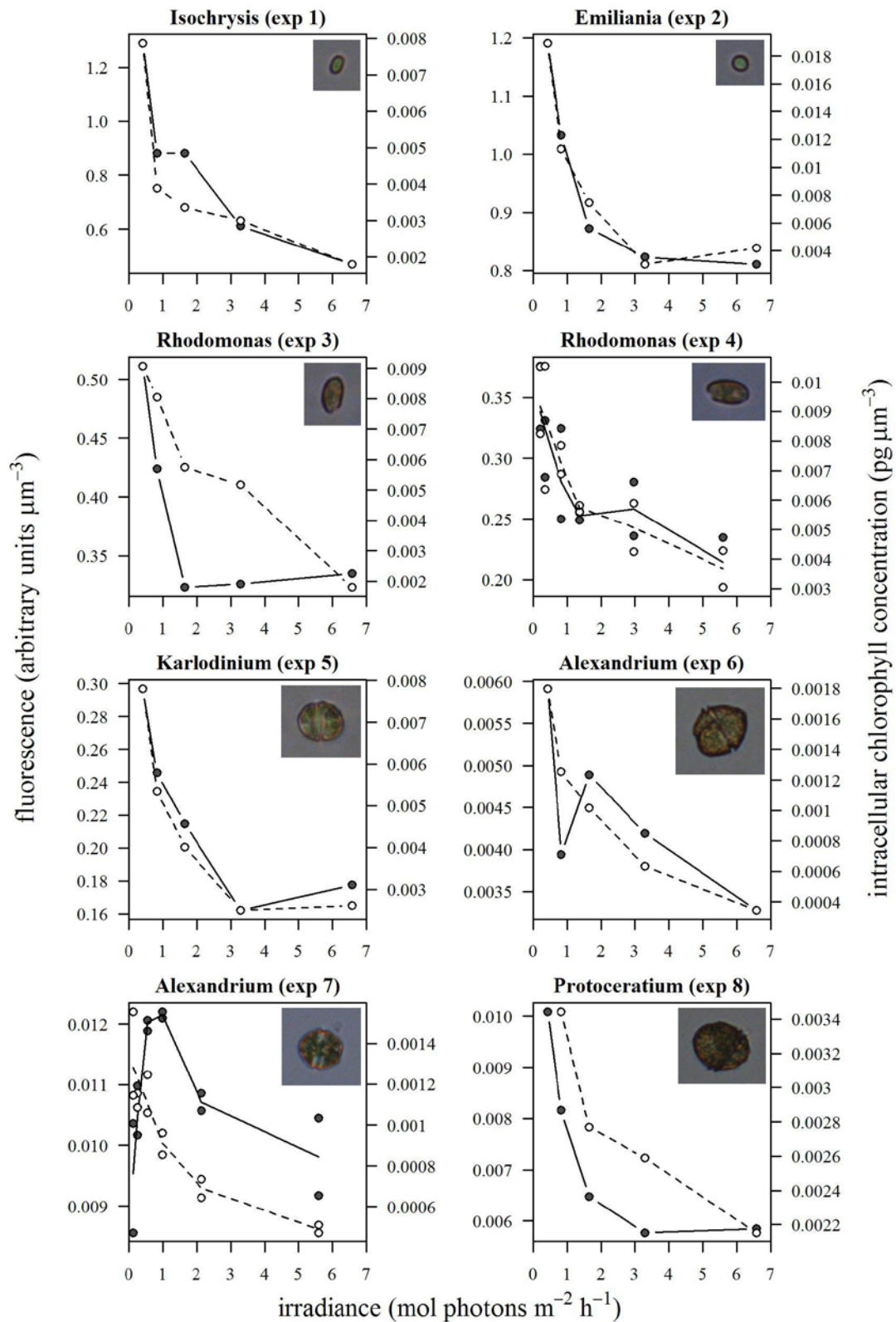


Figure 1 Fluorescence per unit biovolume and intracellular Chl-a concentration as a function of growth irradiance intensity in each experiment (\bullet fluorescence (arbitrary units cell^{-1}), \circ chlorophyll ($\text{pg Chl-a cell}^{-1}$)).

Results

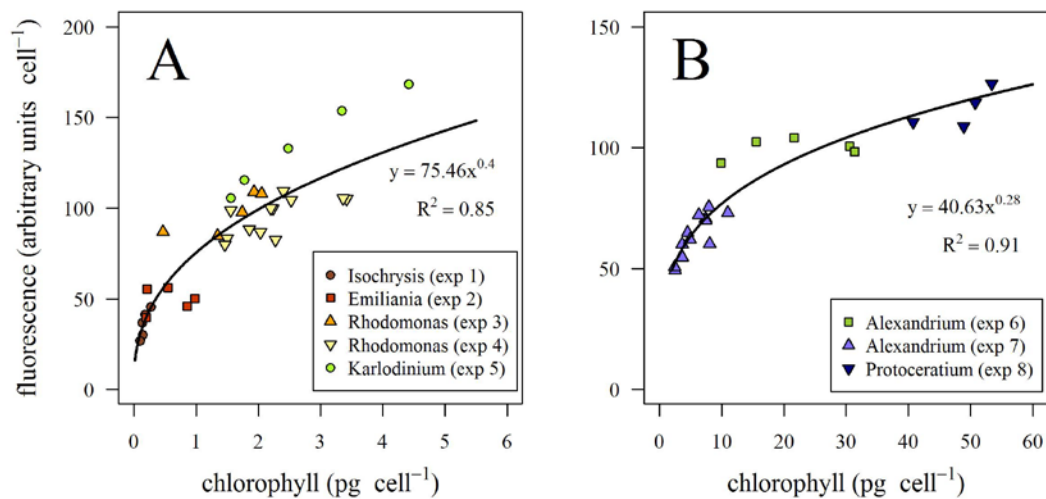


Figure 2 Fluorescence peak per cell measured on the FlowCAM as a function of analytic Chl-a per cell, for the experiments analyzed with the (A) 200×-FC50 and (B) 100×-FC100 lens-flow chamber combinations. Solid line, equation and R^2 indicate the fitted conversion from fluorescence to Chl-a.

Inter-specific scaling

If the fluorescence-to-Chl-a conversion was reliable, the size dependence of the Chl-a predicted from fluorescence is expected to be similar to the size dependence of analytical Chl-a. In Figure 3 we grouped the treatments of the experiments by their growth irradiance level and, for each of them, we explore the relationship between Chl-a content and cell biovolume. The eight experiments distribute linearly in a log-log scale, so we applied a reduced major axis regression, and the exponent of the relationship describes the size dependence of pigment content at each irradiance level.

Considering the analytic Chl-a, each experiment provides a unique Chl-a value, hence vertical error bars are not available. The size dependence of Chl-a content varied as a function of the irradiance treatments, and the exponents increase with irradiance from 0.65 to 0.83 (Fig. 3A-E). The decrease of the size scaling exponent with increasing light limitation (Fig. 3F) compare well with previous experimental (Fujiki & Taguchi, 2002) and theoretical works (Finkel, 2004).

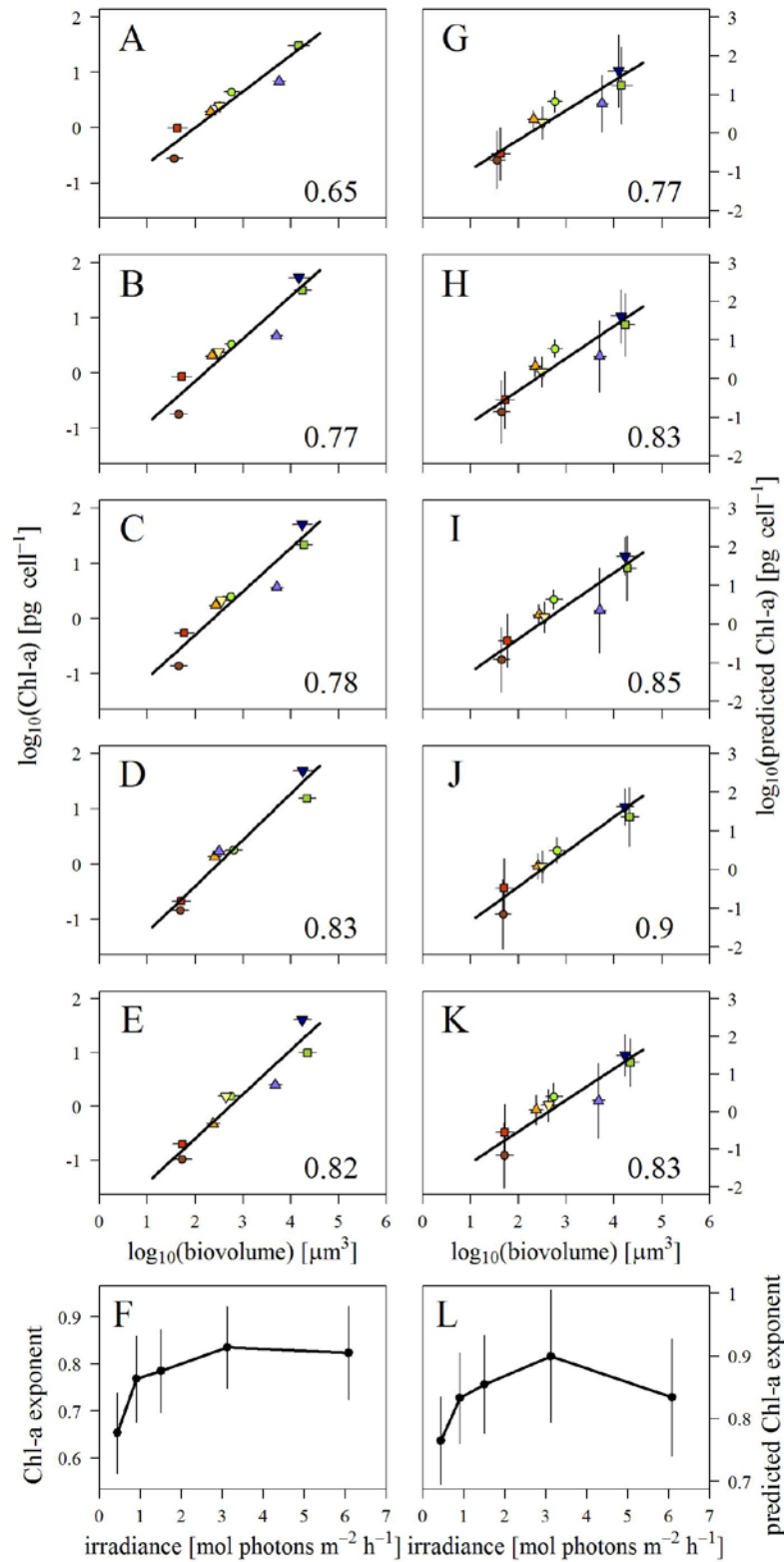


Figure 3 Inter-specific size scaling of Chl-a per cell for the eight experiments in each of the five irradiance treatments: (A to E) for analytic Chl-a and (G to K) for fluorescence-based Chl-a. And size scaling exponent of Chl-a per cell as a function of growth irradiance, (F) analytical Chl-a and (L) fluorescence based Chl-a. Volume scaling exponent was calculated from reduced major axis regression.

Results

The fluorescence values of each single cell were transformed to Chl-a with the fluorescence to Chl-a conversions described above, and averaged to obtain the mean and the standard deviation of fluorescence per species and irradiance level. Considering this Chl-a predicted from fluorescence, the exponents of the size dependence of pigment content at each irradiance level were slightly higher. They varied between 0.77 and 0.99 (Fig. 3G-K). Nevertheless, the pattern of decrease of the size scaling exponent in light limited conditions was captured by the FlowCAM-measured fluorescence (Fig. 3L).

Intra-specific scaling

The measurement of fluorescence on a single-cell basis allowed us to explore the size dependence of Chl-a content within a single population. To analyze the size dependence of Chl-a content as a function of irradiance within each experiment, the fluorescence of each single cell was converted to Chl-a content and plotted against cellular biovolume in a log-log scale. As an example, the five irradiance treatments of experiment 5 (*K. micrum*) are shown in Figure 4 (A-E). The distributions of biovolume and Chl-a per cell were log-normal, as indicated by the inserted bar plots coupled, respectively, to the x and y axis. The data clouds present a high dispersion with several outliers, more evident at high irradiance levels. The size scaling exponent was obtained with a robust linear model, an alternative to least squares regression not as susceptible to the presence of outliers (Venables & Ripley, 2002).

Considering a single species, the size scaling exponent tends to decrease in light limited conditions, similarly to what happens at the inter-specific scale. In Figure 4 we present the variation of the size-scaling exponent as a function of irradiance for each of the eight species (panels F-M). Experiments from 2 to 8 showed the pattern of increase of the size-scaling exponent at increased growth irradiance levels, although it is less clear than at the inter-specific scale. Experiment 1 did not show this pattern, probably due to the small size of *I. galbana*, very close to the detection limit of the FlowCAM.

When explored the intra-specific scaling, the exponents were not limit to 1, as found in the inter-specific scaling, but fluctuated between 0.35 and 3.04 with variability within each experiment ranging between 0.1 and 1.52 units. This means that although the general pattern of decreasing of the size scaling exponent under light limited conditions keeps across species, the relationship between Chl-a content and biovolume is species-specific and other factors play determinant roles in the adjustment of the intracellular Chl-a content. The variability of intra-specific scaling is higher at the small scale of a single species, and body size explains only between 3 and 28% of the variability in the Chl-a content.

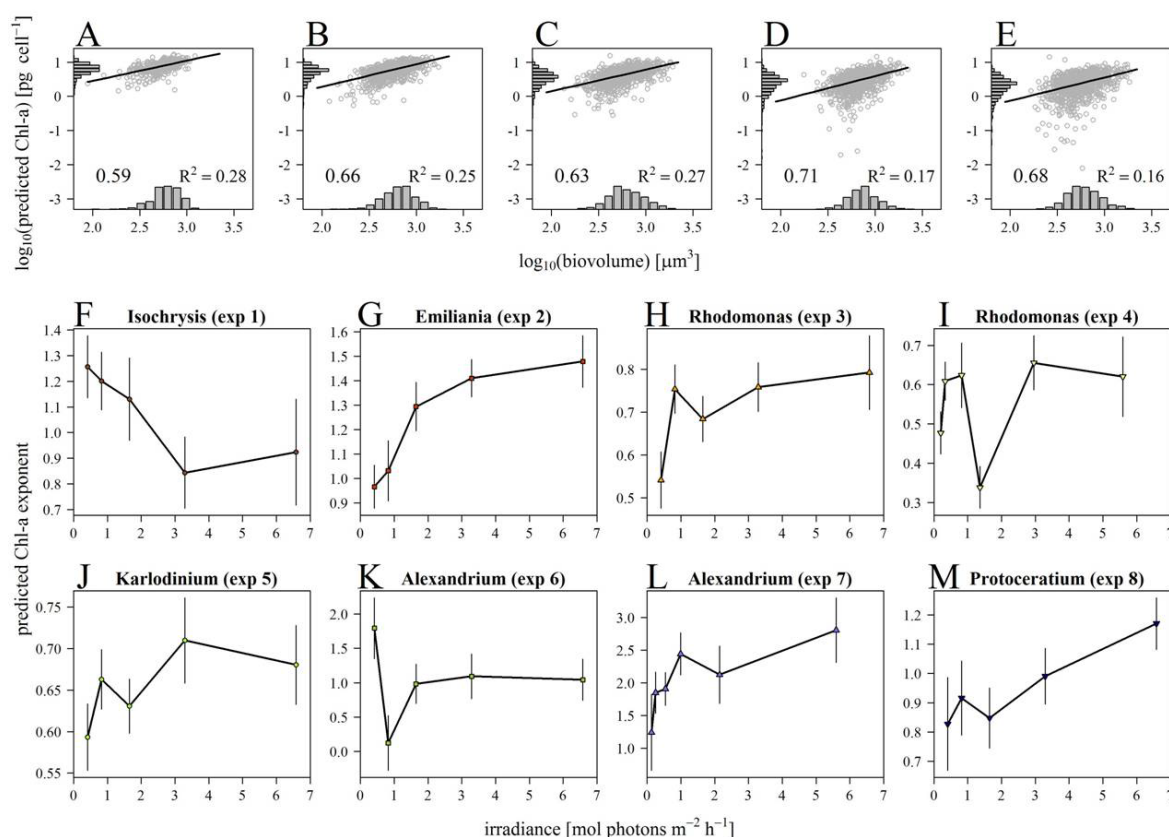


Figure 4 Intra-specific size scaling of Chl-a per cell: (A to E) predicted Chl-a per cell as a function of cell biovolume in the five irradiance treatments for experiment 5 (*K. micrum*) and (F to M) size scaling exponent for predicted Chl-a per cell as a function of growth irradiance for each of the eight experiments.

Field sampling

The size scaling of pigment content is reproduced in the natural samples analyzed. The fluorescence values of the two subsamples analyzed for each sample were converted to Chl-a content and combined to estimate a size scaling exponent for each sample. The exponents of the size dependence were estimated by robust linear regression. Fig. 5A shows an example of a natural sample with cells sampled with the 200 \times /FC50 (light dots) and cells sampled with the 100 \times /F100 (dark dots) and the linear adjustment.

Among all samples, the size scaling ranged from 0.5 to 1 (Fig. 5B), and r squared of predicted intracellular Chl-a content as a function of biovolume ranged from 0.27 to 0.59. At low irradiances, the variation of the exponents as a function of irradiance

Results

tended to increase as expected, while for irradiances higher than $1.0 \text{ mol photons m}^{-2} \text{ h}^{-1}$ the tendency disappeared. In natural samples, the influence of other environmental variables, such as temperature and nutrient concentrations, and the physiological (ontogenetic) status of the cells (exponential growth phase, division or senescence) could mask the expected pattern.

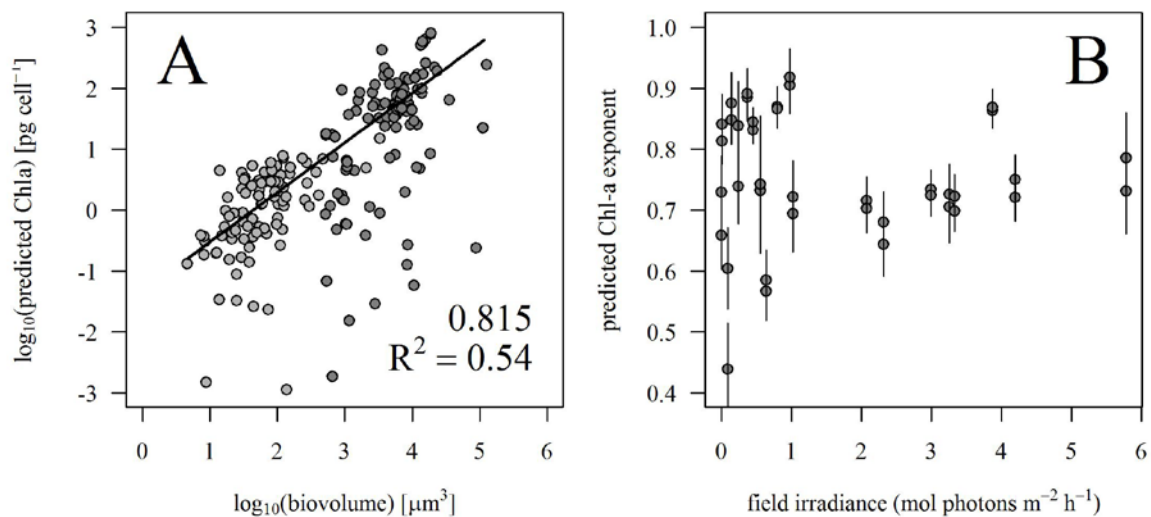


Figure 5 Field sampling: (A) Example of predicted Chl-a per cell as a function of cell biovolume in a natural sample, where the number within the panel indicates the size-scaling exponent. (B) Size scaling exponent of predicted Chl-a per cell as a function of field irradiance.

Discussion

Chlorophyll per single cell

We presented a method to estimate single-cell Chl-a content from FlowCAM measured fluorescence. The existence of a relationship between the fluorescence measured by flow cytometers and the Chl-a per cell has been described before (Sosik *et al.*, 1989) but, for the best of our knowledge, that's the first time for FlowCAM. A priori, it would be expected a linear relationship between fluorescence and the absorption cross section of single cells (Perry & Porter, 1989) which implies a non linear relationship with the Chl-a content given the package effect. If cellular pigment concentration is constant, the efficacy of light absorption by cellular pigment decreases with increasing size, due to pigment shelf-shading (Kirk, 1975a; Kirk, 1975b; Morel & Bricaud, 1986; Finkel, 2001).

The intracellular concentration of Chl-a has been estimated for the whole phytoplankton community or for specific compartments (Sathyendranath, 2009; Wang *et al.*, 2009). We have shown that the simultaneous acquisition of estimates of biovolume and fluorescence per cell by means of FlowCAM analysis offers an integral methodology to estimate intracellular concentration of Chl-a of nano and micro-phytoplankton, on a single cell basis.

Inter-specific size dependence of chlorophyll content

We found a significant size dependence of Chl-a content per cell. In the same way that the mean size of a population is a representative estimate of the species size distribution and the superposition of size distributions give place to linear community size spectra (Giometto *et al.*, 2013), the mean Chl-a content of a population is sufficient to characterize the Chl-a content distribution fully and mean values permit the inter-comparison across all species.

Larger cells tend to have lower cellular pigment concentrations than smaller cells under similar environmental conditions (Agustí, 1991), thereby counteracting the package effect associated with increasing cell size (Finkel, 2004). This means that Chl-a content scale with exponents lower than one, which implies that small cells have higher pigment contents per unit volume or biomass. This is supported by geometrical considerations, which only can be explain by exponents lower than one. That is, indeed, what have been found on empirical data (Fujiki & Taguchi, 2002; Finkel, 2004; Key *et al.*, 2010) and what we have also found with our fluorescence-based Chl-a estimates.

Results

As growth irradiance decreases, the size-scaling of Chl-a content decreases, as described by previous empirical works (Fujiki & Taguchi, 2002). However, our exponents surpass the $\frac{3}{4}$ value predicted by theoretical models (Finkel, 2004). Size scaling of Chl-a content also predicts shifts in the size scaling of growth and photosynthesis with the light regime. All phytoplankton require light for growth and the variable light regimes imposed by mixing may explain the size-structure of phytoplankton community (Karentz *et al.*, 1991; Finkel *et al.*, 2009). The different pigment contents as a function of cell size leads to different physiological strategies and niche partitioning defined by cell size.

Intra-specific size dependence of chlorophyll content

At the intra-specific scale, the variability of fluorescence values and hence Chl-a content is higher than size variability. Size only explains a small part of the variability, since Chl-a content in a single population is subject to several sources of heterogeneity, such as the narrow biovolume range covered, the phenotypic (and at some extent also genotypic) variability among the population members, the phase of the cellular cycle and the physiological differences.

The size-scaling of Chl-a content of a single population had exponents bigger than one in some species, which means that larger cells have higher Chl-a content than smaller cells. This result can be counter-intuitive. However, it can be explained if the difference in cell size and pigment content within the population is given, to great extent, by the phase of the cellular cycle in which the cells are. In unicellular phytoplankton, within a given population small cells are generated from larger cells, which can hide the size dependence of chlorophyll content. A large cell with a given Chl-a concentration that enters the division phase of the cellular cycle will give place to two smaller cells with a Chl-a concentration lower than the potential concentration that their new surface-to-volume ratio may allow. In this case, the concentration of Chl-a will be independent of cell size and the pigment content per cell will scale with size with an exponent around one. On the other extreme, a large cell can increase its pigment content above the limits imposed by its surface-to-volume ratio in order to divide this pigment between the two daughter cells. For instance, the division mechanism of coccolithophorids is characterized by a first phase where the mother cell duplicates their chloroplasts, from two to four, and then enters the division phase in strict sense (Klaveness, 1972). In the case of the smallest species, other biovolume constraints can be considered. The possibility that very small cells are prevented from increasing their scalable components (photosynthetic units) due to the necessity of maintaining a constant quota of non-scalable essential components, such as the gene pool, within a

very small cell biovolume (Raven, 1998). In this case, only those cells above a critical size will be able to increase their intracellular quota of molecules involved in metabolic processes.

The same pattern of decrease of the size scaling exponent of Chl-a content in light limited conditions was found when focusing on a single species. The analysis of single cells is the unique choice to explore this kind of relationships in mono-specific cultures, and also this permits to apply the same methodology to field samples and explore the size scaling of Chl-a content on different environmental conditions.

Regional in situ datasets

Our approach makes possible the measurement of Chl-a content per cell in natural samples and hence the estimation of the size dependence of Chl-a content *in situ*. The natural samples yielded exponents lower than 1, in agreement with the results of inter-specific scaling. However, one can wonder if the upper limit of the exponent is more likely to be 1 or $\frac{3}{4}$. An isometric scaling between cell volume and intracellular Chl-a have been reported on the basis of size-fractionation of Chl-a in natural samples by Marañón and co-workers (Marañón *et al.*, 2007), who argued that the discrepancies regard to the predicted exponents has been caused by different growth conditions experienced by cultured cells and the small number of species used in laboratory studies. To the best of our knowledge, we reported for the first time the size scaling of Chl-a in single cells, and our results showed exponents lower than 1 but larger than $\frac{3}{4}$, both in natural samples and cultures. The estimation on a single cell basis opens the door to the estimation of size-scaling per functional or taxonomic group.

We have also shown that it is possible to estimate simultaneously the Chl-a content of single cells, cell size and cell abundance by means of FlowCAM analysis, allowing the characterization of the size dependence of Chl-a content in natural samples. Under intermediate concentrations of nutrients and photon flux the size scaling of Chl-a content in natural samples must be intermediate between those set by extreme light or nutrient limitation. This can indicate the type of resources limitation that is undergoing the community and hence which is the maximum photosynthetic rate that can be sustained.

However, the variability found on the intra-specific scaling of Chl-a content appears also in natural samples, since different populations of the phytoplankton community present different physiologies and life cycles. Also, we have cultured only spherical or elliptical cells, but, in natural communities, cells have developed strategies to escape from geometrical constraints of pigment content, such as the non-spherical shapes of diatoms and the presence of vacuoles (Raven, 1997).

Results

The analysis of natural samples permits to cover a wide range of environmental conditions, from light or nutrient limiting to light/nutrient saturating conditions, which can help to understand how resource acquisition affect the productivity of natural communities. The size dependence of Chl-a content relates directly with the size scaling of photosynthetic rates (Finkel, 2004). This can be determinant in primary productivity models since phytoplankton production can be modeled on a more realistic way improving current estimates derived from global primary production models.

Net primary production (NPP) begins to be modeled as a function of carbon biomass instead of Chl-a concentration, since variability in intracellular Chl-a content from light acclimation and nutrient stress confounds the relationship between Chl-a and phytoplankton biomass. This Carbon based Productivity Models (Behrenfeld *et al.*, 2005; Westberry *et al.*, 2008) includes information on mixed layer and nitracline depths to parameterize photoacclimation and nutrient stress through the water column, reconstructs the underwater light field and produces profiles of biological properties. Regional in situ datasets as those obtained with FlowCAM can be useful in the validation of these models.

Acknowledgements

We are indebted to the Red Tides and Harmful Algae team of the Centro Oceanográfico de Vigo (IEO) for the supply of the clones of their Toxic Phytoplankton Culture Collection. We thank the captain and crew in the B/O Ángeles Alvariño for their assistance during the RADCAN 0413 cruise. F. Ronzón kindly provided solar radiation data from his meteorological station in Gijón.

Funding

This work was funded by the *Plan de Ciencia, Tecnología e Innovación del Gobierno del Principado de Asturias* [research grant BP07-081 to E.A.], the projects '*Predicción del Balance Metabólico de los Océanos*' (METOCA, CTM2009-13882-MAR) and '*Efecto de las perturbaciones meteorológico-hidrográficas en la estructura de la comunidad planctónica*' (PERPLAN, CTM2006-04854-MAR) funded by the Spanish National Investigation + Development + Innovation (I+D+I) Plan, and the core time-series research Project RADIALES, funded by the *Instituto Español de Oceanografía*.

References

- Agustí, S. (1991) Allometric scaling of light absorption and scattering by phytoplankton cells. *Can J Fish Aquat Sci*, **48**, 763-767.
- Behrenfeld, M. J., Boss, E., Siegel, D. A. and Shea, D. M. (2005) Carbon-based ocean productivity and phytoplankton physiology from space. *Global Biogeochemical Cycles*, **19**.
- Cullen, J. J. (1982) The deep chlorophyll maximum: comparing vertical profiles of chlorophyll a. *Can. J. Fish. Aquat. Sci.*, **39**, 791-803.
- Dodson, A. N. and Thomas, W. H. (1978) Reverse filtration. In: S. A. (ed) *Phytoplankton manual*. UNESCO, Paris, pp. 104-107.
- Falkowski, P. G. and Raven, J. A. (2007) *Aquatic Photosynthesis*. Princeton University Press, Princeton.
- Finkel, Z. V. (2001) Light absorption and size-scaling of light-limited metabolism in marine diatoms. *Limnol. Oceanogr.*, **46**, 86-94.
- Finkel, Z. V. (2004) Resource limitation alters the 3/4 size scaling of metabolic rates in phytoplankton. *Mar Ecol Prog Ser*, **273**, 269-279.
- Finkel, Z. V., Vaillancourt, C. J., Irwin, A. J., Reavie, E. D. and Smol, J. P. (2009) Environmental control of diatom community size structure varies across aquatic ecosystems. *Proc. R. Soc. B*, **276**, 1627-1634.
- Fujiki, T. and Taguchi, S. (2002) Variability in chlorophyll a specific absorption coefficient in marine phytoplankton as a function of cell size and irradiance. *J. Plankton Res.*, **24**, 859-874.
- Geider, R. J. (1987) Light and temperature dependence of the carbon to chlorophyll a ratio in microalgae and cyanobacteria: implications for physiology and growth of phytoplankton. *New Phytologist*, **106**, 1-34.
- Giomettoa, A., Altermatt, F., Carrara, F., Maritan, A. and Rinaldo, A. (2013) Scaling body size fluctuations. *PNAS*, **110**, 4646-4650.
- Huot, Y., Babin, M., Bruyant, F., Grob, C., Twardowski, M. S. and Claustre, H. (2007) Does chlorophyll a provide the best index of phytoplankton biomass for primary productivity studies? *Biogeosciences Discuss.*, **4**, 707-745.
- Jeffrey, S. W. and Humphrey, G. F. (1975) New spectrophotometric equation for determining chlorophyll. *Biochem. Physiol. Pflanz.*, **167**, 194-204.
- Karentz, D., Cleaver, J. E. and Mitchell, D. L. (1991) Cell survival characteristics and molecular responses of Antarctic phytoplankton to ultraviolet-B radiation. *J. Phycol.*, **27**, 326-341.
- Klaveness, D. (1972) *Coccolithus huxleyi* (Lohm.) Kamptn II. The flagellate cell, aberrant cell types, vegetative propagation and life cycles. *British Phycological Journal*, **7**, 309-318.
- Lorenzen, C. J. (1966) A method for the continuous measurement of in vivo chlorophyll concentration. *Deep-Sea Res.*, **13**, 223-227.

Results

- Marañón, E., Cermeño, P., Rodríguez, J., Zubkov, M. V. and Harris, R. P. (2007) Scaling of phytoplankton photosynthesis and cell size in the ocean. *Limnol. Oceanogr.*, **52**, 2190-2198.
- Mei, Z.-P., Finkel, Z. V. and Irwin, A. J. (2009) Light and nutrient availability affect the size-scaling of growth in phytoplankton. *Journal of theoretical biology*, **259**, 582-588.
- Perry, M. J. and Porter, S. M. (1989) Determination of the cross-section absorption coefficient of individual phytoplankton cells by analytical flow cytometry. *Limnol. Oceanogr.*, **34**, 1727-1738.
- Raven, J. A. (1997) The vacuole: a cost-benefit analysis. In: R. A. Leigh and D. Sanders (eds) *The plant vacuole*. Vol. 25. Academic Press, San Diego, pp. 59-82.
- Raven, J. A. (1998) Small is beautiful: the picophytoplankton. *Functional Ecology* **12**, 503-513.
- Sathyendranath, S. (2009) Carbon-to-chlorophyll ratio and growth rate of phytoplankton in the sea. *Mar Ecol Prog Ser*, **383**, 73-84.
- Sieracki, C. K., Sieracki, M. E. and Yentsch, C. S. (1998) An imaging-in-flow system for automated analysis of marine microplankton. *Mar. Ecol. Prog. Ser.*, **168**, 285-296.
- Sosik, H. M., Chisholm, S. W. and Olson, R. J. (1989) Chlorophyll fluorescence from single cells: interpretation of flow cytometric signals. *Limnol. Oceanogr.*, **34**, 1749-1761.
- Venables, W. N. and Ripley, B. D. (2002) *Modern applied statistics with S*. Springer, New York, pp. 139-182.
- Wang, X. J., Behrenfeld, M., Le Borgne, R., Murtugudde, R. and Boss, E. (2009) Regulation of phytoplankton carbon to chlorophyll ratio by light, nutrients and temperature in the Equatorial Pacific Ocean: a basin-scale model. *Biogeosciences*, **6**, 391-404.
- Westberry, T., Behrenfeld, M. J., Siegel, D. A. and Boss, E. (2008) Carbon-based primary productivity modeling with vertically resolved photoacclimation. *Global Biogeochemical Cycles*, **22**, GB2024.
- Yentsch, C. M., Horan, P. K., Muirhead, K., Dortch, Q., Hangen, F., Legendre, L., Murphy, L. S., Perry, M. J., Phinney, D. A., Pomponi, S. A., Spinrad, R. W., Wood, M., Yentsch, C. S. and Zahuranec, B. J. (1983) Flow cytometry and cell sorting: a technique for analysis and sorting of aquatic particles. *Limnol. Oceanogr.*, **28**, 1275-1280.
- Yentsch, C. S. and Menzel, D. W. (1963) A method for the determination of phytoplankton chlorophyll and phaeophytin by fluorescence. *Deep-Sea Res.*, **10**, 221-231.

Chapter VI. Other works related to the Thesis

During the development of this Thesis, I had the opportunity to work in another research projects, such as the one focused on the dynamics of late winter phytoplankton blooms. Also, previous chapters opened research lines that were explored, such as the one related to the improvement of plankton biomass estimates. This additional work gave place to the following publications:

Eva Álvarez, Enrique Nogueira, Jose Luis Acuña, Marcos López-Álvarez and Jorge A. Sostres (2009) Short-term dynamics of late-winter phytoplankton blooms in a temperate ecosystem (Central Cantabrian Sea, Southern Bay of Biscay). *Journal of Plankton Research*, 31(6): 601-617.

Pablo González, Eva Álvarez, Jose Barranquero, Jorge Diez, Rafael González-Quirós, Enrique Nogueira, Ángel López-Urrutia and Juan José Del Coz (2013) Multiclass Support Vector Machines With Example-Dependent Costs Applied to Plankton Biomass Estimation. *IEEE Transactions on Neural Networks and Learning Systems*, 24(11): 1901-1905.

General discussion

The works expounded in this PhD Thesis provide relevant results on the dynamics of the planktonic community obtained from automated image-based methods. We present technological advances that allow to go deeply into the description of the planktonic community, both from structural and physiological points of view. It is outlined the relevance of the sampling and analysis strategy with FlowCAM to assure the reliability of the obtained information. With this information, we contributed to the advance of knowledge about the variability of size-structure of the phytoplankton community at seasonal and short-term scale in the central Cantabrian Sea shelf and about the size-dependence of the chlorophyll content in individual cells.

FlowCAM: a comprehensive and routine sampling

Comparisons between FlowCAM and traditional methods have been carried out in limited ranges of size (See *et al.*, 2005; Buskey & Hyatt, 2006; Ide *et al.*, 2008) and a formal validation of the capacity of the FlowCAM to characterize the size-structure of the planktonic community was absent. In addition, the particle enumeration with image-based methods presents particularities, such as the two-dimensionality of the images, that demand to be carefully designed to guarantee the quality of the obtained information. For the optimization of the sampling technique with FlowCAM, we went through several phases, evaluating its aptitude to characterize the size-structure of the community, estimating the reliability in the assignment of taxonomic categories and improving the calculation of the biovolume of the particles. This development turned the FlowCAM technique into a potential routine methodology for the enumeration of plankton. This was probed by means of a comparison of the time series obtained on a routine basis with FlowCAM and the traditional light microscopy method.

The effect of the size-structure of the biological communities in the efficiency of the inventory with FlowCAM is here considered for the first time in the literature (I). The ability of the FlowCAM to enumerate plankton cells in natural samples is proved over realistic concentrations of particles and size-spectra determined with traditional

microscopy. We provide an analysis which allows the estimation of the sample volume or total number of particles that have to be counted to obtain a representative sample of the size spectrum. Within this framework, we found that FlowCAM cannot only count a mono-specific solution of cells accurately but can also estimate the size structure of natural samples. However, the requirements of the instrument in terms of sample concentration impose certain constraints, so the pre-treatment of the sample should be carefully chosen and some a priori knowledge about the cell density in the sample is required. We conclude that automatic sampling devices could provide a more precise vision of plankton community, avoiding the effects of sampling preservation and storage and increasing the resolution of the surveys.

The next phase of the method design was to implement techniques of automatic classification based on pattern recognition, returning very promising results (II). The automatic classification of images limits the role of the expert taxonomist to the classification of a group of images of example to train the automatic classifier, eliminating the dependence of the taxonomist during the routine sampling. Similar procedures has been applied to a variety of image-based sampling devices (Blaschko *et al.*, 2005; Sosik & Olson, 2007; Gorsky *et al.*, 2010). However, we went further, adapting the automatic classification of images to obtain not only taxonomic but also morphological information about the particles. This approximation was useful to estimate cell biovolume considering the shape of the particles, permitting to consider the three-dimensional shape of the particles to obtain a more reliable value for cell biovolume.

The automatic classification of FlowCAM images presented here only attains a low taxonomic resolution, thus when the aim is high taxonomic resolution, detailed microscopy analysis is still the unique choice. However, we found that a routine sampling with FlowCAM coupled to a system of automatic classification provides comparable results that a routine sampling with microscopy (III). The comprehensive sampling with FlowCAM presented here allows measuring reliably several cell attributes, such as biovolume, morphology and taxonomy. This kind of information was obtained from other image based methods (Moberg & Sosik, 2012; Spaulding *et al.*, 2012), but, to the best of our knowledge that's the first integral sampling methodology developed for FlowCAM.

The strength of single-cells analysis

However, the goal of the FlowCAM technique was not only to obtain the same information than traditional methods. If this was the case, its application would not

make a big difference, more than relatively faster and expert independent sample analysis. From our perspective, the goal is the single-cell approach that FlowCAM provides. From basic attributes obtained on individual cells, such as biovolume, morphology or taxonomy, it is possible to derive more complex variables that allows to explore deeply the dynamics of the phytoplankton community (Marañon, 2008), further than bulk measurements that has been used traditionally. The combination of FlowCAM information with bulk measurements such as fractionated chlorophyll permits the physiological description of the community and the estimation of primary production. Moreover, a frontier that was not explored yet and that would allow the fully description of a community from a single cell perspective was the estimation of cellular composition and pigment content on individual cells.

FlowCAM is a useful advance for size structure studies, providing a way to analyze many samples in a reasonable amount of time and to obtain extensive numeric information also differentiating broad taxonomic categories. FlowCAM complements traditional techniques by improving the sampling resolution available for study of highly dynamic communities. Hence, the method has the potential to be employed in the analysis phytoplankton variability at broad temporal and spatial scales. We described the seasonality of the phytoplankton community with our FlowCAM integral sampling and explored the differences between contrasting meteo-hydrographic situations of August and November in the shelf area of the Southern Bay of Biscay (IV).

The combination of the routine sampling with FlowCAM with auxiliary information, such as chlorophyll concentration, provides derived variables, such as the carbon to chlorophyll ratio, an indicator of the physiological status of the community (Geider, 1987). This approach allowed exploring photoadaptative changes of the phytoplankton community during the seasonal cycle but also between two highly contrasted hydrographical scenarios in summer and autumn. We found that the photoadaptative response was dependent on body size, which was reported in laboratory cultures (Fujiki & Taguchi, 2002; Finkel, 2004) but not yet in field studies. Hence, our approach can go through the physiological description of the community, characterizing cell physiology with a routine sampling. However, although the carbon was computed on single cells, the chlorophyll was still a bulk measurement, with the errors that this can result (Qin *et al.*, 2013).

The introduction of flow cytometric techniques in oceanography allowed the estimate of the optical properties of individual cells and hence, to account for the chlorophyll content of single cells (Yentsch *et al.*, 1983). In this thesis we calibrate the intensity of fluorescence in every cell against the actual concentration of chlorophyll to be used as a quantitative estimate of the abundance of chlorophyll molecules in the cell

(V). Cell size and chlorophyll content both measured on single cells allows exploring the size dependence of chlorophyll content in cultured and natural samples. We confirmed that size-scaling exponents at the inter-specific scale varied with growth irradiance, but also found that the same pattern can be found on single populations, information that could not be gathered before. This opens the door to the analysis of production on single cells, since variations in the size dependence of chlorophyll content are related directly with the size dependence of photosynthetic rates.

In sum, the analysis with FlowCAM does not only permit to estimate production per size fraction when combined with analytical filtered chlorophyll, but a single analysis allows to estimate chlorophyll concentration and hence derive production on single cells of natural samples. This means that the physiology and production can be disaggregated by cell size, taxonomic group, morphology, or any other characteristic that has been measured on single cells. Besides this single cell perspective revealed *in situ* variations in the size dependence of chlorophyll content, carbon to chlorophyll ratios and hence, the physiological status of the phytoplankton cells.

Consequences and further applications

An integral sampling technique as the one developed in this PhD Thesis can improve exponentially the description that is done routinely of the plankton community. With a single analysis, we can explore not only the standing stocks of carbon but also the turnover rates. Availability of primary productivity data with high temporal and spatial resolution would potentially increase our knowledge about conditions favoring or preventing production, as we showed for the central Cantabrian Sea.

The *in situ* analysis of natural samples permits to cover a wide range of environmental conditions, from light and/or nutrient limiting to saturating conditions, which can help to understand how resource availability and acquisition affect the productivity of natural communities. The size dependence of chlorophyll content relates directly with the size scaling of photosynthetic rates (Finkel, 2004). This can be determinant in primary productivity models since phytoplankton production can be modeled more realistically by improving current models for global primary production. Carbon based Productivity Models (Behrenfeld *et al.*, 2005; Westberry *et al.*, 2008) produce profiles of biological properties and realistic chlorophyll to carbon ratios and regional *in situ* datasets as those obtained with FlowCAM can be useful in the validation of these remotely obtained estimates.

General conclusions

1. The FlowCAM have characteristic flow and particle detection systems which impose constraints on the size range that can be effectively sampled in a given amount of time. A planned pre-processing of the samples allows the FlowCAM to estimate reliably the size structure of natural samples.
2. State of the art techniques to classify automatically images from automatic sampling devices can be applied successfully to FlowCAM on a routine basis. Additional steps to filter out non-living particles, based on statistical differences between certain image attributes of detritus and living particles, improve the classification.
3. Cell biovolume estimates obtained from two-dimensional images are biased when applied to cells with cylindrical or more complex shapes. This causes errors in the total biovolume estimate when dealing, for instances, with samples rich in chain-forming diatoms. The automatic classification can be designed to provide morphological information of the cells which permits a more accurate estimation of cell biovolume.
4. FlowCAM based analysis is a useful advance for size structure studies, providing a way to analyze many samples in a reasonable amount of time, obtaining extensive numeric information and differentiating broad taxonomic categories. Hence, FlowCAM complements traditional techniques by improving the sampling resolution available for study highly dynamic communities and providing a detailed description of particle-size distributions.
5. Annual cycles of phytoplankton community in the central Cantabrian Sea show marked seasonality with spring phytoplankton blooms, transitional periods in autumn and stratification situations in summer. The hydrographical conditions determined the characteristics of the phytoplankton community.

6. The transitional situations of August and November presented different attributes of the planktonic community in base to the size-structure and chlorophyll content per size fraction. Acclimation to light regime caused a differentiation in the allometric scaling of chlorophyll content per biomass unit.
7. The exploration of physiological status of the community per size fraction with a routine sampling based on FlowCAM analysis showed that the alometric exponent of chlorophyll content per biomass unit decrease with the increase of light limitation and these changes can be observed on natural samples.
8. The same pattern of increment of the exponent of the size dependence of chlorophyll content on individual cells with increasing growth irradiance was obtained with analytical chlorophyll and from FlowCAM fluorescence which indicates that FlowCAM fluorescence accounts for the chlorophyll content on single cells.
9. The single cells perspective provided by FlowCAM allows the exploration of size dependence of chlorophyll content in single populations, finding the same pattern of increment of size-scaling exponent with growth irradiance. This allows analysis of chlorophyll content on single cells of natural samples and the exploration of the relationship between environmental conditions and *in situ* photosynthesis rates.

Conclusiones generales

1. El característico sistema de detección de partículas del FlowCAM impone limitaciones al rango de tamaño que puede ser muestreado en una cantidad de tiempo determinado. De modo que el tratamiento previo de las muestras es necesario para que el FlowCAM proporcione estimas fiables de la estructura de tamaño de muestras naturales.
2. Las técnicas actuales de clasificación automática de imágenes pueden ser aplicadas a las imágenes obtenidas con FlowCAM con éxito y de forma rutinaria. La eliminación de partículas inertes (detritos) mediante diferencias estadísticas en los atributos de las imágenes adquiridas permite la mejora de los resultados de la clasificación automática.
3. El biovolumen celular obtenido a partir de imágenes bidimensionales está sesgado cuando se estima a partir del área proyectada, particularmente en células cilíndricas o con formas complejas. Esto causa errores en la estimación del biovolumen celular total en muestras con altas abundancias de, por ejemplo, diatomeas formadoras de cadena. Un sistema de clasificación automático diseñado para proporcionar información morfológica de las partículas permite una estima fiable del biovolumen celular.
4. El análisis mediante FlowCAM presenta ventajas aplicables en los estudios de estructura de tamaños, ya que proporciona un método para analizar un alto número de muestras en un tiempo razonable, obteniendo información numérica y taxonómica. Por ello, el análisis mediante FlowCAM complementa la información obtenida mediante técnicas tradicionales, al incrementar la resolución del muestreo necesaria para el estudio de comunidades altamente dinámicas y al proporcionar una descripción detallada de las distribuciones de tamaño.

5. El ciclo anual de la comunidad de organismos autótrofos en el la plataforma continental del Mar Cantábrico muestra una marcada estacionalidad, con proliferaciones de primavera, periodos de transición en otoño y condiciones de estratificación en verano. Las condiciones hidrográficas determinan las características de la comunidad y su dinámica.
6. Las situaciones de transición encontradas en agosto y noviembre de 2008 presentaron diferentes atributos de la comunidad de fitoplancton, en cuanto a estructura de tamaño y contenido en clorofila por fracción de tamaño. La aclimatación al régimen de luz causó una diferenciación en el escalamiento alométrico del contenido en clorofila por unidad de biomasa.
7. El análisis de la fisiología de la comunidad por fracciones de tamaño con un muestreo rutinario basado en el FlowCAM muestra que el exponente alométrico del contenido en clorofila por unidad de biomasa desciende con el incremento de la limitación por luz y que esos cambios pueden observarse en muestras naturales.
8. El mismo patrón de incremento del exponente alométrico con la radiación se observa con la clorofila analítica y con la clorofila predicha a partir de los valores de fluorescencia lo que indica que la señal de fluorescencia detectada por el FlowCAM revela el contenido en clorofila de las células.
9. El análisis de células individuales que proporciona el FlowCAM permite explorar la alometría del contenido en clorofila en poblaciones aisladas, encontrando el mismo patrón de incremento del exponente alométrico con el incremento de la radiación. Esto permite el análisis del contenido en clorofila de células individuales en muestras naturales y explorar la relación entre las condiciones ambientales y las tasas de fotosíntesis *in situ*.

Bibliography

- Agustí, S. (1991) Allometric scaling of light absorption and scattering by phytoplankton cells. *Can J Fish Aquat Sci*, **48**, 763-767.
- Akima, H. (1978) A method of bivariate interpolation and smooth surface fitting for irregularly distributed data points. *ACM Transactions on Mathematical Software*, **4**, 148-164.
- Alcaraz, M. (2003) Estimating zooplankton biomass through image analysis. *Mar. Biol.*, **143**, 307-315.
- Álvarez, E., López-Urrutia, A. and Nogueira, E. (2012) Improvement of plankton biovolume estimates derived from image-based automatic sampling devices: application to FlowCAM. *J. Plankton Res.*, **34**, 454-469.
- Álvarez, E., López-Urrutia, A., Nogueira, E. and Fraga, S. (2011) How to effectively sample the plankton size spectrum? A case study using FlowCAM. *J. Plankton Res.*, **33**, 1119-1133.
- Álvarez, E., Nogueira, E., Acuña, J. L., López-Álvarez, M. and Sostres, J. A. (2009) Short-term dynamics of late-winter phytoplankton blooms in a temperate ecosystem (Central Cantabrian Sea, Southern Bay of Biscay). *J. Plankton Res.*, **31**, 601-617.
- Babin, M., Cullen, J. J., Roesler, C., Donaghay, P., Doucette, G. J., Kahru, M., Lewis, M. R., Scholin, C. A., Sieracki, M. E. and Sosik, H. M. (2005) New approaches and technologies for observing harmful algal blooms. *Oceanography*, **18**, 210-227.
- Bakker, C., Prins, T. C. and Tackx, M. L. M. (1985) Interpretation of particle spectra of electronic counters by microscopical methods. *Hydrobiol. Bull.*, **19**, 49-59.
- Barofsky, A., Simonelli, P., Vidoudez, C., Troedsson, C., Nejstgaard, J. C., Jakobsen, H. H. and Pohnert, G. (2010) Growth phase of the diatom *Skeletonema marinoi* influences the metabolic profile of the cells and the selective feeding of the copepod *Calanus* spp. *J. Plankton Res.*, **32**, 263-272.
- Bauman, A. G., Burt, J. A., Feary, D. A., Marquis, E. and Usseglio, P. (2010) Tropical harmful algal blooms: an emerging threat to coral reef communities? *Mar. Pollut. Bull.*, doi: 10.1016/j.marpolbul.2010.08.015.
- Beaugrand, G., Reid, P. C., Ibañez, F. and Planque, B. (2000) Biodiversity of North Atlantic and North Sea calanoid copepods. *Mar. Ecol. Prog. Ser.*, **204**, 299-303.
- Behrenfeld, M. J., Boss, E., Siegel, D. A. and Shea, D. M. (2005) Carbon-based ocean productivity and phytoplankton physiology from space. *Global Biogeochemical Cycles*, **19**.

Bibliography

- Behrenfeld, M. J., Marañón, E., Siegel, D. A. and Hooker, S. B. (2002) Photoacclimation and nutrient-based model of light-saturated photosynthesis for quantifying oceanic primary production. *Mar Ecol Prog Ser*, **228**, 103-117.
- Benfield, M. C., Grosjean, P., Culverhouse, P., Irigoien, X., Sieracki, M. E., López-Urrutia, A., Dam, H. G., Hu, Q., Davis, C. S., Hansen, A., Pilskaln, C. H., Riseman, E., Schultz, H., Utgoff, P. E. and Gorsky, G. (2007) RAPID: research on automated plankton identification. *Oceanography*, **20**, 12-26.
- Bérard-Therriault, L., Poulin, M. and Bossé, L. (1999) *Guide d'identification du phytoplancton marin de l'estuaire et du Golfe du Saint-Laurent*. CNRC-NRC, Ottawa, Canada, pp. 387.
- Blanco, J. M., Echevarría, F. and García, C. M. (1994) Dealing with size-spectra: some conceptual and mathematical problems. *Sci. Mar.*, **58**, 17-29.
- Blaschko, M. B., Holness, G., Mattar, M. A., Lisin, D., Utgoff, P. E., Hanson, A. R., Schultz, H., Riseman, E. M., Sieracki, M. E., Balch, W. M. and Tupper, B. (2005) Automatic in situ identification of plankton. *Proceedings of the Seventh IEEE Workshops on Application of Computer Vision (WACV/MOTION'05)*, **1**, 79-86.
- Breier, C. F. and Buskey, E. J. (2007) Effects of the red tide dinoflagellate, *Karenia brevis*, on grazing and fecundity in the copepod *Acartia tonsa*. *J. Plankton Res.*, **29**, 115-126.
- Brown, J. H., Gillooly, J., Allen, A. P., Savage, V. M. and West, G. B. (2004) Toward a metabolic theory of ecology. *Ecology*, **85**, 1771-1789.
- Brown, L. (2010) Using laser-scatter triggering in an imaging particle analysis system to increase particle counting accuracy in sparse samples. Fluid Imaging Technologies, Yarmouth, ME, 8 pp.
- Brzezinski, M. A., Baines, S. B., Balch, W. M., Beucher, C. P., Chai, F., Dugdale, R. C., Krause, J. W., Landry, M. R., Marchi, A., Measures, C., Nelson, D. M., Parker, A. E., Poulton, A. J., Selph, K. E., Strutton, P. G., Taylor, A. G. and Twining, B. S. (2010) Co-limitation of diatoms by iron and silicic acid in the equatorial Pacific. *Deep-Sea Res. II*, doi: 10.1016/j.dsr2.2010.08.005
- Buskey, E. J. (2008) How does eutrophication affect the role of grazers in harmful algal bloom dynamics? *Harmful Algae*, **8**, 152-157.
- Buskey, E. J. and Hyatt, C. J. (2006) Use of the FlowCAM for semi-automated recognition and enumeration of red tide cells (*Karenia brevis*) in natural plankton samples. *Harmful Algae*, **5**, 685-692.
- Calvo-Díaz, A. and Morán, X. A. G. (2006) Seasonal dynamics of picoplankton in shelf waters of the southern Bay of Biscay. *Aquat. Microb. Ecol.*, **42**, 159-174.
- Cavender-Bares, K. K., Rinaldo, A. and Chisholm, S. W. (2001) Microbial size-spectra from natural and nutrient enriched ecosystems. *Limnol. Oceanogr.*, **46**, 778-789.
- Cermeño, P. and Figueiras, F. G. (2008) Species richness and cell-size distribution: size structure of phytoplankton communities. *Mar. Ecol. Prog. Ser.*, **357**, 79-85.

- Cermeño, P., Marañón, E., Rodríguez, J. and Fernández, E. (2005) Large-sized phytoplankton sustain higher carbonspecific photosynthesis than smaller cells in a coastal eutrophic ecosystem. *Mar. Ecol. Prog. Ser.*, **297**, 51-60.
- Cloern, J. E., Grenz, C. and Videgar-Lucas, L. (1995) An empirical model of the phytoplankton chlorophyll/carbon ratio - The conversion factor between productivity and growth rate. *Limnol. Oceanogr.*, **40**, 1313-1321.
- Clough, J. and Strom, S. (2005) Effects of *Heterosigma akashiwo* (Raphidophyceae) on protist grazers: laboratory experiments with ciliates and heterotrophic dinoflagellates. *Aquat. Microb. Ecol.*, **39**, 121-134.
- Cotano, U., Irigoien, X., Etxebeste, E., Álvarez, P., Zarauz, L., Mader, J. and Ferrer, L. (2008) Distribution, growth and survival of anchovy larvae (*Engraulis encrasicolus* L.) in relation to hydrodynamic and trophic environment in the Bay of Biscay. *J. Plankton Res.*, **30**, 467-481.
- Culverhouse, P. F. R. W., Beatriz Reguera, Vincent Herry, Sonsoles González-Gil (2003) Do experts make mistakes? A comparison of human and machine identification of dinoflagellates. *Mar. Ecol. Prog. Ser.*, **247**, 17-25.
- Cullen, J. J. (1982) The deep chlorophyll maximum: comparing vertical profiles of chlorophyll a. *Can. J. Fish. Aquat. Sci.*, **39**, 791-803.
- Cupp, E. E. (ed) (1977) *Marine plankton diatoms of the west coast of North America*. Otto Koeltz Science Publishers, Koenigstein, Germany, pp. 237.
- Chang, C.-C. and Lin, C.-J. (2009) LIBSVM: a Library for Support Vector Machines. <http://www.csie.ntu.edu.tw/~cjlin/libsvm/>.
- Chisholm, S. W. (1992) Phytoplankton size. In: P. G. Falkowski and A. D. Woodhead (eds) *Primary Productivity and Biogeochemical Cycles in the Sea*. Plenum Press, New York, pp. 213-237.
- Davis, C. S., Hu, Q., Gallager, S. M., Tang, X. and Ashjian, C. J. (2004) Real-time observation of taxa-specific plankton distributions: an optical sampling method. *Mar. Ecol. Prog. Ser.*, **284**, 77-96.
- Dodge, J. D. (ed) (1982) *Marine dinoflagellates of the British Isles*. Her Majesty's Stationary Office, London, United Kingdom, pp. 303.
- Dodson, A. N. and Thomas, W. H. (1978) Reverse filtration. In: S. A. (ed) *Phytoplankton manual*. UNESCO, Paris, pp. 104-107.
- Edler, L. and Elbrächter, M. (2010) The Utermöhl method for quantitative phytoplankton analysis. In: B. Karlson, C. Cusack and E. Bresnan (eds) *Microscopic and molecular methods for quantitative phytoplankton analysis*. UNESCO, Paris, pp. 13-20.
- Edwards, K. F., Litchman, E. and Klausmeier, C. A. (2013) Functional traits explain phytoplankton community structure and seasonal dynamics in a marine ecosystem. *Ecology Letters*, **16**, 56-63.

Bibliography

- Falkowski, P. G. and Raven, J. A. (2007) *Aquatic Photosynthesis*. Princeton University Press, Princeton.
- Fernández, E. and Bode, A. (1991) Seasonal patterns of primary production in the Central Cantabrian Sea (Bay of Biscay). *Scientia Marina*, **55**, 629-636.
- Finkel, Z. V. (2001) Light absorption and size-scaling of light-limited metabolism in marine diatoms. *Limnol. Oceanogr.*, **46**, 86-94.
- Finkel, Z. V. (2004) Resource limitation alters the 3/4 size scaling of metabolic rates in phytoplankton. *Mar Ecol Prog Ser*, **273**, 269-279.
- Finkel, Z. V., Vaillancourt, C. J., Irwin, A. J., Reavie, E. D. and Smol, J. P. (2009) Environmental control of diatom community size structure varies across aquatic ecosystems. *Proc. R. Soc. B*, **276**, 1627-1634.
- Fujiki, T. and Taguchi, S. (2002) Variability in chlorophyll a specific absorption coefficient in marine phytoplankton as a function of cell size and irradiance. *J. Plankton Res.*, **24**, 859-874.
- García, C. M., Jimenez-Gómez, F. and Rodríguez, J. (1994) The size-structure and functional composition of ultraplankton and nanoplankton at a frontal station in the Alboran Sea. Working groups 2 and 3 report. *Sci. Mar.*, **58**, 43-52.
- Geider, R. J. (1987) Light and temperature dependence of the carbon to chlorophyll a ratio in microalgae and cyanobacteria: implications for physiology and growth of phytoplankton. *New Phytologist*, **106**, 1-34.
- Giometto, A., Altermatt, F., Carrara, F., Maritan, A. and Rinaldo, A. (2013) Scaling body size fluctuations. *PNAS*, **110**, 4646-4650.
- González, P., Díez, J., Del Coz, J. J., Álvarez, E., González-Quirós, R., Nogueira, E. and López-Urrutia, A. (2010) Predicción taxonómica de muestras de microplancton usando técnicas de Aprendizaje Automático. In: A. Troncoso and J. C. Riquelme (eds) *V Simposio de Teoría y Aplicaciones de Minería de Datos (TAMIDA 2010)*. Ibergaceta Publicaciones, Madrid, 2010, Valencia, Spain, pp. 319-328.
- Gorsky, G., Ohman, M. D., Picheral, M., Gasparini, S., Stemmann, L., Romagnan, J. B., Cawood, A., Pesant, S., García-Comas, C. and Prejger, F. (2010) Digital zooplankton image analysis using the ZooScan integrated system. *J. Plankton Res.*, **32**, 285-303.
- Granda, A. P. and Anadón, R. (2008) The annual cycle of nanoflagellates in the Central Cantabrian Sea (Bay of Biscay). *Journal of Marine Systems*, **72**, 298-308.
- Grasshoff, K., Ehrhardt, M. and Kremling, K. (eds) (1983) *Methods of seawater analysis*. Verlag Chemie, Weinheim.
- Gribben, P. E., Wright, J. T., O'connor, W. A., Doblin, M. A., Eyre, B. and Steinberg, P. D. (2009) Reduced performance of native infauna following recruitment to a habitat-forming invasive marine alga. *Oecologia*, **158**, 733-745.

- Grosjean, P. (2005) Analyze your plankton through digitized images. <http://www.sciviews.org/zooimage/index.html>.
- Grosjean, P. (2011) SciViews: A GUI API for R. <http://www.sciviews.org/SciViews-R/>.
- Grosjean, P., Picheral, M., Warembourg, C. and Gorsky, G. (2004) Enumeration, measurement and identification of net zooplankton samples using the ZOOSCAN digital imaging system. *ICES J. Mar. Sci.*, **61**, 518-525.
- Gutiérrez-Rodríguez, A., Latasa, M., Estrada, M., Vidal, M. and Marrasé, C. (2010) Carbon fluxes through major phytoplankton groups during the spring bloom and post-bloom in the Northwestern Mediterranean Sea. *Deep-Sea Research I*, **57**, 486-500.
- Haralick, R. M., Shanmugam, K. and Deinstein, I. (1979) Textural features for image classification. *IEEE T. Syst. Man Cyb.*, **6**, 610-621.
- Haury, L. R., McGowan, J. A. and Wiebe, P. H. (1978) Patterns and processes in the time-space scales of plankton distributions. In: S. J. H. (ed) *Spatial pattern in plankton communities*. Plenum Press, New York, pp. 277-327.
- Hillebrand, H., Dürselen, C.-D., Kirschtel, D., Pollinger, U. and Zohary, T. (1999) Biovolume calculation for pelagic and benthic microalgae. *J. Phycol.*, **35**, 403-4424.
- Hu, M. K. (1962) Visual Pattern Recognition by Moment Invariants. *IRE Trans. Info. Theory*, **8**, 179-187.
- Huete-Ortega, M., Marañón, E., Varela, M. and Bode, A. (2010) General patterns in the size scaling of phytoplankton abundance in coastal waters during a 10-year time series. *J. Plankton Res.*, **32**, 1-14.
- Huot, Y., Babin, M., Bruyant, F., Grob, C., Twardowski, M. S. and Claustre, H. (2007) Does chlorophyll a provide the best index of phytoplankton biomass for primary productivity studies? *Biogeosciences Discuss.*, **4**, 707-745.
- Ide, K., Takahashi, K., Kuwata, A., Nakamachi, M. and Saito, H. (2008) A rapid analysis of copepod feeding using FlowCAM. *J. Plankton Res.*, **30**, 275-281.
- Irigoiien, X., Fernandes, J. A., Grosjean, P., Denis, K., Albaina, A. and Santos, M. (2009) Spring zooplankton distribution in the Bay of Biscay from 1998 to 2006 in relation with anchovy recruitment. *J. Plankton Res.*, **31**, 1-17.
- Jakobsen, H. H. and Carstensen, J. (2011) FlowCAM: Sizing cells and understanding the impact of size distributions on biovolume of planktonic community structure. *Aquat. Microb. Ecol.*, **65**, 75-87.
- James, M. R. (1991) Sampling and preservation methods for the quantitative enumeration of microzooplankton. *New Zeal. J. Mar. Fresh.*, **25**, 305-310.
- Jeffrey, S. W. and Humphrey, G. F. (1975) New spectrophotometric equation for determining chlorophyll. *Biochem. Physiol. Pflanz.*, **167**, 194-204.
- Jennings, S. and Mackinson, S. (2003) Abundance–body mass relationships in size-structured food webs. *Ecol. Lett.*, **6**, 971-974.

Bibliography

- Kara, A. B., Rochford, P. A. and Hurlburt, H. E. (2000) An optimal definition for ocean mixed layer depth. *Journal of Geophysical Research*, **105**, 16803-16821.
- Karatzoglou, A., Meyer, D. and Hornik, K. (2006) Support Vector Machines in R. *J. Stat. Softw.*, **15**, 1-28.
- Karentz, D., Cleaver, J. E. and Mitchell, D. L. (1991) Cell survival characteristics and molecular responses of Antarctic phytoplankton to ultraviolet-B radiation. *J. Phycol.*, **27**, 326-341.
- Kirk, J. T. O. (1975a) A theoretical analysis of the contribution of algal cells to the attenuation of light within natural waters I. General treatment of suspensions of pigmented cells. *New Phytol.*, **75**, 11-20.
- Kirk, J. T. O. (1975b) A theoretical analysis of the contribution of algal cells to the attenuation of light within natural waters II. Spherical cells. *New Phytol.*, **75**, 21-36.
- Kirk, J. T. O. (1994) *Light and photosynthesis in aquatic ecosystems*. Cambridge Univ. Press, New York, pp. 662.
- Klaveness, D. (1972) *Coccolithus huxleyi* (Lohm.) Kamptn II. The flagellate cell, aberrant cell types, vegetative propagation and life cycles. *British Phycological Journal*, **7**, 309-318.
- Koski, M., Breteler, W. K., Schogt, N., Gonzalez, S. and Jakobsen, H. H. (2006) Life-stage-specific differences in exploitation of food mixtures: diet mixing enhances copepod egg production but not juvenile development. *J. Plankton Res.*, **28**, 919-936.
- Kudela, R. M., Lane, J. Q. and Cochlan, W. P. (2008) The potential role of anthropogenically derived nitrogen in the growth of harmful algae in California, USA. *Harmful Algae*, **8**, 103-110.
- Lavrentyev, P. J., McCarthy, M. J., Klarer, D. M., Jochem, F. and Gardner, W. S. (2004) Estuarine microbial food web patterns in a Lake Erie coastal wetland. *Microbial Ecol.*, **48**, 567-577.
- Leakey, R. J. G., Burkill, P. H. and Sleigh, M. A. (1994) A comparison of fixatives for the estimation of abundance and biovolume of marine planktonic ciliate populations. *J. Plankton Res.*, **10**, 375-389.
- Legendre, P. and Legendre, L. (1998) *Numerical Ecology*. Elsevier Science B. V., Amsterdam.
- Litchman, E. and Klausmeier, C. A. (2008) Trait-based community ecology of phytoplankton. *Annu. Rev. Ecol. Evol. Syst.*, **39**, 615-639.
- Littman, R. A., Van Oppen, M. J. H. and Willis, B. L. (2008) Methods for sampling free-living *Symbiodinium* (zooxanthellae) and their distribution and abundance at Lizard Island (Great Barrier Reef). *J. Exp. Mar. Biol. Ecol.*, **364**, 48-53.
- Liu, H., Dagg, M. J. and Strom, S. (2005) Grazing by the calanoid copepod *Neocalanus cristatus* on the microbial food web in the coastal Gulf of Alaska. *J. Plankton Res.*, **27**, 647-662.
- Lorenzen, C. J. (1966) A method for the continuous measurement of in vivo chlorophyll concentration. *Deep-Sea Res.*, **13**, 223-227.

- Luo, T., Kramer, K., Goldgof, D. B., Hall, L. O., Samson, S., Remsen, A. and Hopkins, T. (2004) Recognizing Plankton Images From the Shadow Image Particle Profiling Evaluation Recorder. *IEEE T. Syst. Man Cy. B*, **34**, 1753-1762.
- Macintyre, H. L., Kana, T. M., Anning, J. and Geider, R. (2002) Photoacclimation of photosynthesis irradiance response curves and photosynthetic pigments in microalgae and cyanobacteria. *J. Phycol.*, **38**, 17-38.
- Macleod, N., Benfield, M. and Culverhouse, P. (2010) Time to automate identification. *Nature*, **467**, 154-155.
- Marañón, E. (2008) Inter-specific scaling of phytoplankton production and cell size in the field.
- Marañón, E., Cermeño, P., Rodríguez, J., Zubkov, M. V. and Harris, R. P. (2007) Scaling of phytoplankton photosynthesis and cell size in the ocean. *Limnol. Oceanogr.*, **52**, 2190-2198.
- Mcgill, B. J., Enquist, B. J., Weiher, E. and Westoby, M. (2006) Rebuilding community ecology from functional traits. *Trends Ecol. Evol.*, **21**, 178-185.
- Mei, Z.-P., Finkel, Z. V. and Irwin, A. J. (2009) Light and nutrient availability affect the size-scaling of growth in phytoplankton. *Journal of theoretical biology*, **259**, 582-588.
- Menden-Deuer, S., Lessard, E. J. and Satterberg, J. (2000) Carbon to volume relationships for dinoflagellates, diatoms and other protist plankton. *Limnol. Oceanogr.*, **45**, 569-579.
- Menden-Deuer, S., Lessard, E. J. and Satterberg, J. (2001) Effect of preservation on dinoflagellate and diatom cell volume and consequences for carbon biomass predictions. *Mar. Ecol. Prog. Ser.*, **222**, 41-50.
- Moberg, E. A. and Sosik, H. M. (2012) Distance maps to estimate cell volume from two-dimensional plankton images. *Limnol. Oceanogr.-Meth*, **10**, 278-288.
- Montagnes, D. J. S., Berges, J. A., Harrison, P. J. and Taylor, F. J. R. (1994) Estimating carbon, nitrogen, protein and chlorophyll a from volume in marine phytoplankton. *Limnol. Oceanogr.*, **39**, 1044-1060.
- Nielsen, L. T., Jakobsen, H. H. and Hansen, P. J. (2010) High resilience of two coastal plankton communities to twenty-first century seawater acidification: evidence from microcosm studies. *Mar. Biol. Res*, **1**, 1-14.
- Nielsen, T. G. and Hansen, B. W. (1999) Plankton community structure and carbon cycling on the western coast of Greenland during the stratified summer situation. I. Hydrography, phytoplankton and bacterioplankton. *Aquat Microb Ecol*, **16**, 205-216.
- Nogueira, E., González-Nuevo, G., Bode, A., Varela, M., Morán, X. A. G. and Valdés, L. (2004) Comparison of biomass and size spectra derived from optical plankton counter data and net samples: application to the assessment of mesoplankton distribution along the Northwest and North Iberian Shelf. *ICES Journal of Marine Science*, **61**, 508-517.
- Odum, E. P. (1969) The strategy of ecosystem development. *Science*, **164**, 262-270.

Bibliography

- Olenina, I., Hajdu, S., Edler, L., Andersson, A., Wasmund, N., Busch, S., Göbel, J., Gromisz, S., Huseby, S., Huttunen, M., Jaanus, A., Kokkonen, P., Ledaine, I. and Niemkiewicz, E. (2006) Biovolumes and size-classes of phytoplankton in the Baltic Sea. *HELCOM Balt.Sea Environ. Proc.*, **106**, 144.
- Olson, R. J. and Sosik, H. M. (2007) A submersible imaging-in-flow instrument to analyze nano- and microplankton : Imaging FlowCytobot. *Limnol. Oceanogr.-Meth*, **5**, 195-203.
- Olson, R. J., Zettler, E. R. and Durand, M. D. (1993) Phytoplankton analysis using flow cytometry. In: P. F. Kemp, B. F. Sherr, E. B. Sherr and J. J. Cole (eds) *Handbook of methods in aquatic microbial ecology*. Lewis publishers, Boca Raton, Florida, pp. 175-186.
- Pau, G., Fuchs, F., Sklyar, O., Boutros, M. and Huber, W. (2010) EBImage - an R package for image processing with applications to cellular phenotypes. *Bioinformatics*, **26**, 979-981.
- Pedersen, T. M., Almeda, R., Fotel, F. L., Jakobsen, H. H., Mariani, P. and Hansen, B. W. (2010) Larval growth in the dominant polychaete *Polydora ciliata* is food-limited in a eutrophic Danish estuary (Isefjord) *Mar. Ecol. Prog. Ser.*, **407**, 99-110.
- Peliz, A., Dubert, J., Santos, A. M. P., Oliveira, P. B. and Le Cann, B. (2005) Winter upper ocean circulation in the Western Iberian Basin - fronts, eddies and poleward flows: an overview. *Deep-Sea Research I*, **52**, 621-646.
- Perry, M. J. and Porter, S. M. (1989) Determination of the cross-section absorption coefficient of individual phytoplankton cells by analytical flow cytometry. *Limnol. Oceanogr.*, **34**, 1727-1738.
- Peters, A. and Hothorn, T. (2009) ipred: Improved Predictors. R package version 0.8-8. <http://CRAN.R-project.org/package=ipred>.
- Pingree, R. D. and Lecann, B. (1990) Structure, strength and seasonality of the slope currents in the Bay of Biscay region. *J. Mar. Biol. Assoc. UK*, **70**, 857-885.
- Qin, H., Li, S. and Li, D. (2013) An improved method for determining phytoplankton chlorophyll a concentration without filtration. *Hydrobiologia*, **707**, 81-95.
- Quiñones, R. A., Platt, T. and Rodríguez, J. (2003) Patterns of biomass-size spectra from oligotrophic waters of the Northwest Atlantic. *Prog. Oceanogr.*, **57**, 405-427.
- R_Development_Core_Team (2010) R: A language and environment for statistical computing. <http://www.R-project.org>.
- Raven, J. A. (1997) The vacuole: a cost-benefit analysis. In: R. A. Leigh and D. Sanders (eds) *The plant vacuole*. Vol. 25. Academic Press, San Diego, pp. 59-82.
- Raven, J. A. (1998) Small is beautiful: the picophytoplankton. *Functional Ecology* **12**, 503-513.
- Reynolds, C. S. (1997) Vegetation processes in the pelagic: a model for ecosystem theory. In: O. Kinne (ed) *Excellence in Ecology*. Vol. 9. Ecology Institute, Oldendorf/Luhe, Germany, pp. 371.

- Reynolds, R. A., Stramski, D., Wright, V. M. and Woźniak, S. B. (2010) Measurements and characterization of particle size distributions in coastal waters. *J. Geophys. Res.*, **115**, doi: 10.1029/2009JC005930.
- Rodriguez, J. (1994) Some comments of the size-based structural analysis of the pelagic ecosystems. *Sci. Mar.*, **58**, 1-10.
- Rodriguez, J. and Mullin, M. M. (1986) Relation between biomass and body weight of plankton in a steady state oceanic ecosystem. *Limnol. Oceanogr.*, **31**, 361-370.
- San Martin, E., Harris, R. P. and Irigoien, X. (2006a) Latitudinal variation in plankton size spectra in the Atlantic Ocean. *Deep-Sea Res. II*, **53**, 1560-1572.
- San Martin, E., Irigoien, X., Harris, R. P., López-Urrutia, A., Zubkov, M. V. and Heywood, J. L. (2006b) Variation in the transfer of energy in marine plankton along a productivity gradient in the Atlantic Ocean. *Limnol. Oceanogr.*, **51**, 2084-2091.
- Sathyendranath, S. (2009) Carbon-to-chlorophyll ratio and growth rate of phytoplankton in the sea. *Mar Ecol Prog Ser*, **383**, 73-84.
- See, J. H., Campbell, L., Richardson, T. L., Pinckney, J. L., Shen, R. and Guinasso Jr., N. L. (2005) Combining new technologies for determination of phytoplankton community structure in the northern Gulf of Mexico. *J. Phycol.*, **41**, 305-310.
- Sheldon, R. W. and Parsons, T. R. (1967) *A practical manual on the use of the Coulter counter in marine science*. Coulter Electronics, Toronto, pp. 66.
- Sheldon, R. W., Prakash, A. and Sutcliffe Jr., W. H. (1972) The size distribution of particles in the ocean. *Limnol. Oceanogr.*, **17**, 327-340.
- Sieracki, C. K., Sieracki, M. E. and Yentsch, C. S. (1998) An imaging-in-flow system for automated analysis of marine microplankton. *Mar. Ecol. Prog. Ser.*, **168**, 285-296.
- Sklyar, O. and Huber, W. (2006) Image Analysis for Microscopy Screens - Image analysis and processing with EBImage. *The Newsletter of the R Project*, **6**, 12-16.
- Sklyar, O., Pau, G., Smith, M. and Huber, W. (2011) EBImage: Image processing toolbox for R. <http://bioconductor.org/packages/2.9/bioc/html/EBImage.html>.
- Smayda, T. J. (1998) Patterns of variability characterizing marine phytoplankton, with examples from Narragansett Bay. *ICES Journal of Marine Science*, **55**, 562-573.
- Solow, A., Davis, C. and Hu, Q. (2001) Estimating the taxonomic composition of a sample when individuals are classified with error. *Mar. Ecol. Prog. Ser.*, **216**, 309-311.
- Sosik, H. M., Chisholm, S. W. and Olson, R. J. (1989) Chlorophyll fluorescence from single cells: interpretation of flow cytometric signals. *Limnol. Oceanogr.*, **34**, 1749-1761.
- Sosik, H. M. and Olson, R. J. (2007) Automated taxonomic classification of phytoplankton sampled with imaging-in-flow cytometry. *Limnol. Oceanogr.-Meth*, **5**, 204-216.
- Spaulding, S. A., Jewson, D. H., Bixby, R. J., Nelson, H. and Mcknight, D. M. (2012) Automated measurement of diatom size. *Limnol. Oceanogr.-Meth*, **10**, 882-890.

Bibliography

- Sterling Jr, M. C., Bonner, J. S., Ernest, A. N. S., Page, C. A. and Autenrieth, R. L. (2004) Characterizing aquatic sediment-oil aggregates using in situ instruments. *Mar. Pollut. Bull.*, **48**, 533-542.
- Stoecker, D. K., Gifford, D. J. and Putt, M. (1994) Preservation of marine planktonic ciliates: losses and cell shrinkage during fixation. *Mar. Ecol. Prog. Ser.*, **110**, 293-299.
- Sun, J. and Liu, D. (2003) Geometric models for calculating cell biovolume and surface area for phytoplankton. *J. Plankton Res.*, **25**, 1331-1346.
- Sverdrup, H. U. (1953) On conditions for the vernal blooming of phytoplankton. *Journal du Conseil pour la Exploration de la Mer*, **18**, 287-295.
- Tang, X., Lin, F., Samson, S. and Remsen, A. (2006) Binary Plankton Image Classification. *IEEE J. Oceanic Eng.*, **31**, 728-735.
- Tang, X., Stewart, W. K., Vincent, L., Huang, H., Marra, M., Gallager, S. M. and Davis, C. S. (1998) Automatic Plankton Image Recognition. *Artif. Intell. Rev.*, **12**, 177-199.
- Tanoi, T., Kawachi, M. and Watanabe, M. M. (2010) Effects of carbon source on growth and morphology of *Botryococcus braunii*. *J. Appl. Phycol.*, doi: 10.1007/s10811-010-9528-4.
- Tauxe, L., Steindorf, J. L. and Harris, A. (2006) Depositional remanent magnetization: toward an improved theoretical and experimental foundation. *Earth Planet. Sc. Lett.*, **244**, 515-529.
- Tilman, D. (1999) The ecological consequences of changes in biodiversity: a search for general principles. *Ecology*, **80**, 1455-1474.
- Toepel, J., Langner, U. and Wilhelm, C. (2005) Combination of flow cytometry and single cell absorption spectroscopy to study the phytoplankton structure and to calculate the Chl a specific absorption coefficients at the taxon level. *J. Phycol.*, **41**, 1099-1109.
- Tomas, C. R. (ed) (1997) *Identifying marine phytoplankton*. Academic Press, San Diego, California, pp. 858.
- Töpper, B., Larsen, A., Thingstad, T. F., Thyrrhaug, R. and Sandaa, R.-A. (2010) Bacterial community composition in an Arctic phytoplankton mesocosm bloom: the impact of silicate and glucose *Polar Biol.*, doi: 10.1007/s00300-010-0846-4.
- Townsend, D. W., Keller, M. D., Sieracki, M. E. and Ackleson, S. G. (1992) Spring phytoplankton blooms in the absence of vertical water column stratification. *Nature*, **360**, 59-62.
- Utermöhl, H. (1958) Zur Vervollkommnung der quantitativen Phytoplankton-Methodik. *Mitt. Int. Ver. Theor. Angew. Limnol.*, **9**, 1-38.
- Vaillancourt, R. D., Brown, C. W., Guillard, R. R. L. and Balch, W. M. (2004) Light backscattering properties of marine phytoplankton: relationships to cell size, chemical composition and taxonomy. *J. Plankton Res.*, **26**, 191-212.
- Vázquez-Domínguez, E., Morán, X. A. G. and López-Urrutia, A. (2013) Photoacclimation of picophytoplankton in the central Cantabrian Sea. *Mar Ecol Prog Ser*, **493**, 43-56.

- Venables, W. N. and Ripley, B. D. (2002) *Modern applied statistics with S*. Springer, New York, pp. 139-182.
- Vuorio, K., Lepisto, L. and Holopainen, A.-L. (2007) Intercalibrations of freshwater phytoplankton analyses. *Boreal Environ Res*, **12**, 561-569.
- Wang, X. J., Behrenfeld, M., Le Borgne, R., Murtugudde, R. and Boss, E. (2009) Regulation of phytoplankton carbon to chlorophyll ratio by light, nutrients and temperature in the Equatorial Pacific Ocean: a basin-scale model. *Biogeosciences*, **6**, 391-404.
- Westberry, T., Behrenfeld, M. J., Siegel, D. A. and Boss, E. (2008) Carbon-based primary productivity modeling with vertically resolved photoacclimation. *Global Biogeochemical Cycles*, **22**, GB2024.
- Willén, E. (1976) A simplified method of phytoplankton counting. *Br. phycol. J.*, **11**, 265-278.
- Worden, A. Z., Nolan, J. K. and Palenik, B. (2004) Assessing the dynamics and ecology of marine picophytoplankton: the importance of the eukaryotic component. *Limnol. Oceanogr.*, **49**, 168-179.
- Yentsch, C. M., Horan, P. K., Muirhead, K., Dortch, Q., Hangen, F., Legendre, L., Murphy, L. S., Perry, M. J., Phinney, D. A., Pomponi, S. A., Spinrad, R. W., Wood, M., Yentsch, C. S. and Zahuranec, B. J. (1983) Flow cytometry and cell sorting: a technique for analysis and sorting of aquatic particles. *Limnol. Oceanogr.*, **28**, 1275-1280.
- Yentsch, C. S. and Menzel, D. W. (1963) A method for the determination of phytoplankton chlorophyll and phaeophytin by fluorescence. *Deep-Sea Res.*, **10**, 221-231.
- Zar, J. H. (1999) *Biostatistical Analysis*. Prentice-Hall, Englewood Cliffs, New Jersey, pp. 718.
- Zarauz, L. and Irigoien, X. (2008) Effects of lugol's fixation on the size structure of natural nano-microplankton samples, analyzed by means of an automatic counting method. *J. Plankton Res.*, **30**, 1297-1303.
- Zarauz, L., Irigoien, X. and Fernandes, J. A. (2009) Changes in plankton size structure and composition, during the generation of a phytoplankton bloom, in the central Cantabrian sea. *J. Plankton Res.*, **31**, 193-207.
- Zarauz, L., Irigoien, X., Urtizberea, A. and Gonzalez, M. (2007) Mapping plankton distribution in the Bay of Biscay during three consecutive spring surveys. *Mar. Ecol. Prog. Ser.*, **345**, 27-39.
- Zernike, F. (1934) Beugungstheorie des Schneidenverfahrens und seiner verbesserten Form, der Phasenkontrastmethode (Diffraction theory of the cut procedure and its improved form, the phase contrast method). *Physica*, **1**, 689-704.
- Zubkov, M. V., Sleigh, M. A., Tarran, G. A., Burkill, P. H. and Leakey, R. J. G. (1998) Picoplankton community structure on an Atlantic transect from 50° N to 50° S. *Deep-Sea Res. I.*, **45**, 1339-1355.